A Comprehensive Study on Leprosy and its Control Through Mathematical Standpoint

Thesis
Submitted for the Degree of
Doctor of Philosophy in Science

By

Salil Ghosh

Centre for Mathematical Biology and Ecology
Department of Mathematics
Jadavpur University
Kolkata - 700032
West Bengal, India
October, 2023

যাদবপুর বিশ্ববিদ্যালয়

FACULTY OF SCIENCE
DEPARTMENT OF MATHEMATICS

JADAVPUR UNIVERSITY
Kolkata-700 032, India
Telephone : 91 (33) 2414 6717

CERTIFICATE FROM THE SUPERVISOR

This is to certify that the thesis entitled "**A Comprehensive Study on Leprosy and its Control Through Mathematical Standpoint**" submitted by **Sri Salil Ghosh** who got his name registered on **02.01.2020** for the award of Ph. D. (Science) degree of Jadavpur University, is absolutely based upon his own work under the supervision of **Prof. Priti Kumar Roy** and that neither this thesis nor any part of it has been submitted for either any degree / diploma or any other academic award anywhere before.

Priti Kumar Roy

(Signature of the Supervisor) 09/10/2023.

Prof. (Dr.) Priti Kumar Roy
Professor
Department of Mathematics
Jadavpur University
Kolkata-700 032, West Bengal

I dedicate my thesis to my Father Sri Gayanath Ghosh and my Mother Smt. Shankari Ghosh.

Abstract

Leprosy is a chronic mycobacterial infectious disease that causes peripheral neuropathy in human body which results irreversible nerve damage and loss of sensation in skin and disabilities of various organs. In-depth research of leprosy continues to be a very challenging topic for scientists worldwide as the infection of leprosy is a very complex process and difficult to execute the same in laboratory. In spite of the invention of multi-drug therapy (MDT), leprosy is far from eradicated and still remains a public health problem in many densely populated countries like India, Brazil, China, Indonesia and some parts of Africa, Europe and USA etc. According to WHO (World Health organisation), there were $202,256$ new leprosy cases registered globally in 2019 from 161 countries from the six WHO Regions. Considering this contexts, this thesis deals with several mathematical models demonstrating and decoding the basic infection mechanism and disease dissemination process of leprosy. Also, exploring safe and effective treatment policies and regimens to overcome the hindrance of drug-resistance scenarios, adverse drug impacts and the difficulties in framing a perfect tenure of treatment is the key focus of the thesis. Each chapter of this thesis is divided into two parts: theoretical part and numerical part. In theoretical section, systems are constructed in such a way so that their solutions remain biologically meaningful and also the existence, uniqueness and boundedness of solutions remain biologically plausible. Finally, novel numerical tools and techniques are utilized to illustrate and validate all the analytical outcomes.

Acknowledgements

I am using this opportunity to express my gratitude to everyone who supported me throughout the course of this Ph.D. program. I am thankful for their aspiring guidance, invaluably constructive criticism and friendly advice during this work. I am sincerely grateful to them for sharing their truthful and illuminating views on a number of issues related to the study. At the end of my thesis, it is my pleasure to express my thanks to all those who contributed in many ways to the success of this study and made it an unforgettable experience for me.

Yes, whenever writing this acknowledgement for the thesis, I am really being a little emotional. Firstly, I would like to thank none other than my research supervisor, Prof. (Dr.) Priti Kumar roy for his guidance, endless love, affection and encouragement throughout the journey. Without him, it would not be possible at all to accomplish this rigorous research works and acquire the Ph.D degree. I have faced a certain amount of difficulty in my career before starting Ph.D journey, but thanks to Prof. Roy. He is the person who taught me to stand tall and strong. Prof. Roy firstly motivated me a lot and then, designed the whole outline of the study on which I have started investigating and experimenting in pursuit of fundamental knowledge in my research works.

It has been a great privilege to spend several years in the Department of Mathematics at Jadavpur University. I have started my journey in Jadavpur University as a undergraduate student. Then, after completing the Bachelor of Science degree and Master of of Science degree from this university, I got myself admitted in Jadavpur University in the Ph.D program. It is been a long long journey here and I think, it will be the best part my of life spended here in Jadavpur university. I would like to express my heartiest gratitude to all of respected teachers, official staffs in my department for making those times like a joyful ride.

My heartfelt thanks to my fellow lab-mates - Shubhankar, Amit, Tarun, Sanju, Mosaraf, Tushar, Homagnic and Satyajit for the stimulating discussions and for all the fun we have had in the last four years. These are really memorable to me. My acknowledgement will never be completed without the special mention of my lab seniors: Dr. Shubhankar Saha, Dr. Amit Kumar Roy, Dr. Fahad Al Basir, Dr. Jahangir Chowdhury, Dr. Amar Nath Chatterjee, Dr. Jayanta Mondal, Dr. Abhirup Datta, Dr. Mithun Kumar Ghosh, Dr. Dibyendu Biswas who have taught me the lab culture and the disciplines and dedications required in research. Thank you very much for your guidance, enormous help and suggestions to prepare the entire thesis and they were always there for any kind of help whenever it was needed.

I would also like to thank all my seniors and juniors from the Department of Mathematics, Jadavpur University, for all the love that they have showered upon me. I could not have asked for more than what I got from them.

I would also like to thank specially Prof. Sourav Rana and two of my previously mentioned lab seniors, Dr. Shubhankar Saha, Dr. Amit Kumar Roy who helped me performing several mathematical experiments required in my research work. I am grateful to them for answering all of my research queries, their endless efforts, patience and for their precious times shared with me during my Ph.d works. Furthermore, I thank Debaditya Ghosh and Avik Das, two of my best friends for their unconditional love, support and motivation for nearly the last ten years.

The journey of my study had started from my school Krishnanagar High School and Kavi Bijoylal H.S. institute, which I think is the best part of my memory lane. Here, I pay homage to all my respected teachers for their love, care and motivation. I have got encouragement, motivation and inspiration from there to walk a long way of higher education.

Finally, I would like to thank my parents, Sri Gayanath Ghosh & Smt. Shankari Ghosh and my sister, Joyeeta Ghosh. I just can't describe their contribution in words in pursuing my Ph.d and even in my life. This dissertation stands as a tribute to my beloved grandfather, late Nitaipada Ghosh and also to all of my beloved family members for their unconditional love and encouragement.

Finally, I would like to thank the West Bengal Government State Fellowship, Government of West Bengal, W.B., India and DST-FIST, Department of Mathemetics, Jadavpur University, Kolkata, India, for their financial support. Also, my sincere thanks to all the unknown referees of the journals who referred my research papers for their prompt and constructive comments and suggestions which helped in improving my work.

Last of all, I would like to thank everyone who had helped me and apologize to them whom I could not mention in my acknowledgement.

October, 2023 (Salil Ghosh)

Contents

ACRONYMES AND ABBREVIATIONS

t	time
$\mathbb{R}$	Real line
$\mathbb{R}^n$	n-dimensional euclidean space
WHO	World Health Organization
MDT	Multidrug Therapy
M. leprae	*Mycobacterium leprae*
MB	Multibacillary
PB	Paucibacillary
R-H criterion	Routh Hurwitz criterion

Chapter 1

Introduction

"An end to leprosy can be put only if all of us work in synergy.... Only if we never give up on this disease."

$\sim$ World Leprosy Eradication Day Slogan, 2022 (@bestmessages.org) $\square$

1.1 The Leprosy Epidemic: History of the Disease

[1]Leprosy is a chronic mycobacterial disease caused by the bacterium called *M. leprae*. The disease is also recognized as one of the oldest disease known to mankind. In medieval times, nearly all of Europe have seen the terrifying impact of leprosy at an endemic stage. The burden of leprosy reduced a lot during the period of renaissance in Europe and that was possible due to the strict isolation measure implemented which blocked the transmission of the disease quite successfully. This strategy also enhanced the social stigma greatly. In the 13^{th} century BC, there were as many as 2000 leper colonies in France according to an article in 1864 written by Rudolf Virchow. people used to know very little about the in-depth infection and disease dissemination process about leprosy until the norwegian physician Gerhard Armauer Hansen first experimented in 1873 and discovered that the main causative agent for leprosy is the bacteria *Mycobacterium leprae* (*M. leprae*). After his name, leprosy is also called 'Hansen's disease' nowadays.

[1]*Information given/listed in this chapter are collected from several web links and peer-reviewed journals (cited here).*

1.2 The Epidemiology of Leprosy

Leprosy constitutes a chronic infectious ailment stemming from the bacterium *Mycobacterium leprae*. Its primary afflictions encompass the skin and peripheral nerves, with potential for disfigurement and disability when left untreated [Ploemacher et al. (2020)]. Profound comprehension of leprosy's epidemiological facets is imperative for the effective implementation of prevention and control measures. The subsequent elucidation provides an overview of the epidemiology of leprosy:

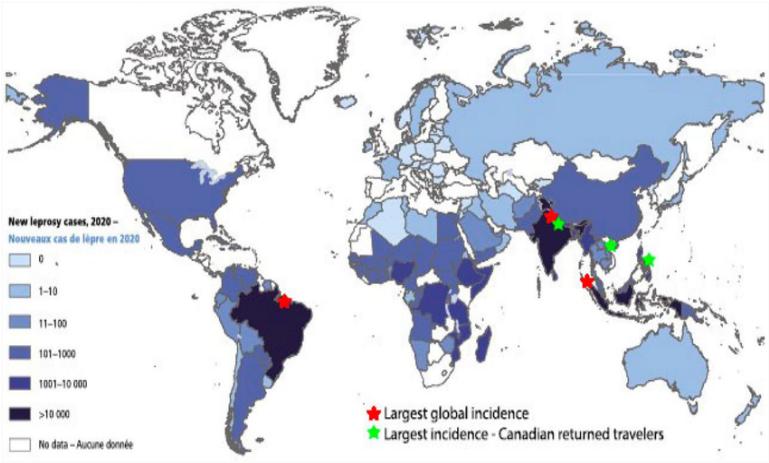

Figure 1.1: Global leprosy update (2019) describing the geographical distribution

- Global Prevalence: Leprosy persists as a salient public health quandary in numerous regions worldwide, prominently within low- and middle-income nations. As of the last data update in September 2021, the World Health Organization (WHO) reported a yearly incidence exceeding 200,000 new leprosy cases globally.

- Geographic Distribution: Leprosy exhibits global dissemination, with its highest prevalence in tropical and subtropical zones, encompassing sections of Asia, Africa, and Latin America [mondiale de la Santé et al. (2016)]. Notably, nations such as India, Brazil, and Indonesia consistently manifest the highest incidence of new leprosy cases [Rao and Suneetha (2018)].

- Clinical Spectrum: Leprosy manifests a spectrum of clinical presentations, encompassing the Paucibacillary (characterized by few bacteria) and multibacillary (characterized by numerous bacteria) forms [Gaschignard et al. (2016); Pardillo et al. (2007)]. The specific type of leprosy an individual manifests influences both the risk of transmission and the duration of treatment. Timely diagnosis and commencement of treatment,

employing multidrug therapy (MDT), are pivotal to averting disability and curtailing further transmission.

- Endeavors Toward Eradication: The WHO initiated the Global Leprosy Strategy 2016–2020 with the overarching objective of diminishing the worldwide burden of leprosy. This strategy centers on early case identification, enhancing access to MDT, and mitigating the societal stigma and discrimination linked with leprosy. Several nations have demonstrated substantial progress in lowering leprosy prevalence, and certain regions have achieved the esteemed status of leprosy elimination, signifying a low rate of incidence [Dogra et al. (2013); Ooi and Srinivasan (2004)].

- Persistent Challenges: Noteworthy hurdles in leprosy control include late case detection, incomplete treatment regimens, and societal ostracism, which can dissuade afflicted individuals from seeking necessary medical care and support [Goulart and Goulart (2008); Rodrigues and Lockwood (2011)]. Furthermore, the fortification of monitoring and surveillance systems is requisite to furnish precise data on leprosy caseloads.

1.3 Transmission Dynamics

The mode of transmission of *M. leprae*, the etiological agent of leprosy, is a very complex phenomenon and not completely understood by researchers till date. Prolonged close contact with untreated individuals with active leprosy is considered the primary route of transmission, although respiratory droplets and nasal secretions also play a pivotal role [Job et al. (2008)]. The disease exhibits a long incubation period, ranging from several months to years, posing challenges in identifying the source and timing of infection.

1.4 Basic Features and Clinical Symptoms

Leprosy primarily affects the skin, peripheral nerves, mucosal surfaces of the upper respiratory tract, and the eyes. The disease has a wide range of clinical manifestations, making it essential to understand its basic features and clinical symptoms. Clinical symptoms of leprosy vary depending on the immune response of the affected individual. The disease can be classified into different types based on the Ridley-Jopling classification [Ridley et al. (1962)] or the World Health Organization (WHO) classification. The two main types of leprosy i.e. paucibacillary (PB) and multibacillary (MB) leprosy are described briefly below.

Paucibacillary leprosy is characterized by a lower bacterial load and a limited number of skin lesions. Skin lesions in PB leprosy are typically hypopigmented or erythematous macules (flat patches) or papules (raised bumps). These lesions may be accompanied by numbness or loss of sensation in the affected area due to nerve involvement. Nerve damage is a crucial aspect of leprosy, and it can lead to sensory loss, muscle weakness, and deformities [Sabin et al. (1969)].

Multibacillary leprosy, on the other hand, is characterized by a higher bacterial load and a larger number of skin lesions. The skin lesions in MB leprosy are often nodules, plaques, or infiltrated areas. Just like in PB leprosy, nerve involvement is common and can result in sensory loss, muscle weakness, and deformities.

Leprosy can affect various systems of the body, leading to complications if left untreated. Common complications include eye involvement (such as lagophthalmos, iridocyclitis, or blindness), nasal septum perforation, and claw hand or foot deformities [Leprosy (2012)]. It's important to note that early diagnosis and treatment play a crucial role in preventing further transmission, irreducible nerve damage and reducing the long-term complications associated with the disease.

1.5 What is Schwann Cell? A Short Review

Schwann cells are a type of glial cell found in the peripheral nervous system (PNS). During the mid nineteenth century while investigating the nervous system, scientist Theodore Schwann, the co-founder of the cell theory, discovered Schwann cells. The primary function of these cells is to support and insulate neurons by producing myelin, a lipid-rich substance that forms a protective sheath around nerve fibers. Schwann cells play a crucial role in nerve development, maintenance, and regeneration [Jessen and Mirsky (2016); Salzer (2015)]. In leprosy, these cells are the principal target of *Mycobacterium leprae*, the causative agent of the disease [Tapinos and Rambukkana (2005)]. The bacteria invade Schwann cells, leading to a cascade of events that result in nerve damage and the characteristic neuropathic symptoms observed in leprosy patients.

M. leprae infects Schwann cells through a process involving adhesion, entry, and intracellular survival. The bacteria first attach to Schwann cell surfaces through interactions with specific receptors. Once attached, they gain entry into the Schwann cells by either receptor-mediated endocytosis or phagocytosis. Once inside, *M. leprae* manipulates the host cellular machinery to ensure its survival [Masaki et al. (2013)]. The bacteria inhibit phagosome maturation, preventing their destruction by lysosomes, and interfere with immune recogni-

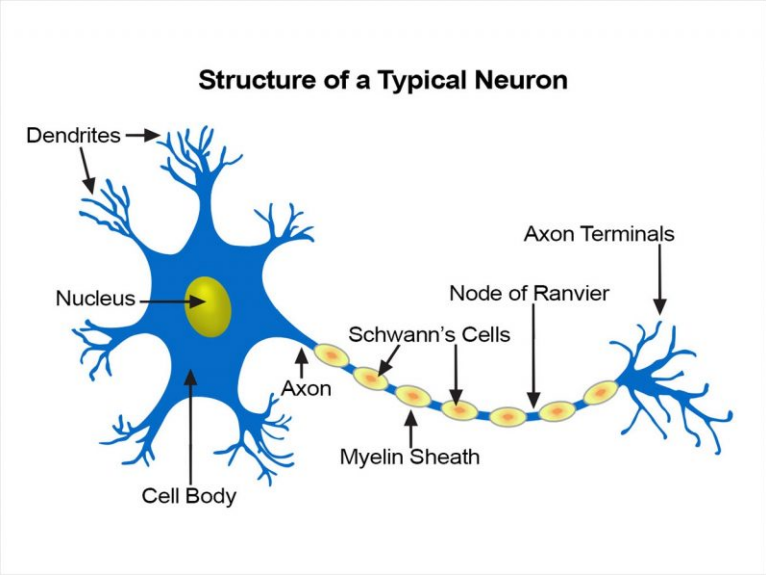

Figure 1.2: Depiction of Schwann cells within a Neuron of Peripheral Nervous System (PNS)

tion mechanisms. They also exploit host lipids and nutrients to support their replication and persistence within Schwann cells. These interactions disrupt normal Schwann cell functions, including myelination, leading to the demyelination and nerve damage characteristic of leprosy. Understanding the biology of Schwann cells in leprosy is essential for developing targeted therapeutic strategies to mitigate the progression of the disease and minimize its neurological complications.

1.6 Infection Mechanism of Schwann cells by *M. leprae* Bacteria

Mycobacterium leprae, the causative agent of leprosy, predominantly infects Schwann cells, leading to the characteristic neuropathic manifestations of the disease. Understanding the infection mechanism of *M. leprae* in Schwann cells is crucial for developing effective therapeutic interventions. The whole infection process involves a series of intricate interactions between the bacteria and Schwann cells, ultimately leading to nerve damage and clinical symptoms.

Crucial steps of the infection mechanism:

- Adhesion and Entry: *M. leprae* first attaches to the surface of Schwann cells, facilitated by various adhesion molecules and receptors. Upon adhesion, the bacteria trigger receptor-mediated endocytosis or phagocytosis, enabling their entry into Schwann cells [Masaki et al. (2013)].

- Intracellular Survival: After entering Schwann cells, the bacteria modifies its intracellular environment to ensure survival. The bacteria employ multiple mechanisms to avoid host immune responses, including inhibition of phagosome maturation and interference with signaling pathways involved in immune recognition.

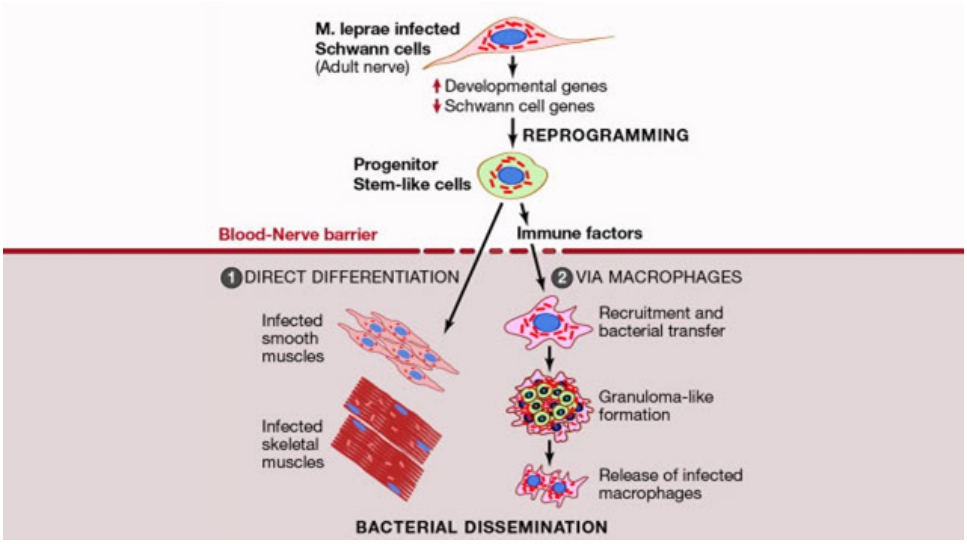

Figure 1.3: Demonstration of the infection procedure by M. leprae bacteria and further, the proliferation and dissemination of the bacteria into the human body

- Replication and Spread: Within the Schwann cell, *M. leprae* undergoes replication, leading to the formation of multiple bacteria-containing vacuoles known as globi. The bacteria strategically avoid host lysosomal degradation mechanisms and utilize host lipids for their growth and persistence [Adams et al. (2012)].

- Interaction with Schwann Cell Signaling: During infection, *M. leprae* manipulates various signaling pathways within Schwann cells, including those involved in myelination, inflammation, and cell survival [Spierings et al. (2000)]. These alterations contribute to the demyelination and nerve damage observed in leprosy.

- Dissemination: *M. leprae* can be transmitted from infected individuals through respiratory droplets. The bacteria exploit nerve pathways and utilize peripheral blood mononuclear cells as a means of transport.

1.7 Risk Factors

Several risk factors influence leprosy transmission and susceptibility. These include genetic predisposition, immunological status, socioeconomic factors, and environmental conditions. Household contacts of leprosy patients are at increased risk of developing the disease, emphasizing the importance of contact tracing and early case detection.

1.8 Prevention of the Disease

Leprosy control programs aim to interrupt transmission, prevent disabilities, and provide timely treatment. Active case finding, starting the treatment at an early stage are vital components of disease control strategies. Multidrug therapy (MDT), consisting of a combination of antibiotics, has proven effective in curing leprosy and reducing transmission [Becx-Bleumink and Berhe (1992)]. However, challenges such as finding the perfect drug dose regimen which also supports cost-effectiveness strategies, drug resistance, adverse therapeutic effects, and the persistence of leprosy in certain endemic pockets require ongoing surveillance and research for tailored interventions.

Understanding the epidemiology of leprosy is crucial for effective disease control. Continued research, surveillance, and targeted interventions are needed to achieve global leprosy elimination goals.

1.9 Drug Therapies Invented so far

MDT stands for Multidrug Therapy, which is the standard treatment regimen for leprosy recommended by the World Health Organization (WHO). MDT is a combination of antibiotics that effectively target and kill the *Mycobacterium leprae* bacteria [Smith et al. (2017)]. The components of MDT include three main drugs:

- **Rifampicin:** Rifampicin is a bactericidal antibiotic that targets actively dividing bacteria, including *M. leprae* [Moet et al. (2008)]. It inhibits the synthesis of bacterial RNA, thereby preventing protein production and ultimately killing the bacteria.

- **Dapsone:** Dapsone is a bacteriostatic antibiotic that inhibits the synthesis of dihydrofolic acid, a crucial component required for bacterial DNA synthesis. By interfering with this process, Dapsone slows down the growth of *M. leprae*, allowing the immune system to effectively control and eliminate the bacteria [Zuidema et al. (1986)].

- **Clofazimine:** Clofazimine is a bactericidal antibiotic that exerts its antimicrobial activity by binding to bacterial DNA, leading to the inhibition of DNA replication and transcription. It also possesses anti-inflammatory properties that help reduce the immune response and limit tissue damage caused by leprosy [Fischer (2017)].

  The combination of these three drugs in MDT helps to eliminate *M. leprae* bacteria, and reduce the risk of relapse. The specific duration and dosage of MDT depend on the classification and severity of the disease. MDT not only acts on active leprosy infections but also prevents transmission by rapidly reducing the bacterial load, thereby reducing the chances of spreading the disease to others. It is highly effective in preventing disabilities if administered early and completed as prescribed. Some of the other novel drug therapies invented for the treatment of leprosy as listed as:

- **Minocycline:** Minocycline is a broad-spectrum antibiotic belonging to the tetracycline class. It has shown efficacy in the treatment of leprosy and is often used as an alternative to Dapsone in cases of Dapsone resistance or intolerance. Minocycline works by inhibiting bacterial protein synthesis, thereby preventing the growth and spread of *M. leprae*. It is commonly used in combination with Rifampicin and Clofazimine in multidrug therapy (MDT) regimens for leprosy treatment [Gelber et al. (1992)].

- **Ofloxacin:** Ofloxacin is a fluoroquinolone antibiotic with potent antimycobacterial activity. It is primarily used in the treatment of multibacillary leprosy and is included as an additional drug in the WHO-recommended MDT regimen for this form of the disease [Grosset et al. (1990)]. Ofloxacin inhibits bacterial DNA gyrase, an enzyme essential for DNA replication, thereby preventing the growth of *M. leprae*. It has shown good efficacy, especially in cases of Rifampicin resistance, and has the advantage of being available in oral form [Setia et al. (2011)].

- **Clarithromycin:** Clarithromycin is a macrolide antibiotic that exhibits antimicrobial activity against a wide range of bacteria, including *M. leprae*. It inhibits bacterial protein synthesis. Clarithromycin is used as an alternative drug in the treatment of leprosy and often used in combination with other antibiotics, such as Ofloxacin or Minocycline, to enhance its effectiveness.

These additional drugs, namely Minocycline, Ofloxacin, and Clarithromycin, provide valuable alternatives in cases of drug resistance or intolerance to the standard MDT regimen [Williams and Gillis (2012)]. They have demonstrated efficacy in treating leprosy and are commonly used as part of multidrug combinations to achieve optimal treatment outcomes. However, it is important to note that the choice and use of these drugs should be guided by the specific characteristics of the patient's health situation and should be done under the supervision of efficient healthcare professionals.

1.10 Mathematical Methods and Their Applications

In this Section, we have discussed about some mathematical techniques that are generally required to investigate the dynamical behavior of a system. The following qualitative methods of dynamical systems have been applied to analyze various models proposed in this thesis.

1.10.1 Equilibrium analysis:

Let us assume the following system of first order autonomous difference equation:

$$X_{t+1} = f(X_t) \quad \text{or} \quad X \to f(X), \tag{1.10.1}$$

where

$$\begin{aligned} & X = (X^1, X^2, ..., X^k) \in \mathbb{R}^k, \\ & f = (f^1, f^2, ..., f^k) \in \mathbb{R}^k, \\ \text{and} \quad & f : \mathbb{R}^k \to \mathbb{R}^k. \end{aligned}$$

Here X_t denotes the state of the system (1.10.1) at discrete time $t \in \mathbb{T}$ and the corresponding initial conditions are:

$$X_{t=0} = X_0, X_0 = ({X^1}_0, {X^2}_0, ..., {X^k}_0).$$

Definition 1.10.1 *A point X^* of the system (1.10.1) is said to be an **Equilibrium point** or **Fixed point** or **Critical point** if it satisfies $f(X^*) = X^*$.*

It is also very crucial to determine the behavior of a non-linear system in the neighbourhood of equilibrium points. In order to analyze the behaviour of the systems' trajectories, we have described the stability criteria of the possible equilibrium points.

Local stability analysis:

It is one of the most fundamental topics in applied mathematics, especially in the field mathematical biology. Several existing literatures have addressed this topic lately [Lakshmikantham et al. (1989); Lakshmanan and Rajaseekar (2012); Hale (1977); Guckenheimer et al. (1977)].

Definition 1.10.2 *The equilibrium point Y^* of the system (1.10.1) is said to be **Locally stable**, if for each $\epsilon > 0$ there exists $\delta > 0$ such that*

$$||f^n(X_0) - X^*|| < \epsilon \text{ whenever } ||X_0 - X^*|| < \delta. \tag{1.10.2}$$

Note that, if X^* is locally stable then any solution trajectory starts from any nearest point to X^* will remain closed to it.

Definition 1.10.3 *If the fixed point X^* of the system (1.10.1) is not stable then it is **Unstable fixed point**.*

If the solution trajectories start from any initial point which nearest to X^* not only remain close to it but also converge to that fixed point, is called locally asymptotically stable fixed point.

Definition 1.10.4 *The critical point X^* of the system (1.10.1) is said to be **Local asymptotic stable**, if X^* is locally stable and there exists a $\delta > 0$ such that*

$$f^n(X) = X^* \text{ as } n \to \infty \text{ when } ||X_0 - X^*|| < \delta. \tag{1.10.3}$$

Let us assume X be any solution in the neighborhood of X^* and $\lambda = \lambda_1, \lambda_2, ..., \lambda_n$ is a small perturbation from that fixed point (X^*), then we have

$$\begin{cases} X = X^* + \lambda, \\ \lambda_{n+1} = \mathcal{N}\lambda_n, \end{cases} \tag{1.10.4}$$

where, $\mathcal{N} = (p_{ij})|_{Y^*}$, $(i, j = 1, 2, 3, ..., n)$ is the *Variational* or *Jacobian Matrix* at the fixed point X^*. The linear system (1.10.4) corresponding to the Jacobian matrix is called linearization of the non-linear system (1.10.1) at X^*. If λ_0 be the initial perturbation from the fixed point X^* then

$$\lambda_n = \mathcal{N}^n\lambda_0. \tag{1.10.5}$$

The stable or unstable nature of the fixed point X^* of system (1.10.1) can be determined by the eigenvalues of the linearized system (1.10.4). Let, ζ be the eigenvalue corresponding to

the eigenvector υ of the matrix $\mathcal{N}$. Then the characteristic equation is given by

$$\det(\mathcal{N} - \zeta I) = p_0\zeta^n + p_1\zeta^{n-1} + p_2\zeta^{n-2} + ... + p_n, \quad p_0 \neq 0. \tag{1.10.6}$$

The necessary and sufficient condition for being the fixed point locally stable is that the eigenvalues of the linearized matrix lie in the unit circle [Robinson (1998)].

Definition 1.10.5 *A fixed point X^* of the system (1.10.1) is called **Saddle point** if the maximum modulus of at least one eigenvalue of $\mathcal{N}$ is less than unity with the other eigenvalues are greater than unity.*

Definition 1.10.6 *A fixed point X^* is said to be a **Hyperbolic fixed point** of the system (1.10.1) if none of the eigenvalues of $\mathcal{N}$ have unit modulus.*

Definition 1.10.7 *An equilibrium point X^* is called **Non-Hyperbolic fixed point** of a system if*

- *at least one eigenvalue of $\mathcal{N}$ is 1 and other eigenvalues having moduli not equal to 1.*
- *at least one eigenvalue of $\mathcal{N}$ is -1 and other eigenvalues having moduli not equal to 1.*
- *at least $\mathcal{N}$ has two complex conjugate eigenvalues with modulus 1 and other eigenvalues having moduli not equal to 1.*

1.10.2 Bifurcation analysis

Whenever studying a dynamical system, bifurcation analysis is a very well-known tool to investigate the changes in the qualitative or topological structure of the solutions of a family of differential equations. A bifurcation occurs in both continuous and discrete systems when a small smooth change made to the parameter values (the bifurcation parameters) of the system. There are mainly four types of bifurcations viz. Saddle-node bifurcation, Transcritical bifurcation, Pitchfork bifurcation and Hopf bifurcation.

Let us consider the following continuous dynamical system described by the ODE:

$$\dot{x} = f(x, \lambda), \quad f : \mathbb{R}^n \times \mathbb{R} \to \mathbb{R}^n, \tag{1.10.7}$$

with an equilibrium (x_0, λ_0) and corresponding Jacobian matrix $df_{(x_0,\lambda_0)}$.

Definition 1.10.8 *A **Bifurcation** occurs at the fixed point (x_0, λ_0) for the system (1.10.7) if the Jacobian matrix $df_{(x_0,\lambda_0)}$ has at least one eigenvalue with real part equals to zero.*

Definition 1.10.9 *Let the system (1.10.7) has two fixed points namely* (x_0, λ_0) *and* (x_1, λ_1) *and the two fixed points (or equilibria) collide and annihilate each other then a* ***Saddle-node bifurcation*** *occurs.*

Definition 1.10.10 ***Transcritical bifurcation*** *is characterized by an equilibrium of the system (1.10.7) having an eigenvalue whose real part passes through zero.*

Definition 1.10.11 ***Pitchfork bifurcation*** *is a particular type of bifurcation where the system (1.10.7) transitions from one fixed point to three fixed points.*

Definition 1.10.12 ***Hopf bifurcation*** *occurs if near a critical point system (1.10.7) losses its stability and a periodic solution arises.*

In this thesis, we have focused on Hopf-bifurcation, associated with the appearance or the disappearance of a periodic orbit through a local change in the stability properties of a fixed point. By the following theorem, Hale et al. [Hale and Koçak (2012)] have described the conditions under which Hopf-bifurcation phenomenon occurs

Theorem 1.10.1 *Suppose that all eigenvalues of* $df_{(x_0,\lambda_0)}$ *corresponding to the steady state* (x_0, λ_0) *have negative real parts except one conjugate nonzero purely imaginary pair* $\pm i\beta$*. A Hopf-bifurcation arises when these two eigenvalues cross the imaginary axis because of a variation of the system parameters.*

1.10.3 Delay differential equation

A delayed differential equation (DDE) is a type of differential equation where the rate of change of a variable does not solely depend on its current value but also on its past values, with a time delay. In other words, the state variable appears with delayed argument i.e. the derivative of the variable at a given time depends on its values at previous times.

A delayed differential equation can be generally written in the form:

$$\frac{dx(t)}{dt} = f(x(t), x(t-\tau_1), x(t-\tau_2), ..., x(t-\tau_n)) \tag{1.10.8}$$

where $x(t)$ is the variable of interest at time t and f is a function that describes how the variable changes based on its current and past values at specific delays $(\tau_1, \tau_2, \tau_3, ..., \tau_n)$. Here, τ_1, $\tau_2, \tau_3, ..., \tau_n$ are considered as constant delays.

DDEs can model various real-world phenomena where the past history of a system affects its future behavior. They have applications in biology, physics, engineering, economics, and

other fields. Analyzing and solving DDEs can be more challenging compared to ordinary differential equations due to the presence of delay terms, which can lead to complex dynamics and sometimes require specialized techniques for analysis and numerical solutions. Overall, we can say that a system based on delayed differential equations offers a way to capture systems where time delays play a significant role in determining the system's behavior and evolution over time.

Example: Let us consider a simple example of a population growth model that incorporates a time delay. Suppose we have a population of rabbits, and we want to model their growth over time, taking into account a delay in the reproductive process.

Let,

- $X(t)$ be the population of rabbits at time t,
- ν be the intrinsic growth rate of the rabbit population,
- K be the carrying capacity of the environment (maximum sustainable population size),
- τ be a time delay representing the time it takes for a rabbit to mature and start reproducing.

According to these assumptions, the delayed differential equation-based system can be written as:

$$\frac{dX(t)}{dt} = \nu X(t).\left(1 - \frac{X(t-\tau)}{K}\right)$$

This equation describes the rate of change of the rabbit population at time t. The growth rate ν is scaled by the current population size $X(t)$ and is dampened by the term $\frac{X(t-\tau)}{K}$, which represents the effect of the delayed reproduction.

In this model, the delay τ accounts for the time it takes for a newborn rabbit to reach maturity and contribute to population growth. The equation essentially says that the rate of change of the population depends on the current population size and the population size τ units of time ago. This simple delayed differential equation captures how the history of the rabbit population affects its future growth. The dynamics of this model can lead to interesting behaviors, including oscillations and stability, depending on the parameter values ν, K, and τ. Solving and analyzing this equation would involve considering the impact of the delay on the stability and behavior of the rabbit population over time.

• Linearization process for autonomous delay differential equation (DDE) with constant delay

Suppose, $g(x, y)$ is chosen so that it satisfies $g(0, 0) = 0$ and $x = 0$ is a steady state. Then,

$$\dot{x}(t) = g(x(t), x(t-\tau)) = g_x(0,0)x(t) + g_y(0,0)x(t-\tau) + \text{h.o.t.}$$

The corresponding linearization is given as

$$\dot{x}(t) = g_x(0,0)x(t) + g_y(0,0)x(t-\tau) = \sigma_1 x(t) + \sigma_2 x(t-\tau).$$

Now, putting $x(t) = e^{\lambda t}$, we get the following transcendental characteristic equation given as:

$$\lambda - \sigma_1 - \sigma_2 e^{-\lambda\tau} = 0.$$

Considering $\lambda = \alpha + i\beta$, we have the following:

$$\alpha - \sigma_1 - \sigma_2 e^{-\alpha\tau}\cos(\tau\beta) = \beta + \sigma_2 e^{-\alpha\tau}\sin(\tau\beta) = 0.$$

The equation given above has infinitely many roots and all of them lie on the curve $g(\alpha) = \pm\sqrt{\sigma_2^2 e^{-2\tau\alpha} - (\alpha - \sigma_1)^2}$ From the above discussion, we can observe the following points:

1. The fact that all the solutions are exponential can be viewed using Laplace transform.
2. On the right-hand side of any vertical line in the complex plane, there exists finitely many roots.
3. Each stable manifold is infinitesimal here.
4. The inequality $\alpha < |\sigma_1| + |\sigma_2|$ is necessarily satisfied by all the characteristic roots.

• Important results and theorems related to a general delayed dynamical system

A dynamical system based on delayed differential equation exhibits various phenomena and properties. Here, we note some of the important theorems, properties, and results that commonly occur during the analytical and numerical investigation of such a system in general.

1. **Existence and Uniqueness Theorems:** For the justification of biological validity and plausibility of a dynamical system, demonstration of the existence and uniqueness of the solutions of a delayed system is essential. Similar to ordinary differential equations, delayed differential equations also have existence and uniqueness theorems that ensure the existence of solutions and their uniqueness under certain conditions, specifically based on the initial conditions. These theorems provide a foundation for studying the behavior of solutions to delayed dynamical systems.

2. **Characteristic Equation:** The characteristic equation of a delay differential equation-based system is important for stability analysis. From this, we can obtain the eigenvalues of the system, which actually supply the necessary information about the stability and oscillatory behavior of the solutions of the system.

3. **Stability Criteria:** Lyapunov's direct method, as well as other stability criteria such as the delay-independent stability criterion and delay-dependent stability criterion, are used to analyze the stability of equilibrium points in delayed systems.

4. **Hopf Bifurcation:** Delayed systems can exhibit Hopf bifurcations, leading to the emergence of stable periodic solutions from equilibrium points as a parameter is varied. The delayed nature of the system can induce interesting and complex oscillatory behavior.

5. **State-Dependent Delays and Neutral Delay Differential Equations:** In some systems, the delay itself can depend on the state of the system while Neutral Delay is a special class of delayed systems where both the current state and its past values impact the dynamics. Both these types of delayed systems can lead to more intricate dynamics and analyzing the stability and behavior of these systems often involves more advanced mathematical tools.

6. **Delay Compensation and Control:** Understanding and designing controllers for systems with delays is an important practical application. Methods like Smith predictors and model predictive control are used to compensate for delays and stabilize systems.

7. **Chaos and Complex Behavior:** Delayed dynamical systems can exhibit chaotic behavior, leading to sensitive dependence on initial conditions and complex patterns of evolution.

8. **Numerical Methods:** Numerical techniques for solving delayed differential equations, such as Runge-Kutta methods and collocation methods, need to be adapted to handle the time delays. These methods are crucial for approximating solutions and studying the behavior of delayed dynamical systems.

These are just a few aspects of the rich and diverse field of delayed dynamical systems. The study of such systems requires a combination of mathematical analysis, numerical methods, and sometimes specialized tools to unravel the complex behavior and properties of the system.

1.10.4 Optimal control theory

Let us consider an ordinary differential equation (ODE) having the form

$$\begin{aligned} \frac{dX(t)}{dt} &= f(X(t)) \qquad (t > 0) \\ X(0) &= X_0. \end{aligned}$$

Here $X_0 \in \mathbb{R}^n$ is the given initial point and the function f is defined from $\mathbb{R}^n$ to $\mathbb{R}^n$. The unknown is the curve $X : [0, \infty) \to \mathbb{R}^n$, which we interpret as the dynamical evolution of the state of some "system".
Now by generalizing, we suppose that f depends also upon some "control" parameters belonging to a set $A \subset \mathbb{R}^m$; so that $f : \mathbb{R}^n \times A \to \mathbb{R}^n$. Then if we select some value $a \in A$ and consider the corresponding dynamics:

$$\begin{aligned} \frac{dX(t)}{dt} &= f(X(t), a) \qquad (t > 0) \\ X(0) &= X_0, \end{aligned} \tag{1.10.9}$$

we obtain the evolution of our system when the parameter is constantly set to the value a.
The next possibility is that we change the value of the parameter as the system evolves. For instance, suppose we define the function $\alpha : [0, \infty) \to A$ this way:

$$\alpha(t) = \begin{cases} a_1, & 0 \le t \le t_1 \\ a_2, & t_1 \le t \le t_2 \\ a_3, & t_2 \le t \le t_3 \text{ etc.} \end{cases} \tag{1.10.10}$$

for times $0 < t_1 < t_2 < t_3 ...$ and parameter values $a_1, a_2, a_3, ... \in A$; and we then solve the dynamical equation

$$\begin{aligned} \frac{dX(t)}{dt} &= f(X(t), a(t)) \qquad (t > 0) \\ X(0) &= X_0. \end{aligned} \tag{1.10.11}$$

It is important to note here that the system may behave quite differently as we change the control parameters. More generally, we call a function $\alpha : [0, \infty) \to A$ a *control*. Corresponding to each control, we consider the ODE system (1.10.11) and regard the trajectory $X(\cdot)$ as the corresponding *response* of the system. The set $\mathcal{A} = \{\alpha : [0, \infty) \to A \mid \alpha(\cdot) \text{ is measurable}\}$ denotes the collection of all *admissible controls*.

Note that our solution $X(\cdot)$ of (1.10.11) depends upon $\alpha(\cdot)$ and the initial condition. Consequently our notation would be more precise, but more complicated if we were to write

$$X(\cdot) = X(\cdot, \alpha(\cdot), X_0),$$

displaying the dependence of the response $X(\cdot)$ upon the control and the initial value.

Let us now define the *payoff functional*

$$J[\alpha(\cdot)] := \int_{t_0}^{t_f} [r(X(t), \alpha(t))]dt + g(X(T)), \tag{1.10.12}$$

where $X(\cdot)$ solves (1.10.11) for the control $\alpha(\cdot)$. Here $r : \mathbb{R}^n \times A \to \mathbb{R}$ and $g : \mathbb{R}^n \to \mathbb{R}$ are given, and we call r the *running payoff* and g the *terminal payoff*. The terminal time $t_f > 0$ is given as well.

Our aim is to find a control $\alpha^*(\cdot)$, which maximizes or minimizes the payoff function $J[\alpha(\cdot)]$. In other words, we want

$$J[\alpha^*(\cdot)] \geq \text{or} \leq J[\alpha(\cdot)]$$

for all controls $\alpha(\cdot) \in \mathcal{A}$. Such a control $\alpha^*(\cdot)$ is called *optimal*.

1.10.5 Preliminaries on fractional derivatives and integration

Recently, analysis of fractionalized mathematical models has gained a huge importance for any biological system equipped with memory phenomena. In this Subsection, some crucial fundamental definitions from the theory of fractional calculus are presented.

Definition 1.10.13 *The Caputo fractional derivative operator of order ζ ($\zeta \geq 0$) & $n \in \mathbb{N} \cup \{0\}$ is defined by Vellappandi et al. (2022) as:*

$$D_t^{\zeta}(u(t)) = \frac{1}{\Gamma(n-\zeta)} \int_0^t (t-\xi)^{n-\zeta-1} \frac{d^n}{dt^n} u(\xi) d\xi \tag{1.10.13}$$

where $n - 1 \leq \zeta < n$.

Definition 1.10.14 *Let $v \in H'(a, b)$, $b > a$, $0 < \zeta < 1$. Then, the time-fractional Caputo–*

Fabrizio fractional differential operator is defined as [Caputo and Fabrizio (2015)]:

$$^{CF}D_t^{\zeta}(v(t)) = \frac{M(\zeta)}{1-\zeta}\int_0^t \exp\left[-\frac{\zeta(t-\xi)}{1-\zeta}\right] v'(\xi)d\xi, \quad t \geq 0, \quad 0 < \zeta < 1 \tag{1.10.14}$$

where $M(\zeta)$ is a normalization function which depends on ζ and satisfies the condition $M(0) = M(1) = 1$.

Definition 1.10.15 *The Caputo–Fabrizio (CF) fractional integral operator of order $0 < \zeta < 1$ is given by Losada and Nieto (2015) as:*

$$^{CF}\mathcal{I}_t^{\zeta}(v(t)) = \frac{2(1-\zeta)}{(2-\zeta)M(\zeta)}v(t) + \frac{2\zeta}{(2-\zeta)M(\zeta)}\int_0^t v(\xi)d\xi, \quad t \geq 0. \tag{1.10.15}$$

Here, it is important to note that

$$^{CF}D_t^{\zeta}(v(t)) = 0 \quad \textit{if} \quad v\textit{s. is a constant function.}$$

Furthermore, it is imperative to observe that the previous definitions completely suggest that the fractional integral of a function of order $0 < \zeta < 1$ is actually represented by the average of the respective functions and their integral of order one. Furthermore, the equation

$$\frac{2(1-\zeta)}{(2-\zeta)M(\zeta)} + \frac{2\zeta}{(2-\zeta)M(\zeta)} = 1 \tag{1.10.16}$$

holds true, which provides the following formula:

$$M(\zeta) = \frac{2}{(2-\zeta)}, \quad 0 \leq \zeta < 1. \tag{1.10.17}$$

Here, the specific form of the normalizing function $M(\zeta)$ given in (1.10.17) along with the boundary conditions is used throughout the study and more specifically, for the purpose of numerical simulations.

Definition 1.10.16 *The Laplace transform for the CF fractional operator of order $0 < \zeta \leq 1$ for $k \in \mathbb{N}$ is given as follows [Caputo and Fabrizio (2015)]:*

$$\begin{aligned}\mathcal{L}\left(^{CF}D_t^{k+\zeta}(v(t))\right)(p) &= \frac{1}{1-\zeta}\mathcal{L}\left(v^{k+1}(t)\mathcal{L}\left(\exp\left(-\frac{\zeta}{1-\zeta}t\right)\right)\right) \\ &= \frac{p^{k+1}\mathcal{L}(v(t)) - p^k v(0) - p^{k-1}v'(0)\ldots - v^k(0)}{p+\zeta(1-p)}.\end{aligned}$$

To be precise, we can say that

$$\begin{aligned}\mathcal{L}\left({}^{CF}D_t^{\zeta}(v(t))\right)(p) &= \frac{p\mathcal{L}(v(t))}{p+\zeta(1-p)}, \quad k=0\\ \mathcal{L}\left({}^{CF}D_t^{\zeta+1}(v(t))\right)(p) &= \frac{p^2\mathcal{L}(v(t))-pv(0)-v'(0)}{p+\zeta(1-p)}, \quad k=1.\end{aligned}$$

1.11 Mathematical Contribution and Motivation of the Study

Mathematical model and its control therapeutic approaches provide an efficient way to understand and unravel different dynamics of the disease leprosy and help us to obtain futuristic predictions. The outcomes based on the mathematical investigations are of utmost importance to the clinical scientists and pharmacists as well as the policymakers who are trying to achieve a perfect drug dose regimen and complete eradication of leprosy from mankind.

Firstly, we note some of the previous clinical studies that actually made the pathway for performing mathematical investigations on leprosy. Several clinical and experimental studies have been performed on the leprosy disease lately. Sharma et al. (2013) reported that among infected armadillos, concentrations of 10^9 to 10^{11} *M. leprae*/gram of liver, spleen or lymph node has been observed. Through an electron microscopic study, Job et al. (1975) reported that *M. leprae* is engulfed by Schwann cells and the bacteria survive and replicate inside the cells by constructing protective responses against the disastrous activities taken by Schwann cells by losing its phagosomal membrane. The clinical works thus clearly constitute the basic background of mathematical model formulations on leprosy which deals with ordinary differential equations (ODEs) and incorporates control therapeutic approaches as standard treatment methods.

The control theoretic concepts have been considered important in a wide variety of disciplines. Too large dosage may not be beneficial for the patient and also too small dosage may not be effective as well. This is the main reason why we require optimal treatment strategies which can reduce the possibility of bacterial transmission and proliferation, pharmaceutical side effects and complex, expansive medication burden. The basic equation of the optimal control theory may be derived by different approach which comprises the well-known theorem called Pontryagin's Minimum Principle [Pontryagin (1987)]. Pontryagin et al. also developed the maximum principle for the optimal control of finite dimensional problems governed by ODEs. The application and necessity of the theorems provided by Pontryagin et al. is very much important for the drug treatment in different treatment setup. We have used the theory

and by the help of these theorems, we have derived optimal drug dosages for different optimal control-induced systems for which better treatment can be achieved.

For leprosy patients, two of the most commonly used drugs in combined control therapeutic treatment procedures are Ofloxacin and Dapsone. Ofloxacin displayed powerful bactericidal activity against *M. leprae* and can be chosen as an important component of new multidrug therapy for the treatment of leprosy. Ji et al. (1994) experimented over 24 patients with newly diagnosed leprosy and treated them for 56 days with 400 mg of ofloxacin daily and demonstrated significant clinical developments along with major decline of the MI index (morphological index) in the skin smears during the treatment period. Dapsone (diaminodiphenylsulphone) is also a key part of multidrug therapy (MDT). Following this direction, some mathematicians have contributed in exploring the leprosy dynamics by formulating mathematical models on leprosy regulation through Ordinary Differential Equations. Blok et al. (2015) developed a stochastic individual-based model, SIMCOLEP, which was able to take into account transmission of leprosy in households and test for different assumptions on heterogeneity in susceptibility to leprosy. Recently in 2018, Giraldo et al. (2018) constructed a mathematical simulation model describing the transmission dynamics of the multibacillary leprosy (MB) and paucibacillary leprosy (PB) including a delay. However, all these works are based on human population dynamics, but the detailed fundamental cell dynamical characteristics of leprosy has not been examined yet.

During the last few decades, mathematical modeling on living organisms in the discrete-time setup is gaining much interest and is considered a very crucial and significant tool by many researchers [Franke and Yakubu (2008); Sekiguchi and Ishiwata (2010)]. There are some specific advantages of discrete-time models compared with continuous-time models. Discrete-time models manifest a much richer set of system dynamics. It offers a more convenient and precise approach to formulate a mathematical model than continuous-time models [Hu et al. (2012); Chen et al. (2009)]. Through the discretization, numerical simulations for continuous models can be obtained. These suggest that it is more appropriate to elucidate Schwann cell infection by *M. leprae* and the disease transmission through a discretized system while categorically focusing on the per capita growth rate of the bacterium.

Analysis of mathematical models based on delayed differential equations instead of simple ODE-based systems has acquired major importance in current times and several mathematical studies on various infectious and non-infectious diseases like HIV-1, dengue, malaria, tumor and cutaneous leishmaniasis have been performed recently that primarily focuses on the delayed dynamics of the systems [Banerjee and Sarkar (2008); Ruan et al. (2008); Roy, Chatterjee, Greenhalgh and Khan (2013)]. Most interestingly, previous outcomes from existing literature on various diseases and moreover, on several biological problems, it is observed

that optimal control theory whenever applied on delayed differential equation-based systems produces much accurate result. There has been significant progress in the development of optimal control-induced delayed mathematical models and various research works have been performed in this direction in recent times [Al Basir (2020); Ali and Zaman (2021); Hattaf and Yousfi (2012)]. It is important to note that implementing optimal control theory on delayed systems instead of simple ODE-based systems has some certain benefits in general. The state-of-the-art of this type of system involves the use of advanced numerical methods which allows for more efficient numerical simulations of the system dynamics. Besides, for a fixed duration, in comparison to optimal therapy, a constant control therapy requires a high dose of drug therapy for the whole treatment tenure which usually results in a high cost of combined drug therapy and simultaneously, induces the risks related to drug overdose situations.

Before 1982, the only available treatment for leprosy was Dapsone monotherapy but drug resistance to Dapsone was observed in a large number of patients suffering from leprosy. So, multidrug therapy (MDT) was implemented according to the recommendation of World Health Organization in 1982 [Walker and Lockwood (2006)]. The components of MDT are Dapsone, Rifampicin and Clofazimine. Among these, Rifampicin has a bactericidal effect on *M. leprae* while Clofazimine mainly acts as an anti-inflammatory drug [Fischer (2017)]. Still, there are evidences in recent times in which cases MDT with the standard components was not completely successful. Results from clinical trials conducted in 2012 indicates that bacteriological index (BI) are observed to be decreased significantly over time in patients taking U-MDT compared to the regular MDT therapy but the relapse rates for U-MDT regimen are still a matter of concern for the clinical scientists [Kroger et al. (2008); Penna, Buhrer-Sekula, Pontes, Cruz, Gonçalves and Penna (2014)]. In a recent study, it is suggested that the rate at which infected nerve regenerates is nearly about 60% to 70% and the recovery rate is relatively slow for patients with chronic and recurrent nerve impairment [Britton and Lockwood (2004)]. These observations together indicate the essence of investigating a safe and unsafe zone of MDT depending on the drug-efficacy rate of the therapy. There are some previous works on various infectious diseases such as HIV which dealt with the infection of healthy cells, stable production of virus [Ikeda et al. (2003)] and the key relationships in between the disease prevalence or infection rate, drug-efficacy and dosing regimen of the prescribed combined or single-drug therapy into a human body [Smith and Wahl (2005); Saha et al. (2018); Cao et al. (2019)]. As far as finding a perfect drug dose regimen for both paucibacillary (PB) and multibacillary (MB) leprosy is our foremost goal, in depth investigation of the drug efficacy of the existing MDT therapy and its correlations with various pathogenetic components of leprosy must be given major importance to eradicate the

disease permanently from mankind.

In 2016, Westerlund pointed out that every matter has a memory [Westerlund (1991)]. The dynamic behavior of living microorganisms such as *M. leprae* bacteria not only depends on the conditions of their current state but also on those of their previous states to better predict and interpret the pattern of the states at some point in the future [Wolf et al. (2008); Yang et al. (2020)]. It is to be noted that integer-order (IO) derivatives only take into account the local properties (at time t). In the real-world explanation, the IO differentiation explores the dynamics between two different points. In such a situation, a natural question may arise about the non-local behavior of the two points. To solve such limitations of local differentiation, researchers like Riemann and Liouville first introduced the concept of differentiation with non-local or fractional-order operators [Samko et al. (1993)]. A fractional (fractional-order) derivative is a generalization of the integer-order (IO) derivative and integral. In order to investigate the pathogenesis of leprosy from a completely novel analytical and numerical point of view, considering only systems involving ordinary differential equations (ODE) with integer-order (IO) derivatives is not sufficient, and introducing fractionalized mathematical systems to introspect various aspects of memory effect on leprosy dynamics becomes mandatory in this scenario.

All of our investigations are mainly based on deterministic modeling. Deterministic modeling produces consistent outcomes for a given set of inputs, regardless of how many times the model is recalculated. The mathematical characteristics are known in this case. It deals with the definitive outcomes as opposed to random results and doesn't make allowances for error. A deterministic model is applied where outcomes are precisely determined through a known relationship between states and events where there is no randomness or uncertainty. In contrast, stochastic modelling is intrinsically unpredictable, and the unknown components are integrated into the model. When the relationship between variables is unknown or uncertain then stochastic modelling could be used because it relies on likelihood estimation of the probability of events. There are several stochastic mathematical models [Nåsell (1999); Matis et al. (2003)] that have been developed to describe the extinction process both at cellular and population level. Wang et al. (2013) investigated the behavior of a hospital infection before extinction and also, the time to extinction. In a HIV disease mathematical model, the authors focused about the distribution function and expected time to extinction of the infected cells [Cao et al. (2019)].

From the above discussion, it is clear that though a few mathematical models have been developed previously on the disease leprosy in human population level, but the in depth analysis of the cell dynamical structure has not been explored yet mathematically. Furthermore, predictions on various aspects of the density dependent growth of the bacteria, the important

effects of intracellular delays to unravel the complex infection mechanism in leprosy, investigation of the corresponding optimal control-induced systems for finding suitable drug dose regimen in a safe, cost-effective way and evaluation of the critical drug efficacy rate of the MDT are still untouched by the researchers. In addition, besides the ODE-based systems, the novel aspects of the fractionalized models considering the memory effects and the expected time to extinction of the infected Schwann cells in the leprosy neuropathy are yet to be studied by the mathematicians. Such unknown issues of the previous studies lead us to generate new ideas and determination in the development of theoretical research on leprosy. Research is an original contribution to the existing stock of knowledge making for its advancement and it is indeed the pursuit of truth with the help of study, observation, comparison and experiment. This thesis obeys this law and contributes the systematic approach concerning generalization and the formulation of a theory.

1.12 Outline of the Contribution

The thesis has been organized in the following manner:

- In *Chapter 2*, we have formulated a three dimensional nonlinear ODE-based mathematical model comprising of the concentrations of healthy Schwann cells, infected Schwann cells and *M. leprae* bacteria and explored the interlink between these system population on how they contribute to progress the infection into the human body. Moreover, the optimal control-induced system consisting of a combined drug therapy of Ofloxacin and Dapsone has been investigated in detail to predict a suitable optimal control strategy for the eradication of leprosy.

- Next, in *Chapter 3*, the previously formulated ODE-based continuous system has been discretized. Here, in this chapter theta logistic growth rate of *M. leprae* bacteria has been incorporated into the system instead of the classical logistic growth rate. Besides performing the stability analysis in discrete setup, we have also determined θ^* i.e. the critical value of the radius of curvature of the density dependant bacterial growth curve through Hopf-bifurcation analysis. Also, different behaviours of the system cell populations arising for both $\theta < 1$ and $\theta > 1$ have been manifested in detail.

- In *Chapter 4*, the necessary aspects of intracellular delay has been considered to formulate and examine two different variants of delay induced systems. We have also discussed the impact of optimal control strategy into the systems while simultaneously considering the time-lag appeared into the bacterial attachment and bacterial prolifer-

ation process for finding a cost effective and safe combined therapeutic regimen more accurately and realistically.

- *Chapter 5* deals with a four dimensional ODE-based mathematical model consisting of the concentrations of healthy Schwann cells, infected Schwann cells, *M. leprae* bacteria and the amount of MDT drug concentrations administered into the human body during the treatment. Through Hopf-bifurcation analysis for inquiring oscillatory periodic solutions, Poincare section analysis and and Lyapunov's exponent method, we have systematically determined and distinguished a safe and an adversely impactful zone of the drug efficacy rate of MDT. Moreover, critical efficacy rate of MDT has been found for different classifications (according to the World Health Organization (W.H.O) and also, the Ridley-Jopling classification) for both the Paucibacillary (PB) and Multibacillary (MB) leprosy cases.

- In *Chapter 6*, a fractionalized mathematical model has been introduced by incorporating the well-known Caputo-Fabrizio (CF) fractional derivative for fractional order $\zeta \in (0, 1)$ instead of classical integer-order (IO) derivative. A generalized fractional optimal control problem (FOCP) has been formulated in CF sense. Utilizing the results derived from this general case, we have studied the control-induced CF fractional system. As a consequence, we have evaluated a standard tenure of treatment and optimal control profiles for a double-drug therapeutic schedule to overcome the drug-resistance scenario emerging due to the memorial effect of the bacteria.

- In *Chapter 7*, we have derived a stochastic mathematical model from the previously studied four dimensional deterministic system. Constructing Kolmogorov's forward equation by applying Joint probability distribution of infected Schwann cells and *M. leprae* bacteria along with quasi-stationary distribution, normal approximation, comparison between approximate and exact solutions of the system are demonstrated. Finally, utilising Ornstein-Uhlenbeck Process, expected time to extinction of the infected Schwann cells are estimated for our formulated model and all of our analytical observations are verified through numerical investigations in detail.

- Finally, *Chapter 8*, we have reviewed all the research conclusions of the thesis and presented some important future aims and scope for research in these directions.

Chapter 2

Basic Framework of Mathematical Modelling on Leprosy by Introducing Optimal Control Therapeutic Approach

Leprosy (Hansen's disease) is an infectious, neglected tropical disease caused by the bacterium scientifically called *Mycobacterium leprae* (*M. leprae*) and the disease is characterized by damage and impairment of nerve-function through infection of untreated wounds, which reveals of debilitating ulcers on palms and soles, chronic disability of several organs. Leprosy affects the skin or more precisely epidermal layer but *M. leprae* specifically targets the Schwann cells of myelinated axons. In this Chapter[2], we have proposed a three dimensional mathematical model involving the concentrations of healthy Schwann cells, infected Schwann cells and bacteria (*M. leprae*) to predict the dynamical changes of the cells during this disease progression. We have also studied the control-induced mathematical model by introducing two bounded control parameters into our model. For detailed analysis of this controlled system, by considering a minimization problem for the concentration of infected Schwann cells and bacteria, we have applied the Pontryagin maximum principle. As a result of this analysis, the properties of the optimal controls and their possible types have been established. All analytical outcomes have been verified by numerical simulations.

[2] *The major portion of this chapter is published in Computational Mathematics and Modeling, Springer, Vol. 32, No. 1, January, 2021.*

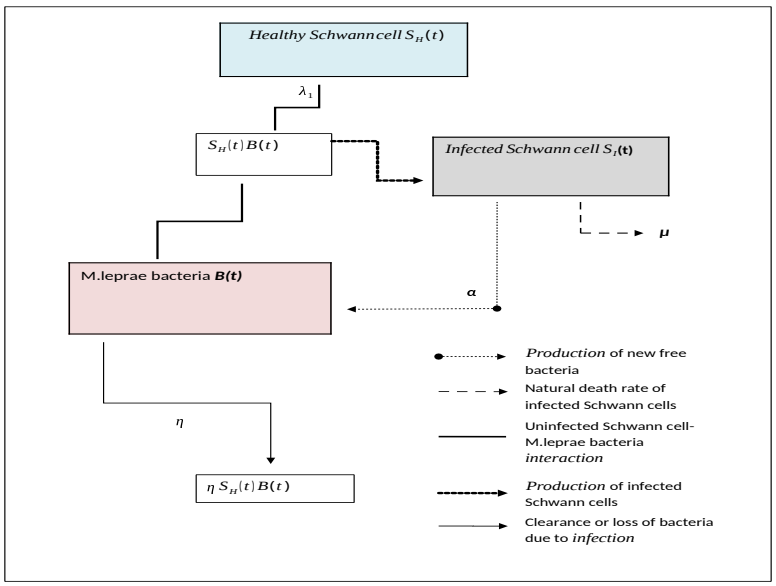

Figure 2.1: Schematic of the interactions between the components of the model.

2.1 The Basic Assumptions and the Mathematical Model

In order to formulate the mathematical model, we assume $S_H(t)$, $S_I(t)$ and $B(t)$ are the concentrations of healthy Schwann cells, infected Schwann cells and *M. leprae* bacteria, respectively, for any time t. Following assumptions are to be considered in creating the mathematical model.

(A1): We have considered the logistic function as a growth function of healthy Schwann cells, where r_1 is the growth rate and k_1 is the carrying capacity. Schwann cells are the main target for the bacterium Mycobacterium Leprae. Healthy Schwann cells become infected at the rate λ_1 by the bacteria through receptor mediated mechanisms regulated by Mitogen-activated protein kinases (MAPK) cascade. So, the term $-\lambda_1 S_H B$ is added to the first equation.

(A2): It is to be assumed that newborn bacteria may be created by proliferation of existing *M. leprae* bacteria and the total number of bacteria can not increase unboundedly. Here, we represent the proliferation of bacteria by a logistic fashion, in which r_2 is the maximum proliferation rate constant and it proliferates to the maximum given by k_2, denoting the bacteria's population density at which proliferation shuts off. *M. leprae* takes entry into healthy Schwann cells and hence, the Schwann cells become infected. The interaction rate of bacteria and healthy Schwann cells is denoted by λ_1 (same as infection rate). Now, due to the interaction of bacteria with healthy Schwann cells and the infection of healthy cells, a certain

portion of bacteria is cleared. We have denoted the rate of loss of bacteria or clearance rate of bacteria by the parameter η. So, -$\eta S_H B$ is also added to the third equation. Infected Schwann cells produce new free bacteria at the rate α.

(A3): From the above assumptions, it is imperative to include another variable S_I to represent the density of the infected Schwann cells. The growth of the infected Schwann cells is represented by term $\lambda_1 S_H B$. The natural mortality rate of the infected Schwann cells is denoted by μ.

The above assumptions **(A1)**–**(A3)** lead us to formulate the model equations as follows

$$\begin{aligned} \frac{dS_H}{dt} &= r_1 S_H \left(1 - \frac{S_H}{k_1}\right) - \lambda_1 S_H B, \\ \frac{dS_I}{dt} &= \lambda_1 S_H B - \mu S_I, \\ \frac{dB}{dt} &= r_2 B \left(1 - \frac{B}{k_2}\right) - \eta S_H B + \alpha S_I \end{aligned} \tag{2.1.1}$$

with the initial conditions

$$S_H(0) \geq 0, \quad S_I(0) \geq 0, \quad B(0) \geq 0. \tag{2.1.2}$$

Various cell-to-cell interactions between our model cell populations are demonstrated through a schematic diagram in Figure 2.1.

2.2 Theoretical Study of the System

2.2.1 Non-negative invariance and boundedness

Let us demonstrate the non-negativity and boundedness of the solutions, which imply that the system (2.1.1) is well-posed and biologically realistic. The following theorem is true.

Theorem 2.2.1 *The solutions of system (2.1.1) with the non-negative initial conditions (2.1.2) are non-negative:*

$$S_H(t) \geq 0, \quad S_I(t) \geq 0, \quad B(t) \geq 0$$

for all possible $t > 0$. All such solutions are located in the region $\Omega \subset \mathbb{R}^3_+$ and are ultimately

bounded, where Ω *is defined as*

$$\Omega = \Big\{(S_H, S_I, B) : 0 \le S_H \le M,\ 0 \le S_H + S_I \le M\left(\frac{r_1}{\mu} + 1\right),$$
$$0 \le B \le \frac{k_2}{2} + \sqrt{\frac{k_2^2}{4} + \frac{\alpha k_2 M}{r_2}\left(\frac{r_1}{\mu} + 1\right)}\Big\},$$

where $M = \max\{k_1; S_H(0)\}$.

Proof. In order to justify the non-negativity of the solutions $S_H(t)$, $S_I(t)$, $B(t)$ to the system (2.1.1) under initial conditions (2.1.2), let us check the necessary and sufficient condition for these solutions to be non-negative [Krasnosel (1968)]. It consists in satisfying the quasi-positivity condition:

$$\begin{cases} \Phi_H(0, S_I, B) \ge 0 \text{ for all } \ S_I \ge 0,\ B \ge 0, \\ \Phi_I(S_H, 0, B) \ge 0 \text{ for all } \ S_H \ge 0,\ B \ge 0, \\ \Phi_B(S_H, S_I, 0) \ge 0 \text{ for all } \ S_H \ge 0,\ S_I \ge 0, \end{cases}$$

where

$$\begin{cases} \Phi_H(S_H, S_I, B) = r_1 S_H\left(1 - \dfrac{S_H}{k_1}\right) - \lambda_1 S_H B, \\ \Phi_I(S_H, S_I, B) = \lambda_1 S_H B - \mu S_I, \\ \Phi_B(S_H, S_I, B) = r_2 B\left(1 - \dfrac{B}{k_2}\right) - \eta S_H B + \alpha S_I \end{cases}$$

are the right-hand sides of the equations of the system (2.1.1).

It is easy to see that

$$\begin{cases} \Phi_H(0, S_I, B) = 0, \\ \Phi_I(S_H, 0, B) = \lambda_1 S_H B \ge 0 \text{ for all } \ S_H \ge 0,\ B \ge 0, \\ \Phi_B(S_H, S_I, 0) = \alpha S_I \ge 0 \text{ for all } \ S_I \ge 0. \end{cases}$$

Thus, the non-negativity of the solutions $S_H(t)$, $S_I(t)$, $B(t)$ for the system (2.1.1) with the non-negativity initial conditions (2.1.2) is established. It means that the non-negative octant $\mathbb{R}^3_+$ is an invariant region for this system.

Now we will study the behavior of non-negative solutions $S_H(t)$, $S_I(t)$, $B(t)$ for the system (2.1.1) with respect to the region Ω. To do this, first, we consider the first equation

of the system. It implies the following inequality:

$$\frac{dS_H}{dt} \leq r_1 S_H \left(1 - \frac{S_H}{k_1}\right).$$

Integrating this inequality with the corresponding initial condition from (2.1.2), we find that

$$S_H(t) \leq \frac{k_1 S_H(0)}{S_H(0)\left(1 - e^{-r_1 t}\right) + k_1 e^{-r_1 t}} \leq M. \tag{2.2.1}$$

Now we consider the first and second equations of system (2.1.1). Adding these two equations and using (2.2.1), we obtain the relationships:

$$\begin{aligned}\frac{d(S_H + S_I)}{dt} &= r_1 S_H \left(1 - \frac{S_H}{k_1}\right) - \mu S_I \\ &\leq r_1 S_H - \mu S_I = (r_1 + \mu) S_H - \mu (S_H + S_I) \\ &\leq (r_1 + \mu) M - \mu (S_H + S_I)\end{aligned}$$

from which we find the inequality:

$$\frac{d(S_H + S_I)}{dt} \leq (r_1 + \mu) M - \mu (S_H + S_I).$$

Integrating it with the necessary initial condition, we conclude that

$$S_H(t) + S_I(t) \leq \left(S_H(0) + S_I(0)\right) e^{-\mu t} + M \left(\frac{r_1}{\mu} + 1\right) \left(1 - e^{-\mu t}\right),$$

which implies the inequality

$$S_H(t) + S_I(t) \leq M \left(\frac{r_1}{\mu} + 1\right), \tag{2.2.2}$$

if $S_H(0) + S_I(0) \leq M \left(\frac{r_1}{\mu} + 1\right)$. Moreover, inequality (2.2.2) also implies

$$S_I(t) \leq M \left(\frac{r_1}{\mu} + 1\right). \tag{2.2.3}$$

Finally, we consider the last equation of system (2.1.1). Inequality (2.2.3) implies that

$$\frac{dB}{dt} \leq r_2 B - \frac{r_2}{k_2} B^2 + \alpha M \left(\frac{r_1}{\mu} + 1\right), \tag{2.2.4}$$

or performing the change of variable

$$z = \frac{r_2}{k_2}B - \frac{r_2}{2},$$

we obtain the differential inequality:

$$\frac{dz}{dt} \leq \xi^2 - z^2, \tag{2.2.5}$$

where

$$\xi = \sqrt{\frac{r_2^2}{4} + \alpha M \frac{r_2}{k_2}\left(\frac{r_1}{\mu} + 1\right)}.$$

Assuming the inequality $z^2(0) \leq \xi^2$, we can integrate the inequality (2.2.5) with the initial condition $z(0)$. As a result, the following inequality can be found

$$\frac{z(t) - \xi}{z(t) + \xi} \leq \frac{z(0) - \xi}{z(0) + \xi} e^{-2\xi t} d$$

which implies that $z(t) \leq \xi$ if $z(0) \leq \xi$. Returning to the original variable, we obtain

$$B(t) \leq \frac{k_2}{2} + \sqrt{\frac{k_2^2}{4} + \alpha M \frac{k_2}{r_2}\left(\frac{r_1}{\mu} + 1\right)}.$$

Thus, all solutions $(S_H(t), S_I(t), B(t))$ of system (2.1.1) that start in Ω, remain in this set for all $t > 0$. It means that Ω is an invariant set of this system. Moreover, the region Ω is bounded and therefore all mentioned solutions ultimately bounded as well. Moreover, all such solutions finally come into the region Ω and stay in it. This property is provided by the definition of the region Ω and the following relationships:

$$\frac{dS_H}{dt}(t)\Big|_{\partial\Omega} < 0, \quad \frac{dS_I}{dt}(t)\Big|_{\partial\Omega} < 0, \quad \frac{dB}{dt}(t)\Big|_{\partial\Omega} < 0$$

which are carried out at the points of the boundary $\partial\Omega$ of the region Ω.

2.2.2 Equilibrium analysis

Existence conditions

In system (2.1.1), endemic equilibrium point E^* is steady state solution. For the existence of endemic equilibrium $E^* = (S_H^*, S_I^*, B^*)$, its coordinates should satisfy the conditions: $E^* = (S_H^*, S_I^*, B^*) \neq 0$, where $S_H^* > 0$, $S_I^* > 0$, $B^* > 0$. The endemic equilibrium point is

obtained by setting equations of the system (2.1.1) to zero. Solving state variables in terms of the model parameters we get:

$$\begin{aligned} S_H^* &= \frac{r_2 k_1 \mu(\lambda_1 k_2 - r_1)}{[\lambda_1 k_1 k_2(\lambda_1\alpha - \mu\eta) - \mu r_1 r_2]}, \\ S_I^* &= [\lambda_1 k_2(\lambda_1^2 k_1 k_2 \alpha + r_1 r_2 \mu + r_1 k_1 \mu\eta + r_1 r_2 \mu) \\ &\quad - \lambda_1^2 k_2(k_1 k_2 \mu\eta + k_2 r_2 \mu + k_1 r_1 \alpha) - r_1^2 r_2 \mu] \times \frac{\lambda_1 k_1 r_2}{[\lambda_1 k_1 k_2(\lambda_1\alpha - \mu\eta) - \mu r_1 r_2]^2} \\ B^* &= \frac{r_1 \lambda_1^{-1}[(\lambda_1^2 k_1 k_2 \alpha + r_1 r_2 \mu) - (\lambda_1 k_1 k_2 \mu\eta + \lambda_1 k_2 r_2 \mu)]}{[\lambda_1 k_1 k_2(\lambda_1\alpha - \mu\eta) - \mu r_1 r_2]}. \end{aligned} \tag{2.2.6}$$

Now, assuming that

$$\begin{aligned} C_0 &= \lambda_1^2 k_1 k_2 \alpha + r_1 r_2 \mu + r_1 k_1 \mu\eta + r_1 r_2 \mu, \\ C_1 &= \lambda_1^2 k_2(k_1 k_2 \mu\eta + k_2 r_2 \mu + k_1 r_1 \alpha) + r_1^2 r_2 \mu, \end{aligned}$$

and using the formulas (2.2.6), we can state the following lemma.

Lemma 2.2.1 *System (2.1.1) possesses positive endemic equilibrium $E^* = (S_H^*, S_I^*, B^*)$ if the following conditions are valid:*

i) $\lambda_1\alpha > \mu r_1 r_2 (\lambda_1 k_1 k_2)^{-1} + \mu\eta$,

ii) $\lambda_1 k_2 > r_1$,

iii) $\lambda_1 k_2 C_0 > C_1$,

iv) $\lambda_1^2 k_1 k_2 \alpha + r_1 r_2 \mu > \lambda_1 k_2 \mu(k_1\eta + r_2)$

2.2.3 Stability criteria

The Jacobian matrix for the endemic equilibrium E^* of system (2.1.1) is given by

$$J(S_H^*, S_I^*, B^*) = \begin{pmatrix} \left[r_1 - 2r_1 k_1^{-1} S_H^* - \lambda_1 B^*\right] & 0 & -\lambda_1 S_H^* \\ \lambda_1 B^* & -\mu & \lambda_1 S_H^* \\ -\eta B^* & \alpha & \left[r_2 - 2r_2 k_2^{-1} B^* - \eta S_H^*\right] \end{pmatrix}.$$

The characteristic equation of the Jacobian matrix can be written in the form

$$\xi^3 + A_2\xi^2 + A_1\xi + A_0 = 0, \tag{2.2.7}$$

where

$$
\begin{aligned}
A_2 &= \left(\frac{2r_1}{k_1}+\eta\right)S_H^* + \left(\frac{2r_2}{k_2}+\lambda_1\right)B^* + (\mu - r_2),\\
A_1 &= \frac{4r_1r_2}{k_1k_2}S_H^*B^* + \frac{2r_1\eta}{k_1}(S_H^*)^2 + \frac{2r_2\lambda_1}{k_2}(B^*)^2\\
&\quad + \left(\frac{2r_1\mu}{k_1} + \mu\eta - \frac{2r_1r_2}{k_1} - \lambda_1\alpha - r_1\eta\right)S_H^*\\
&\quad + \left(\frac{2r_2\mu}{k_2} + \lambda_1\mu - \frac{2r_1r_2}{k_2} - \lambda_1r_2\right)B^* + \left(r_1r_2 - \mu[r_1+r_2]\right),\\
A_0 &= \frac{4r_1r_2\mu}{k_1k_2}S_H^*B^* - \frac{2r_1\lambda_1\alpha}{k_1}(S_H^*)^2 + \frac{2\lambda_1r_2\mu}{k_2}(B^*)^2 + \mu r_1r_2\\
&\quad + \left(\frac{2r_1\eta\mu}{k_1} + \lambda_1r_1\alpha - \frac{2r_1r_2\mu}{k_1} - r_1\mu\eta\right)S_H^* - \left(\frac{2r_1r_2}{k_2} + \lambda_1\mu r_2\right)B^*.
\end{aligned}
$$

By the Routh-Hurwitz criteria (R-H criteria) [Gantmacher (1959)], if the following three conditions:

$$A_0 > 0, \quad A_2 > 0, \quad A_1A_2 > A_0 \tag{2.2.8}$$

are satisfied, then the characteristic Eq. (2.2.7) has all the roots lying in the open left half plane, i.e. all the roots have negative real parts. Hence, using the R-H criteria, we can describe the stability situation of our system by the following theorem.

Theorem 2.2.2 *The system (2.1.1) will be locally asymptotically stable at the endemic equilibrium point $E^* = (S_H^*, S_I^*, B^*)$ if the inequalities (2.2.8) are fulfilled.*

2.2.4 Disease free equilibrium and basic reproduction ratio $\Re_0$

The system (2.1.1) has always a disease-free equilibrium $E_0 = (k_1, 0, 0)$. Local stability of E_0 is governed by basic reproduction ratio $\Re_0$. Biologically, $\Re_0$ is the average number of new secondary infections in a completely susceptible Schwann cell population, generated by a single infected Schwann cell. It can be determined by the next generation method [Van den Driessche and Watmough (2002)]. Using this approach, we need to renumber the model variables in such a way that the compartments reflecting infected individuals are at the beginning. So, we have $x = (S_I, B, S_H)$, with the number of infected compartments equal to 2. Now, by $\mathcal{X}_S$ we denote the set of all disease-free states, i.e.

$$\mathcal{X}_S = \{x \geq 0 : x_i = 0,\ i = 1, 2\}.$$

System (2.1.1) shall be written in the form

$$x_i' = f_i(x) = \mathcal{F}_i(x) - \mathcal{V}_i(x), \quad i = 1, 2, 3,$$

where $\mathcal{F}_i(x)$ describes the rate of appearance of new infections in compartment i. Moreover, $\mathcal{V}_i(x) = \mathcal{V}_i^-(x) - \mathcal{V}_i^+(x)$, and $\mathcal{V}_i^+(x)$ is the rate of transfer into the compartment i, $\mathcal{V}_i^-(x)$ is the rate of transfer out of this compartment. The following assumptions are to be posed:

- (A1) $\mathcal{F}_i(x) \geq 0$, $\mathcal{V}_i^-(x) \geq 0$, $\mathcal{V}_i^+(x) \geq 0$ for any $x \geq 0$;
- (A2) if $x_i = 0$, then $\mathcal{V}_i^- = 0$;
- (A3) $\mathcal{F}_i = 0$ for $i = 3$;
- (A4) if $x \in \mathcal{X}_S$, then $\mathcal{F}_i(x) = 0$ and $\mathcal{V}_i^+(x) = 0$ for $i = 1, 2$;
- (A5) if x_0 is the disease free equilibrium (DFE), then the Jacobi matrix $Df(x_0)$ restricted to the subspace $\mathcal{F} = 0$ has all eigenvalues with negative real parts.

Now, we can form the next generation matrix FV^{-1} [Heffernan et al. (2005); Van den Driessche and Watmough (2002)] from matrices of partial derivatives of $\mathcal{F}_i$ and $\mathcal{V}_i$. Specifically,

$$F = \left[\frac{\partial \mathcal{F}_i(x_0)}{\partial x_j}\right], \qquad V = \left[\frac{\partial \mathcal{V}_i(x_0)}{\partial x_j}\right],$$

where $i, j = 1, 2$. Here F and V are the squared matrices of dimension 2 and $\Re_0 = \varrho(FV^{-1})$ (ϱ denotes a spectral radius of the matrix).

In case of system (2.1.1), we have

$$\mathcal{F} = \begin{pmatrix} \lambda_1 S_H B \\ 0 \\ 0 \end{pmatrix}, \qquad \mathcal{V} = \begin{pmatrix} \mu S_I \\ \eta S_H B - r_2 B\left(1 - k_2^{-1} B\right) - \alpha S_I \\ \lambda_1 S_H B - r_1 S_H \left(1 - k_1^{-1} S_H\right) \end{pmatrix}.$$

Here, the infected compartments are S_I and B. The matrices F and V for the new infection terms and the remaining transfer terms are given by

$$F = \begin{pmatrix} 0 & \lambda_1 k_1 \\ 0 & 0 \end{pmatrix}, \qquad V = \begin{pmatrix} \mu & 0 \\ -\alpha & \eta k_1 - r_2 \end{pmatrix}.$$

A threshold criteria, or reproduction ratio $\Re_0$, can be derived using the spectral radius of the next-generation matrix. Therefore, to find $\Re_0$, we have to find the largest eigenvalue of FV^{-1}. It easy to find that

$$V^{-1} = [\mu(\eta k_1 - r_2)]^{-1} \begin{pmatrix} \eta k_1 - r_2 & 0 \\ \alpha & \mu \end{pmatrix}.$$

Hence, we calculate

$$FV^{-1} = [\mu(\eta k_1 - r_2)]^{-1} \begin{pmatrix} \alpha\lambda_1 k_1 & \mu\lambda_1 k_1 \\ 0 & 0 \end{pmatrix}.$$

Finally, we obtain

$$\Re_0 = \varrho(FV^{-1}) = \frac{\alpha\lambda_1 k_1}{\mu(\eta k_1 - r_2)}.$$

Now, the Jacobian matrix at the disease-free equilibrium E_0 of system (2.1.1) is given by

$$J(E_0) = \begin{pmatrix} -r_1 & 0 & -\lambda_1 k_1 \\ 0 & -\mu & \lambda_1 k_1 \\ 0 & \alpha & r_2 - \eta k_1 \end{pmatrix}.$$

After expanding we get the characteristic polynomial of the Jacobian matrix $J(E_0)$ as follows

$$(\xi + r_1)\left(\xi^2 + D_1\xi + D_0\right) = 0, \tag{2.2.9}$$

where $D_1 = \mu + \eta k_1 - r_2$, $D_0 = \mu(\eta k_1 - r_2) - \alpha\lambda_1 k_1$.

Now $E_0 = (k_1, 0, 0)$ to be locally asymptotically stable, polynomial in (2.2.9) should have all the roots with negative real parts. Equation (2.2.9) has already a negative root which is $\xi = -r_1$. Now, it is easy to note that if $D_0 \geq 0$, then $D_1 > 0$. Therefore, all the roots of the Eq. (2.2.9) will be negative real if $D_0 > 0$ [Heffernan et al. (2005)]. Now, we can see that $D_0 > 0$ gives us a threshold criteria to determine the stability of the disease-free equilibrium and actually $D_0 > 0$ is equivalent to $\Re_0 < 1$. When $\Re_0 > 1$, leprosy infection can take hold. Otherwise, the infection will be eliminated. Hence, we state the following theorem.

Theorem 2.2.3 *For $\Re_0 < 1$ the disease-free equilibrium E_0 is locally asymptotically stable and unstable otherwise.*

Remark 2.2.1 *When $\Re_0 < 1$, disease-free equilibrium E_0 exists as the only equilibrium but for $\Re_0 > 1$, E_0 becomes unstable and endemic equilibrium E^* exists.*

Remark 2.2.2 *From the expression of $\Re_0 = \alpha\lambda_1 k_1[\mu(\eta k_1 - r_2)]^{-1}$ it is observed that parameters appearing in $\Re_0$ are biologically valid. With the increase of the values of parameters λ_1, α and r_2, an average number of new secondary infected Schwann cells will increase and with the increase of the values of parameters μ, η, the number of new secondary cases will decrease.*

2.2.5 Sensitivity analysis

In this Section, we use sensitivity analysis to investigate the impact of various intervention measures. By this method, we can determine the model robustness to parameter values. More precisely, sensitivity indices allows us to measure the relative change in a variable when a parameter changes. Also we can identify the parameters that have high impact on the basic reproductive ratio $\Re_0$ as well as on the disease transmission. Here we derive the sensitivity index by using partial rank correlation coefficients (PRCC) of the basic reproductive ratio with respect to parameters. The normalized forward sensitivity index [Okosun and Makinde (2013)] of a variable v which is differentiable with respect to a given parameter p, is defined as:

$$\Upsilon_p^v := \frac{\partial v}{\partial p} \times \frac{p}{v} .$$

Therefore the normalized forward sensitivity index of $\Re_0$ with respect to a parameter c is defined as follows:

$$\Upsilon_c^{\Re_0} = \frac{\partial \Re_0}{\partial c} \times \frac{c}{\Re_0} .$$

By using this formula, we have written the signs sensitivity index of $\Re_0$ with respect to each of the six different parameters in Table 2.1.

Table 2.1: **Sensitivity analysis of parameters of system (2.1.1)**

Parameter	Assigned value	Sensitivity index of $\Re_0$	(Positive/Negative)
λ_1	5×10^{-4}	1.0	+
k_1	1200	-0.081	–
α	0.4	1	+
μ	0.1	-1	–
η	4×10^{-4}	-1.09	–
r_2	0.036	0.081	+

Sensitivity indices of $\Re_0$ with respect to the six parameters are obtained as

$$\Upsilon_{\lambda_1}^{\Re_0} = 1, \quad \Upsilon_{k_1}^{\Re_0} = -0.081, \quad \Upsilon_{\alpha}^{\Re_0} = 1,$$
$$\Upsilon_{\mu}^{\Re_0} = -1, \quad \Upsilon_{\eta}^{\Re_0} = -1.09, \quad \Upsilon_{r_2}^{\Re_0} = 0.081.$$

Increasing (or decreasing) λ_1 by 10% would increase (or decrease) $\Re_0$ by 10% and increasing (or decreasing) k_1 by 10% would decrease (or increase) $\Re_0$ by 0.81%. This suggests that $\Re_0$ is most positively sensitive to the interaction rate of bacteria and healthy Schwann cells, i.e. the infection rate (λ_1) and the proliferation rate of new free bacteria from infected Schwann cell

population (α), which implies that if we can decrease the values of λ_1 and α, the number of new infected Schwann cells and disease prevalence will be reduced. On the other hand, η and μ have most negative effect on $\Re_0$. So, with the increase of the values of bacteria clearance rate and mortality rate of the infected cells, the value of $\Re_0$ will be decreased. From our knowledge of sensitivity analysis, the control theoretic approach to our system can be very beneficial and accurate as we can identify the most sensitive parameters by this method and use some of them as control parameters. In contrast, the other parameters, k_1 and r_2 do not require as much attention because of their low value in the magnitude of the sensitivity indices.

2.3 Optimal Control Approach

Optimal control is a well-known mathematical tool which is used to control a mathematical model of biological or medical processes. On a given treatment time interval, we usually solve these types of problems through finding the time dependent values of the control functions. Previously several mathematicians have successfully developed control based mathematical models to achieve ideal drug dose regimen in a cost-effective manner for various diseases. Chatterjee and Roy (2012) studied optimal schedule treatment by systematic drug therapy for HIV infection. In the article [Roy, Chowdhury, Chatterjee, Chattopadhyay and Norman (2013)], the author have investigated optimal control therapy and the effect of delay in the positive feedback control for HIV. Effect of Th_1-cells and cytokines have been explored through a control-based mathematical model in psoriasis regulation by Roy et al. (2017). Since leprosy is a skin disease which occurs due to the effect of *M. leprae* bacterium on healthy Schwann cells, then it is obligatory that to control this disease we have to suppress the effect of *M. leprae* bacterium on the susceptible Schwann cells and also the natural replication of the bacterium. In this Section, we have analyzed our formulated model with an addition of two control functions $u_1(t)$ and $u_2(t)$, one is an effect of the drug Ofloxacin and another is Dapsone on various cell densities. Dapsone works by preventing the formation of folic acid and thus inhibits the organism *Mycobacterium leprae*'s replication. Ofloxacin is also a very effective drug in killing the leprosy bacterium. This drug works by disrupting the activity of Gyrase (an enzyme) in the bacterium. Gyrase actually cuts DNA of the bacterium at specific points so that the DNA is able to uncoil to be transcribed. Thus, the control $u_1(t)$ represents the drug therapy Ofloxacin which prevents the new infection, and control $u_2(t)$ is the drug therapy Dapsone which acts against new replication of the bacteria.

As a result, at a given time interval $[0, t_f]$, which is the leprosy treatment period, we

consider the control system:

$$\begin{cases} \dfrac{dS_H}{dt} = r_1 S_H \left(1 - \dfrac{S_H}{k_1}\right) - \lambda_1(1-u_1) S_H B, \\ \dfrac{dS_I}{dt} = \lambda_1(1-u_1) S_H B - \mu S_I, \\ \dfrac{dB}{dt} = r_2(1-u_2) B \left(1 - \dfrac{B}{k_2}\right) - \eta(1-u_1) S_H B + \alpha S_I \end{cases} \tag{2.3.1}$$

with the known initial values for the state variables $S_H(t)$, $S_I(t)$ and $B(t)$:

$$S_H(0) = S_H^0 \geq 0, \quad S_I(0) = S_I^0 \geq 0, \quad B(0) = B^0 \geq 0. \tag{2.3.2}$$

We will consider that the set $\mathcal{U}$ of admissible controls consists of all Lebesgue measurable functions $(u_1(t), u_2(t))$, which for almost all the values of t from the time interval $[0, t_f]$ satisfy the following constraints:

$$0 \leq u_1(t) \leq 1, \qquad 0 \leq u_2(t) \leq 1. \tag{2.3.3}$$

The following theorem ensures that the solutions of system (2.3.1),(2.3.2) are bounded.

Theorem 2.3.1 *For any admissible controls $(u_1(t), u_2(t))$ the corresponding absolutely continuous solution $(S_H(t), S_I(t), B(t))$ to system (2.3.1),(2.3.2) is defined on the entire interval $[0, t_f]$, and for its components $S_H(t)$, $S_I(t)$, $B(t)$ the inequalities:*

$$0 \leq S_H(t) \leq S_H^{\max}, \quad 0 \leq S_I(t) \leq S_I^{\max}, \quad 0 \leq B(t) \leq B^{\max}, \tag{2.3.4}$$

where

$$S_H^{\max} = \max\left\{k_1; S_H^0\right\}, \quad S_I^{\max} = \max\left\{k_1; S_H^0\right\}\left(\frac{r_1}{\mu} + 1\right),$$

$$B^{\max} = B^0 e^{r_2 t_f} + \frac{\alpha \max\left\{k_1; S_H^0\right\}}{r_2}\left(\frac{r_1}{\mu} + 1\right)\left(e^{r_2 t_f} - 1\right)$$

hold for all $t \in [0, t_f]$.

Proof. Let the solution $(S_H(t), S_I(t), B(t))$ be defined on some interval $[0, t_0)$, which is the maximum possible interval of its existence. Without loss of generality, we will assume that $t_0 \leq t_f$. Then, the nonnegativity of the solutions $S_H(t)$, $S_I(t)$, $B(t)$ is justified as in Theorem 2.2.1. The right bounds $S_H^{\max}$ and $S_I^{\max}$ result from the inequalities similar to (2.2.1) and (2.2.3) of Theorem 2.2.1. The bound $B^{\max}$ results from integrating the differential

inequality

$$\frac{dB}{dt} \leq r_2 B + \alpha M \left(\frac{r_1}{\mu} + 1 \right),$$

following from (2.2.4), with the appropriate initial condition from (2.3.2).

Thus, we substantiated the validity of inequalities (2.3.4) on the maximum possible interval of existence of the solution $(S_H(t), S_I(t), B(t))$. This means their implementation on the entire interval $[0, t_f]$ [Hartman (1964)].

Now, on the set $\mathcal{U}$ of admissible controls for the control system (2.3.1),(2.3.2) we define the objective function

$$\mathcal{J}(u_1(\cdot), u_2(\cdot)) = \int_0^{t_f} \left[P u_1^2(t) + Q u_2^2(t) + S_I^2(t) - S_H^2(t) \right] dt, \tag{2.3.5}$$

where the term $Pu_1^2(t)$ represents the cost of the Ofloxacin drug therapy that prevents the new infection. The term $Qu_2^2(t)$ is the cost of the Dapsone drug therapy, which acts against new replication of the bacteria. P and Q are positive balancing coefficients (weights) that regularize the optimal controls. The quadratic expressions for the controls included in (2.3.5) indicate nonlinear costs potentially arising at high intervention levels [Neilan (2009)].

Our goal is to minimize the objective function (2.3.5) on the set $\mathcal{U}$ for the state system (2.3.1),(2.3.2) and find the corresponding optimal controls $(u_1^*(t), u_1^*(t))$, such that

$$\inf_{(u_1(\cdot), u_2(\cdot)) \in \mathcal{U}} \mathcal{J}(u_1(\cdot), u_2(\cdot)) = \mathcal{J}(u_1^*(\cdot), u_2^*(\cdot)). \tag{2.3.6}$$

In order to show the existence of the optimal solution in problem (2.3.6), we will use the well-known result from [Lee and Markus (1967)]. Indeed, for any admissible controls $(u_1(t), u_2(t))$ from $\mathcal{U}$ and the given non-negative initial conditions (2.3.2), it is obvious that the non-negative uniformly bounded on the whole interval $[0, t_f]$ solutions $S_H(t)$, $S_I(t)$, $B(t)$ to the state system (2.3.1) exist (see Theorem 2.3.1). Also, we note that the equations of this system are linear in the controls u_1 and u_2. Next, the set $\mathcal{U} = \{(u_1, u_2) : 0 \leq u_i \leq 1,\ i = 1, 2\}$, in which these controls take on their values (see (2.3.3)), is convex and compact. Finally, the integrand $\left[P u_1^2 + Q u_2^2 + S_I^2 - S_H^2 \right]$ in the objective function (2.3.5) is convex in variables u_1, u_2 on the set $\mathcal{U}$.

Then, we can state the existence of the optimal solution by the following theorem.

Theorem 2.3.2 *There exists the optimal solution in problem (2.3.6), which consists of the optimal controls $(u_1^*(t), u_2^*(t))$ and the appropriate optimal solution $(S_H^*(t), S_I^*(t), B^*(t))$ for*

system (2.3.1),(2.3.2), such that

$$\inf_{(u_1(\cdot),u_2(\cdot))\in\mathcal{U}} \mathcal{J}(u_1(\cdot),u_2(\cdot)) = \min_{(u_1(\cdot),u_2(\cdot))\in\mathcal{U}} \mathcal{J}(u_1(\cdot),u_2(\cdot)) = \mathcal{J}(u_1^*(\cdot),u_2^*(\cdot)). \tag{2.3.7}$$

2.3.1 Properties of the optimal controls

For the analysis of the controls $u_1^*(t)$, $u_2^*(t)$ and the corresponding solutions $S_H^*(t)$, $S_I^*(t)$, $B^*(t)$) we apply the Pontryagin maximum principle [Pontryagin (2018)]. First, we define the Hamiltonian:

$$\begin{aligned}\mathcal{H}(S_H,S_I,B,&u_1,u_2,\psi_1,\psi_2,\psi_3) = Pu_1^2 + Qu_2^2 + S_I^2 - S_H^2\\ &+\left\{r_1 S_H\left(1-\frac{S_H}{k_1}\right) - \lambda_1(1-u_1)S_H B\right\}\psi_1\\ &+\left\{\lambda_1(1-u_1)S_H B - \mu S_I\right\}\psi_2\\ &+\left\{r_2(1-u_2)B\left(1-\frac{B}{k_2}\right) - \eta(1-u_1)S_H B + \alpha S_I\right\}\psi_3,\end{aligned}$$

where ψ_1, ψ_2, ψ_3 are the adjoint variables.

Next, we evaluate all the required partial derivatives of the Hamiltonian with respect to the variables S_H, S_I, B:

$$\begin{aligned}\mathcal{H}'_{S_H}(S_H,S_I,B,u_1,u_2,\psi_1,\psi_2,\psi_3) =& -2S_H + \left\{r_1\left(1-\frac{2S_H}{k_1}\right) - \lambda_1(1-u_1)B\right\}\psi_1\\ &+\lambda_1(1-u_1)B\psi_2 - \eta(1-u_1)B\psi_3,\\ \mathcal{H}'_{S_I}(S_H,S_I,B,u_1,u_2,\psi_1,\psi_2,\psi_3) =& \ 2S_I - \mu\psi_2 + \alpha\psi_3,\\ \mathcal{H}'_{B}(S_H,S_I,B,u_1,u_2,\psi_1,\psi_2,\psi_3) =& -\lambda_1(1-u_1)S_H\psi_1 + \lambda_1(1-u_1)S_H\psi_2\\ &+\left\{r_2(1-u_2)\left(1-\frac{2B}{k_2}\right) - \eta(1-u_1)S_H\right\}\psi_3,\end{aligned}$$

and also with respect to controls u_1 and u_2:

$$\begin{aligned}\mathcal{H}'_{u_1}(S_H,S_I,B,u_1,u_2,\psi_1,\psi_2,\psi_3) &= 2Pu_1 + \lambda_1 S_H B\psi_1 - \lambda_1 S_H B\psi_2 + \eta S_H B\psi_3,\\ \mathcal{H}'_{u_2}(S_H,S_I,B,u_1,u_2,\psi_1,\psi_2,\psi_3) &= 2Qu_2 - r_2 B\left(1-\frac{B}{k_2}\right)\psi_3.\end{aligned} \tag{2.3.8}$$

Then, by the Pontryagin maximum principle, for optimal controls $u_1^*(t)$, $u_2^*(t)$ and the corresponding optimal solutions $S_H^*(t)$, $S_I^*(t)$, $B^*(t)$ there exists the vector-function $\psi_*(t) = (\psi_1^*(t),\psi_2^*(t),\psi_3^*(t))$, such that:

- $\psi_*(t)$ is the nontrivial solution of the adjoint system:

$$\begin{cases} \psi_1^{*\prime}(t) = -\mathcal{H}'_{S_H}(S_H^*(t), S_I^*(t), B^*(t), u_1^*(t), u_2^*(t), \psi_1^*(t), \psi_2^*(t), \psi_3^*(t)) \\ \qquad = 2S_H^*(t) - \left\{ r_1 \left(1 - \dfrac{2S_H^*(t)}{k_1}\right) - \lambda_1(1-u_1^*(t))B^*(t) \right\} \psi_1^*(t) \\ \qquad\quad - \lambda_1(1-u_1^*(t))B^*(t)\psi_2^*(t) + \eta(1-u_1^*(t))B^*(t)\psi_3^*(t), \\ \psi_2^{*\prime}(t) = -\mathcal{H}'_{S_I}(S_H^*(t), S_I^*(t), B^*(t), u_1^*(t), u_2^*(t), \psi_1^*(t), \psi_2^*(t), \psi_3^*(t)) \\ \qquad = -2S_I^*(t) + \mu\psi_2^*(t) - \alpha\psi_3^*(t), \\ \psi_3^{*\prime}(t) = -\mathcal{H}'_{B}(S_H^*(t), S_I^*(t), B^*(t), u_1^*(t), u_2^*(t), \psi_1^*(t), \psi_2^*(t), \psi_3^*(t)) \\ \qquad = \lambda_1(1-u_1^*(t))S_H^*(t)\psi_1^*(t) - \lambda_1(1-u_1^*(t))S_H^*(t)\psi_2^*(t) \\ \qquad\quad - \left\{ r_2(1-u_2^*(t)) \left(1 - \dfrac{2B^*(t)}{k_2}\right) - \eta(1-u_1^*(t))S_H^*(t) \right\} \psi_3^*(t) \end{cases} \tag{2.3.9}$$

with the corresponding initial conditions:

$$\psi_1^*(t_f) = 0, \quad \psi_2^*(t_f) = 0, \quad \psi_3^*(t_f) = 0; \tag{2.3.10}$$

- the controls $u_1^*(t)$ and $u_2^*(t)$ maximize the Hamiltonian

$$\mathcal{H}(S_H^*(t), S_I^*(t), B^*(t), u_1, u_2, \psi_1^*(t), \psi_2^*(t), \psi_3^*(t)) \tag{2.3.11}$$

with respect to $u_i \in [0,1]$, $i = 1,2$ for almost all $t \in [0, t_f]$, and therefore, due to the corresponding formulas from (2.3.8), the following relationships hold:

$$u_1^*(t) = \begin{cases} 1 & , \text{ if } \quad \phi_{u_1}(t) \geq 1, \\ \phi_{u_1}(t) & , \text{ if } \quad 0 < \phi_{u_1}(t) < 1, \\ 0 & , \text{ if } \quad \phi_{u_1}(t) \leq 0, \end{cases} \tag{2.3.12}$$

$$u_2^*(t) = \begin{cases} 1 & , \text{ if } \quad \phi_{u_2}(t) \geq 1, \\ \phi_{u_2}(t) & , \text{ if } \quad 0 < \phi_{u_2}(t) < 1, \\ 0 & , \text{ if } \quad \phi_{u_2}(t) \leq 0, \end{cases} \tag{2.3.13}$$

where

$$\begin{aligned} \phi_{u_1}(t) &= 0.5P^{-1}S_H^*(t)B^*(t)(\lambda_1(\psi_2^*(t) - \psi_1^*(t)) - \eta\psi_3^*(t)), \\ \phi_{u_2}(t) &= 0.5Q^{-1}r_2B^*(t)\left(1 - \frac{B^*(t)}{k_2}\right)\psi_3^*(t). \end{aligned} \tag{2.3.14}$$

are the so-called the indicator functions [Schättler and Ledzewicz (2015)], which determine the

behavior of the corresponding optimal controls $u_1^*(t)$ and $u_2^*(t)$ according to formulas (2.3.12) and (2.3.13).

Study of relationships (2.3.12) and (2.3.13) shows that for all values of $t \in [0, t_f]$, the maximum of the Hamiltonian (2.3.11) is reached with unique values $u_1 = u_1^*(t)$, $u_2 = u_2^*(t)$. Therefore, Theorem 6.1 in the article [Flemming and RISHEL (1975)] implies the continuity of controls $u_1^*(t)$ and $u_2^*(t)$. Adding to this result, the analysis of the adjoint system (2.3.9),(2.3.10) and formulas (2.3.14), and again relationships (2.3.12) and (2.3.13) leads us to the validity of the following theorem.

Theorem 2.3.3 *The optimal controls $u_1^*(t)$ and $u_2^*(t)$ are continuous functions on the interval $[0, t_f]$, which satisfy the equalities:*

$$u_1^*(t_f) = 0, \qquad u_2^*(t_f) = 0.$$

Also we note that the uniqueness of the optimal controls $(u_1^*(t), u_2^*(t))$ is due to the boundedness of the state and adjoint variables and the Lipschitz properties of the systems (2.3.1),(2.3.2) and (2.3.9),(2.3.10) defining these variables [see Jung et al. (2002); Mateus et al. (2017); Silva and Torres (2013) and references cited therein].

Due to relationships (2.3.14), we will rewrite the formulas (2.3.12) and (2.3.13) in a more convenient and compact form:

$$u_1^*(t) = \max\Big\{\min\Big\{1; 0.5P^{-1}S_H^*(t)B^*(t)(\lambda_1(\psi_2^*(t) - \psi_1^*(t)) - \eta\psi_3^*(t))\Big\}; 0\Big\}, \tag{2.3.15}$$

$$u_2^*(t) = \max\left\{\min\left\{1; 0.5Q^{-1}r_2B^*(t)\left(1 - \frac{B^*(t)}{k_2}\right)\psi_3^*(t)\right\}; 0\right\}. \tag{2.3.16}$$

Finally, the boundary value problem for the maximum principle arises, which is formed by systems (2.3.1) and (2.3.9) with the corresponding initial conditions (2.3.2) and (2.3.10), as well as relationships (2.3.15) and (2.3.16). The results of numerical analysis of this boundary value problem are presented in Section 2.4.

2.3.2 Efficiency analysis

In this Section, we consider three strategies (Strategy-I, Strategy-II and Strategy-III). Strategy-I is the strategy where $u_1 \neq 0$, $u_2 = 0$ and for Strategy-II, $u_1 = 0$, $u_2 \neq 0$. Strategy-III is the combination of the drug therapy where $u_1 \neq 0$, $u_2 \neq 0$. Here we shall

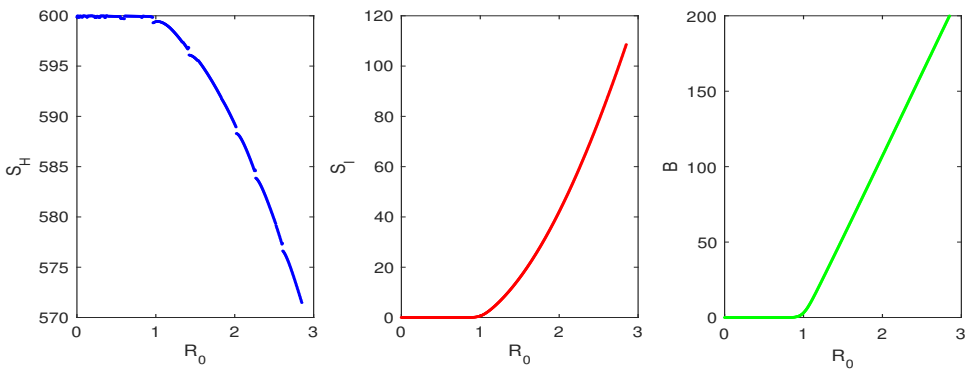

Figure 2.2: Transcritical bifurcation: steady state value of infected cell are plotted versus basic reproduction ratio $\Re_0$ using the set of parameters as given in Table 2.3 except disease transmission rate λ_1. Endemic steady state feasible when $\Re_0 > 1$. λ_1 is varied in plotting the Figure.

calculate the efficiency index $\sum$ which is defined as

$$\sum = \left(1 - \frac{A_c}{A_s}\right) \times 100\%,$$

where A_c represents the area under the infected Schwann cells concentration as a function of time when the control is used and A_s is the area under the infected total population curve in absence of control input. The cumulative number of infected Schwann cells during the time interval $[0, 1]$ is defined by

$$\mathbb{A} = \int_0^{t_f} S_I(t)dt.$$

By calculating the efficiency index we can adopt the best strategy whose efficiency index [Yang and Ferreira (2008); Abboubakar et al. (2018)] will be the biggest. The values of A_c and the efficiency index for two strategies are given in Table 2.2.

Table 2.2: **Table of efficiency index for system (2.1.1)**

Strategy	$\mathbb{A} = \int_0^{t_f} S_I(t)dt$	$\sum = \left(1 - \frac{A_c}{A_s}\right) \times 100\%$
No control	4.8558×10^5	0%
Strategy-I	2.0034×10^5	58.74%
Strategy-II	2.3858×10^5	50.85%
Strategy-III	1.3812×10^5	71.56%

From the Table 2.2, we can conclude that Strategy-I is more effective than Strategy-II. However, Strategy-III (which is the combination of two drug therapy) is the best strategy.

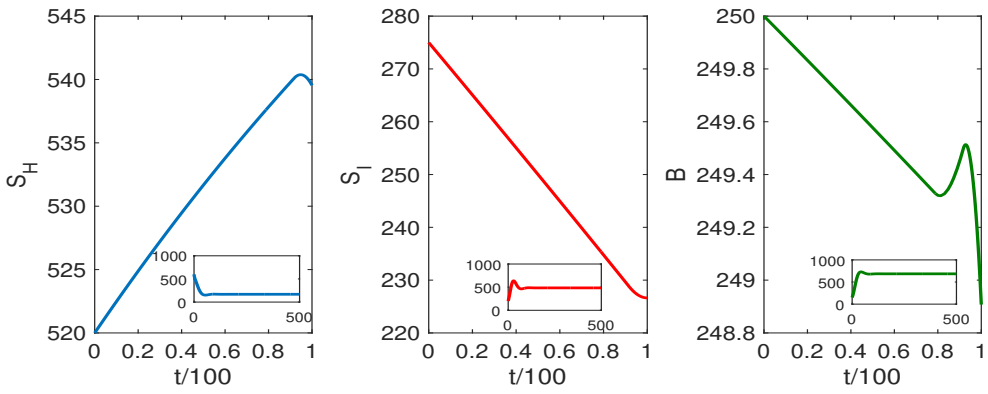

Figure 2.3: Trajectories with fixed controls $u_1 = 0.7$, $u_2 = 0.7$. Inset Figure shows model trajectories without controls.

2.4 Numerical Simulations

In this Section, we have studied the numerical simulations of our model on the basis of analytical findings in order to have an understanding of the detailed dynamics of the system comprising of three different cell populations. For numerical simulations, we take a set of parameter values given in Table 2.3. Some parameter values are estimated and the remaining values are assumed. We choose the initial values in number dependant according to cardinal rule of scientific hypothesis.

In Figure 2.2, we have described that our system (2.1.1) exhibits a transcritical bifurcation at the threshold $\Re_0 = 1$. Here the three steady state values of our model three cell populations have been plotted versus basic reproduction ratio $\Re_0$. From the three Subfigures of Figure 2.2, we can clearly observe that for $\Re_0 < 1$, the healthy Schwann cells (S_H) remain at its maximum possible density level, i.e. at 600 mm^{-3} and the densities of infected Schwann cells (S_I) and *M. leprae* bacteria (B) remain zero. As the value of $\Re_0$ is increased and becomes greater than 1, the density of healthy cells starts decreasing and the concentrations of infected cells and bacteria begin to increase rapidly and thus the endemic steady state E^* becomes feasible. Biologically speaking, for $\Re_0 < 1$, the disease-free state E_0 becomes stable and for $\Re_0 > 1$, the endemic state E^* exists and hence, the disease leprosy persists. Infection rate λ_1 is varied within the permissible range listed in Table 2.3 in plotting the graphs in this Figure.

In Figure 2.3, we have demonstrated the trajectories of healthy Schwann cells, infected

Table 2.3: **List of parameter values used in numerical simulation for system (2.1.1)**

Parameter	Parameter definition	Assigned Value (Unit)
r_1	growth rate of healthy Schwann cell	$0.4(\text{day}^{-1})$
r_2	growth rate of *M. leprae* bacteria	$0.1(\text{day}^{-1})$
k_1	carrying capacity of healthy Schwann cell	$600(\text{mm}^{-3})$
k_2	carrying capacity of bacteria	$500(\text{mm}^{-3})$
μ	natural death rate of infected Schwann cell	$0.1(\text{day}^{-1})$
λ_1	infection rate of healthy cell and bacteria	$0.00042(\text{mm}^3$ $\text{day}^{-1})$
α	proliferation of new free bacteria	$0.1(\text{day}^{-1})$
η	bacteria clearance rate due to infection	$0.0003(\text{mm}^3$ $\text{day}^{-1})$

Schwann cells and *M. leprae* bacteria at a constant value of both controls. The inset Figures in each Subfigure represents the behavior of the curves of the corresponding cell populations without controls. The values of constant controls u_1 and u_2 are taken as $u_1 = 0.7$, $u_2 = 0.7$ to produce the graphs in Figure 2.3. The trajectories of S_H and S_I indicate that without controls, the density of healthy Schwann cells decreases from 500 mm^{-3} to 280 mm^{-3} and in case of infected cells it increases up to 480 mm^{-3} from 250 mm^{-3} in 100 days. Trajectory of *M. leprae* bacteria shows a quite similar behavior like infected cells as both of them decreases gradually to 248 mm^{-3} and 227 mm^{-3} with controls from their initial cell concentrations. Also, the healthy cell concentration S_H increases from 520 mm^{-3} to 539 mm^{-3} in 100 days if we use fixed control values of both the control functions u_1 and u_2. It is evident from this Figure that the fixed control therapy has a great impact on both healthy and infected Schwann cells by increasing and decreasing the cell concentrations respectively in comparison with the scenario of the cell dynamics without controls. Also, if we use higher values of both the control functions u_1 and u_2, it will be easier to handle the condition of a patient but using high dosages of these two drugs (Ofloxacin and Dapsone) for a long period of time can cause potentially irreversible serious adverse reactions (skin rashes, hypersensitivity, peripheral neuropathies, hemolytic anemia etc.) in a leprosy patient. Therefore, we need to provide the optimal control therapy of leprosy.

Next, we solve the optimal control problem (2.3.7) for the control system (2.3.1) numerically and we have explored the effect of optimal controls $u_1^*(t)$ and $u_2^*(t)$. In Section 2.3.2, we

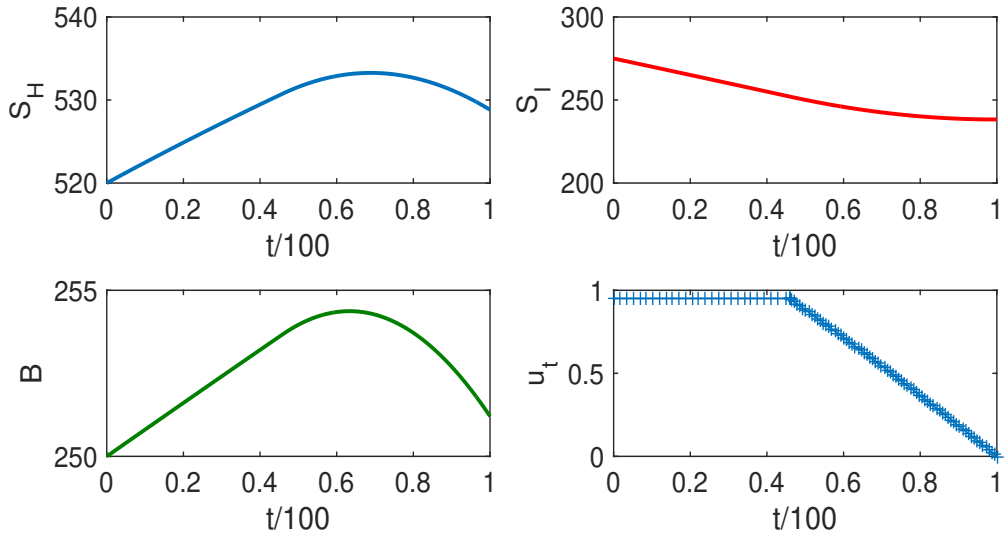

Figure 2.4: Strategy-I: $u_1(t) \neq 0$, $u_2(t) = 0$ *with* $P = 30000$.

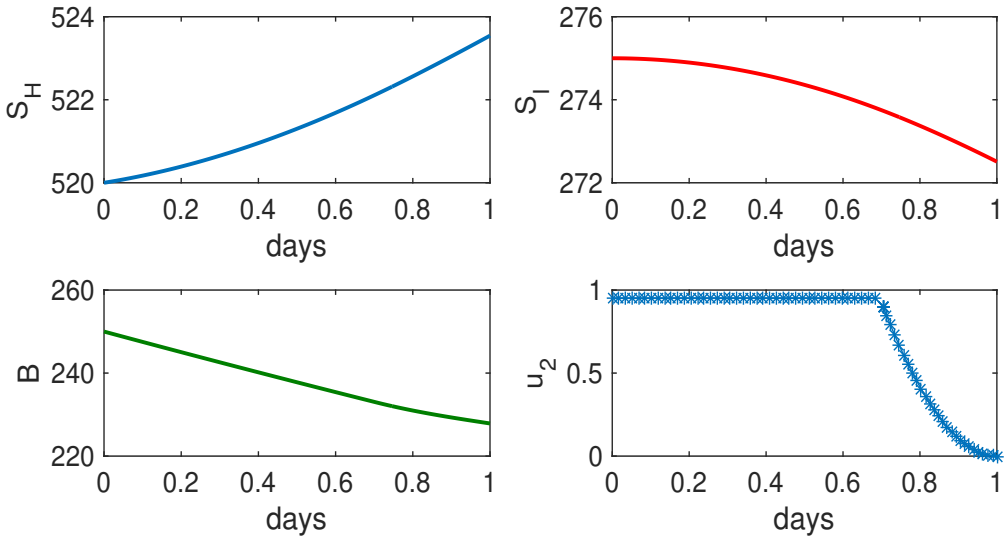

Figure 2.5: Strategy-II: $u_1(t) = 0$, $u_2(t) \neq 0$ *with* $Q = 100$.

have performed an efficiency analysis on the three previously mentioned control strategies. Efficiency analysis is actually a comparative study of these three strategies to discover which one of them is the strongest and the most effective. The effect of optimal control Strategy-I, Strategy-II and Strategy-III on the three cell populations S_H, S_I, and B have been illustrated in Figure 2.4, Figure 2.5, and Figure 2.6, respectively. Values of the parameters P and Q,

which are actually the weight constants on the benefit of the cost, have been chosen suitably as $P = 30000$ and $Q = 100$ for these three Figures. The graphs of the optimal control functions $u_1^*(t)$, $u_2^*(t)$ plotted with respect to the time scale $t/100$ in each of these Figures suggests that after a certain number of days (after approximately 40 days for $u_1^*(t)$ and after 60 days for $u_2^*(t)$ in case of Strategy-III) when the infected Schwann cells and bacteria population density reduces remarkably, the drug dose declines gradually to 0. From Figure 2.4 and Figure 2.5 we can observe that for Strategy-I, the healthy Schwann cell concentration increases up to 530 mm^{-3} where for Strategy-II, healthy cell density increases up to 523 mm^{-3} in 100 days. Also for Strategy-II, infected cell (S_I) density declines to 273 mm^{-3}, but for Strategy-I, density of S_I reduces to a relatively lower level i.e. 230 mm^{-3} in 100 days. So, Strategy-I is more effective than Strategy-II but Figure 2.6 demonstrates that in case of Strategy-III, density of S_H increases to 529 mm^{-3} and both infected cell population (S_I) and *M. leprae* bacteria (B) population density decrease significantly to 238 mm^{-3} and 245 mm^{-3}, respectively, in 100 days. So finally, Strategy-III appears to be the best and strongest strategy among these three strategies according to our numerical findings and it clearly supports our analytical findings as well in Section 2.3.2.

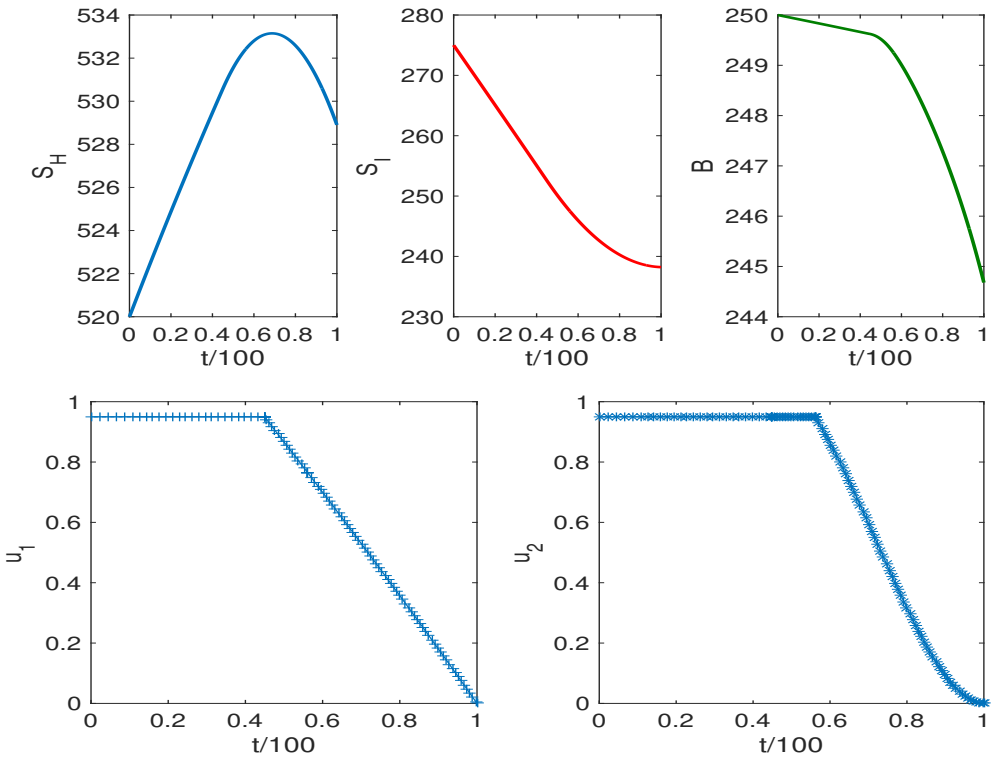

Figure 2.6: Strategy-III: $u_1(t) \neq 0$, $u_2(t) \neq 0$ with $P = 30000$ and $Q = 100$.

In Figure 2.6, we have also illustrated the dynamics of the optimal controls with respect to time. At the early stage of the disease leprosy, high drug doses (0.8–0.9) of both Ofloxacin and Dapsone are needed to control the infection as extreme bacterial density has been observed in the skin smears of leprosy patients at this time. Once the infections start decreasing, drug dose needs to be reduced after 40 days for Ofloxacin and after 60 days in case of Dapsone. We have used the drug dose of 0.7 for both the two drugs throughout 100 days during the fixed control therapy. Optimal control treatment for the combined drug therapy also requires the dosage of 0.7 in between 55–60 days for Ofloxacin and in between 65–70 days for Dapsone. After that, the drug dose needs to be decreased gradually and after 90 days, a very low amount of drug dosage is required. We can clearly observe from our numerical analysis of the cell dynamics and the control functions $u_1^*(t)$, $u_2^*(t)$ under the optimal treatment policy that by maintaining an optimum level of drug dose for 100 days, the disease can be brought under control and it also eliminates the possibility of severe adverse drug reactions. It is important to note that we have re-scaled the time axis in $t/100$ for the sake of simplicity of numerical simulations (i.e. 0.6 in the time axis actually represents 60 days). Therefore the optimal control therapy has the capability to stabilize the system by reducing infected cells and bacteria and by increasing the healthy Schwann cell population in a leprosy patient.

2.5 Discussion

In this chapter, we have established a three dimensional non-linear mathematical model to discover the effect of *M. leprae* bacteria on healthy Schwann cells and to perceive the dynamical changes of our model cell populations during the disease progression. Our model exhibits two equilibria which are the disease-free equilibrium and the endemic equilibrium. Existence of these equilibria has been shown both analytically and through numerical simulations. We have shown the stability of disease-free equilibrium and also proved the stability of endemic equilibrium E^* by using R-H criteria. We have evaluated the basic reproduction ratio $\Re_0$ and studied its significance in determining the persistence of the disease leprosy. For $\Re_0$ less than unity, the disease leprosy is eliminated from human body. For the value of $\Re_0$ greater than unity, endemic equilibrium E^* exists according to Lemma 2.2.1 and hence, the disease continues to persist. Sensitivity analysis has been done to find the sensitivity indices for each of our model parameter. It is observed that all the parameters are sensitive for leprosy pathogenesis.

In this Chapter, we have compared the cell dynamical behavior of our model without and with the control therapy. Furthermore, the fixed control method and optimal control

method have been compared in our study. Our findings related to the optimality system and the control pairs (u_1^*, u_2^*) suggest that optimal control policy of introducing the combined drugs (Ofloxacin and Dapsone) is more effective for reducing the bacterial load, inhibiting new infections and stopping the spread of the infection by killing the infected Schwann cells. Because of extreme side-effects and high cost of the combined drug therapy, we recommend the optimal control method as a standard treatment policy for leprosy.

Chapter 3

Mathematical Insights on Density Dependent growth of *Mycobacterium leprae* Bacteria for the Disease Leprosy

In the previous Chapter, we have described a basic three dimensional ODE-based mathematical model for exploring the fundamental features of the disease leprosy. While dealing with continuous systems, a discrete cell dynamical model of leprosy has not yet been proposed and investigated. In this regard, recent experimental studies suggests that population growth rate plays a synergistic effect in describing the various aspects of the proliferation of *Mycobacterium leprae* bacteria. It is necessary to understand the density-dependent growth to forecast a more realistic population trend of *M. leprae* into the human body. Introducing theta logistic growth rate instead of classical logistic growth not only makes the dynamics of a living system more complicated but it adds more pliability and flexibility in terms of the key relationship of per capita growth rate with the population density of *M. leprae*. Indeed, the intraspecific competition for a safe and sustainable intracellular environment with necessary metabolic activities performed by the organism inside Schwann cells ensure the density dependency when abundance in the bacterial concentration increases. Also, this approach is mathematically more practical and plausible as it considers the bacteria population not to grow unboundedly. In this Chapter[3], we have considered a three-dimensional non-linear

[3] *The major portion of this chapter is published in Diferential Equations and Dynamical Systems, Springer, August, 2022.*

mathematical model with healthy Schwann cell, infected Schwann cell, and *M. leprae* bacteria population. We have incorporated a theta logistic growth in the *M. leprae* bacteria population due to its vital density dependence property. We have discussed how different values of the shape parameter θ plays a key role on interpreting the impacts for the infection and dissemination of leprosy through cell-to-cell interactions into the human body. The stability of the system and also bifurcation analysis has been investigated in detail. Also, all of our analytical outcomes have been verified and validated through numerical simulations.

3.1 Model Formulation with Suitable Assumptions

Firstly, we have reconsidered the following three dimensional mathematical model already developed in Chapter 2.

$$\begin{aligned} \frac{dx_h}{dt} &= r_1 x_h(1-\frac{x_h}{K}) - \lambda x_h M_l, \\ \frac{dx_i}{dt} &= \lambda x_h M_l - \delta x_i, \\ \frac{dM_l}{dt} &= r_2 M_l(1-\frac{M_l}{N}) - \gamma x_h M_l + \nu x_i. \end{aligned} \tag{3.1.1}$$

Here, $x_h(t)$, $x_i(t)$ and $M_l(t)$ are the concentrations of healthy Schwann cells, infected Schwann cells and *M. leprae* bacteria, respectively, for any time t. Logistic growth rate is assumed for both healthy Schwann cells and bacteria population where we have denoted the intrinsic growth rate and the carrying capacity of the healthy Schwann cell population by r_1 and K and the same for the bacteria population are denoted by r_2 and N respectively. The rate at which healthy Schwann cells getting infected by the *M. leprae* bacteria is represented by λ. New free bacteria proliferates from infected cells at a rate ν. The natural mortality rate of infected Schwann cells and the rate of bacterial clearance due to infection are represented by δ and γ, respectively.

Theta logistic growth curve is more realistic and accurate than the classical logistic growth model. Here, we incorporate the discrete version of the model (3.1.1). Based on the above perception along with the theta logistic growth in *M. leprae* bacteria population using the

Forward Euler Scheme for discretization, we have revised the system (3.1.1) as follows:

$$\begin{aligned} x_{h_{t+1}} &= x_{h_t} + p\left[r_1 x_{h_t}(1-\frac{x_{h_t}}{K}) - \lambda x_{h_t} M_{l_t}\right], \\ x_{i_{t+1}} &= x_{i_t} + p\left[\lambda x_{h_t} M_{l_t} - \delta x_{i_t}\right], \\ M_{l_{t+1}} &= M_{l_t} + p\left[r_2 M_{l_t}\left[1-\left(\frac{M_{l_t}}{N}\right)^{\theta}\right] - \gamma x_{h_t} M_{l_t} + \nu x_{i_t}\right]. \end{aligned} \tag{3.1.2}$$

Here, $\theta(>0)$ describes the curvature of the relationship and the parameter $p(>0)$ denotes the step size.

3.2 Equilibria and Stability Analysis

System (3.1.2) has two equilibrium points, namely, the disease-free equilibrium $E_0 = (K, 0, 0)$ and the unique positive interior equilibrium $E^* = (x_h^*, x_i^*, M_l^*)$, where the values of x_h^*, x_i^*, M_l^* are given by

$$x_i^* = \frac{r_1}{\delta} x_h^* \left(1 - \frac{x_h^*}{K}\right), \quad M_l^* = \frac{r_1}{\lambda}\left(1 - \frac{x_h^*}{K}\right)$$

and x_h^* is the positive root of the following equation,

$$g(x_h^*) = r_2\left[1 - \left\{1 - \frac{r_1}{\lambda N}(1 - \frac{x_h^*}{K})\right\}^{\theta}\right] + \left(\frac{\nu\lambda}{\delta} - \gamma\right) x_h^* = 0.$$

Here, it is important to note that both $x_i^* > 0$ and $M_l^* > 0$ because $x_h^* < K$ always holds true as the density of healthy Schwann cells can never exceed its carrying capacity K at the endemic steady state. Now, from the second equation of system (3.1.2), it follows that the values of x_h^*, x_i^*, M_l^* are interconnected and actually, x_h^* can be written as

$$x_h^* = \frac{\delta}{\lambda}\frac{x_i^*}{M_l^*}. \tag{3.2.1}$$

Now, as we have already obtained $x_i^* > 0$, $M_l^* > 0$, we can see that equation (3.2.1) clearly ensures the positivity of x_h^*.

3.2.1 Stability of the disease-free equilibrium

The Jacobian matrix of the system (3.1.2) at the disease-free equilibrium point $E_0 = (K, 0, 0)$ is as follows:

$$\mathcal{J}_0 = \begin{pmatrix} 1-pr_1 & 0 & -p\lambda K \\ 0 & 1-p\delta & p\lambda K \\ 0 & p\nu & 1+p(r_2-\gamma K) \end{pmatrix}. \tag{3.2.2}$$

The eigenvalues of $\mathcal{J}_0$ are ζ_i for $i = 1, 2, 3$ where $\zeta_1 = 1 - pr_1$ and ζ_2, ζ_3 are the roots of the following equation:

$$f(\zeta) = \zeta^2 + A_1\zeta + A_2 = 0. \tag{3.2.3}$$

Here,

$$A_1 = p(\gamma K + \delta - r_2) - 2,$$
$$A_2 = 1 + p(r_2 - \gamma K - \delta) - p^2(\lambda\nu K + \delta(r_2 - \gamma K)).$$

Now, by analyzing the nature of the roots ζ_i for $i = 1, 2, 3$ of equation (3.2.3) according to the well-known Jury conditions [Murray (1989)], we can conclude the following theorem about the stability situation of E_0.

Theorem 3.2.1 *The disease-free equilibrium $E_0 = (K, 0, 0)$ of system (3.1.2) will be locally asymptotically stable if $|\zeta_1| < 1$ and also if the following three conditions are satisfied:*

$$f(1) > 0, \quad f(-1) > 0 \quad \textit{and} \quad A_2 < 1. \tag{3.2.4}$$

3.2.2 Stability analysis of the interior equilibrium

Here, we will discuss the stability of the system (3.1.2) at the interior equilibrium point $E^* = (x_h^*, x_i^*, M_l^*)$. The Jacobian matrix of system (3.1.2) at E^* is given by,

$$\mathcal{J}(E^*) = \begin{pmatrix} M_{11} & 0 & -p\lambda x_h^* \\ p\lambda M_l^* & 1-p\delta & p\lambda x_h^* \\ -p\gamma M_l^* & p\nu & M_{33} \end{pmatrix} \tag{3.2.5}$$

where,

$$M_{11} = 1 + p(r_1 - \frac{2r_1}{K}x_h^* - \lambda M_l^*),$$
$$M_{33} = p[r_2 - r_2(\theta+1)(\frac{M_l^*}{N}) - \gamma x_h^*].$$

From the Jacobian matrix $\mathcal{J}(E^*)$ given by (3.2.5), we get the characteristic equation of system (3.1.2) at E^* as follows:

$$|\mathcal{J}(E^*) - \xi I| = 0. \tag{3.2.6}$$

Expanding equation (3.2.6), we get

$$\xi^3 + \varphi_1\xi^2 + \varphi_2\xi + \varphi_3 = 0 \tag{3.2.7}$$

where,

$$\begin{aligned}
\varphi_1 &= \delta p - M_{11} - M_{33} - 1,\\
\varphi_2 &= M_{11} + M_{33} + M_{11}M_{33} - \delta p(M_{11} + M_{33}) - p^2\lambda x_h^*(\nu + \gamma M_l^*),\\
\varphi_3 &= M_{11}M_{33}(\delta p - 1) + p^2\lambda x_h^*(\nu M_{11} + \gamma M_l^*) + p^3\lambda x_h^* M_l^*(\lambda\nu + \gamma\delta).
\end{aligned}$$

Hence, using the Jury conditions [Sen and Mukhejee (2011)], we now obtain the following theorem which ensures the stability of E^*. This clearly indicates the following theorem.

Theorem 3.2.2 *System (3.1.2) will be locally asymptotically stable at the the interior equilibrium E^* if and only if*

$$|\varphi_1 + \varphi_3| < 1 + \varphi_2, \quad |\varphi_3| < 1 \quad \textit{and} \quad |\varphi_2 - \varphi_1\varphi_3| < |1 - \varphi_3^2|. \tag{3.2.8}$$

3.3 Hopf Bifurcation Analysis

In this Section, we will derive conditions for which Hopf bifurcation occurs around the interior equilibrium E^* as θ varies in the open interval $(0, 1)$.
Let, $\Psi : (0, \infty) \to \mathbb{R}$ be a continuously differentiable function of θ defined by

$$\Psi(\theta) = \varphi_1(\theta)\varphi_2(\theta) - \varphi_3(\theta). \tag{3.3.1}$$

For the occurrence of Hopf bifurcation there should exist a $\theta^* \in (0, 1)$ such that $Re\ \xi(\theta^*) = 0$ and $Im\ \xi(\theta^*) = \omega_0 > 0$ where the complex conjugate pair of eigenvalues $\xi(\theta^*)$, $\bar{\xi}(\theta^*) \in \sigma(\theta)$. The transversality condition is given by

$$\frac{d(Re\xi(\theta))}{d\theta}\Big|_{\theta=\theta^*} \neq 0; \tag{3.3.2}$$

Also, let us define $\sigma(\theta) = \{\rho : D(\rho) = 0\}$ is the spectrum of the characteristic equation

(3.2.7). For the appearance of Hopf bifurcation, it is necessary for all the other elements of $\sigma(\theta)$ to have negative real parts.

To prove the existence of such θ^*, we have to solve the equation for $\xi(\theta^*)$. Now using equation (3.3.1), we can rewrite the characteristic equation (3.2.7) as

$$\begin{aligned} \xi^3 + \varphi_1\xi^2 + \varphi_2\xi + \varphi_1\varphi_2 = 0 \quad [\ As\ \varphi_1\varphi_2 - \varphi_3 = 0] \\ \Rightarrow \xi^2(\xi + \varphi_1) + \varphi_2(\xi + \varphi_1) = 0 \\ \Rightarrow (\xi + \varphi_1)(\xi^2 + \varphi_2) = 0. \end{aligned} \tag{3.3.3}$$

This equation contains three roots ξ_i for $i = 1, 2, 3$ which are given by

$$\begin{aligned} \xi_1 &= +i\sqrt{\varphi_2}, \\ \xi_2 &= -i\sqrt{\varphi_2}, \\ \xi_3 &= -\varphi_1. \end{aligned}$$

So, there exists a pair of purely imaginary eigenvalues for $\varphi_1\varphi_2 - \varphi_3 = 0$. To obtain the transversality condition, differentiating equation (3.2.7) with respect to θ, we get that

$$\begin{aligned} \frac{d\xi}{d\theta} &= -\frac{\xi^2\dot{\varphi}_1 + \xi\dot{\varphi}_2 + \dot{\varphi}_3}{3\xi^2 + 2\xi\varphi_1 + \varphi_2}\Big|_{\xi=i\sqrt{\varphi_2}} \\ &= -\frac{(\dot{\varphi}_3 - \varphi_2\dot{\varphi}_1 + i\sqrt{\varphi_2}\dot{\varphi}_2)}{(-2\varphi_2 + 2i\sqrt{\varphi_2}\varphi_1)} \\ &= \frac{(\dot{\varphi}_3\sqrt{\varphi_2} - \varphi_2\sqrt{\varphi_2}\dot{\varphi}_1 - \sqrt{\varphi_2}\varphi_1\dot{\varphi}_2) + i(\varphi_1\dot{\varphi}_3 - \varphi_1\varphi_2\dot{\varphi}_1 + \varphi_2\dot{\varphi}_2)}{2\sqrt{\varphi_2}(\varphi_1^2 + \varphi_2)} \\ &= \frac{\dot{\varphi}_3 - (\dot{\varphi}_1\varphi_2 + \dot{\varphi}_2\varphi_1)}{2(\varphi_1^2 + \varphi_2)} + i\frac{\sqrt{\varphi_2}(\varphi_1\dot{\varphi}_3 + \varphi_2\dot{\varphi}_2 - \dot{\varphi}_1\varphi_1\varphi_2)}{2\varphi_2(\varphi_1^2 + \varphi_2)}. \end{aligned} \tag{3.3.4}$$

Now, using (3.3.4),

$$\begin{aligned} Re\left(\frac{d\xi}{d\theta}\right)\Big|_{\theta=\theta^*} &= \frac{d(Re\xi)}{d\theta}\Big|_{\theta=\theta^*} \\ &= \frac{\dot{\varphi}_3 - (\dot{\varphi}_1\varphi_2 + \dot{\varphi}_2\varphi_1)}{2(\varphi_1^2 + \varphi_2)} > 0. \end{aligned} \tag{3.3.5}$$

i.e.

$$\dot{\varphi}_3 > (\dot{\varphi}_1\varphi_2 + \dot{\varphi}_2\varphi_1). \tag{3.3.6}$$

Thus, we achieve the transversality condition (3.3.6) for which Hopf bifurcation occurs at the critical value of $\theta = \theta^*$.
In view of the above discussion, we now present the following theorem.

Theorem 3.3.1 *The system (3.1.2) exhibits Hopf bifurcation around the interior equilibrium E^* at $\theta = \theta^* \in (0, 1)$ if and only if the following conditions hold:*

1. $\Psi(\theta^*) = 0$
2. $\dot{\varphi}_3 > (\dot{\varphi}_1\varphi_2 + \dot{\varphi}_2\varphi_1)$
3. *All the other eigenvalues have negative real parts*

where $\xi(\theta)$ is purely imaginary at the critical value of $\theta = \theta^*$.

Table 3.1: **List of parameter values used in numerical simulation for system (3.1.2)**

Parameter	Parameter definition	Assigned Value (Unit)	Range
r_1	growth rate of healthy cell	$0.4(\text{day}^{-1})$	-
r_2	growth rate of *M. leprae*	$0.1(\text{day}^{-1})$	-
K	carrying capacity of healthy cell	$800(\text{mm}^{-3})$	500- 1200
N	carrying capacity of bacteria	$530(\text{mm}^{-3})$	500-600
δ	natural death rate of infected cell	$0.1(\text{day}^{-1})$	-
λ	infection rate of healthy cell	$0.00032(\text{mm}^3$ $\text{day}^{-1})$	0.00032-0.0005
ν	proliferation rate of free bacteria	$0.3(\text{day}^{-1})$	0.04-0.4
γ	bacteria clearance rate	$0.00024(\text{mm}^3$ $\text{day}^{-1})$	0.0002-0.00034
t_{max}	maximum time	3000	-
p	step size parameter	0.1	-

3.4 Numerical Simulations

In this Section, we have studied the dynamics of our system represented by system (3.1.2) numerically by using Matlab 2016A and also validated these results with our analytical findings. For numerical simulation, most of the parameter values and their ranges have been chosen from Table 3.1 and collected from Chapter 2 and some previous experimental studies [Wilder-Smith and Van Brakel (2008); Rees (1994)]. We choose the initial values in number dependent according to the cardinal rule of scientific hypothesis. For all of our numerical results, we have chosen the value of the step size parameter $p = 0.1$.

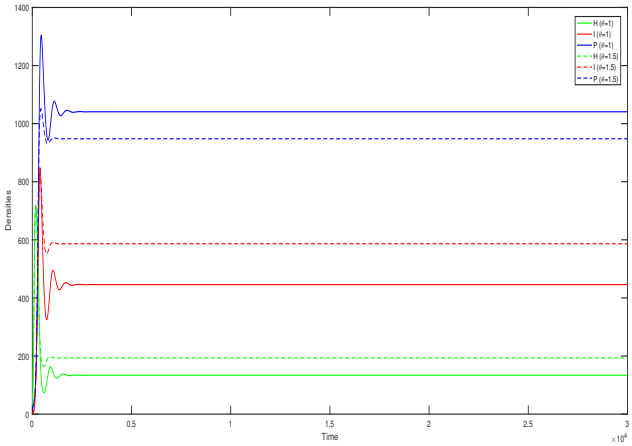

Figure 3.1: Time series plot of the densities of healthy Schwann cells, infected Schwann cells and M. leprae bacteria for $\theta = 1$ (denoted by solid lines) and the same for $\theta = 1.5$ (denoted by the dotted lines) for system (3.1.2). Here, we have chosen the values of $r_1 = 0.4$, $r_2 = 0.1$, $K = 800$, $N = 530$, $\lambda = 0.00034$, $\nu = 0.29$, $\gamma = 0.0003$ and the other parameter values are taken from Table 3.1.

In Figure 3.1, we have demonstrated the behaviour of the trajectories of our model cell populations for system (3.1.2) by the solid lines, choosing the value of the shape parameter $\theta = 1$. Incorporating the value of $\theta = 1$ in system (3.1.2) actually makes the theta-logistic growth of *M. leprae* bacteria into a simple classical logistic growth. All of our model cell population trajectories fluctuate slightly at the beginning and after almost 1200 days, a stable density of 170 mm^{-3}, 420 mm^{-3} and 1030 mm^{-3} are attained by the healthy Schwann cells (x_h), infected Schwann cells(x_i) and *M. leprae* bacteria (M_l), respectively. Also, in Figure 3.1, the densities of our system populations are plotted as time increases for the value of $\theta = 1.5$ and it is represented by the dotted line trajectories. We can see that a stable cell concentration of 195 mm^{-3}, 590 mm^{-3} and 970 mm^{-3} are achieved by the healthy

Schwann cells, infected Schwann cells and *M. leprae* bacteria, respectively, after 1000 days. In comparison with the solid line trajectories for $\theta = 1$, we can get a conclusion that after a little initial oscillations, densities of the system populations achieve stability more early if the value of θ increases from $\theta = 1$ to $\theta = 1.5$.

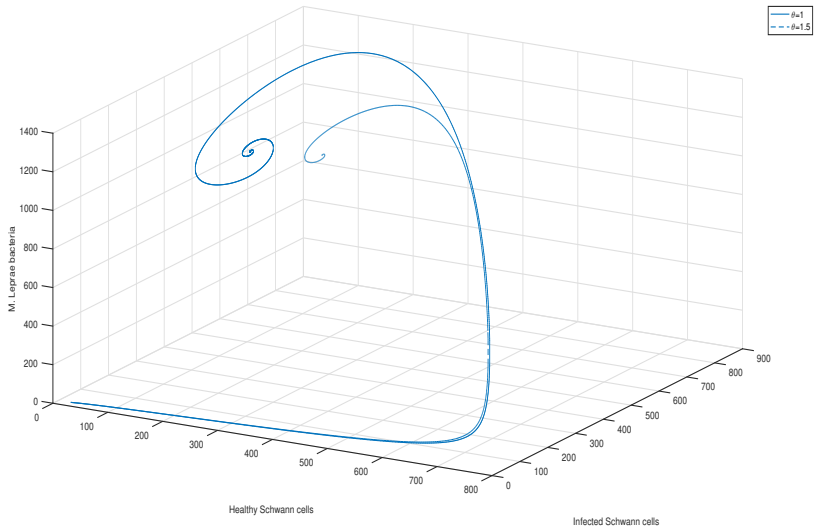

Figure 3.2: Phase plots of x_h cells, x_i cells and M_l bacteria population for system (3.1.2) corresponding to Figure 3.1. Here, the two values of θ are taken as $\theta = 1$ and $\theta = 1.5$ for generating the Figures. The initial values are taken as $(x_h, x_i, M_l) = (30, 5, 15)$. Other parameter values are collected from Table 3.1.

Phase diagrams of x_h, x_i and M_l corresponding to Figure 3.1 for both the values of $\theta = 1$ and $\theta = 1.5$ have been depicted in Figure 3.2.

In Figure 3.3, we have shown that for $\theta = 0.5$, trajectories of the cell populations oscillate more rapidly about 1.2×10^4 days and then gradually tend to proceed toward its stable region. If the value of θ is decreased further to $\theta = 0.3$ then behaviour of the system trajectories suddenly alters which is illustrated in Figure 3.4. For $\theta = 0.3 < 0.48$, the system (3.1.2) becomes unstable and periodic oscillations are observed after almost 2000 days. From this findings, it is evident that for $\theta > 0.48$, our system is asymptotically stable at the interior equilibrium point $E^* = (x_h^*, x_i^*, M_l^*)$ and for $\theta < 0.48$, Hopf bifurcating periodic solution begins to exist. Hence, we can interpret that our system (3.1.2) exhibits a rich dynamics if the value of θ decreases from the value of $\theta = 1$. Thus, incorporating theta-logistic growth instead of classical logistic one for the growth rate of *M. leprae* bacteria is more realistic and flexible in nature.

Figure 3.5 exhibits the phase portrait of x_h cells, x_i cells and M_l bacteria population for

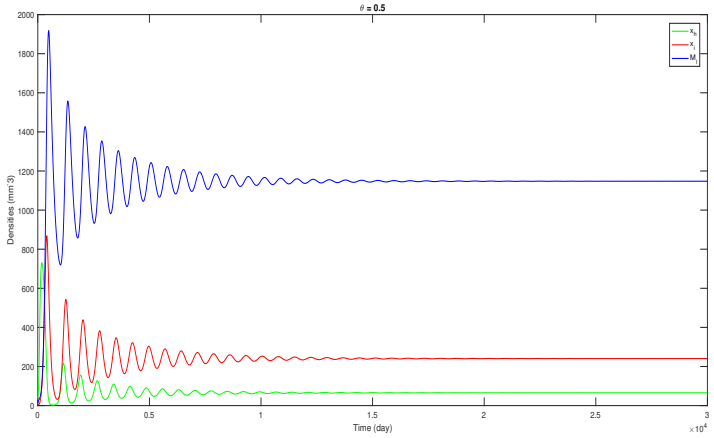

Figure 3.3: Time series plot of the densities of x_h, x_i and M_l for $\theta = 0.5$. Values of the parameters are chosen as $K = 800$, $N = 530$, $\lambda = 0.00038$, $\nu = 0.34$, $\gamma = 0.0003$ and the other parameter values are taken from Table 3.1.

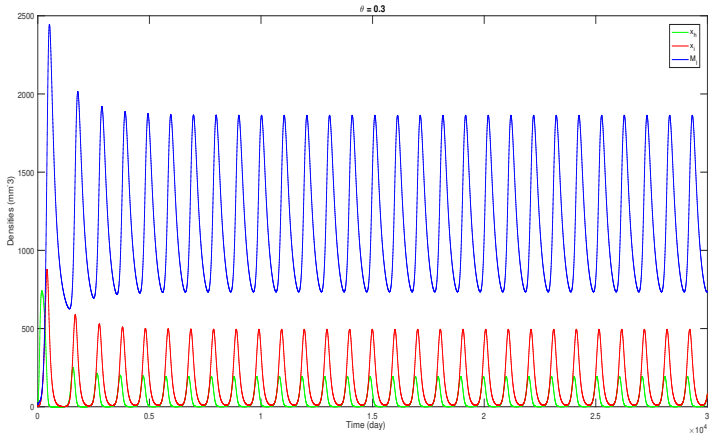

Figure 3.4: Time series plot of the densities of x_h, x_i and M_l for $\theta = 0.3$. We choose the values of the parameters as $K = 800$, $N = 530$, $\lambda = 0.00038$, $\nu = 0.34$, $\gamma = 0.0003$ and the other parameter values are taken from Table 3.1.

system (3.1.2) for $\theta = 0.5$ while phase diagram of system (3.1.2) for the value of $\theta = 0.3$ has been illustrated in Figure 3.6. From Figure 3.5, we can clearly see that system (3.1.2) starting with the initial values $(30, 5, 15)$ and finally converges to the interior equilibrium point $E^* = (x_h^*, x_i^*, M_l^*)$. Also, the phase portrait of the system populations displayed in Figure 3.6 indicates occurrence of limit cycles. In particular, it reflects the periodic oscillatory behaviour of the densities of the model cell populations starting from the same initial values.

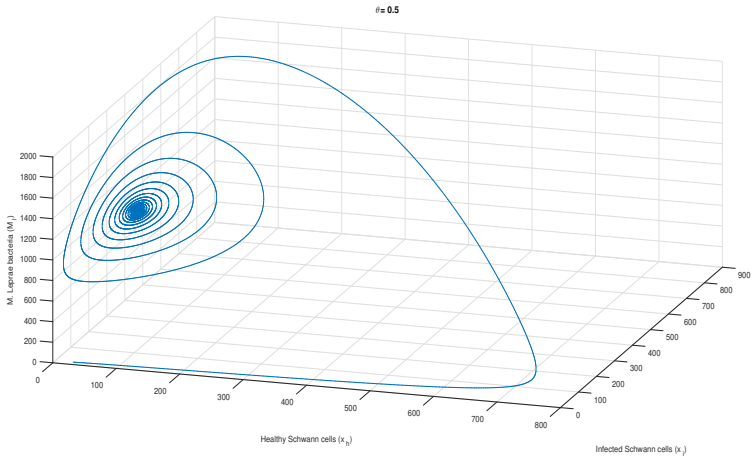

Figure 3.5: Phase plot of x_h cells, x_i cells and M_l bacteria population for system (3.1.2) for the value of $\theta = 0.5$ corresponding to Figure 3.3. The initial values are taken as $(x_h, x_i, M_l) = (30, 5, 15)$. The other parameter values are collected from Table 3.1.

Our present study emphasizes a special importance for the investigation of Hopf bifurcation for our discrete-time based system (3.1.2). The bifurcation diagram of the densities of our model populations with respect to the shape parameter θ has been depicted in Figure 3.7. From the appearance of periodic solutions and presence of limit cycles in the phase diagram, we can confirm that system (3.1.2) undergoes a Hopf bifurcation whenever the value of θ crosses the critical value $\theta = \theta^* = 0.48$, which completely clarifies our analytical findings in Section 3.3. Here, all the other parameter values are chosen from Table 3.1.

In Figure 3.8, the domain of stability of the interior equilibrium $E^* = (x_h^*, x_i^*, M_l^*)$ of system (3.1.2) has been manifested by varying r_2 i.e. the intrinsic growth rate of *M. leprae* bacteria and the shape parameter θ. This completely justifies the analytical findings described in (3.2.2). If all the conditions denoted by (3.2.8) hold true, then the endemic equilibrium E^* of system (3.1.2) exist and it will be locally asymptotically stable for any value of θ as depicted in Figure 3.8.

3.5 Discussion

In this Chapter, we have constituted and experimented with a discrete-time-based cell dynamical mathematical model on leprosy. As we have discussed previously, that mathematical model in a discrete-time setup exhibits a much more versatile set of results in terms of numerical simulations than continuous-time models. We have studied system (3.1.2) for different values of shape parameter θ. For the values of $\theta = 1$ i.e. in the classical logistic scenario

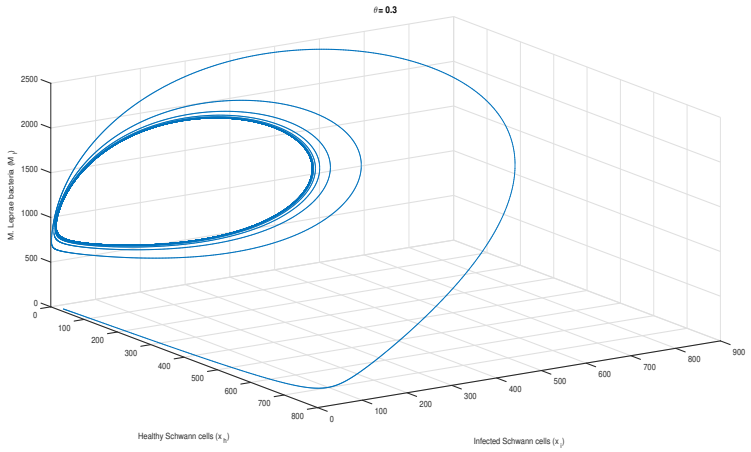

Figure 3.6: Phase plot of x_h cells, x_i cells and M_l for system (3.1.2) for the value of $\theta = 0.3$ corresponding to Figure 3.4. The initial values are taken as $(x_h, x_i, M_l) = (30, 5, 15)$.

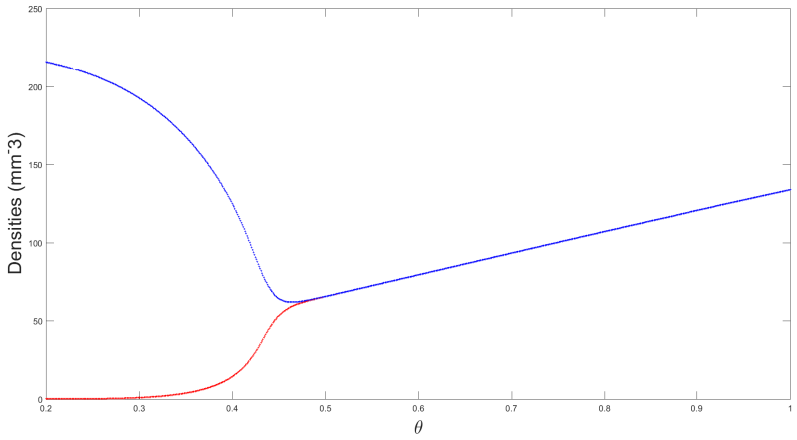

Figure 3.7: Bifurcation diagram of the densities of x_h cells, x_i cells and M_l bacteria with respect to the shape parameter θ for system (3.1.2). Values of the parameters used here are given as: $r_1 = 0.4$, $r_2 = 0.1$, $K = 780$, $N = 550$, $\lambda = 0.00036$, $\nu = 0.31$, $\gamma = 0.0003$ and the other parameter values are collected from Table 3.1.

and also for $\theta = 1.5 > 1$, the system has responded almost similarly. From the time series plots depicted in Figure 3.1, we can see that all the model population densities gain stability after slight initial fluctuations while for the values of $\theta < 1$, a high range of oscillations are noticed for a larger period of time. Actually for the value of $\theta = 0.3 < 0.48$, the system becomes unstable because the value of θ crosses the critical value $\theta^* = 0.48$ in this case.

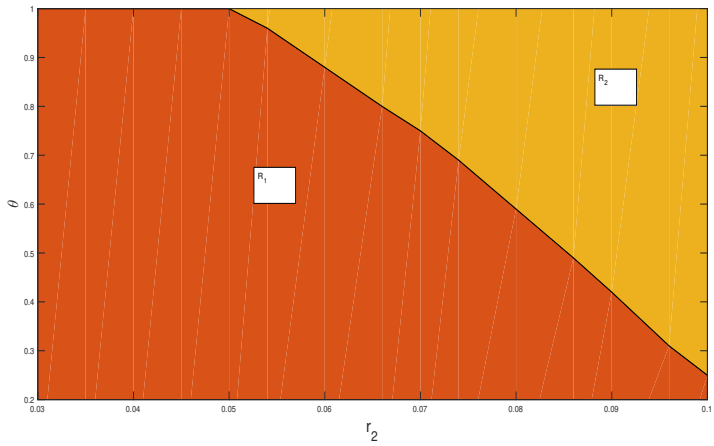

Figure 3.8: Stability region of the interior equilibrium with respect to θ and r_2. Values of the parameters used here are given as: $r_1 = 0.4$, $K = 820$, $N = 530$, $\lambda = 0.00034$, $\nu = 0.32$, $\gamma = 0.00028$. All the other parameter values are chosen from Table 3.1.

The phase diagram demonstrated in Figure 3.5 suggests that all the cell populations with initial values $(30, 5, 15)$ ultimately converge to E^* while on the contrary, the phase plot in Figure 3.6 portrays that for $\theta = 0.3$, the system gives rise to limit cycles. The occurrence of Hopf bifurcation for our formulated system has been confirmed in Section 3.3. Also, we have derived the transversality conditions given by (3.3.6) in Theorem 3.3.1 for which Hopf bifurcating periodic solutions appear for our system (3.1.2) around the interior equilibrium E^*.

Our present study explicitly suggests that choosing the growth of *M. leprae* in a density-dependence manner is certainly needed to decode the disease dissemination process. Both the analytical and numerical findings indicate that the per capita growth rate of *M. leprae* not only controls the infection progression but it also strongly regulates the generation of free bacteria which are capable of further transmitting the infection to the whole human body. Finally, we can conclude our current study by asserting that considering the density-dependent theta logistic approach for *M. leprae* bacteria is certainly a very beneficial and essential tool to overcome the obstacles for constructing a perfect control strategy for leprosy and it should definitely be adopted for any future attempt to implement a novel drug therapeutic regimen more accurately to eliminate the disease from mankind.

Chapter 4

Comparisons Between Two Different Variants of Delay-induced Mathematical Models for Interpreting Leprosy Pathogenesis and the Corresponding Optimal Control Schedules

Involving intracellular delay into a mathematical model and investigating the delayed systems by incorporating optimal control is of great importance to study the cell-to-cell interactions of the disease leprosy. Keeping this in mind, shifting our focus from the discretized system developed in the previous Chapter, we have now proposed two different variants of delay-induced mathematical models with time delay in the process of proliferation of *M. leprae* bacteria from the infected cells and a similar delay to indicate the time-lag both in the proliferation process and the infection of healthy cells after getting attached with the bacterium. In this Chapter[4], we have performed a comparative study between these two delayed systems equipped with optimal control therapeutic approach to determine which one acts better to unravel the complexities of the transmission and dissemination of leprosy into a human body as far as scheduling a perfect drug dose regime depending on this analysis remains our

[4] *The major portion of this chapter is published in the journal Optimal Control, Applications and Methods, Wiley, 2023.*

main priority. Stability analysis, Hopf-bifurcation analysis, existence of oscillatory solutions are examined and corresponding transversality conditions are evaluated analytically. Also, existence of optimal control solutions are demonstrated in detail. To achieve the optimal control profiles of the drug therapies and to obtain the whole optimality systems, Pontryagin's Minimum principle with delay in state are employed for our controlled systems. All the mathematical results are verified numerically and comparison of the numerical results with some recent clinical data are presented in this Chapter as well.

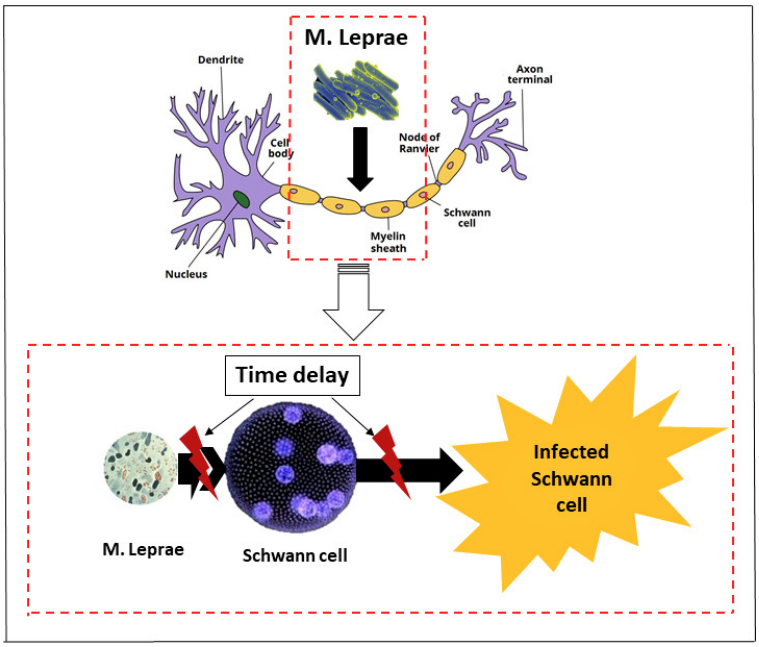

Figure 4.1: Schematic diagram of the interactions between the components of the model including the time delay factors.

4.1 Delayed Mathematical Model-I

4.1.1 Model formulation and uniqueness of the system solutions:

At first, we consider the three-dimensional ODE model on leprosy described in Chapter 2:

$$\begin{cases} \dfrac{dS_H(t)}{dt} = r_1 S_H(t)\Big(1 - \dfrac{S_H(t)}{k_1}\Big) - \lambda_1 S_H(t) B(t), \\ \dfrac{dS_I(t)}{dt} = \lambda_1 S_H(t) B(t) - \mu S_I(t), \\ \dfrac{dB(t)}{dt} = r_2 B(t)\Big(1 - \dfrac{B(t)}{k_2}\Big) - \eta S_H(t) B(t) + \alpha S_I(t). \end{cases} \tag{4.1.1}$$

- $S_H(t)$, $S_I(t)$ and $B(t)$ are the concentrations of healthy Schwann cells, infected Schwann cells and *M. leprae* bacteria, respectively, for any time t.

- Logistic growth rate is assumed for both healthy Schwann cells and bacteria population where we have denoted the intrinsic growth rate and the carrying capacity of the healthy Schwann cell population by r_1 and k_1 and the same for the bacteria population are denoted by r_2 and k_2, respectively.

- The interaction rate of *M. leprae* bacteria and healthy Schwann cells is considered the same as the infection rate of healthy Schwann cells by bacteria and it is represented by λ_1. New free bacteria proliferate from infected cells at a rate α.

- The natural mortality rate of infected Schwann cells and the rate of bacterial clearance due to infection are represented by μ and η, respectively.

  Based on these definitions of the system parameters from the physical interpretations presented above, we can see that the parameters denote different rates such as growth rates, death rates, interaction rate and proliferation rate and hence, can never be negative or zero. Thus, all the parameters $r_1, k_1, r_2, k_2, \lambda_1, \mu, \eta, \alpha$ used in the system (4.1.1) are assumed to be positive from the fundamental biological point of view.

The process of production of new free bacteria from an infected Schwann cell is not instantaneous. Here, we have introduced a discrete intracellular time delay into system (4.1.1) to describe specifically the time between the infection of a Schwann cell and proliferation of new free *M. leprae* bacteria from the infected cells. The interaction process has been depicted in Figure 4.1. Hence, based on the above assumptions, the delayed mathematical model is

constructed as follows:

$$\begin{cases} \dfrac{dS_H(t)}{dt} = r_1 S_H(t)\Big(1 - \dfrac{S_H(t)}{k_1}\Big) - \lambda_1 S_H(t) B(t), \\ \dfrac{dS_I(t)}{dt} = \lambda_1 S_H(t-\tau) B(t-\tau) - \mu S_I(t), \\ \dfrac{dB(t)}{dt} = r_2 B(t)\Big(1 - \dfrac{B(t)}{k_2}\Big) - \eta S_H(t) B(t) + \alpha S_I(t), \end{cases} \tag{4.1.2}$$

with initial conditions:

$$S_H(\theta) > 0, \quad S_I(\theta) > 0 \; and \; B(\theta) > 0 \;\text{ where }\; \theta \in [-\tau, 0]. \tag{4.1.3}$$

Here, τ represents the time delay in days. Let us denote $C = C([-\tau, 0], \mathbb{R}^3_+)$ be the Banach space of all continuous functions $\varphi : [-\tau, 0] \longrightarrow \mathbb{R}^3_+$ equipped with the usual supremum norm defined by

$$\|\varphi\| = \sup_{-\tau<\theta<0} \{|\varphi_1(\theta)|, |\varphi_2(\theta)|, |\varphi_3(\theta)|\},$$

where $\varphi = (\varphi_1, \varphi_2, \varphi_3)$. The initial conditions for system (2.1.1) are given as: $S_H(\theta) = \varphi_1(\theta)$, $S_I(\theta) = \varphi_2(\theta)$, $B(\theta) = \varphi_3(\theta)$ with $\theta \in [-\tau, 0]$. To make the model biologically justified, the initial functions are assumed as $\varphi_i(\theta) \geq 0$ for $\theta \in [-\tau, 0]$ and $\varphi_i(0) > 0$ for all $i = 1, 2, 3$. Now, by using the fundamental theory of functional differential equations, we can guarantee the uniqueness of solutions of system (4.1.2) with initial conditions (4.1.3).

4.1.2 Positivity and boundedness:

Positivity of the solutions of a system means the survival of the model populations. In this Subsection, we have established the positivity of the solutions of system (2.1.1) by the following theorem and also evaluated the region where system (2.1.1) is bounded.

Theorem 4.1.1 *All the solutions of system (4.1.2) with given initial conditions (4.1.3) are positive.*

Proof. We can see that the region $\mathbb{R}^3_+$ contains the solutions of system (4.1.2) and non-negativity of all these solutions for all $t > 0$ is a simple consequence of the application of Lemma 2 described in the article by [Yang et al. (1996)]. Let, $X = col(S_H(t), S_I(t), B(t)) \in \mathbb{R}^3_+$, $(\varphi_1(\theta), \varphi_2(\theta), \varphi_3(\theta)) \in C = C([-\tau, 0], \mathbb{R}^3_+)$ and

$$P(X) = \begin{pmatrix} P_1(X) \\ P_2(X) \\ P_3(X) \end{pmatrix} = \begin{pmatrix} r_1 S_H(t)\Big(1 - \frac{S_H(t)}{k_1}\Big) - \lambda_1 S_H(t) B(t) \\ \lambda_1 S_H(t-\tau) B(t-\tau) - \mu S_I(t) \\ r_2 B(t)\Big(1 - \frac{B(t)}{k_2}\Big) - \eta S_H(t) B(t) + \alpha S_I(t) \end{pmatrix}. \tag{4.1.4}$$

Then, system (4.1.2) can be re-written in the following form:

$$\frac{dX}{dt} = P(X) \tag{4.1.5}$$

where $X(\theta) = (\varphi_1(\theta), \varphi_2(\theta), \varphi_3(\theta)) \in C$ and $\varphi_1(0) > 0$, $\varphi_2(0) > 0$, $\varphi_3(0) > 0$. Now, from equation (4.1.4), we can see that whenever we choose $X(\theta) \in C$ with $S_H = 0$, $S_I = 0$ or $B = 0$, we obtain

$$P_i(X)|_{x_i=0,\ X\in\mathbb{R}^3_+} \geq 0, \quad i = 1, 2, 3$$

where $x_1(t) = S_H(t)$, $x_2(t) = S_I(t)$, $x_3(t) = B(t)$. Now, using the Lemma 2 by Yang et al. (1996) and the Theorem 1.1 by Bodnar et al. [Bodnar (2000)], any solution of (4.1.5) with $X(\theta) \in C$, say $X(t) = X(t, X(\theta))$, satisfies $X(\theta) \in \mathbb{R}^3_+$ for all $t \geq 0$. Hence, we can conclude that the solution of system (4.1.2) exists in $\mathbb{R}^3_+$ and remains non-negative for all $t > 0$. So, $\mathbb{R}^3_+$ is an invariant region for system (4.1.2).

The next theorem describes the boundedness and positive invariance of the delayed system (4.1.2). Before starting to prove the theorem, let us first present and briefly prove the following lemma.

Lemma 4.1.1 *Consider the following differential inequality given as:*

$$\frac{dU(t)}{dt} \leq A^2 - U^2(t)$$

where A is a positive real constant. Then, $U(t) \leq A$ holds whenever $U(0) \leq A$.

Proof. Rearranging the inequality

$$\frac{dU(t)}{dt} \leq A^2 - U^2(t),$$

we get that

$$\frac{dU(t)}{(A^2 - U^2(t))} \leq dt, \quad \text{where} \quad A > 0. \tag{4.1.6}$$

We now integrate (4.1.6) with the initial condition $U(0)$. Thus, we obtain the following inequality,

$$\frac{U(t) - A}{U(t) + A} \leq \frac{U(0) - A}{U(0) + A} e^{-2At}$$

which clearly indicates that $U(0) \leq A$ implies $U(t) \leq A$.

Another way of interpreting the result of Lemma 4.1.1 is to use the appearance of the slope field of an autonomous equation as a verification for the asymptotic behaviour of its

solutions without actually computing this rigorously. we can see that $\frac{dU(t)}{dt} = A^2 - U^2(t)$ is an autonomous differential equation of order 1 and $U(t) = A$ is a stable equilibrium solution of it. So, all the solutions $U(t)$ of this differential equation with initial condition $U(0) < A$, will surely approach $U(t) = A$ as $t \to \infty$.

Theorem 4.1.2 *Every positive solution of the system (4.1.2) with the given initial conditions (4.1.3) is ultimately bounded. Also, all such solutions of system (4.1.2) which starts within D_1 i.e. initiating or with initial values in D_1, finally come into the region D_1 and stay in it for all $t > 0$. D_1 is a region of attraction for system (4.1.2) and actually attracts all solutions initiating in the interior of the positive octant where D_1 is defined by*

$$D_1 = \Bigg\{ (S_H(t), S_I(t), B(t)) : 0 \le S_H(t) \le M,\ 0 \le S_H(t) + S_I(t) \le M\left(\frac{r_1}{\mu} + 1\right), \\ 0 \le B(t) \le \frac{k_2}{2} + \sqrt{\frac{k_2^2}{4} + \frac{\alpha k_2 M}{r_2}\left(\frac{r_1}{\mu} + 1\right)} \Bigg\},$$

where $M = \max\{k_1; S_H(0)\}$.

Proof. To prove the boundedness and to find the invariant region for system (4.1.2), we now consider the first equation of system (4.1.2) and try to predict the maximum concentration of healthy Schwann cells from which it follows that $\frac{dS_H}{dt} \le r_1 S_H\left(1 - \frac{S_H}{k_1}\right)$. Solving the above inequality and using a standard comparison argument, we get that

$$\limsup_{t\to\infty} S_H(t) \le M \tag{4.1.7}$$

where $M = \max\{k_1,\ S_H(0)\}$. Now, we consider the first and second equations of system (4.1.2). Adding these two equations while using (4.1.7) and assuming $(S_H + S_I)(t) = X(t)$, we get,

$$\frac{dX(t)}{dt} \le M(r_1 + \mu) - \mu X(t). \tag{4.1.8}$$

Applying the well-known comparison principle [Birkhoff and Rota (1978)] to (4.1.8), we obtain the inequality :

$$X(t) \le M\frac{(r_1 + \mu)}{\mu}(1 - e^{-\mu t}) + X(0)e^{-\mu t}, \quad t > 0. \tag{4.1.9}$$

For large values of t, we get $X(t) \le M\frac{(r_1+\mu)}{\mu}$ if $X(0) \le M\frac{(r_1+\mu)}{\mu}$ i.e.

$$S_H(t) + S_I(t) \le M\frac{(r_1 + \mu)}{\mu} \tag{4.1.10}$$

and it also implies

$$S_I(t) \leq M\frac{(r_1+\mu)}{\mu}. \tag{4.1.11}$$

Now, we consider the third equation of system (4.1.2) and using the inequality (4.1.11), we have

$$\frac{dB}{dt} \leq r_2 B - \frac{r_2 B^2}{k_2} + \alpha M(\frac{r_1}{\mu}+1). \tag{4.1.12}$$

Now, denoting $Z(t) = B(t) - \frac{k_2}{2}$, we can write the above inequation in the form

$$\frac{dZ}{dt} \leq \frac{r_2}{k_2}(\zeta^2 - Z^2) \tag{4.1.13}$$

where $\zeta = \sqrt{\frac{\alpha k_2 M}{r_2}(\frac{r_1}{\mu}+1) + \frac{k_2^2}{4}}$.
Now, applying the result of Lemma 4.1.1 to the inequality (4.1.13), we get

$$\limsup_{t\to\infty} Z(t) \leq \zeta \quad \text{if} \quad Z(0) \leq \zeta.$$

Returning to the original variable, this implies that

$$\limsup_{t\to\infty} B(t) \leq \frac{k_2}{2} + \sqrt{\frac{\alpha k_2 M}{r_2}(\frac{r_1}{\mu}+1) + \frac{k_2^2}{4}} \tag{4.1.14}$$

if

$$B(0) \leq \frac{k_2}{2} + \sqrt{\frac{\alpha k_2 M}{r_2}(\frac{r_1}{\mu}+1) + \frac{k_2^2}{4}}. \tag{4.1.15}$$

Thus, the region D_1 is bounded and all the solutions $(S_H(\mathrm{t}), S_I(\mathrm{t}), \mathrm{B(t)})^\top$ of system (4.1.2) with the non-negative initial conditions are ultimately bounded. All such solutions of system (4.1.2) that start within D_1, remain in the region for all $t > 0$. So, the set D_1 is a positively invariant set and acts as the region of attraction for system (4.1.2).

4.1.3 Stability of disease-free equilibrium and the basic reproduction number:

The non-delayed system (4.1.1) has two steady states. One is the disease-free equilibrium $E_0 = (k_1, 0, 0)$ and the another one is the positive endemic equilibrium $E^* = (S_H^*, S_I^*, B^*)$. Here, the basic reproduction number is defined as

$$\Re_0 = \frac{\alpha\lambda_1 k_1}{\mu(\eta k_1 - r_2)}. \tag{4.1.16}$$

We find that the delayed model given by system (4.1.2) also has two steady states. Without loss of generalization, we denote them by $E_0 = (k_1, 0, 0)$ and $E_1^* = (S_H^*, S_I^*, B^*)$. The values of S_H^*, S_I^* and B^* already have been established in Chapter 2.

Let us first define $x(t) = S_H(t) - \tilde{S_H}$, $y(t) = S_I(t) - \tilde{S}_I$ and $z(t) = B(t) - \tilde{B}$ where $\tilde{E} = (\tilde{S_H}, \tilde{S}_I, \tilde{B})$ is any steady state of the delayed system (4.1.2). Then the linearized form of the system (4.1.2) at $\tilde{E} = (\tilde{S_H}, \tilde{S}_I, \tilde{B})$ is given by

$$\begin{cases} \dfrac{dx(t)}{dt} = \Big(r_1 - \dfrac{2r_1\tilde{S_H}}{k_1} - \lambda_1\tilde{B}\Big)x(t) - \lambda_1\tilde{S_H}z(t), \\ \dfrac{dy(t)}{dt} = \lambda_1\tilde{B}x(t-\tau) - \mu y(t) + \lambda_1\tilde{S_H}z(t-\tau), \\ \dfrac{dz(t)}{dt} = -\eta\tilde{B}x(t) + \alpha y(t) + \Big(r_2 - \dfrac{2r_2\tilde{B}}{k_2} - \eta\tilde{S_H}\Big)z(t). \end{cases} \tag{4.1.17}$$

Now system (4.1.17) can be represented in following matrix form:

$$\frac{d}{dt}\begin{pmatrix} x(t) \\ y(t) \\ z(t) \end{pmatrix} = P\begin{pmatrix} x(t) \\ y(t) \\ z(t) \end{pmatrix} + Q\begin{pmatrix} x(t-\tau) \\ y(t-\tau) \\ z(t-\tau) \end{pmatrix} \tag{4.1.18}$$

where the 3×3 matrices P and Q are given by

$$P = \begin{pmatrix} (r_1 - \frac{2r_1}{k_1}\tilde{S_H} - \lambda_1\tilde{B}) & 0 & -\lambda_1\tilde{S_H} \\ 0 & -\mu & 0 \\ -\eta\tilde{B} & \alpha & (r_2 - \frac{2r_2}{k_2}\tilde{B} - \eta\tilde{S_H}) \end{pmatrix} \text{ and } Q = \begin{pmatrix} 0 & 0 & 0 \\ \lambda_1\tilde{B} & 0 & \lambda_1\tilde{S_H} \\ 0 & 0 & 0 \end{pmatrix}.$$

The characteristic equation of system (4.1.17) is given by

$$\Delta(\lambda) = |\lambda I - P - e^{-\lambda\tau}Q| = 0 \tag{4.1.19}$$

which implies that the characteristic equation of the jacobian matrix of the linearized form of system (4.1.2) at E_0 becomes $(\lambda + r_1)[(\lambda + \mu)(\lambda + \eta k_1 - r_2) - \lambda_1 k_1 \alpha e^{-\lambda\tau}] = 0$. From this equation, we can see clearly that $\lambda = -r_1$ is a negative root of the equation. So, the sign of the roots of the following equation will be dominant in determining the stability of E_0:

$$(\lambda + \mu)(\lambda + \eta k_1 - r_2) - \lambda_1 k_1 \alpha e^{-\lambda\tau} = 0. \tag{4.1.20}$$

By the following two cases, we can discuss the stability of the disease-free equilibrium E_0 for the system (4.1.2).

- **Case - I ($R_0 < 1$ and $\tau \geq 0$):** For $\tau = 0$, equation (4.1.20) becomes

$$\lambda^2 + (\eta k_1 - r_2 + \mu)\lambda + \mu(\eta k_1 - r_2) - \lambda_1 k_1 \alpha = 0. \tag{4.1.21}$$

For $\Re_0 < 1$, we get that $\lambda_1 k_1 \alpha < \mu(\eta k_1 - r_2) \implies (\eta k_1 - r_2) > \frac{\lambda_1 k_1 \alpha}{\mu} > 0$ which actually confirms that $(\eta k_1 - r_2 + \mu) > 0$. This implies that both the roots of equation (4.1.21) are negative and hence, for $\tau = 0$, E_0 is locally asymptotically stable whenever $\Re_0 < 1$. Let us assume, for $\tau > 0$, $\lambda = \kappa(\tau) + i\omega(\tau)$ is an eigenvalue of the characteristic equation (4.1.20) where $\omega(\tau) > 0$. Suppose, $\kappa(\tau) = 0$ for some $\tau > 0$. Now, substituting $\lambda = i\omega(\tau)$ in equation (4.1.20) and denoting $\omega(\tau)$ by simply ω , we obtain

$$-\omega^2 + i(\eta k_1 - r_2 + \mu)\omega - \lambda_1 k_1 \alpha(\cos \omega\tau - i \sin \omega\tau) + \mu(\eta k_1 - r_2) = 0. \tag{4.1.22}$$

Comparing the real and imaginary parts of equation (4.1.22), we get two equations. Squaring and adding these gives us:

$$\omega^4 + [(\eta k_1 - r_2)^2 + \mu^2]\omega^2 + [\mu^2(\eta k_1 - r_2)^2 - \lambda_1^2 k_1^2 \alpha^2] = 0. \tag{4.1.23}$$

Let, $z = \omega^2$ and hence, equation (4.1.23) becomes the following:

$$z^2 + [(\eta k_1 - r_2)^2 + \mu^2]z + [\mu^2(\eta k_1 - r_2)^2 - \lambda_1^2 k_1^2 \alpha^2] = 0 \tag{4.1.24}$$

It is evident that $\Re_0 < 1$ implies $\mu^2(\eta k_1 - r_2)^2 > \lambda_1^2 k_1^2 \alpha^2$ and thus, it follows that equation (4.1.24) does not possess any positive root. This implies that there exists no such ω for which $\lambda = i\omega(\tau)$ is a purely imaginary eigenvalue of the characteristic equation (4.1.20). As E_0 is locally asymptotically stable for $\tau = 0$ with $R_0 < 1$, it indicates that $\kappa(0) < 0$. Now, using the continuity in τ of the delayed system and the fact that $\kappa(\tau)$ is never zero for all values of τ, we have that $\kappa(\tau) < 0$ for all $\tau > 0$ with $R_0 < 1$. So, finally, we can conclude that equation (4.1.20) have all the roots with negative real parts and thus, E_0 is locally asymptotically stable for $\Re_0 < 1$ and for all values of $\tau > 0$.

- **Case - II ($R_0 > 1$ and $\tau \geq 0$):** Let us assume that $h(\omega) = \omega^4 + [(\eta k_1 - r_2)^2 + \mu^2]\omega^2 + [\mu^2(\eta k_1 - r_2)^2 - \lambda_1^2 k_1^2 \alpha^2]$. For $\Re_0 > 1$, we can observe that $\mu(\eta k_1 - r_2) < \lambda_1 k_1 \alpha$ and it follows that there exists a positive root of equation (4.1.21). So, E_0 becomes unstable

in this case. Also,

$$\frac{\partial h}{\partial \omega} = 4\omega^3 + 2[(\eta k_1 - r_2)^2 + \mu^2]\omega > 0.$$

Using this inequality and the results [Cooke and Van Den Driessche (1986); Freedman and Kuang (1991)], we can say that E_0 is unstable for all values of $\tau \geq 0$ whenever $\Re_0 > 1$.

Finally, in view of the previous two cases, we can conclude the result about local asymptotic stability of disease-free equilibrium E_0 for system (4.1.2) by the following theorem.

Theorem 4.1.3 *The disease-free equilibrium E_0 of system (4.1.2) is locally asymptotically stable for $\Re_0 < 1$ and becomes unstable for $\Re_0 > 1$ for all values of $\tau \geq 0$.*

4.1.4 Stability analysis of the endemic equilibrium:

Assuming $a_0 = [\lambda_1 k_1 k_2(\lambda_1\alpha - \mu\eta) - \mu r_1 r_2]$, the values of S_H^*, S_I^* and B^* are given by the formulae: $S_H^* = r_2 k_1 \mu a_0^{-1}(\lambda_1 k_2 - r_1)$, $S_I^* = \lambda_1 k_1 r_2 a_0^{-2}[\lambda_1 k_2(\lambda_1^2 k_1 k_2\alpha + r_1 r_2\mu + r_1 k_1\mu\eta + r_1 r_2\mu) - \lambda_1^2 k_2(k_1 k_2\mu\eta + k_2 r_2\mu + k_1 r_1\alpha) - r_1^2 r_2\mu]$ and $B^* = r_1 a_0^{-1}\lambda_1^{-1}[(\lambda_1^2 k_1 k_2\alpha + r_1 r_2\mu) - (\lambda_1 k_1 k_2\mu\eta + \lambda_1 k_2 r_2\mu)]$. Now, using (4.1.19), we obtain the characteristic equation of the linearized form of system (4.1.2) at E_1^* as

$$\lambda^3 + A_1\lambda^2 + A_2\lambda + A_3\lambda e^{-\lambda\tau} + A_4 e^{-\lambda\tau} + A_5 = 0 \tag{4.1.25}$$

where the coefficients are

$$A_1 = \mu + \Big(\lambda_1 + \frac{2r_2}{k_2}\Big)B^* + \Big(\eta + \frac{2r_1}{k_1}\Big)S_H^* - (r_1 + r_2), \quad A_2 = \mu(a_1 + a_2) + a_1 a_2 - \lambda_1\eta S_H^* B^*, \tag{4.1.26}$$

$$A_3 = -\lambda_1\alpha S_H^*, \quad A_4 = \lambda_1^2\alpha S_H^* B^* - a_1\lambda_1\alpha S_H^*, \quad A_5 = a_1 a_2\mu - \lambda_1\mu\eta S_H^* B^* \quad \text{and} \tag{4.1.27}$$

$$a_1 = \lambda_1 B^* + \frac{2r_1}{k_1}S_H^* - r_1, \quad a_2 = \eta S_H^* + \frac{2r_2}{k_2}B^* - r_2. \tag{4.1.28}$$

The condition for E_1^* to be asymptotically stable is that equation (4.1.25) will have all the roots with negative real parts. Let us put $\tau = 0$ in equation (4.1.25). Hence, we will get equation (2.2.7) in the Chapter 2 which actually refers to the characteristic equation of the non-delayed system (4.1.1) and let us assume that all the roots of this equation have negative real parts. This assumption clearly leads us to the conditions derived in Chapter 2 obtained as an application of the well-known Routh-Hurwitz criteria. Let $\lambda = \sigma_1(\tau) + i\sigma_2(\tau)$ with $\sigma_2 > 0$ where σ_1, σ_2 are both dependent on τ. Here, stability of the endemic equilibrium E^* of the system without delay (4.1.1) implies that for $\tau = 0$, $\sigma_1(0) < 0$. Using the neighbourhood

property of continuous function, we can also say that there exists $\epsilon > 0$ such that for all values of $\tau \in (0, \epsilon)$, $\sigma_1(\tau)$ remains negative. Let us assume that there exists a value of $\tau = \tau^{'} > 0$ for which $\sigma_1(\tau^{'}) = 0$ i.e $\lambda = i\sigma_2(\tau^{'})$. For this specific value of λ (as a root of the characteristic equation (4.1.25)) with $Re(\lambda) = \sigma_1(\tau^{'}) = 0$ and also for any other values of λ with $Re(\lambda) = \sigma_1(\tau) > 0$, E_1^* simply becomes unstable as stability requires all the roots of equation (4.1.25) with negative real parts. Now, putting $\lambda = i\sigma_2$ in (4.1.25),

$$-i(\sigma_2(\tau^{'}))^3 - A_1(\sigma_2(\tau^{'}))^2 + iA_2\sigma_2(\tau^{'}) + iA_3\sigma_2(\tau^{'})e^{-i\sigma_2(\tau^{'})\tau} + A_4e^{-i\sigma_2(\tau^{'})\tau} + A_5 = 0. \quad (4.1.29)$$

Comparing the real and imaginary parts of both sides of equation (4.1.29), two new equations will be obtained. Squaring these two equations and then adding, we get that $\Big((\sigma_2(\tau^{'}))^3 - A_2\sigma_2(\tau^{'})\Big)^2 + \Big(A_5 - A_1(\sigma_2(\tau^{'}))^2\Big)^2 = A_4^2 + A_3^2(\sigma_2(\tau^{'}))^2$. This equation can be rewritten as

$$f(\xi) = \xi^3 + p\xi^2 + q\xi + r = 0 \quad (4.1.30)$$

where $p = A_1^2 - 2A_2$, $q = A_2^2 - A_3^2 - 2A_1A_5$, $r = A_5^2 - A_4^2$, $\xi = \sigma_2(\tau^{'})^2$. We can see that the derived equation is $f'(\xi) = 3\xi^2 + 2p\xi + q = 0$. Now, if the following two conditions i.e. (1) $A_5^2 - A_4^2 \geq 0$ and (2) $(A_1^2 - 2A_2)^2 \leq 3(A_2^2 - A_3^2 - 2A_1A_5)$ hold then firstly, $f(0) = r \geq 0$ and also $f'(\xi) = 3\xi^2 + 2p\xi + q \geq 0$ for all $\xi > 0$. There exists at most one value of ξ for which $f'(\xi) = 0$. Hence, we can see that $f(\xi) > 0$ for all $\xi > 0$ and it implies that equation (2.2.6) can not have any positive real root. This contradiction leads us to the fact that $\lambda = i\sigma_2(\tau^{'})$ can not be an eigenvalue of the characteristic equation (4.1.25). So, equation (4.1.25) does not have any purely imaginary eigenvalue for all values of $\tau > 0$. Now, Rouche's Theorem for transcendental equation [Dieudonné (2011)] tells us that equation (4.1.25) can have roots with positive real parts if and only if it has purely imaginary roots. Hence, we can get the conclusion that every root of (4.1.25) lies in the open left half plane and it certainly makes E_1^* asymptotically stable for all $\tau > 0$.

In view of the above investigations for the stability of the interior equilibrium $E_1^* = (S_H^*, S_I^*, B^*)$ of the delay-induced system (4.1.2), we can construct the following theorem.

Theorem 4.1.4 *Suppose, Routh-Hurwitz criteria for the non-delayed system (4.1.1) holds along with the following two inequalities i.e.*
(1) $A_5^2 - A_4^2 \geq 0$,
(2) $(A_1^2 - 2A_2)^2 \leq 3(A_2^2 - A_3^2 - 2A_1A_5)$,
where the $A_i's$ *for* $i = 1, 2$ *are given by formulae (4.1.26) - (4.1.28). Then, the positive endemic equilibrium* E_1^* *of the delay-induced system (4.1.2) is locally asymptotically stable for all values of the time delay* $\tau \geq 0$.

4.2 Delayed Mathematical Model-II

We now introduce the same amount of time delay τ in the second term of the first equation in our first delayed system (4.1.2) i.e. in the term $-\lambda_1 S_H B$ to precisely indicate the necessary time lag between the attachment of *M. leprae* bacteria with the healthy Schwann cells via different receptor-mediated mechanisms and finally the healthy cells getting infected. The interaction process has been described in Figure 4.1. So, our second delayed mathematical model takes the following form:

$$\begin{cases} \dfrac{dS_H(t)}{dt} = r_1 S_H(t)(1 - \dfrac{S_H(t)}{k_1}) - \lambda_1 S_H(t-\tau)B(t-\tau), \\ \dfrac{dS_I(t)}{dt} = \lambda_1 S_H(t-\tau)B(t-\tau) - \mu S_I(t), \\ \dfrac{dB(t)}{dt} = r_2 B(t)(1 - \dfrac{B(t)}{k_2}) - \eta S_H(t)B(t) + \alpha S_I(t), \end{cases} \tag{4.2.1}$$

where the initial conditions are given as

$$S_H(\theta) > 0, \quad S_I(\theta) > 0 \; and \; B(\theta) > 0 \;\text{ where }\; \theta \in [-\tau, 0]. \tag{4.2.2}$$

4.2.1 Positive invariance and boundedness:

To make a mathematical model biologically realistic, showing positivity of the populations of the model is very important. We now have the following theorem to demonstrate the positive invariance of the delayed system (4.2.1).

Theorem 4.2.1 *All the solutions of system (4.2.1) with the given initial conditions (4.2.2) are positive.*

Proof. We skip the detailed proof of this theorem as it is straightforward and similar to the proof of (4.1.1) in the Subsection 2.2. Using Lemma 2 [Yang et al. (1996)], it is easy to observe that all the solutions of system (4.2.1) with the initial conditions lie in $\mathbb{R}^3_+$ and remain non-negative for all $t > 0$ and as a result of this, $\mathbb{R}^3_+$ becomes an invariant region for system (4.2.1).

To show the boundedness of system (4.2.1), we need to look at the basic non-delayed mathematical model (4.1.1) for which boundedness is established already. Similarly, approaching in the manner as demonstrated in Theorem 4.1.2 in Section 4.1.2, we obtain that

the region of attraction D_2 of the delayed system (4.2.1) also becomes the following:

$$D_2 = \Big\{(S_H(t), S_I(t), B(t)) : 0 \leq S_H(t) \leq M,\ 0 \leq S_H(t) + S_I(t) \leq M\left(\frac{r_1}{\mu} + 1\right),$$
$$0 \leq B(t) \leq \frac{k_2}{2} + \sqrt{\frac{k_2^2}{4} + \frac{\alpha k_2 M}{r_2}\left(\frac{r_1}{\mu} + 1\right)}\Big\},$$

where $M = \max\{k_1; S_H(0)\}$. Thus, the result implies that D_2 is a positively invariant set and all the solutions of system (4.2.1) with initial values in D_2 are also attracted and lie in the region D_2.

Remark 4.2.1 *The disease-free equilibrium for system (4.2.1) is also denoted by* $E_0 = (k_1, 0, 0)$ *where* k_1 *is the carrying capacity of the healthy Schwann cell population. In an approach similar to the analysis of the disease-free equilibrium of system (4.1.2), we can state that for all values of* $\tau \geq 0$*, the disease-free equilibrium* E_0 *of system (4.2.1) also remains locally asymptotically stable whenever the basic reproduction number* $\Re_0 < 1$ *and becomes unstable otherwise. In the very next Section, we are now interested to proceed to the detailed discussion of the stability analysis of the positive endemic equilibrium for system (4.2.1).*

4.2.2 Asymptotic stability of the endemic equilibrium:

System (4.2.1) possesses an endemic equilibrium point which we denote by $E_2^* = (S_H^*, S_I^*, B^*)$ where values of S_H^*, S_I^*, B^* are same as given by the formulae in Appendix C. To demonstrate the local asymptotic stability of E_2^*, let us assume $u(t) = S_H(t) - S_H^*$, $v(t) = S_I(t) - S_I^*$ and $w(t) = B(t) - B^*$ be the perturbed variables. Then, linearizing system (4.2.1) about E_2^*, we have

$$\frac{dY}{dt} = M_0 Y(t) + N_0 Y(t - \tau), \tag{4.2.3}$$

where $Y(t) = (u(t), v(t), w(t))^\top$ and matrices M_0 and N_0 are given by

$$M_0 = \begin{pmatrix} (r_1 - \frac{2r_1}{k_1}S_H{}^*) & 0 & 0 \\ 0 & -\mu & 0 \\ -\eta B^* & \alpha & (r_2 - \frac{2r_2}{k_2}B^* - \eta S_H^*) \end{pmatrix} \text{ and } N_0 = \begin{pmatrix} -\lambda_1 B^* & 0 & -\lambda_1 S_H^* \\ \lambda_1 B^* & 0 & \lambda_1 S_H^* \\ 0 & 0 & 0 \end{pmatrix}.$$

The characteristic equation of the delayed system (4.2.1) is given by $\det[\varrho I - M_0 - e^{-\varrho\tau} N_0] = 0$. Expanding this equation, we get

$$\varrho^3 + L_1\varrho^2 + L_2\varrho + L_3\varrho^2 e^{-\varrho\tau} + L_4\varrho e^{-\varrho\tau} + L_5 e^{-\varrho\tau} + L_6 = 0 \tag{4.2.4}$$

where

$$L_1 = \mu + a_1 + a_2 - \lambda_1 B^*, \quad L_2 = \mu a_2 + (a_1 - \lambda_1 B^*)(\mu + a_2), \quad L_3 = \lambda_1 B^*,$$
$$L_4 = (\mu + a_2)\lambda_1 B^* - \lambda_1 \alpha S_H^* - \eta \lambda_1 S_H^* B^*,$$
$$L_5 = \lambda_1 \mu a_2 B^* - (a_1 - \lambda_1 B^*)\lambda_1 \alpha S_H^* - \lambda_1 \eta \mu S_H^* B^*, \quad L_6 = (a_1 - \lambda_1 B^*)\mu a_2.$$

Now, E_2^* is locally asymptotically stable if all the roots of the transcendental equation (4.2.4) have negative real parts. Also, we need to check here the possible occurrence of Hopf-bifurcation as a system exhibits Hopf-bifurcating periodic solutions if the corresponding characteristic equation have purely imaginary eigenvalues. To proceed, let us assume, for $\tau > 0$, $\varrho = i\omega(\tau)$ be a root of (4.2.4) with $\omega(\tau) > 0$. Putting $\varrho = i\omega(\tau)$ in equation (4.2.4) and separating the real and imaginary parts, we get these following pair of equations in ω.

$$\begin{cases} L_2\omega - \omega^3 = (L_5 - L_3\omega^2)\sin\omega\tau - L_4\omega\cos\omega\tau \\ L_1\omega^2 - L_6 = (L_5 - L_3\omega^2)\cos\omega\tau + L_4\omega\sin\omega\tau \end{cases}$$

Squaring and then adding these two equations, it follows that

$$\omega^6 + (L_1^2 - 2L_2 - L_3^2)\omega^4 + (L_2^2 + 2L_3L_5 - 2L_1L_6 - L_4^2)\omega^2 + (L_6^2 - L_5^2) = 0. \tag{4.2.5}$$

We can rewrite the equation (4.2.5) in the form,

$$g(l) = l^3 + \gamma_1 l^2 + \gamma_2 l + \gamma_3 = 0, \tag{4.2.6}$$

where $l = \omega^2$, $\gamma_1 = (L_1^2 - 2L_2 - L_3^2)$, $\gamma_2 = (L_2^2 + 2L_3L_5 - 2L_1L_6 - L_4^2)$, $\gamma_3 = (L_6^2 - L_5^2)$. From equation (4.2.6), we get that

$$\frac{dg(l)}{dl} = 3l^2 + 2\gamma_1 l + \gamma_2 = 0. \tag{4.2.7}$$

Roots of equation (4.2.7) are given by

$$l_1 = \frac{-\gamma_1 + \sqrt{\gamma_1^2 - 3\gamma_2}}{3} \quad \text{and} \quad l_2 = \frac{-\gamma_1 - \sqrt{\gamma_1^2 - 3\gamma_2}}{3}.$$

We can observe that both the roots of equation (4.2.7) are negative if $\gamma_1 > 0$ and $\gamma_2 > 0$. Also, if $g(0) = \gamma_3 \geq 0$ holds then (4.2.6) does not contain any positive root. This way, we can conclude that $g(l)$ doesn't satisfy $\omega(\tau) > 0$, and proceeding as before, E_2^* is locally asymptotically stable for $\tau \geq 0$. Now, we summarize our previous discussion in the following

theorem.

Theorem 4.2.2 . *If the endemic equilibrium of the non-delayed system (4.1.1) is stable and if the three conditions $\gamma_1 > 0$, $\gamma_2 > 0$ and $\gamma_3 \geq 0$ hold true, then the endemic equilibrium E_2^* of the delayed system (4.2.1) is locally asymptotically stable for all $\tau \geq 0$.*

Remark: If the values of all the parameters listed in Table 4.1 satisfies all the conditions of Theorem 4.2.2 then the steady state E_2^* of the delayed model (4.2.1) is locally asymptotically stable for all $\tau \geq 0$ which indicates that E_2^* is independent of the delay values in this scenario. However, we now describe that if the conditions mentioned in Theorem 4.2.2 are not satisfied, the stability of E_2^* becomes dependent on the values of delay.

4.2.3 Bifurcation analysis:

In this Subsection, we now analyze the stability switch or stability changes of the endemic equilibrium E_2^* by investigating the emergence of Hopf-bifurcating periodic solutions of the system (4.2.1). To perform this, especially, we concentrate on establishing conditions for which purely imaginary eigenvalues exist for the characteristic equation (4.2.4).

From equation (4.2.6), we can see that $\gamma_3 < 0 \Rightarrow g(0) < 0$. Therefore, since $\lim_{l\to+\infty} g(l) = +\infty$, the existence of a positive root l_0 of equation (4.2.6) (which also implies the existence of at least one positive root, say ω_0 of equation (4.2.5)) is guaranteed. On the other hand, if $\gamma_2 < 0$, we get that $\sqrt{\gamma_1^2 - 3\gamma_2} > \gamma_1$. So, from equation (4.2.7), it follows that $l_1 = \frac{-\gamma_1+\sqrt{\gamma_1^2-3\gamma_2}}{3} > 0$ and consequently, a minimum of $g(l)$ takes place at the right side. In addition, if $g(l_1) < 0$ holds true, then it implies that equation (4.2.6) and hence, equation (4.2.5), have at least one positive root. Therefore, we can conclude that the characteristic equation (4.2.4) has a pair of purely imaginary roots, says $\pm i\omega_0$, for the aforementioned cases.

Now, we consider again the following pair of equations.

$$\begin{cases} L_2\omega - \omega^3 = (L_5 - L_3\omega^2)\sin\omega\tau - L_4\omega\cos\omega\tau, \\ L_1\omega^2 - L_6 = (L_5 - L_3\omega^2)\cos\omega\tau + L_4\omega\sin\omega\tau. \end{cases}$$

From these two equations, we get the value of τ^* as follows.

$$\tau^n = \frac{1}{\omega}\arccos\Big[\frac{(L_4 - L_1L_3)\omega^4 + (L_1L_5 + L_3L_6 - L_2L_4)\omega^2 - L_5L_6}{L_3^2\omega^4 + (L_4^2 - 2L_3L_5)\omega^2 + L_5^2}\Big] + \frac{2n\pi}{\omega}, \qquad (4.2.8)$$

where $n = 0, 1, 2, 3...$ Let us assume $\tau_2^* = \min_{n\geq 0}\{\tau^n\}$ and $\omega_0 = \omega(\tau_2^*)$. Now, denoting

$\varrho(\tau) = \varrho$ and differentiating equation (4.2.4) with respect to τ, we get that

$$\left(\frac{d\varrho(\tau)}{d\tau}\right)^{-1} = -\frac{3\varrho^2 + 2L_1\varrho + L_2}{3(\varrho^3 + L_1\varrho^2 + L_2\varrho + L_6)} + \frac{2L_3\varrho + L_4}{3(L_3\varrho^2 + L_4\varrho + L_5)} - \frac{\tau}{\varrho}. \tag{4.2.9}$$

From this equation, we obtain

$$\begin{aligned}
\operatorname{sign}\left\{\operatorname{Re}\left(\frac{d\varrho(\tau)}{d\tau}\right)_{\tau=\tau_2^*}\right\} &= \operatorname{sign}\left\{\operatorname{Re}\left(\frac{d\varrho(\tau)}{d\tau}\right)^{-1}_{\tau=\tau_2^*}\right\} \\
&= \operatorname{sign}\left\{3\omega_0^4 + (2L_1^2 - 4L_2 - 2L_3^2)\omega_0^2 + (L_2^2 + 2L_3L_5 - 2L_1L_6 - L_4^2)\right\} \\
&= \operatorname{sign}\left\{3\omega_0^4 + 2\omega_0^2\gamma_1 + \gamma_2\right\}.
\end{aligned}$$

Now, $\operatorname{Re}\left(\frac{d\varrho}{d\tau}\right)_{\tau=\tau_2^*} > 0$ means $3\omega_0^4 + 2\omega_0^2\gamma_1 + \gamma_2 > 0$. Hence, the transversality condition is proved and we can conclude that at the value of $\tau = \tau_2^*$, Hopf bifurcation occurs for system (4.2.1) provided the transversality condition holds. Summarising the above discussions, we now have the following theorem.

Theorem 4.2.3 *Suppose, the endemic equilibrium of the non-delayed system (4.1.1) is stable. Consider, the root l_1 of the equation given as (4.2.7). If, any one of the following two conditions*

- $\gamma_3 < 0$
- $\gamma_3 \geq 0$, $\gamma_2 < 0$ *and* $g(l_1) < 0$

is satisfied then by using Butler's lemma [Freedman and Kuang (1991)], E_2^* is asymptotically stable for $\tau < \tau_2^*$ and unstable for $\tau > \tau_2^*$, where

$$\tau_2^* = \frac{1}{\omega_0}\arccos\Big[\frac{(L_4 - L_1L_3)\omega_0^4 + (L_1L_5 + L_3L_6 - L_2L_4)\omega_0^2 - L_5L_6}{L_3^2\omega_0^4 + (L_4^2 - 2L_3L_5)\omega_0^2 + L_5^2}\Big]. \tag{4.2.10}$$

Thus, when $\tau = \tau_2^*$, bifurcation occurs i.e. a family of periodic solutions bifurcate as τ crosses the critical value τ_2^* with the transversality condition

$$3\omega_0^4 + 2\omega_0^2\gamma_1 + \gamma_2 > 0.$$

Note: Our first delay-induced mathematical model i.e. system (4.1.2) also undergoes Hopf bifurcation as the value of time delay τ passes through a critical value. Approaching very similarly like system (4.2.1), we can find out that there exists a critical value of $\tau = \tau_1^*$ such that the positive endemic equilibrium E_1^* remains stable for all the values of $\tau < \tau_1^*$

and becomes unstable whenever $\tau > \tau_1^*$. Avoiding the similar analytical calculations, we have demonstrated the appearance of Hopf bifurcating periodic solutions for system (4.1.2) numerically and further, provided the necessary biological interpretations.

4.3 Delayed Systems with Optimal Control

Optimal control approach is a very popular and effective mathematical tool to predict the optimal treatment policy of a disease by analyzing a mathematical system [Al Basir (2020); Ali and Zaman (2021)]. Optimal control treatment policy whenever applied on the delay-induced systems instead of the non-delayed mathematical model produces a much accurate and realistic result in achieving a perfect drug therapeutic schedule for leprosy. In this Section, we have discussed the effect of optimal control on both of the two delay induced systems i.e. on system (4.1.2) and system (4.2.1). We introduce the parameters $u_1(t)$ and $u_2(t)$ as control parameters where $u_1(t)$ represents the Ofloxacin drug therapy and $u_2(t)$ denotes the Dapsone drug therapy. Delayed model (4.1.2) equipped with optimal control is of the form:

$$\begin{aligned}
\frac{dS_H(t)}{dt} &= r_1 S_H(t)(1-\frac{S_H(t)}{k_1}) - \lambda_1(1-u_1)S_H(t)B(t), \\
\frac{dS_I(t)}{dt} &= \lambda_1(1-u_1)S_H(t-\tau)B(t-\tau) - \mu S_I(t), \qquad (4.3.1)\\
\frac{dB(t)}{dt} &= r_2(1-u_2)B(t)(1-\frac{B(t)}{k_2}) - \eta(1-u_1)S_H(t)B(t) + \alpha S_I(t).
\end{aligned}$$

$$\text{with} \quad S_H(0) = S_{H_0}, S_I(0) = S_{I_0}, B(0) = B_0. \qquad (4.3.2)$$

It is easy to prove that a unique solution $(S_H(t), S_I(t), B(t))$ of system (4.3.1) with initial data given as $(S_{H_0}, S_{I_0}, B_0) \in C = C([-\tau, 0], \mathbb{R}^3_+)$ exists. Additionally, for biological justifications, let us assume that the initial data for system (4.3.1) satisfy the following :

$$S_{H_0}(t) > 0, \quad S_{I_0}(t) > 0, \quad B_0(t) > 0 \ \forall t \in [-\tau, 0].$$

4.3.1 Objective functional and its description

The problem is to minimize the objective cost functional described as:

$$J(u_1(t), u_2(t)) = \int_0^{t_f} \left[P_1 u_1^2(t) + P_2 u_2^2(t) + A_1 S_I^2(t) - A_2 S_H^2(t)\right] dt \qquad (4.3.3)$$

subject to the optimal control induced delayed system (4.3.1). Here, in the first two terms in the objective functional i.e. $P_i u_i^2$, $i = 1, 2$, P_i is the positive weight parameters associated

with the control $u_i(t)$ and the square of the control variables indicate the severity of the side effects of the Ofloxacin and Dapsone drug therapies. Also, A_1, A_2 are chosen as the penalty multipliers on the benefit of the cost where both $A_1 > 0$, $A_2 > 0$. Our main aim is to reduce the concentrations of the infected Schwann cells and the *M. leprae* bacteria population so as to increase the density of the healthy Schwann cells into the human body while minimizing the cost of implementing the control therapies, $u_i(t),\ i = 1, 2$. The control set is defined on the interval $[0, t_f]$ where t_f is the final time of control. Let us define the control set as

$$U = \{u(t) = (u_1(t), u_2(t))) : u_i \text{ is Lebesgue measurable on}, 0 \leq u_i(t) \leq 1,\ t \in [0, t_f], i = 1, 2\}. \tag{4.3.4}$$

The objective of the optimal control problem is to achieve optimal control function denoted as $(u_1^*(t), u_2^*(t))$ for system (4.3.1) such that

$$J(u_1^*, u_2^*) = \min\{J(u_1(t), u_2(t)) : (u_1(t), u_2(t)) \in U\}. \tag{4.3.5}$$

To obtain the necessary conditions for solving this optimal control problem, we have used Pontryagin's Minimum Principle [Göllmann and Maurer (2013); Pontryagin (1987)]. For the bounded Lebesgue measurable controls and the non-negative initial conditions, there exist non-negative bounded solutions [Birkhoff et al. (1989)] to the optimal control induced delayed system (4.3.1), (4.3.2). Now, first, we investigate the existence of an optimal control for system (4.3.1) in the next Subsection.

4.3.2 Existence of an optimal control

To prove the existence of an optimal control pair for system (4.3.1), we use the results described in the articles [Lukes (1982); Fleming and Rishel (2012)]. For the control induced delayed system (4.3.1), (4.3.2), the objective functional described in (4.3.3) and the control set defined by (4.3.4), firstly, note the following:

1. The control and state variables are non-negative. Also, the set of controls and the state variables are non-empty.

2. The control set U is convex and closed by definition.

3. In this minimization problem, the necessary convexity of the objective functional (4.3.3) are satisfied in u_1 and u_2.

4. The control induced system (4.3.1) is bounded which provides the required compactness for the existence of the optimal control.

5. The integrand $\left[P_1 u_1^2(t) + P_1 u_1^2(t) + A_1 S_I^2(t) - A_2 S_H^2(t)\right]$ of the objective functional (4.3.3) is convex on the control set U.

Additionally, we can see that there exists constants $\kappa_1, \kappa_2 > 0$ and $\rho > 1$ such that

$$J(u_1, u_2) \geq \kappa_1(\mid u_1 \mid^2 + \mid u_2 \mid^2)^{\frac{\rho}{2}} - \kappa_2 \text{ as the state variables are bounded.}$$

Now, using the Theorem 4.1 in Fleming and Rishel (2012), existence of an optimal control solution is guaranteed, and hence, summarizing the previous discussions, we now present the following theorem.

Theorem 4.3.1 *There exists an optimal control pair $(u_1^*(t), u_2^*(t)) \in U$ subject to the control induced system (4.3.1), (4.3.2) such that*

$$J(u_1^*, u_2^*) = \min\left\{J(u_1(t), u_2(t)) : (u_1(t), u_2(t)) \in U\right\}. \tag{4.3.6}$$

Next, we evaluate the optimal control functions and derive the optimality system for the optimal control problem.

4.3.3 Characterization of the optimal control

For characterizing the optimal control, we use Pontryagin's Minimum Principle with delay in state [Göllmann and Maurer (2013)]. To do this, let us first define the hamiltonian H for the control problem (4.3.1)-(4.3.5) as

$$H = P_1 u_1^2(t) + P_2 u_2^2(t) + A_1 S_I^2(t) - A_2 S_H^2(t) + \xi_1 f_1 + \xi_2 f_2 + \xi_3 f_3 \tag{4.3.7}$$

where f_i' s, for $i = 1, 2, 3$, are the right hand sides of system (4.3.1) and ξ_i' s for $i = 1, 2, 3$ are adjoint functions to be determined suitably. Now, applying Pontryagin's Minimum Principle with delay in state [Göllmann and Maurer (2013); Rodrigues et al. (2017)] to the hamiltonian H, we have the following theorem.

Theorem 4.3.2 *If the objective cost function $J(u_1, u_2)$ is minimum for the optimal control pair $(u_1^*(t), u_2^*(t))$ for the optimal control problem (4.3.1)-(4.3.5) and (S_H^*, S_I^*, B^*) be corresponding optimal state, then there exist adjoint variables ξ_1, ξ_2 and ξ_3 which satisfy the*

corresponding transversality conditions. Moreover, the optimal control solution is given by:

$$\begin{aligned} u_1^*(t) &= \max\left\{0, \min\left\{1, \frac{-(\xi_1(t)\lambda_1 + \xi_3(t)\eta)S_H^*(t)B^*(t) + \xi_2(t)\lambda_1 S_H^*(t-\tau)B^*(t-\tau)}{2P_1}\right\}\right\}, \\ u_2^*(t) &= \max\left\{(0, \min\left\{1, \frac{\xi_3(t)r_2B^*(t)(1-\frac{B^*(t)}{k_2})}{2P_2}\right\}\right\}. \end{aligned} \tag{4.3.8}$$

Proof. We use the Pontryagin's Minimum Principle [Göllmann and Maurer (2013)] to obtain the adjoint system as

$$\begin{aligned} \frac{d\xi_1}{dt} &= -\frac{\partial H}{\partial S_H}(t) - \chi[0, t_f - \tau](t)\frac{\partial H}{\partial S_H}(t+\tau), \\ \frac{d\xi_2}{dt} &= -\frac{\partial H}{\partial S_I}(t), \\ \frac{d\xi_3}{dt} &= -\frac{\partial H}{\partial B}(t) - \chi[0, t_f - \tau](t)\frac{\partial H}{\partial B}(t+\tau) \end{aligned}$$

with the transversality conditions $\xi_i(t_f) = 0$ for all $i = 1, 2, 3$ and $\chi[0, t_f - \tau]$ is the characteristic function defined on the interval $[0, t_f - \tau]$. So, the adjoint system takes the form

$$\begin{aligned} \frac{d\xi_1}{dt} &= 2A_2S_H^* - \xi_1(t)\left[r_1(1-\frac{2S_H^*}{k_1}) - \lambda_1(1-u_1^*)B^*\right] + \xi_3(t)\left[\eta(1-u_1^*)B^*\right] \\ &\quad -\chi[0, t_f-\tau](t)\xi_2(t+\tau)\lambda_1(1-u_1^*)B^*, \\ \frac{d\xi_2}{dt} &= -2A_1S_I^* + \mu\xi_2(t) - \alpha\xi_3(t), \\ \frac{d\xi_3}{dt} &= \xi_1(t)\left[\lambda_1(1-u_1^*)S_H^*\right] - \xi_3(t)\left[r_2(1-u_2^*)(1-\frac{2B^*}{k_2}) - \eta(1-u_1^*)S_H^*\right] \\ &\quad -\chi[0, t_f-\tau](t)\xi_2(t+\tau)\lambda_1(1-u_1^*)S_H^*, \end{aligned} \tag{4.3.9}$$

where $\xi_i(t_f) = 0$ for all $i = 1, 2, 3$. Now, to obtain the optimal controls $u_1^*(t)$ and $u_2^*(t)$, we use the optimality condition given as

$$\frac{\partial H}{\partial u_1}\Big|_{u_1 = u_1^*(t)} = 0, \tag{4.3.10}$$

$$\frac{\partial H}{\partial u_2}\Big|_{u_2 = u_2^*(t)} = 0. \tag{4.3.11}$$

The hamiltonian equation (4.3.7) can be rewritten as:

$$\begin{aligned} H &= P_1 u_1^2(t) + P_2 u_2^2(t) + A_1 S_I^2(t) - A_2 S_H^2(t) \\ &+ \xi_1 \left[r_1 S_H(t)(1 - \frac{S_H(t)}{k_1}) - \lambda_1(1-u_1) S_H(t) B(t) \right] \\ &+ \xi_2 \left[\lambda_1(1-u_1) S_H(t-\tau) B(t-\tau) - \mu S_I(t) \right] \\ &+ \xi_3 \left[r_2(1-u_2) B(t)(1 - \frac{B(t)}{k_2}) - \eta(1-u_1) S_H(t) B(t) + \alpha S_I(t) \right]. \end{aligned} \tag{4.3.12}$$

Differentiating equation (4.3.12) with respect to u_1 partially and using condition (4.3.10), we get

$$u_1^*(t) = \frac{-(\xi_1(t)\lambda_1 + \xi_3(t)\eta) S_H^*(t) B^*(t) + \xi_2(t)\lambda_1 S_H^*(t-\tau) B^*(t-\tau)}{2P_1}.$$

Similarly, from condition (4.3.11), we obtain

$$u_2^*(t) = \frac{\xi_3(t) r_2 B^*(t)(1 - \frac{B^*(t)}{k_2})}{2P_2}.$$

Using boundedness properties of the standard control i.e. using the properties of the control set U that admissible controls take values such that $0 \leq u_i(t) \leq 1$, $i = 1, 2$, we can write

$$u_1^*(t) = \begin{cases} 0 \\ \frac{-(\xi_1(t)\lambda_1 + \xi_3(t)\eta) S_H^*(t) B^*(t) + \xi_2(t)\lambda_1 S_H^*(t-\tau) B^*(t-\tau)}{2P_1} \\ 1 \end{cases}$$

if respectively,

$$\begin{aligned} &\frac{-(\xi_1(t)\lambda_1 + \xi_3(t)\eta) S_H^*(t) B^*(t) + \xi_2(t)\lambda_1 S_H^*(t-\tau) B^*(t-\tau)}{2P_1} \leq o, \\ &\frac{-(\xi_1(t)\lambda_1 + \xi_3(t)\eta) S_H^*(t) B^*(t) + \xi_2(t)\lambda_1 S_H^*(t-\tau) B^*(t-\tau)}{2P_1} \in (0, 1), \\ &\frac{-(\xi_1(t)\lambda_1 + \xi_3(t)\eta) S_H^*(t) B^*(t) + \xi_2(t)\lambda_1 S_H^*(t-\tau) B^*(t-\tau)}{2P_1} \geq 1. \end{aligned}$$

and

$$u_2^*(t) = \begin{cases} 0 & if \quad \frac{\xi_3(t) r_2 B^*(t)(1 - \frac{B^*(t)}{k_2})}{2P_2} \leq 0, \\ \frac{\xi_3(t) r_2 B^*(t)(1 - \frac{B^*(t)}{k_2})}{2P_2} & if \quad 0 < \frac{\xi_3(t) r_2 B^*(t)(1 - \frac{B^*(t)}{k_2})}{2P_2} < 1, \\ 1 & if \quad \frac{\xi_3(t) r_2 B^*(t)(1 - \frac{B^*(t)}{k_2})}{2P_2} \geq 1. \end{cases}$$

Hence, representing the values of $u_1^*(t)$ and $u_2^*(t)$ in a more compact and convenient form, we get the optimal control solutions as given in (4.3.8) for the optimal control problem (4.3.1)-(4.3.5).

The optimal control pair and states are obtained by solving the optimality system which consists of the state system (4.3.1) along with the boundary condition (4.3.2), the adjoint system (4.3.9) with the corresponding transversality conditions and the characterization of the optimal control $(u_1^*(t), u_2^*(t))$ given by (4.3.8).

Also, we describe the delayed model (4.2.1) equipped with optimal control below.

$$\begin{aligned}
\frac{dS_H(t)}{dt} &= r_1 S_H(t)(1-\frac{S_H(t)}{k_1}) - \lambda_1(1-u_1)S_H(t-\tau)B(t-\tau), \\
\frac{dS_I(t)}{dt} &= \lambda_1(1-u_1)S_H(t-\tau)B(t-\tau) - \mu S_I(t), \qquad (4.3.13)\\
\frac{dB(t)}{dt} &= r_2(1-u_2)B(t)(1-\frac{B(t)}{k_2}) - \eta(1-u_1)S_H(t)B(t) + \alpha S_I(t)
\end{aligned}$$

$$\text{with} \quad S_H(0) = S_{H_0}, S_I(0) = S_{I_0}, B(0) = B_0 \qquad (4.3.14)$$

and the initial data given as $(S_{H_0}, S_{I_0}, B_0) \in C = C([-\tau, 0], \mathbb{R}^3_+)$.

In a similar approach, using the same objective functional and control problem (4.3.3),(4.3.5), control set (4.3.4) and hamiltonian (4.3.7) for the control induced system (4.3.13),(4.3.14), we can easily obtain the values of $u_1^*(t)$ and $u_2^*(t)$. The values of optimal control solutions for the delayed system equipped with optimal control (4.3.13) are given by

$$\begin{aligned}
u_1^*(t) &= \max\left\{0, \min\left\{1, \frac{(\xi_2(t)-\xi_1(t))\lambda_1 S_H^*(t-\tau)B^*(t-\tau) - \xi_3(t)\eta S_H^*(t)B^*(t)}{2P_1}\right\}\right\}, \\
u_2^*(t) &= \max\left\{0, \min\left\{1, \frac{\xi_3(t) r_2 B^*(t)(1-\frac{B^*(t)}{k_2})}{2P_2}\right\}\right\}. \qquad (4.3.15)
\end{aligned}$$

4.4 Numerical Simulation

In this Section, we have performed numerical simulations for both the delayed systems i.e. system (4.1.2) and system (4.2.1) and validated these findings with our analytical and the theoretical outcomes. We choose the initial values in number dependant according to the cardinal rule of scientific hypothesis. The values of the parameters which we have used here are described in the following table denoted by Table 4.1. All of our numerical findings are obtained here by using Matlab 2016A.

In Figure 4.2, we have compared the system (4.1.2) with delay and the non-delayed system

Parameter	Parameter definition	Assigned Value (Unit)
r_1	growth rate of healthy Schwann cell	0.4 (day^{-1})
r_2	growth rate of *M. leprae* bacteria	0.01 (day^{-1})
k_1	carrying capacity of healthy Schwann cell	600 (mm^{-3})
k_2	carrying capacity of bacteria	400 (mm^{-3})
μ	natural death rate of infected Schwann cell	0.1 (day^{-1})
λ_1	infection rate of healthy cell and bacteria	0.00035 (day^{-1})
α	proliferation rate of new free bacteria	0.1 (day^{-1})
η	bacteria clearance rate due to infection	0.0003 (day^{-1})

Table 4.1: Values of the system parameters used in numerical simulations for system (4.1.2) and system (4.2.1). For the choice of parameters values, we have found the ranges of few parameters from the numerical tables described in Chapter 2 and Chapter 3. Some of the model parameters are estimated from literature [Masaki et al. (2013); Fischer (2017)]. Due lack of sufficient primary data related with inter-cellular delay factors, we have chosen some parameter values that allowed model behaviour to be biologically feasible. We have also varied the values of our assumed parameters to predict the different scenario.

(4.1.1). Here, trajectories coloured in red are describing the dynamics of healthy Schwann cells, infected Schwann cells and *M. leprae* bacteria in a non-delayed system i.e. trajectories for system with $\tau = 0$ while trajectories in blue demonstrate the behavior of our model cell populations for the delayed system (4.1.2) assuming the value of intracellular time delay $\tau = 2$ (in days). All the other parameter values used here for numerical simulations are mentioned in Table 4.1. This Figure depicts that at the infected steady state, the cell populations of the non-delayed system i.e. S_H, S_I and B attain a stable concentration of 180 mm^{-3}, 500 mm^{-3} and 800 mm^{-3}. On the other hand, it is interesting to see that introducing time lag or time delay into the system (4.1.1) makes the cell populations oscillate i.e. periodic oscillatory solutions appear for system (4.1.2).

In Figure 4.3, behavior of the solutions of the cell populations of delay-induced system (4.1.2) have been depicted for different values of time delay τ (i.e. $\tau = 0.01$, $\tau = 2$ and $\tau = 5$). Here, we have used three different values of τ i.e. $\tau = 0.01$, $\tau = 2$ and $\tau = 5$ to achieve the trajectories of the healthy Schwann cells (S_H), infected Schwann cells(S_I) and *M. leprae* bacterial population (B). For the value of $\tau = 0.01$, the healthy cell, infected cell and *M. leprae* densities oscillate at the beginning and achieve local asymptotic stability after a certain period of time. It completely supports our analytical findings in the Subsection 4.1.4.

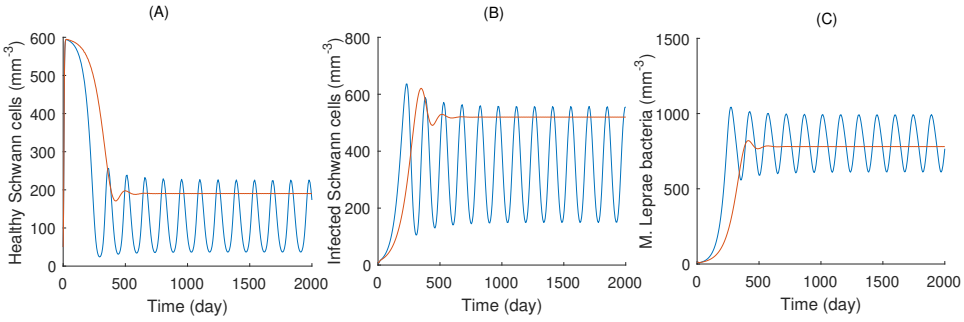

Figure 4.2: Comparison of the behavior of the trajectories of S_H, S_I and B of the non-delayed system (4.1.1) and the delayed system (4.1.2). For the delayed system, the value of time delay is taken as $\tau = 2$. Red color represents system (4.1.1) and blue represents system (4.1.2).

Indeed, if all the conditions of Theorem 4.1.4 are satisfied then the endemic equilibrium E_1^* of the delayed system (4.1.2) becomes locally asymptotically stable for all values of $\tau > 0$ i.e. stability of the endemic equilibrium E_1^* does not depend on the value of time-delay τ if the previously stated conditions are satisfied. Regular oscillatory solutions appear for larger values of τ. Biologically, it means that if the amount of time lag between a susceptible Schwann cell getting infected and production of new free bacteria from that infected cell is increased, the model cell concentrations fluctuate more quickly and this fluctuation of the population densities occur in an oscillatory manner. This happens due to the effect of the formation of reprogrammed Schwann cells which stimulate the dissemination of the disease by releasing free bacteria and also by exploiting the natural high plasticity property of the infected Schwann cells during the progression of infection.

Figure 4.4 illustrates the chaotic nature of the trajectories of the cell populations of the delayed system (4.1.2) for the value of $\tau = 40$. When the value of time delay becomes very large (i.e $\tau = 40$) in comparison to the values used previously to achieve the trajectories in Figure 4.2 and Figure 4.3, the concentration of S_H cells, S_I cells and B of system (4.1.2) oscillate but an irregular pattern is observed which is completely chaotic in nature. Actually, for all types of leprosy, whenever slowly progressive, insidious neuropathy occurs in patients, sudden, unexplained and spontaneous enhancement of an individual's immune response to *M. leprae* is noted [Scollard et al. (2006)]. Also, the immunologic mechanisms which characterize the skin smears and inflammations, act indiscriminately during the dissemination of the bacteria into different body parts. This certainly explains and confirms

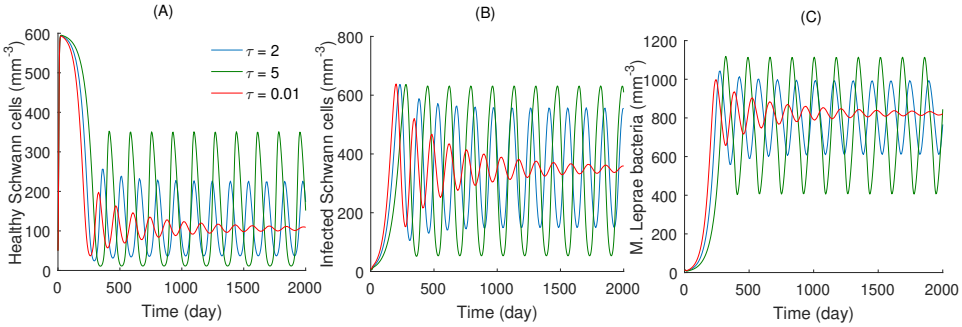

Figure 4.3: Time series solution of the model variables of the delayed system (4.1.2) for different values of time delay τ. Trajectories coloured in red, blue and green are obtained by considering the values of $\tau = 0.01$, $\tau = 2$ and $\tau = 5$ respectively. Values of rest of the parameters are chosen from Table 4.1.

the chaotic behavior of the delayed system (4.1.2) around the infected steady state when the time required for production of free *M. leprae* bacteria from infected Schwann cells is sufficiently large.

In Figure 4.5, bifurcation diagrams of E_1^* for system (4.1.2) have been depicted by taking τ as the bifurcation parameter. Here, we obtain a critical value of time delay $\tau = \tau_1^* \approx 1.81$ for which Hopf bifurcation occurs. System (4.1.2) exhibits a stable behaviour for the values of $\tau < \tau_1^*$ but loses its stability for $\tau > \tau_1^*$. We have also demonstrated a feasible limit cycle on the $S_H - S_I - B$ phase plane appearing around the infected steady state E_1^* for the delayed system (4.1.2). In order to simulate this picture, we have chosen suitable initial values of the system cell populations and the value of time delay is taken as $\tau = 1.82$. All the other parameter values are chosen from Table 4.1.

Figure 4.6 describes the comparison of the three systems i.e. the non-delayed system (4.1.1) and the delayed system (4.1.2) and system (4.2.1) for $\tau = 2$. It is quite interesting to note that the amplitude of the periodic oscillations is relatively high for the second delayed system (4.2.1) compared to the first delayed system (4.1.2) but the period of the oscillations does not change remarkably. The biological interpretation behind this behavior lies in the presence of an additional intracellular delay into system (4.2.1) which is necessary to describe the time for getting a healthy Schwann cell finally being infected after binding to *M. leprae* through various receptor mediated mechanisms. This whole attachment-infection process is somehow complicated but significantly effective on the population cell densities

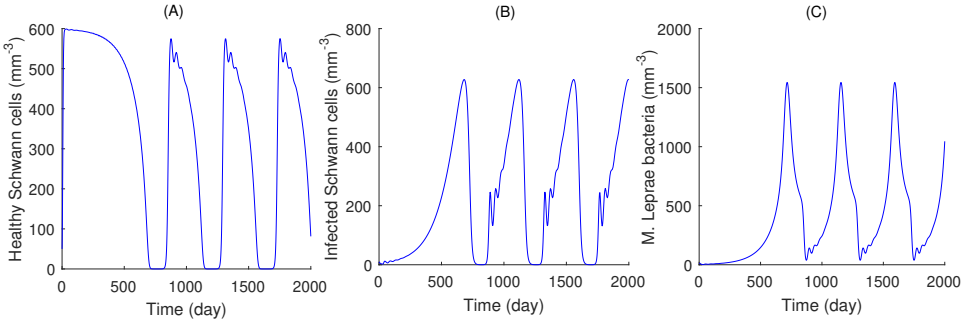

Figure 4.4: Description of the chaotic situation of the delay-induced system (4.1.2) for the value of $\tau = 40$. Rest of the parameters are the same as listed in Table 4.1.

and eventually contributes to more rapid fluctuations of the system solution trajectories.

In Figure 4.7, we numerically investigate the dynamics of the trajectories of the delayed system (4.2.1) for different values of time delay τ (i.e. $\tau = 0.0002$, $\tau = 0.5$, $\tau = 2$). For the value of $\tau = 0.0002$, solutions of the system fluctuate at the beginning and then, arrive at a stable steady state concentration after almost 1000 days. For $\tau = 0.5$, behavior of the trajectories is quite similar to the case of $\tau = 0.0002$ but cell densities attain local asymptotic stability after approximately 1200 days and the initial fluctuation of the trajectories is more evident in this scenario. This indicate that the cell densities of both healthy and infected Schwann cells and also the bacterial load will be sometimes high and sometimes low. From this Figure it is clear that if we vary the value of τ from very low value to higher values, the delayed system (4.2.1) exhibits a rich dynamics in terms of behavior of the trajectories of the system cell populations. The endemic equilibrium E_2^* of system (4.2.1) remains locally asymptotically stable for all the values of $\tau < \tau_2^*$ and becomes unstable when $\tau > \tau_2^*$. Whenever τ crosses the threshold value τ_2^*, system (4.2.1) undergoes a Hopf-bifurcation which means bifurcating periodic solutions appear around the infected steady state. Indeed, we can clearly observe that the densities of the model cell populations fluctuate and display regular periodic oscillation for the value of $\tau = 2 > \tau_2^*$. Also, initiation of stable periodic solutions implies existence of limit cycle for system (4.2.1) for the values of $\tau > \tau^*$. The feasible limit cycle solution of the delayed system (4.2.1) has been illustrated next.

In Figure 4.8, we have demonstrated the bifurcation diagrams of the model cell densities of system (4.2.1) at the endemic equilibrium E_2^* by considering τ as a bifurcation parameter.

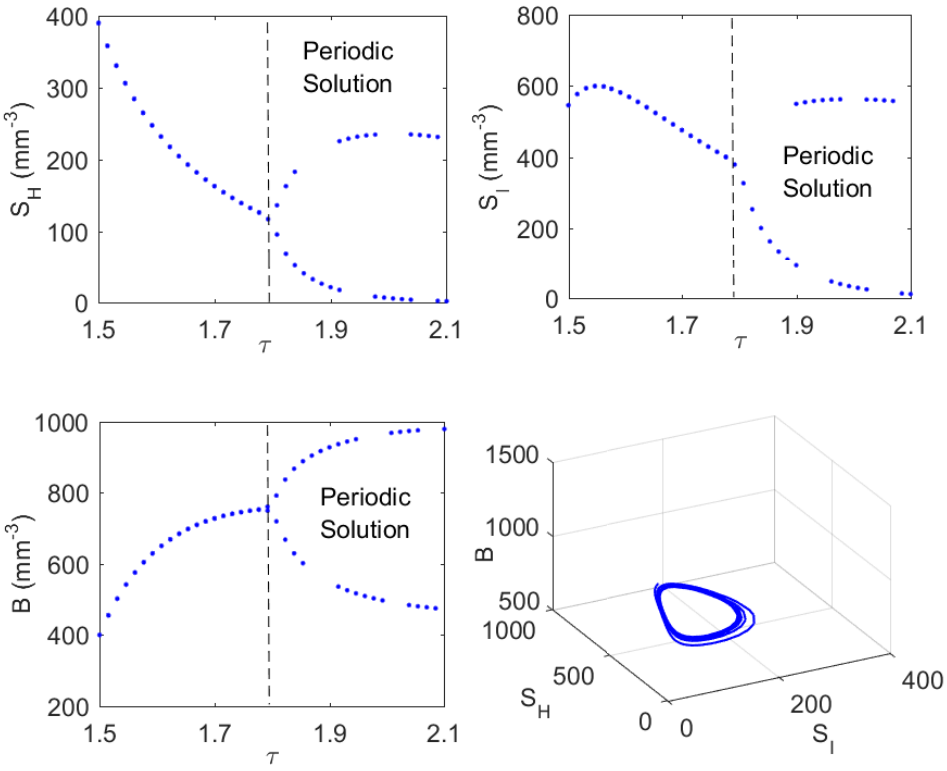

Figure 4.5: Bifurcation diagram of the densities of S_H cell, S_I cell and bacteria B of the delayed system (4.1.2) taking time delay τ as the bifurcation parameter. The value of the parameters are same as given in Table 4.1. Here, the steady state values of all populations are plotted with the minimum/maximum of the periodic solution when it exists. The feasible limit cycle of the system (4.1.2) on $S_H - S_I - B$ phase plane by considering the value of $\tau = 1.82$.

Time delay τ is chosen as the bifurcation parameter for these diagrams. Figure 4.8 clearly indicates that for $\tau > 0$, E_2^* is locally asymptotically stable when time delay is suitably small i.e for $\tau < \tau_2^* \approx 1.39$ and the system becomes unstable whenever $\tau > \tau_2^*$. The delayed system (4.2.1) undergoes Hopf-bifurcation when τ crosses the critical value τ_2^*. These findings evidently justifies all of our analytical findings in Subsection 4.2.3 and especially Theorem 4.2.3. For $\tau > \tau_2^*$, regular oscillatory periodic solutions begins to generate and it confirms the presence of stable limit cycles for system (4.2.1).

In Figure 4.9, the effect of optimal control therapy has been investigated for both of the control-induced delayed mathematical models i.e. on system (4.3.1) and system (4.3.13) by

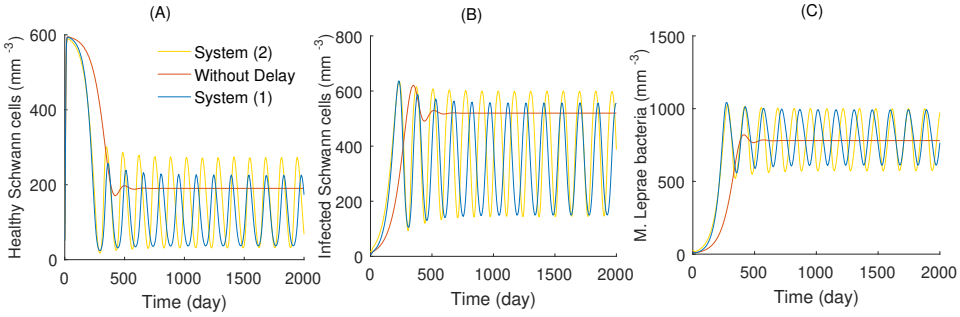

Figure 4.6: Comparison of the dynamical behaviour of between the system without delay(4.1.1), System (4.1.2) and System (4.2.1). To exhibit the impact of delay, we choose the value of $\tau = 2$ here.

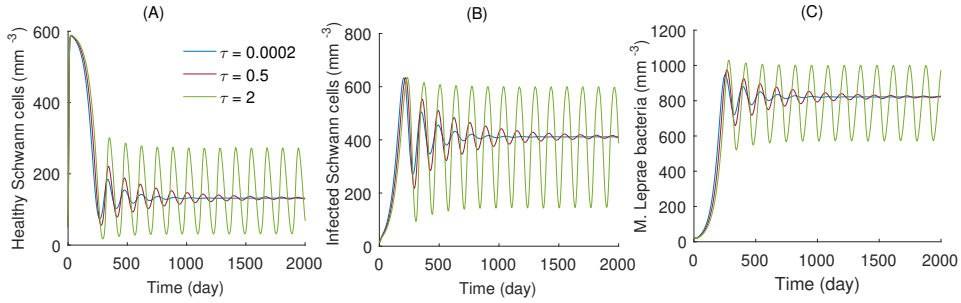

Figure 4.7: Qualitative behavior of the model cell populations of system (4.2.1) for three different values of τ.

considering a fixed value of time delay $\tau = 2$. Due to the effect of Ofloxacin and Dapsone drug therapy denoted by $u_1^*(t)$, $u_2^*(t)$ respectively, bacterial load decreases and densities of healthy cells climbs up significantly. Healthy cell density increases up to 320 mm^{-3} for system (4.3.1) while for the system (4.3.13), it reaches a higher value of 500 mm^{-3} after 2000 days. From the Subfigures (B) and (C) of Figure 4.9, we can observe that densities of infected Schwann cells (S_I) and *M. leprae* bacteria (B) decline to 410 mm^{-3} and 405 mm^{-3} for system (4.3.1) equipped with optimal control but quite interestingly, system (4.3.13) provides a much better result in this context. Infected cell density and bacterial load for system (4.3.13) with control decrease up to 320 mm^{-3} and 290 mm^{-3} after 2000 days of treatment which clearly represents a much improved scenario in comparison to system (4.3.1). Thus, optimal control policy applied on the delayed systems by means of double drug

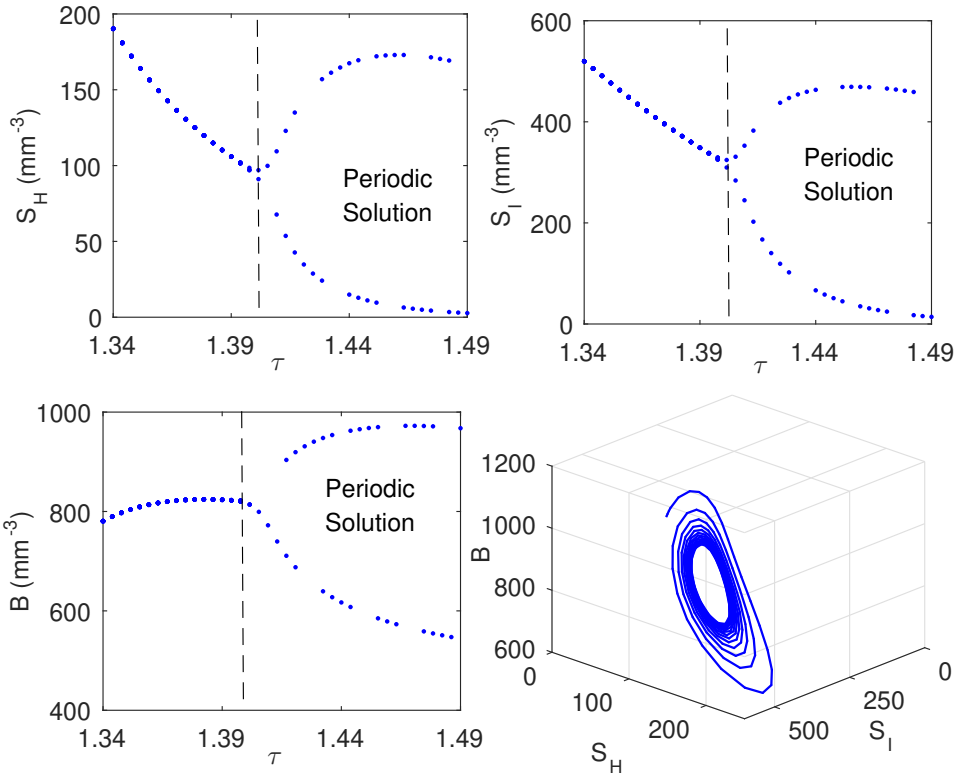

Figure 4.8: Bifurcation diagram of the system cell populations for the delayed model (4.2.1) taking τ as the main bifurcation parameter. Values of the other parameters are chosen the same as given in Table (4.1). Here, the steady state values of all populations are plotted with the minimum/maximum of the periodic solutions when it exists. Hopf bifurcation occurs at the critical value of the time delay $\tau = \tau_2^* = 1.39$. The feasible limit cycle of the system (4.1.17) on $S_H - S_I - B$ phase plane has also been depicted as a Subfigure by considering $\tau = 1.4$.

therapy contributes remarkably on controlling the delay-induced instability and also successfully inhibiting the new infections and declining the huge bacterial load into the human body.

In Figure 4.10, the optimal control profiles u_1^* and u_2^* are exhibited for both of the delayed control system (4.3.1) and system (4.3.13) in the Subfigure (A) and Subfigure (B), respectively. We can observe from the Subfigures (A) and (B) that the optimal control profiles of u_2^* remain almost same for both the systems (4.3.1) and system (4.3.13). But notable differences are observed by looking into the optimal drug doses schedule for the drug therapy Ofloxacin denoted by u_1^*. At the beginning of the treatment, Ofloxacin therapy should be applied in a very low amount and then, after approximately 200 days, the drug dose should be increased

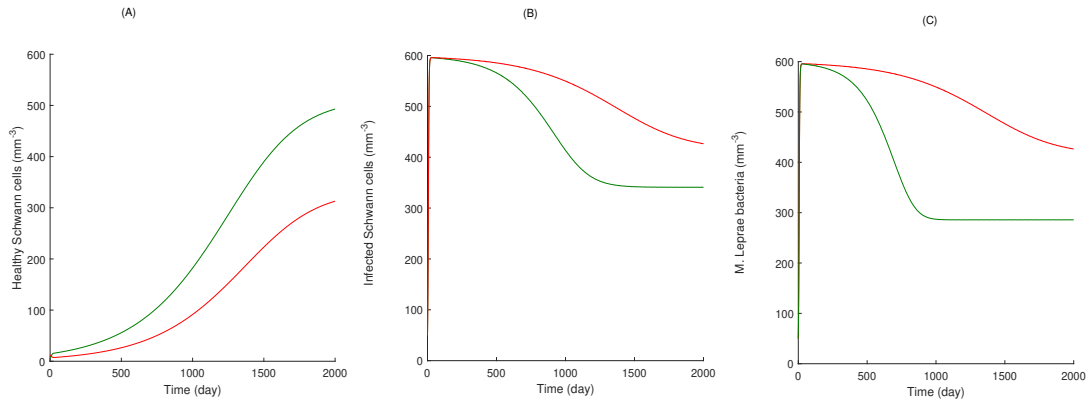

Figure 4.9: Qualitative behaviour of both the optimal control-induced delayed systems denoted as the system (4.3.1) and the system (4.3.13). Trajectories colored in red and green depict the behavior of the system populations for systems (4.3.1) and (4.3.13), respectively. This simulation has been made by taking $\tau = 2$ *and* $p_1 = p_2 = 0.003$, $A_1 = A_2 = 0.15$. *The other parameter values are taken from Table 4.1.*

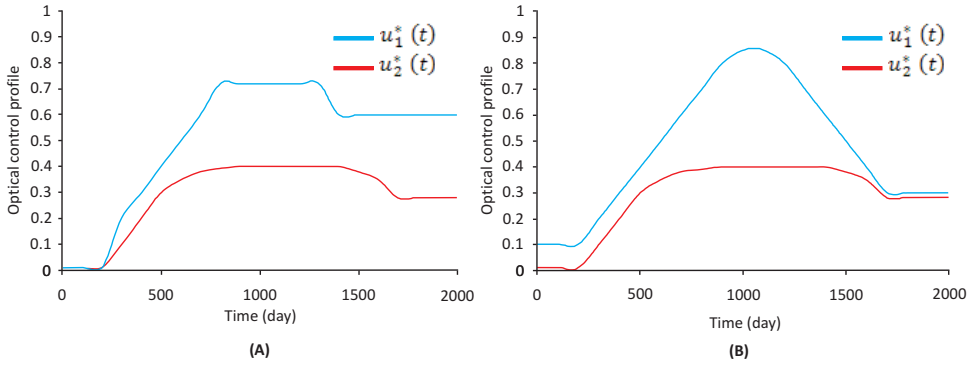

Figure 4.10: Optimal control profiles $u_1^*(t)$ *and* $u_2^*(t)$ *for the optimal control induced delayed systems (4.3.1) and (4.3.13) are presented in Subfigure (A) and Subfigure (B), respectively. This simulation has been made by taking* $\tau = 2$. *Values of the other parameters are chosen from Table 4.1.*

upto the range $0.7 - 0.8$ for system (4.3.1). Maintaining this drug dosing up to 1200 days, the values of $u_1^*(t)$ should be decreased a little and can be applied in the dosing range in between 0.5 - 0.6 throughout the completion of the treatment i.e. up to 2000 days. In comparison to these findings for the controlled system (4.3.1), we can observe that, from the range $0.8 - 0.9$, control $u_1^*(t)$ can be decreased up to $0.3 - 0.4$ after nearly 1100 days for system (4.3.13). The

main reason behind this behavioral pattern of the control profiles of the drug therapies is that initially, bacterial concentrations remain very low into the human body. After a certain period of time, as soon as *M. leprae* starts accumulating necessary nutrients for performing metabolic activities inside Schwann cells, proliferation of infected cells and eventually the bacterial load into the body climbs up rapidly [Masaki et al. (2013)]. After 1100 days, as the overall progression of the disease gets controlled and bacterial concentration gets stabilized to a certain stage, dosing of both $u_1^*(t)$ and $u_2^*(t)$ can be reduced and a moderate optimal drug dose should be maintained up to the completion of the therapy for establishing a cost-effective and efficient treatment policy according to the numerical findings in Subfigure (B).

4.5 Discussion

In this Chapter, we have proposed and investigated two delay induced mathematical models referred by system (4.1.2) and system (4.2.1). The fundamental biological understandings involving the cell-to-cell interactions of our system populations as an effect of intracellular delays with control theoretic approach remains our key point and focus throughout the Chapter. Our analytical and numerical findings suggest that for each of the delayed systems, E_0 remains stable whenever $\Re_0 < 1$ while it loses stability and endemic equilibrium becomes feasible for $\Re_0 > 1$ for all values of time delay $\tau \geq 0$ which shows that the basic reproduction number $\Re_0$ plays a pivotal role in determining the local asymptotic stability of E_0. Amount of time lag or delay is small in quantity up to which both the endemic equilibriums E_1^* and E_2^* exhibit a stable situation. Therefore, early diagnosis is very much important for leprosy patients to rule out the possibility of irreversible nerve damages [Camuset et al. (2016)] so that we can prevent the rapid production of free *M. leprae* bacteria at an early stage after its first entry into the human body. These analytical findings for our systems are well supported and confirmed by several experimental studies [Bekri et al. (1998); Chu et al. (2020); Ffytche (1989); Duthie et al. (2011)] where the authors have clearly explained the essence of early detection and hence, starting the optimal control treatment for eliminating leprosy. In a mouse footprint experiment, Gelber (1987) described the delayed proliferation of *M. leprae* which was also confirmed later in 2021 in the form of a delayed response [van Hooij and Geluk (2021)] of the infected cells contributing to the peripheral injury. These observations are validated also by our numerical findings which describe that both the systems undergo Hopf bifurcations at the critical values τ_1^* and τ_2^* where $\tau_1^* > \tau_2^*$. System (4.1.2) becomes unstable for $\tau > \tau_1^* = 1.81$ while system (4.2.1) loses its stability much earlier i.e for $\tau > \tau_2^* = 1.39$ as suggested by Theorem 4.2.3 which actually

implicates that Hopf bifurcating periodic solution arises for system (4.2.1) at a lesser value of time delay. Indeed, system (4.2.1) is more realistic and flexible in nature than system (4.1.2) as two different aspects of intracellular delays have been incorporated in system (4.2.1).

According to the numerical findings in Figure 4.9, we can claim that delay-induced instability can effectively be reduced and even removed by applying the optimal control therapy which is also suggested by Ji et al. (1994) in their clinical study with Ofloxacin and Dapsone for lepromatous leprosy patients. Both of our proposed optimal treatment policies developed in (4.3.1) and (4.3.13) are found to be preferable to the fixed control therapy as it reduces the concerns of the high cost-burden and adverse impacts of Ofloxacin and Dapsone for maintaining long term treatment schedules. In this context, it is to be noted that both of our control-induced delayed systems act noticeably but the system (4.3.13) emerges as a far better option as it declines the bacterial load as well as inhibits occurrence of new infections more prominently as a crucial impact of administering the optimal control treatment policy. Although the disease progression gets controlled as infected and bacterial densities become stabilized after 1000 days of treatment, to attain complete eradication and elimination of bacterial load from the skin smears especially for the patients with high initial bacteriological index (B.I.) [Kar et al. (2004); Gupta et al. (2005)], the proposed optimal control treatment should be continued up to $1500 - 2000$ days as suggested by Figure 4.10 for system (4.3.13). Furthermore, comparing the Subfigures (A) and (B) in Figure 4.10, we can observe that after 1100 days, the optimal drug dose of u_1^* can be reduced and maintained up to completion of the therapy in the range $0.3 - 0.4$ for system (4.3.13) and hence, we can conclude that the delayed control system (4.3.13) provides us the best cost-effective profiles of the combined drug therapy. Results obtained from our investigations related to the optimal treatment policy predict that as we recommend the combination of Dapsone and Ofloxacin drug therapy instead of three different drugs (classical W.H.O. MDT regimen), our control induced delayed system exhibits a stable behaviour after approximately 1000 days. Morphological index (M.I.) in skin smears during the combined treatment verifies that more than 90% of viable *M. leprae* are killed after 56 days [Ji et al. (1994)] of therapy but because of the crucial interplay of the delay factors in the infection process, our system in the form of a more realistic approach to decode the *M. leprae* induced infection suggests that the combined therapy equipped with optimal control should necessarily be applied on a leprosy patient for at least $800 - 1000$ days. Thus, the re-occurrence of leprosy into a human body can also be inhibited effectively by adopting our prescribed regime. Our proposed combined treatment method is scheduled for a little longer period of time than the W.H.O. recommended regime as we intend to successfully avoid the concerns of high cost and drug

resistance effects of Rifampicin [Organization et al. (1982); Cambau and Williams (2019)]. This completely supports and justifies our analytical and numerical findings of optimal control therapeutic approach for finding a cost-effective and safe drug dose policy.

Chapter 5

Critical Observation of WHO Recommended Multidrug Therapy on the Disease Leprosy through Mathematical Study

For finding suitable leprosy control strategies, we now specifically concentrate on gaining a much deeper insight on the efficacy of the WHO recommended MDT therapy. In this Chapter[5], we have formulated a four-dimensional ODE-based mathematical model which consists of the densities of healthy Schwann cells, infected Schwann cells, *M. leprae* bacteria, and the concentration of multidrug therapy (MDT). This Chapter primarily aims on exploring the dynamical changes and interrelations of the system cell populations during the disease progression. Also, evaluating a critical value of the drug efficacy rate of MDT remains our key focus so that a safe drug dose regimen for leprosy can be framed more effectively. We have examined the stability scenario of different equilibria, the Poincare section and Lyapunov's exponent analysis method for our proposed system, and the occurrence of Hopf-bifurcation for the densities of our system cell populations with respect to the drug efficacy rate of MDT to decode the precise impact of the efficiency rate on both the infected Schwann cells and the bacterial populations. Throughout the Chapter, our main objective remains to explore the variety of neurological manifestations and pathophysiology of nerve damage in leprosy which enables us to predict the perfect drug dose regimen for the treatment of the nerve-

[5] *The major portion of this chapter is published in the Journal of Theoretical Biology, Elsevier, 567, 111496, April 2023.*

function impairment. Also, we have studied the precise effects of multidrug therapy on various system cell populations. In particular, we have investigated how MDT treatment regulates the recovery of infected cells and the infection process of the healthy cells due to the waning effect of MDT and established that it is actually the drug efficacy rate of MDT which plays a significant dominant role in the pathogenesis and treatment of leprosy. All the analytical outcomes obtained in this Chapter have been verified through numerical simulations. Furthermore, based on the clinical, histological and immunological differences, Ridley–Jopling classification of leprosy provides a complete spectrum of five main categories i.e. TT, BT, BB, BL and LL [Ridéey et al. (1966)]. Ridley's bacterial index (BI) with BI ≥ 2 (skin lesions > 5) forms the multibacillary group (MB) consisting of BB, BL and LL patients while BT and TT leprosy patients are categorized as paucibacillary group (PB) [Parkash (2009)]. In real life scenario, clinical correlations of our findings in this Chapter are also compared and discussed in detail with the U-MDT regimen, Ridley–Jopling classification and WHO recommended guidelines for leprosy.

5.1 Formulation of the Mathematical Model

Following assumptions are made for the formulation of desired mathematical model:

- The concentrations of healthy Schwann cells, infected Schwann cells, *M. leprae* bacteria and MDT drug therapy are represented by $S_h(t)$, $S_i(t)$, $B(t)$ and $X(t)$ respectively, at any time t.

- Π denotes the constant production rate of healthy Schwann cells from neural crest cells into human body. β is the effective contact rate between the healthy Schwann cells and the bacteria. α be the rate at which infected cells become recovered due to the effect of MDT. The rate at which healthy Schwann cells are getting infected again as a result of waning effect of MDT is indicated by λ.

- The parameters, r and K describe the intrinsic growth rate and carrying capacity of *M. leprae* bacteria as presented in a logistic manner.

- The level of treatment i.e. the concentration of MDT is proportional to the number of infected Schwann cells and it is represented by the term, $e\eta S_i$, where e denotes the proportionality constant and η denotes the efficacy rate of MDT. Moreover, θ reflects the natural drug washout rate through various physiological processes into a human body.

- d, d_i and d_b signify the natural death rate or mortality rate healthy Schwann cells, infected Schwann cells and the rate at which *M. leprae* bacteria is killed by MDT, respectively.

- The effective drug-treatments is directed by the increasing function, $f(X)$ with $f(0) = 0$ and $\sup f(X) = 1$. It is considered that the effectiveness of drug is fading for which the healthy Schwann cells are becoming infected again. Therefore, $g(X)$ is chosen as a decreasing function of X with $g(0) = 1$ and $\inf g(X) = 0$.

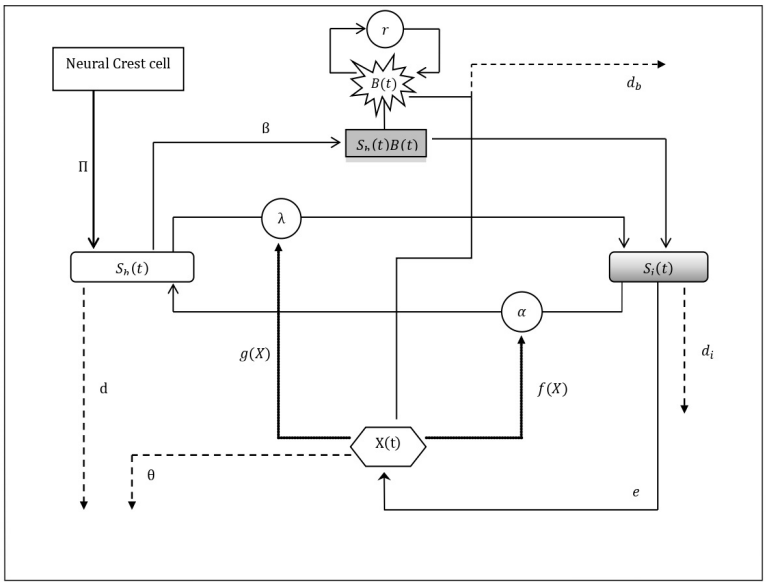

Figure 5.1: Schematic diagram of the interactions of the cell populations for system (5.1.1)

Based on the above assumptions, we have the following mathematical model which depict the various interactions between the compartments (see the Schematic diagram in Figure 5.1):

$$\begin{aligned}
\frac{dS_h}{dt} &= \Pi - \beta S_h B + \alpha f(X) S_i - \lambda g(X) S_h - d S_h, \\
\frac{dS_i}{dt} &= \beta S_h B - \alpha f(X) S_i + \lambda g(X) S_h - d_i S_i, \\
\frac{dB}{dt} &= rB\Big(1 - \frac{B}{K}\Big) - d_b X B, \\
\frac{dX}{dt} &= e\eta S_i - \theta X
\end{aligned} \tag{5.1.1}$$

with initial values $S_h(0) = S_{h0} > 0$, $S_i(0) = S_{i0} > 0$ and $B(0) = B_0 > 0$ and $X(0) = X_0 > 0$ at $t = 0$.

5.2 Model Properties

5.2.1 Non-negative invariance and boundedness

In this Subsection, we discuss the non-negativity of the solutions and boundedness of our proposed mathematical model to prove that the system (5.1.1) is biologically well-posed and plausible. We now present the following theorem which ensures the non-negativity of the solutions of system (5.1.1).

Theorem 5.2.1 *All the solutions of the system (5.1.1) along with the initial conditions are non-negative for all $t > 0$.*

Proof. To prove the theorem, let us first assume that $y_1(t) = S_h(t)$, $y_2(t) = S_i(t)$, $y_3(t) = B(t)$ and $y_4(t) = X(t)$. Now, we can rewrite system (1) in the following form:

$$\frac{dY}{dt} = \Gamma(Y), \quad \Gamma = (\Gamma_1, \Gamma_2, \Gamma_3, \Gamma_4)^\top, \quad Y = (y_1, y_2, y_3, y_4)^\top \tag{5.2.1}$$

where $^\top$ denotes the transpose and Γ_i's denote the right hand sides of system (5.1.1).

Now, for system (5.2.1), it is easy to check that

$$\Gamma_i(Y)|_{y_i=0,\ Y\in\mathbb{R}^4_+} \geq 0. \tag{5.2.2}$$

Indeed, we can see that the following relations hold.

$$\begin{aligned}
&\Gamma_1(0, y_2, y_3, y_4) = \Pi + \alpha f(y_4) y_2 \geq 0, \quad \text{whenever} \quad y_2 \geq 0, y_3 \geq 0, y_4 \geq 0,\\
&\Gamma_2(y_1, 0, y_3, y_4) = \beta y_1 y_3 + \lambda g(y_4) y_1 \geq 0, \quad \text{whenever} \quad y_1 \geq 0, y_3 \geq 0, y_4 \geq 0,\\
&\Gamma_3(y_1, y_2, 0, y_4) = 0, \quad \text{whenever} \quad y_1 \geq 0, y_2 \geq 0, y_4 \geq 0,\\
&\Gamma_4(y_1, y_2, y_3, 0) = e\eta y_2 \geq 0, \quad \text{whenever} \quad y_1 \geq 0, y_3 \geq 0, y_4 \geq 0.
\end{aligned}$$

Thus, using the result in the article [Krasnosel'skii (1968)], we can say that the conditions denoted by (5.2.2) clearly ensures the non-negativity of the solutions $y_1(t)$, $y_2(t)$, $y_3(t)$ and $y_4(t)$ of system (5.1.1) under the given initial conditions. It means that all the solutions of the system (5.1.1) exists in the region $\mathbb{R}^4_+$ and the solutions remain non-negative for all $t > 0$. This also implies that the non-negative octant $\mathbb{R}^4_+$ becomes an invariant region for system (5.1.1).

It is also very essential to prove that all the model cell populations of system (5.1.1) are bounded for all time $t > 0$. This justifies that the system (5.1.1) is well-posed and realistic. The next theorem demonstrates the boundedness of the solutions of system (5.1.1).

Theorem 5.2.2 *All the non-negative solutions of system (5.1.1) enter the domain denoted by* $\mathcal{D} \subset \mathbb{R}^4_+$ *and are ultimately bounded for all possible time* $t > 0$ *where the region* $\mathcal{B}$ *is defined as:*

$$\mathcal{B} = \left\{ (S_h, S_i, B, X) \in \mathbb{R}^4_+ : 0 \leq S_h + S_i \leq \mathcal{D}_1, 0 \leq B \leq \mathcal{D}_2, 0 \leq X \leq \mathcal{D}_3 \right\} \tag{5.2.3}$$

where $\mathcal{D}_i$*'s for* $i = 1, 2, 3$ *are given as:*

$$\mathcal{D}_1 = \frac{\Pi}{d}, \quad \mathcal{D}_2 = max\ \{K, B(0)\} \quad and \quad \mathcal{D}_3 = \frac{e\eta\Pi}{\theta d}.$$

Proof. First, let us consider the first two equations of system (5.1.1). Adding these two equations, we get

$$\frac{d(S_h + S_i)(t)}{dt} = \Pi - (d + d_i)(S_h + S_i)(t)$$

which implies

$$\frac{dU(t)}{dt} \leq \Pi - dU(t) = d\mathcal{D}_1 - dU(t), \tag{5.2.4}$$

where $U(t) = (S_h + S_i)(t)$. Now, using the well-known comparison principle [Birkhoff and Rota (1978)] to (5.2.4), we achieve the following inequality:

$$0 < U(t) < \mathcal{D}_1(1 - e^{-dt}) + U(0)e^{-dt} \quad \text{for} \quad t > 0. \tag{5.2.5}$$

This implies that $U(t) \leq \mathcal{D}_1$ if $U(0) \leq \mathcal{D}_1$.

Now, we consider the third equation of system (5.1.1). Using Theorem 5.2.1, we can write the following inequality:

$$\frac{dB(t)}{dt} \leq rB(t)(1 - \frac{B(t)}{K}). \tag{5.2.6}$$

Integrating this inequality with the corresponding initial condition i.e. $B(0) > 0$, we get

$$0 \leq B(t) \leq \frac{KB(0)}{B(0)(1 - e^{-rt}) + Ke^{-rt}} \leq \mathcal{D}_2 \tag{5.2.7}$$

where $\mathcal{D}_2 = max\ \{K, B(0)\}$.

Again, using the result $0 \leq S_i \leq \frac{\Pi}{d}$ and repeating the similar argument, we also obtain the following:

$$0 < X(t) < \mathcal{D}_3(1 - e^{-\theta t}) + X(0)e^{-\theta t} \quad \text{for} \quad t > 0 \tag{5.2.8}$$

which implies that $X(t) \leq \mathcal{D}_3$ if $X(0) \leq \mathcal{D}_3$.

Hence, all the solutions (S_h, S_i, B, X) of system (5.1.1) which start in the region $\mathcal{B}$, remain within it for all $t > 0$. This evidently makes $\mathcal{B}$ an invariant region for system (5.1.1). Also, the region $\mathcal{B}$ is bounded and this implies that all the mentioned solutions of the system (5.1.1) are ultimately bounded.

Here, it is important to note that all such solutions of system (5.1.1) with the non-negative initial conditions finally arrive into $\mathcal{B}$ and stay in it. This property is justified by the definition of the region $\mathcal{B}$ and the following relationships:

$$\begin{aligned} \frac{dS_h}{dt}(t)\bigg|_{\partial\mathcal{B}} < 0, \qquad \frac{dS_i}{dt}(t)\bigg|_{\partial\mathcal{B}} < 0, \\ \frac{dB}{dt}(t)\bigg|_{\partial\mathcal{B}} < 0, \qquad \frac{dX}{dt}(t)\bigg|_{\partial\mathcal{B}} < 0, \end{aligned} \tag{5.2.9}$$

which are actually carried out at the points of the boundary $\partial\mathcal{B}$ of $\mathcal{B}$. Also, note that, the relationships in (5.2.9) hold outside the region $\mathcal{B}$ which completely ensures the boundedness of all solutions (S_h, S_i, B, X) of system (5.1.1) with the above mentioned non-negative initial conditions.

5.2.2 Equilibrium points and their existence

In this Section, some basic properties such as existence and stability of equilibria for system (5.1.1) are illustrated.

The equilibrium points are obtained by equating the right-hand side of each equation in (5.1.1) to zero and it is found that system (5.1.1) has two non-negative equilibria, namely

- the trivial disease-free equilibria $E_0 = \left(\frac{\Pi}{d}, 0, 0, 0\right)$, which always exists,
- for the endemic equilibrium $E^*(S_h^*, S_i^*, B^*, X^*) \neq 0$ to exist, its coordinates must satisfy the following conditions: $S_h^* > 0$, $S_i^* > 0$, $B^* > 0$ and $X^* > 0$ where

$$S_h^* = \frac{r[\alpha f(X^*) + d_i]\theta X^*}{e\eta[\beta K(r - d_b X^*) + r\lambda g(X^*)]}, \; S_i^* = \frac{\theta X^*}{e\eta}, \; B^* = \frac{K}{r}(r - d_b X^*) \text{ and } X^* = \frac{r}{d_b}(1 - \frac{B^*}{K}).$$

Here, using Theorem 5.2.2 i.e the fact that the bacterial concentration $B(t)$ can not exceed the carrying capacity K of the *M. leprae* bacterial population, it follows that

$X^* = \frac{r}{d_b}(1 - \frac{B^*}{K}) > 0$. Also, this implies that $S_i^* = \frac{\theta X^*}{e\eta} > 0$ as $X^* > 0$.

Now, considering the formulas of S_h^* and B^*, we can see that both $S_h^* > 0$ and $B^* > 0$ provided that the condition $r > d_b X^*$ holds. This ensures the existence of positive endemic equilibrium E^* of system (5.1.1). We now summarize the previous discussions by constructing the following lemma.

Lemma 5.2.1 *The positive endemic equilibrium E^* of system (5.1.1) exists if $r > d_b X^*$ is satisfied.*

Remark 5.2.1 *The sufficient condition for the existence of the endemic equilibrium E^* is that whenever the ratio of intrinsic growth rate and the rate at which* M. leprae *bacteria is killed by the drug therapy, exceeds X^*. Biologically, this is well supported as it means that the growth rate (r) of the bacterial population and the killing rate (d_b) of the bacteria by MDT plays a crucial role in this scenario and if the ratio becomes relatively higher than endemic state MDT concentration X^*, the infected steady state becomes feasible i.e begins to exist.*

5.2.3 Stability analysis

In this Section, at first, we deduce the basic reproduction number R_0 and discuss the local asymptotic stability of the disease-free equilibrium E_0.

Biologically, we can say that R_0 is the average number of new secondary infections in a completely susceptible Schwann cell population. To evaluate R_0, we choose the next-generation matrix method [Heffernan et al. (2005)]. We consider only the infected compartments ($S_i(t)$, $B(t)$ and $X(t)$) of system (5.1.1) i.e. to be precise, the second, third and fourth equations of system (5.1.1). Now, let us define the three dimensional matrices $\mathcal{F}$ and $\mathcal{V}$ as the matrices describing the new infection terms and the remaining transfer terms evaluated at the disease-free equilibrium $E_0 = \left(\frac{\Pi}{d}, 0, 0, 0\right)$, respectively. The linearization of the second, third and fourth equations of system (5.1.1) at the disease-free state E_0 can be rewritten in the following form:

$$\frac{dW}{dt} = (\mathcal{F} - \mathcal{V})W$$

where $W = (S_i, B, X)^\top$ and the matrices $\mathcal{F}$ and $\mathcal{V}$ are given as:

$$\mathcal{F} = \begin{pmatrix} 0 & \frac{\beta\Pi}{d} & \frac{\lambda q\Pi}{d} \\ 0 & 0 & 0 \\ e\eta & 0 & 0 \end{pmatrix} \quad \text{and} \quad \mathcal{V} = \begin{pmatrix} d_i & 0 & 0 \\ 0 & -r & 0 \\ 0 & 0 & \theta \end{pmatrix}. \tag{5.2.10}$$

Using the spectral radius of the next-generation matrix a threshold criterion i.e. the basic reproduction number R_0 can be determined which is actually the largest eigenvalue (ρ) of the matrix $\mathcal{F}\mathcal{V}^{-1}$. Hence,

$$R_0 = \rho(\mathcal{F}\mathcal{V}^{-1}) = \max_{|\kappa|} \det(\kappa I - \mathcal{F}\mathcal{V}^{-1})$$

where I is the identity matrix of order 3 and

$$\mathcal{F}\mathcal{V}^{-1} = \begin{pmatrix} 0 & -\frac{\beta\Pi}{dr} & \frac{\lambda q\Pi}{d\theta} \\ 0 & 0 & 0 \\ \frac{e\eta}{d_i} & 0 & 0 \end{pmatrix}. \tag{5.2.11}$$

So, finally we have

$$R_0 = \sqrt{\frac{\lambda\Pi q e\eta}{dd_i\theta}}. \tag{5.2.12}$$

Now, the discussion of local stability of the disease-free equilibrium E_0 with respect to the basic reproduction number R_0 can be summarised in the following theorem.

Theorem 5.2.3 *The system is stable at E_0 if $R_0 < 1$ and becomes unstable for $R_0 > 1$. Consequently, a transcritical bifurcation occurs at the critical value $R_0 = 1$.*

At the endemic equilibrium $E^* = (S_h^*, S_i^*, B^*, X^*)$, the Jacobian matrix of system (5.1.1) takes the following form:

$$\mathcal{J}(E^*) = \begin{pmatrix} M_{11}^* & M_{12}^* & -M_{13}^* & -M_{14}^* \\ M_{21}^* & M_{22}^* & M_{13}^* & M_{14}^* \\ 0 & 0 & M_{33}^* & M_{34}^* \\ 0 & M_{42}^* & 0 & M_{44}^* \end{pmatrix}.$$

where
$M_{11}^* = -(\beta B^* + \lambda g(X^*) + d) = -(M_{21}^* + d)$, $M_{12}^* = \alpha f(X^*)$, $M_{13}^* = \beta S_h^*$, $M_{14}^* = -\alpha f'(X^*)S_i^* + \lambda g'(X^*)S_h^*$, $M_{21}^* = \beta B^* + \lambda g(X^*)$, $M_{22}^* = -\alpha f(X^*) - d_i$, $M_{33}^* = r - \frac{2rB^*}{K} - d_b X^*$, $M_{34}^* = -d_b B^*$, $M_{42}^* = e\eta$, $M_{44}^* = -\theta$.

Expanding $\det(\mathcal{J} - \upsilon I) = 0$, we get the characteristic equation of system (5.1.1) at the endemic equilibrium point E^* as follows:

$$Y(\upsilon) = \upsilon^4 + \psi_1\upsilon^3 + \psi_2\upsilon^2 + \psi_3\upsilon + \psi_4 = 0 \tag{5.2.13}$$

where

$$\psi_1 = -(M^*_{11} + M^*_{22} + M^*_{33} + M^*_{44}),$$
$$\psi_2 = M^*_{33}M^*_{44} + M^*_{33}(M^*_{11} + M^*_{22}) + M^*_{44}(M^*_{11} + M^*_{22}) + M^*_{11}M^*_{22} - M^*_{42}M^*_{14} - M^*_{21}M^*_{12},$$
$$\psi_3 = M^*_{42}M^*_{14}(M^*_{11} + M^*_{21} + M^*_{33}) - M^*_{33}M^*_{44}(M^*_{11} + M^*_{22}) - M^*_{33}(M^*_{11}M^*_{22} - M^*_{21}M^*_{12})$$
$$- M^*_{44}(M^*_{11}M^*_{22} - M^*_{21}M^*_{12}) - M^*_{13}M^*_{34}M^*_{42},$$
$$\psi_4 = M^*_{13}M^*_{34}M^*_{42}(M^*_{11} + M^*_{21}) + M^*_{33}M^*_{44}(M^*_{11}M^*_{22} - M^*_{21}M^*_{12}) - M^*_{14}M^*_{33}M^*_{42}(M^*_{11} + M^*_{21}).$$

The characteristic equation $Y(\upsilon) = \upsilon^4 + \psi_1\upsilon^3 + \psi_2\upsilon^2 + \psi_3\upsilon + \psi_4 = 0$ denoted by equation (5.2.13) will play the dominant role in determining the local asymptotic stability of E^* for system (5.1.1). Hence, using Routh-Hurwitz criterion for system (5.1.1), we can obtain the following theorem:

Theorem 5.2.4 *At the endemic equilibrium point E^*, all the roots of the characteristic polynomial of system (5.1.1) will be negative real or possess negative real parts i.e. system (5.1.1) will be locally asymptotically stable at E^* if the following four conditions hold true:*

$$\psi_1 > 0, \quad \psi_4 > 0, \quad \psi_1\psi_2 > \psi_3 \quad \textit{and} \quad \psi_1\psi_2\psi_3 - \psi_3^2 - \psi_1^2\psi_4. \tag{5.2.14}$$

In view of the above discussion, we can also present the following result.

Proposition 5.2.1 *The endemic equilibrium point E^* is stable if the condition $R_0 > 1$ is satisfied.*

5.3 Hopf-bifurcation Analysis of the System

A system exhibits Hopf-bifurcation at the endemic steady state if the characteristic equation of the system at that state possesses a pair of purely imaginary eigenvalues and all the other eigenvalues are negative real or with negative real parts. We now study the local Hopf-bifurcation at the endemic equilibrium E^*. Here, for E^*, we consider $\zeta(= (\Pi, \beta, \alpha, \lambda, d, d_i, r, K, d_b, e, \eta, \theta)) \in \mathbb{R}$ is the generic bifurcation parameter of the system. Let, $\Phi : (0, \infty) \longrightarrow \mathbb{R}$ be a continuously differentiable function of ζ defined as

$$\Phi(\zeta) = \psi_1(\zeta)\psi_2(\zeta)\psi_3(\zeta) - \psi_3^2(\zeta) - \psi_4(\zeta)\psi_1^2(\zeta). \tag{5.3.1}$$

For the Hopf-bifurcation to occur, there exists a $\zeta^* \in (0, \infty)$ in the spectrum $\psi(\zeta) = \{\upsilon : Y(\upsilon) = 0\}$ of the characteristic equation (5.2.13), at which a pair of complex eigenvalues

$\upsilon(\zeta^*)$ and $\bar{\upsilon}(\zeta^*) \in \psi(\zeta)$ satisfy the following two conditions:

$$\mathfrak{Re}[\upsilon(\zeta^*)] = 0, \quad \mathfrak{Im}[\upsilon(\zeta^*)] = \omega_0 > 0.$$

In addition, the following transversality condition also must have to be satisfied :

$$\left.\frac{d\mathfrak{Re}(\upsilon_j(\zeta))}{d\zeta}\right|_{\zeta=\zeta^*} \neq 0 \quad \text{for} \quad j = 1, 2. \tag{5.3.2}$$

Theorem 5.3.1 *The endemic equilibrium E^* of system (5.1.1) undergoes Hopf-bifurcation at $\zeta = \zeta^* \in (0, \infty)$ if and only if*

$$\psi_2(\zeta^*) > 0, \quad \psi_3(\zeta^*) > 0, \quad \psi_4(\zeta^*) > 0, \quad \psi_1(\zeta^*)\psi_2(\zeta^*) - \psi_3(\zeta^*) > 0, \tag{5.3.3}$$

$$\Phi(\zeta^*) = 0 \quad \textit{and} \quad \psi_1^3\psi_2'\psi_3(\psi_1 - 3\psi_3) - (\psi_2\psi_1^2 - 2\psi_3^2)(\psi_3'\psi_1^2 - \psi_1'\psi_3^2) \neq 0. \tag{5.3.4}$$

In addition, at $\zeta = \zeta^*$, the characteristic equation contains a pair of purely imaginary eigenvalues and the other two eigenvalues will be negative real or having negative real parts where differentiation with respect to ζ is denoted by primes.

Proof. From the condition, $\Phi(\zeta^*) = 0$, the characteristic equation (5.2.13) can be rewritten in the form

$$(\upsilon^2 + \frac{\psi_3}{\psi_1})(\upsilon^3 + \psi_1\upsilon + \frac{\psi_1\psi_4}{\psi_3}) = 0. \tag{5.3.5}$$

We now denote the four roots of equation (5.3.5) in the complex domain by υ_i for $i = 1, 2, 3, 4$ and let, the pair of imaginary roots at $\zeta = \zeta^*$ being $\upsilon_1 = \bar{\upsilon}_2$. Hence, we get that

$$\begin{cases} \upsilon_3 + \upsilon_4 = -\psi_1, \quad \omega_0^2 + \upsilon_3 + \upsilon_4 = \psi_2, \\ \omega_0^2(\upsilon_3 + \upsilon_4) = -\psi_3, \quad \omega_0^2\upsilon_3\upsilon_4 = \psi_4 \end{cases}$$

where $\omega_0 = \mathfrak{Im}[\upsilon_1(\zeta^*)]$. Considering this set of equations, we can see that $\omega_0 = \sqrt{\frac{\psi_3}{\psi_1}}$ and if ψ_3, ψ_4 are chosen as complex conjugates then we have that $2\mathfrak{Re}[\upsilon_3] = -\psi_1$. From the characteristic equation (5.2.13), it follows that $\upsilon_3 < 0$, $\upsilon_4 < 0$ if υ_3, υ_4 are real roots. Now, to verify the transversality conditions, we substitute $\upsilon_j(\zeta) = \sigma_1(\zeta) \pm i\sigma_2(\zeta)$ in equation (5.2.13) and differentiating, it follows that

$$\begin{cases} K(\zeta)\sigma_1'(\zeta) - L(\zeta)\sigma_2'(\zeta) + M(\zeta) = 0, \\ L(\zeta)\sigma_1'(\zeta) + K(\zeta)\sigma_2'(\zeta) + N(\zeta) = 0, \end{cases} \tag{5.3.6}$$

where the values of $K(\zeta)$, $L(\zeta)$, $M(\zeta)$ and $N(\zeta)$ are given as

$$
\begin{aligned}
K(\zeta) &= 4\sigma_1^3 - 12\sigma_1\sigma_2 + 3\psi_1(\sigma_1^2 - \sigma_2^2) + 2\psi_2\sigma_1 + \psi_3,\\
L(\zeta) &= 12\sigma_1^2\sigma_2 + 6\psi_1\sigma_1\sigma_2 - 4\sigma_1^3 + 2\psi_2\sigma_1,\\
M(\zeta) &= \psi_1\sigma_1^3 - 3\psi_1'\sigma_1\sigma_2^2 + \psi_2'(\sigma_1^2 - \sigma_2^2) + \psi_3'\sigma_1,\\
N(\zeta) &= 3\psi_1'\sigma_1^2\sigma_2 - \psi_1'\sigma_2^3 + 2\psi_2'\sigma_1\sigma_2 + \psi_3'\sigma_1.
\end{aligned}
$$

Now, solving (5.3.6) for $\sigma_1'(\zeta)$, we get that

$$
\begin{aligned}
\left.\frac{d\mathfrak{Re}(\upsilon_j(\zeta))}{d\zeta}\right|_{\zeta=\zeta^*} &= \sigma_1'(\zeta)\big|_{\zeta=\zeta^*}\\
&= -\frac{[L(\zeta^*)N(\zeta^*) + K(\zeta^*)M(\zeta^*)]}{K^2(\zeta^*) + L^2(\zeta^*)}\\
&= \frac{\psi_1^3\psi_2'\psi_3(\psi_1 - 3\psi_3) - 2(\psi_2\psi_1^2 - 2\psi_3^2)(\psi_3'\psi_1^2 - \psi_1'\psi_3^2)}{\psi_1^4(\psi_1 - 3\psi_3)^2 + 4(\psi_2\psi_1^2 - 2\psi_3^2)^2}.
\end{aligned}
$$

From this result, we can see that $\psi_1^4(\psi_1 - 3\psi_3)^2 + 4(\psi_2\psi_1^2 - 2\psi_3^2)^2 > 0$ always. Hence,

$$
\left.\frac{d\mathfrak{Re}(\upsilon_j(\zeta))}{d\zeta}\right|_{\zeta=\zeta^*} \neq 0
$$

holds if

$$
\psi_1^3\psi_2'\psi_3(\psi_1 - 3\psi_3) - 2(\psi_2\psi_1^2 - 2\psi_3^2)(\psi_3'\psi_1^2 - \psi_1'\psi_3^2) \neq 0.
$$

Thus, Hopf-bifurcation occurs for the critical value $\zeta = \zeta^*$ at a neighbourhood of the endemic equilibrium E^* of system (5.1.1).

Remark 5.3.1 *Hopf-bifurcating periodic solutions appear for our system cell populations in the neighbourhood of E^*. This indicates that the system (5.1.1) undergoes stability switches as an effect of administering MDT drug concentrations into the human body. The impact of λ as well as the infection rate β is notable here while the drug efficacy rate of MDT η contributes most significantly to this behavior of the densities of the steady state populations.*

5.4 Numerical Simulations

In this Section, we perform numerical simulations for our four dimensional mathematical model using Matlab 2016A to validate and justify all of our analytical findings achieved in the Subsections 5.2.2, 5.2.3 and Section 5.3. These numerical findings help us interpreting the dynamical shifts of our system cell populations in presence of MDT and more specifically, the procedure of infection of recovered Schwann cells as a resultant of gradually waning drug

Table 5.1: **List of parameter values used in numerical simulations for system (2.1.1)**

Parameter	Assigned Value (Unit)	Range
Π	35 (cells day^{-1})	20-50
β	0.0022 (mm^3 day^{-1})	0.0012-0.0058
α	0.0001 (mm^3 day^{-1})	0.00008-0.0002
λ	0.00042 (mm^3 day^{-1})	0.0002-0.00045
d	0.004 (day^{-1})	0.0015-0.006
d_i	0.0036 (day^{-1})	0.0001-0.0046
η	0.026	-
r	0.1 (day^{-1})	-
K	500 (mm^{-3})	200-700
d_b	0.0022 (day^{-1})	0.0014-0.003
e	1.1	-
θ	0.00012 (μM day^{-1})	0.0001-0.0002

dose efficiency. Separate simulations have been performed for PB and MB cases considering different values of infection rates depending on bacterial index (BI) and drug efficacy rates. To carry this out, we use a set of parameters provided in Table 5.1. Some of the values of these parameters for system (5.1.1) are assumed and other values are either obtained from several literatures or estimated from different elemental sources [Fischer (2017); Talhari et al. (2015)]. For the purpose of numerical simulations, we have used the explicit forms as $f(X) = \frac{X}{1+X}$ and $g(X) = \frac{1}{1+X}$. We choose the initial values in number dependant according to the cardinal rule of scientific hypothesis.

In Figure 5.2, we have demonstrated the behaviour of the trajectories of the system without drugs for $R_0 > 1$ at the endemic state E^*. It is evident that in this scenario, system cell populations exhibits periodic oscillatory solutions i.e. the densities of healthy Schwann cells ($S_H(t)$), infected Schwann cells ($S_I(t)$) and *M. leprae* bacteria ($B(t)$) fluctuate rapidly in the neighbourhood of E^* in the absence of drug. Biologically, it clearly justifies the essence of incorporating MDT therapy into the system for the densities of the system populations to arrive in a stable state.

Next, in Figure 5.3, solution trajectories of the populations of system (5.1.1) the endemic state E^* have been described for three different values of η i.e. for the values of $\eta = 0.018, 0.02, 0.022$. Our findings suggests that amplitude of the fluctuation in the

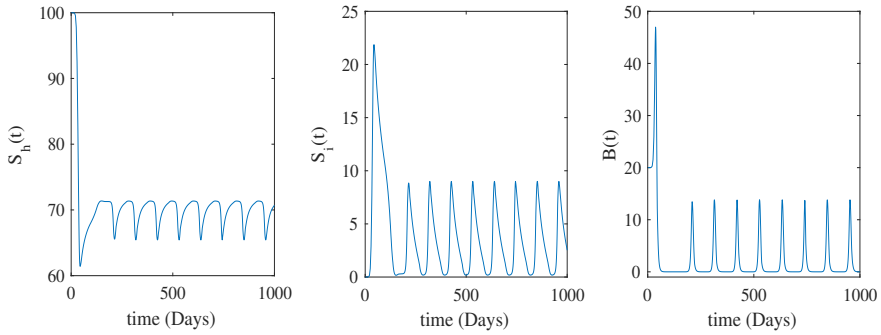

Figure 5.2: Dynamical nature of the trajectories the healthy Schwann cells ($S_H(t)$), infected Schwann cells ($S_I(t)$), M. leprae *bacteria ($B(t)$) of the system without drugs at the endemic state E^* for $R_0 > 1$. The initial values of the system populations are considered as: $S_H(0) = 100$, $S_I(0) = 5$, $B(0) = 20$ and values of all the other parameters are chosen from Table 5.1.*

densities of S_H cells, S_I cells and *M. leprae* bacteria B decreases as η is increased from the value 0.018. This specific pattern indicates that the system populations tends to a stable concentration gradually with the increasing of the value of the drug efficacy rate η of MDT.

In Figure 5.4, bifurcation diagrams of the populations of system (5.1.1) with respect to the efficacy rate η are depicted at a neighbourhood of the endemic equilibrium E^*. For the value of $\eta < 0.024$, periodic oscillatory solutions are observed but as the value of η crosses the critical value $\eta = \eta^* = 0.024$, system becomes stable. Thus, it clearly indicates that the efficacy rate of MDT, η plays a crucial role in leprosy pathogenesis as the whole dynamical shifting of the behaviour of the trajectories of the system cell populations depends primarily on this parameter. Biologically, this reflects that MDT therapy with an efficacy rate η greater than the threshold value $\eta = \eta^*$ is strictly recommended to reduce the disease dissemination process effectively into the human body.

In Figure 5.5, we have demonstrated the Poincare section for the parameter values of

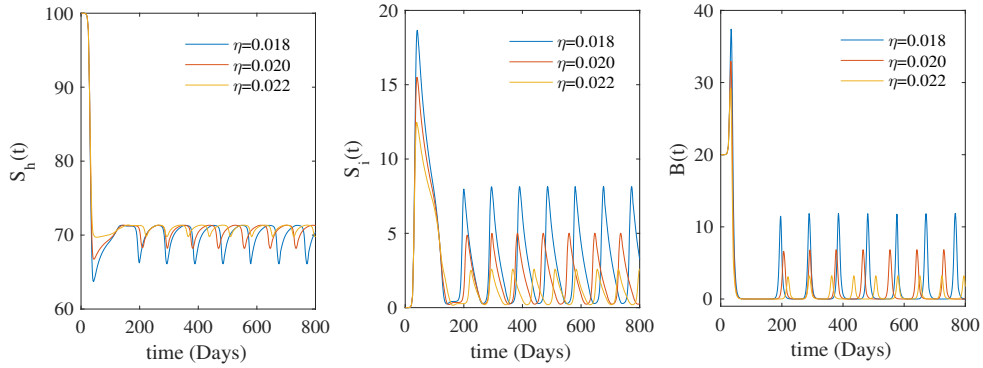

Figure 5.3: Comparison of the oscillatory solutions of the healthy Schwann cells ($S_H(t)$), infected Schwann cells ($S_I(t)$), M. leprae bacteria ($B(t)$) of system (5.1.1) for different values of drug efficacy rate η at the steady state when $R_0 > 1$. Trajectories coloured in blue, red and brown indicate the densities of the system population for the values of $\eta = 0.018$, $\eta = 0.02$ and $\eta = 0.022$. Values of rest of the parameters used in the simulation of this Figure are taken from Table 5.1.

system (5.1.1) represented in Table 5.1. Here, we have actually plotted $\dot{S}_i(t)$ vs $S_i(t)$ using six different values of η. The discrete dynamical behaviour of our continuous system (5.1.1) through the intersection of periodic orbits in the state space is investigated and represented here to establish a permissible range of drug efficacy η for which the system remains stable. This Figure describes that the points assemble together to form a definite pattern occupying a subset of the phase space. The values of $\dot{S}_i(t)$ ranges over nearly ≈ 1 to 3.56 for all the Subfigures but we can see that this specific pattern is not deviated or more particularly, for the values of $\eta = 0.024, 0.025, 0.026$, it does not lose the shape as the values of $S_i(t)$ is increased. This dynamical nature of system (5.1.1) precisely forms the origination of an attractor such that the system trajectories intersect the plane in this pattern. This attractor is a limit cycle and hence, we can conclude that the system is stable for this specific ranges of values of η. Also, from this Figure, our findings confirm the global asymptotical stability of system (5.1.1) as we have opted for Poincare section method here in exhibiting this

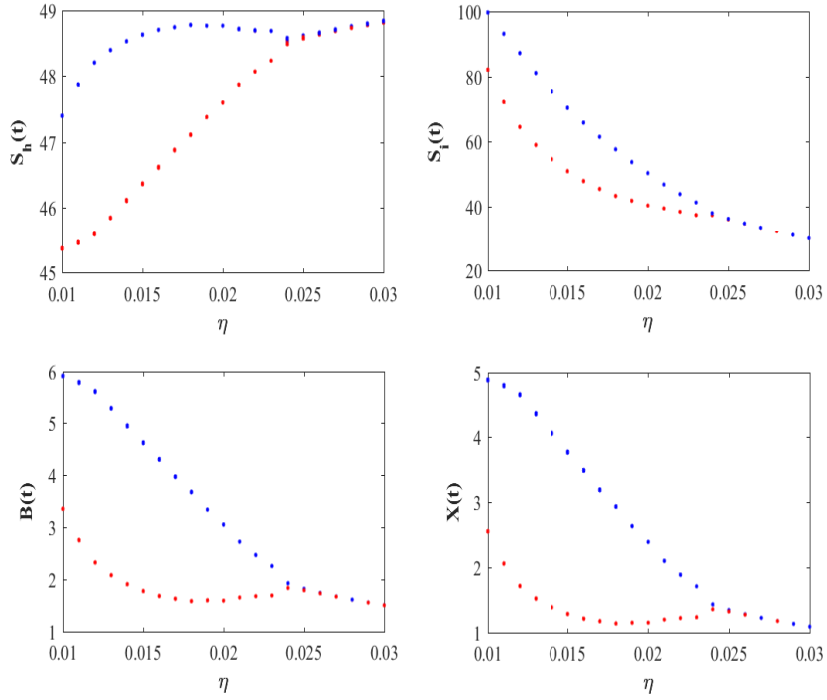

Figure 5.4: Demonstration of bifurcation diagrams and oscillation of the model populations for system (5.1.1) plotted as a function of drug efficacy rate η for $R_0 > 1$. Here, steady state values of all the populations are plotted together with the minimum/maximum of the periodic solutions when it exists. We choose the values of the parameters as given in Table 5.1. Unstable and stable zones are clearly displayed by the dotted vertical line drawn at the critical value $\eta = \eta^* = 0.024$.

phenomenon instead of extensive and tedious analytical calculations.

Next, in Figure 5.6, we have plotted time evolution of the sum of all four Lyapunov's exponents of the model populations for system (5.1.1) for different values of η and the corresponding dynamics of Lyapunov's exponents are described. To indicate the PB types of cases, the value of β is chosen considerably low i.e. $\beta = 0.0032$ mm^3 day^{-1}. The values of drug-efficacy rate η are chosen as $\eta = 0.027, 0.06$ and 0.07 and all the other parameter values are chosen here according to the values given in Table 5.1. Investigating the Lyapunov's exponents for our system enables us to detect the presence of chaos and quantify the stability or instability of the system. Figure 5.6 actually determines the system's sensitivity to initial conditions and more precisely, measures the robustness of the densities of the system populations: S_{h_0}, S_{i_0}, B_0 and X_0 at the time $t = 0$. Moreover, positivity of the

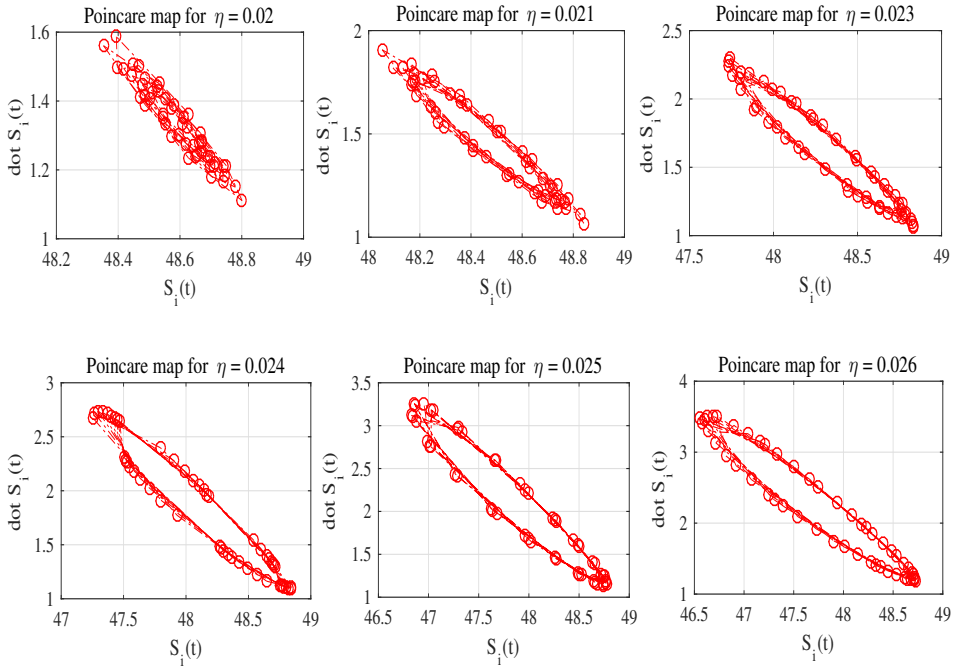

Figure 5.5: Poincare section for the set of parameter values for system (5.1.1). Here, the investigation is performed for six different values of efficacy rate η to achieve the six Subfigures. The values of parameters are chosen as $\Pi = 50$ cells day^{-1}, $\beta = 0.00014$ mm^3 day^{-1} and all the other parameters are taken from Table 5.1.

sum of Lyapunov's exponents means that the system is sensitive to the initial values and possesses chaotic nature. The obtained dynamics of Lyapunov's exponents explains that for $\eta = 0.027$, the sum of the exponents remains negative suggesting that system (5.1.1) remains stable in this case. This finding also supports the results achieved in Figure 5.4. Also, for higher values of efficacy rate i.e. for $\eta = 0.06, 0.07$, system exhibits chaotic behaviour and ultimately, becomes unstable again which is validated by the positive values of sum of Lyapunov's exponents of all the system populations. Specifically, it suggests us that applying MDT for a prolonged period of time i.e. from 6 months to 12 months in PB cases with a very high efficacy rate (i.e. for $\eta > 0.059$) on a leprosy affected person, does not actually exhibit any fruitful result [Narang et al. (2022)]. Rather, it induces substantial drug resistance [Sansarricq et al. (2004)] and severe adverse drug effects [Deps et al. (2007); Kaluarachchi et al. (2001)] into the human body. This indicates a treatment tenure of at least 120 days for PB cases which also supports the WHO recommended PB multidrug

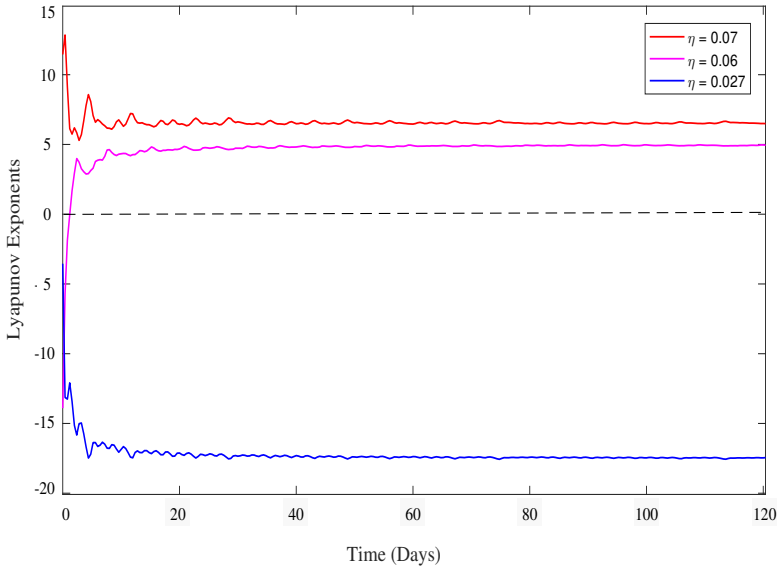

Figure 5.6: Plot of the sum of all the Lyapunov's exponents of the model cell populations for system (5.1.1) for Paucibacillary (PB) types of infection. Values of the parameters are taken $\beta = 0.0032\ mm^3\ day^{-1}$ *and* $K = 420\ mm^{-3}$ *and the values of the other parameters are chosen from Table 5.1. Trajectories coloured in blue, pink and red indicate the dynamics of the sum of the exponents of* S_H *cells,* S_I *cells, bacteria* $B(t)$ *and MDT concentration* $X(t)$ *with time for the values of* $\eta = 0.027$, $\eta = 0.06$ *and* $\eta = 0.07$ *respectively.*

therapy regimen completely [Organization et al. (2012)].

Similarly, in Figure 5.7, time evolution of the sum of all the Lyapunov's exponents of our system cell populations are demonstrated for the values of $\eta = 0.055, 0.06$ and 0.07 for 300 days. To simulate this Figure, value of β is considered as $\beta = 0.0071$ to specifically indicate the infection rate of multibacillary (MB) types of leprosy patients. Simulation shows that our system populations starts getting stabilized after 300 days of treatment with safe and effective efficacy zone of $\eta \in (0.025, 0.059)$ which is also recognized by the WHO mentioned guidelines for multibacillary leprosy patients.

Figure 5.8 investigates and presents the sensitivity of the level of treatment i.e. the drug efficacy rate (η) which we incorporate in the system with time as the infection rate (β) increases. The values of β has been varied in the range $0.001 - 0.009$ to simulate this Figure.

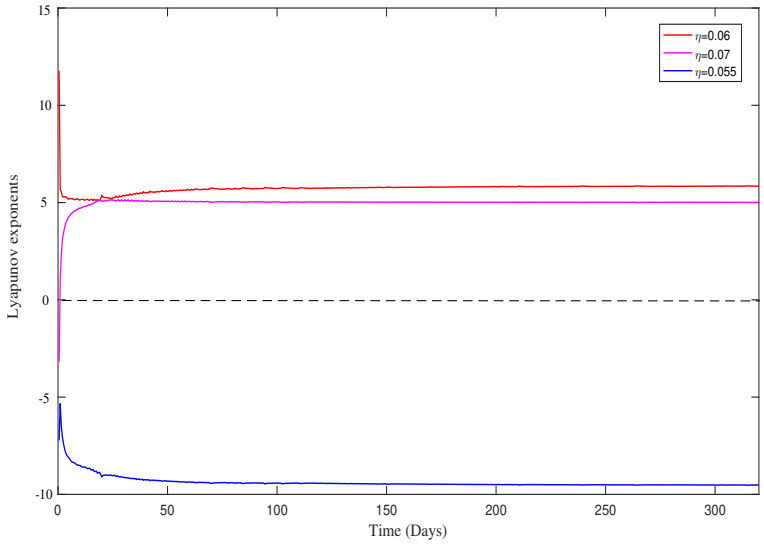

Figure 5.7: Plot of the sum of all the Lyapunov's exponents of the model cell populations for system (5.1.1) for Multiibacillary (MB) types of infection. Values of the parameters are taken $\beta = 0.0071\ mm^3\ day^{-1}$ *and* $K = 480\ mm^{-3}$ *and the values of the other parameters are chosen from Table 5.1. Trajectories coloured in blue, pink and red indicate the dynamics of the sum of the exponents of* S_H *cells,* S_I *cells, bacteria* $B(t)$ *and MDT concentration* $X(t)$ *with time for the values of* $\eta = 0.055$, $\eta = 0.07$ *and* $\eta = 0.06$ *respectively.*

According to the sensitivity profile displayed in this Figure, we can clearly see that η is highly sensitive to the infection rate β which regulates the overall progression of infection into a leprosy patient.

Finally, the combined impact of η and λ on the basic reproduction number R_0 and also the impact of η and β on R_0 has been displayed in the Subfigure (a) and Subfigure (b) respectively in Figure 5.9. In Subfigure (a), we have demonstrated the contour plot of η, λ and R_0 in the three dimensional space where both the values of η and λ are varied over the interval $(0, 1)$. The plane denoted by $R_0 = 1$ plays a decisive role here as it intersects the other two planes. This intersection particularly contributes to present the coupled threshold values of level of treatment where η plays a determining role for the control of the disease progression. In the contour plot denoted by Subfigure (b), the intersection of the plane $R_0 = 1$ provides us a decisive criteria for the feasibility of the endemic state E^* and its

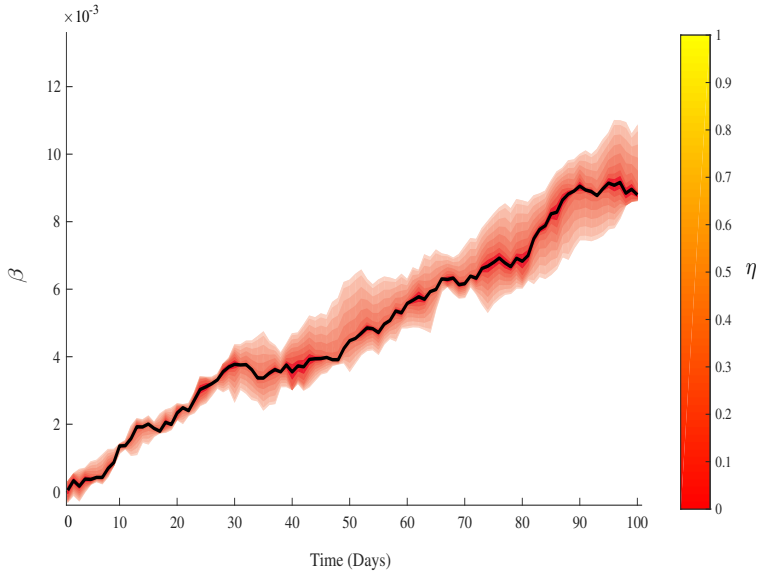

Figure 5.8: Analysis of the sensitivity of the drug efficacy rate (η) with time as the infection rate (β) increases for system (5.1.1) for 100 *days of treatment. As the colour becomes darker from light, the figure indicates a higher sensitivity profile. All the parameter values are chosen from Table 5.1 to simulate this Figure.*

dependency on the two most significant parameters η and β for finding an effective yet safe drug dose regimen for leprosy.

In view of the above numerical simulations and the analytical results obtained in the previous Sections, we now present the following Table 5.2 which describes the dynamical behaviour of the system and overall impact of the multidrug therapy for different values of efficacy rate η into a leprosy affected person.

Table 5.2: **Classification of the influence of MDT based on the values of η for system (5.1.1)**

Range of values of η	Overall impact of MDT on a leprosy patient
$0 < \eta \leq 0.024$	Ineffective or mildly effective
$0.025 < \eta < 0.059$	Safe and strongly effective
$\eta \geq 0.06$	Unsafe

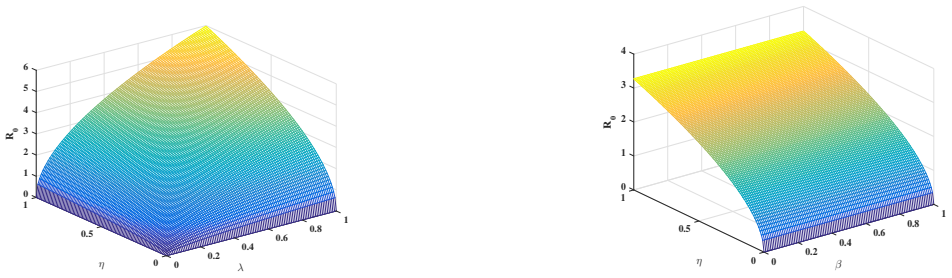

(a) contour plot of η, λ and R_0

(b) contour plot of η, β and R_0

Figure 5.9: Three dimensional contour plots of different pairs of parameters with the basic reproduction number R_0 for system (5.1.1). Values of rest of the parameters used here are chosen from Table 5.1.

5.5 Discussion

Fundamental issues involving the drug-effectiveness of MDT therapy, drug overdose situation, proper length or duration of treatment, adverse therapeutic effects and re-emergence of the infection [Sales et al. (2013); Gelber and Grosset (2012); Penna et al. (2014)] in leprosy are hardly investigated and analyzed from a mathematical point of view. To fill these gaps, we have presented a four dimensional nonlinear ODE based mathematical model describing the infection of healthy Schwann cells and recovery of the infected cells through multidrug therapy and reinfection of the recovered cells of the peripheral nervous system.

In this Chapter, we have obtained mathematical constraint about the existence of the positive endemic equilibrium E^* in Lemma 5.2.1 in Section 5.2.2 and the local asymptotical stability conditions of system (5.1.1) at E^* in Theorem 5.2.4 by using the well-known Routh-Hurwitz criterion. We have also derived the basic reproduction number R_0 for system (5.1.1). For $R_0 < 1$, the disease leprosy is eliminated and this clearly indicates occurrence of a transcritical bifurcation at the critical value $R_0 = 1$. The necessarily required transversality condition for the occurrence of Hopf-bifurcation is established by the Theorem 5.3.1 in Section 5.3 which indicates that system (5.1.1) behaves in a stable manner as η crosses the threshold value η^*. This behavioural change in the pattern of the solutions of the system is observed due to the downregulating and reprogramming effect of healthy adult cells within the body of a leprosy affected person as demonstrated by Masaki et al. (2013). The numer-

ical interpretations in Figure 5.3, Figure 5.4, Figure 5.5 and Figure 5.6 completely suggest us that varying the drug efficacy rate of all the three components of MDT within the fixed range $0.025 - 0.059$ for approximately 120 days in PB cases and 300 days in MB cases helps the system getting stabilized and thus, the dissemination of leprosy to different human organs can evidently be controlled. Impact of MDT has explored two simultaneously occurring phenomenon i.e. the spontaneous recovery of the infected cells S_i and the re-infection of the recovered cells due to the waning effect of MDT which predicts that the drug efficacy rate η of MDT is the most influential parameter for system (5.1.1) monitoring the overall stability situation and dynamical shift of the system. For very low efficacy rate, weak bactericidal activity of MDT against *M. leprae* is noted. Due to this, for $\eta \leq \eta^* = 0.024$, oscillatory periodic solutions of system (5.1.1) are noticed which indicates that MDT in this low efficacy zone is ineffective and any notable improvement in the reduction of the bacterial load are not observed [Shepard et al. (1981); Prasad and Kaviarasan (2010)]. This findings is also supported by the recent clinical studies [Penna, Buhrer-Sekula, Pontes, Cruz, Gonçalves and Penna (2014); Penna et al. (2017)] where based on the randomized and controlled clinical trial on 613 newly diagonized untreated leprosy patients in China, India and Bangladesh, the authors have confirmed that an uniform treatment method called uniform multidrug therapy (U-MDT) can be an acceptable option for future treatment of leprosy worldwide especially in the endemic countries. Moreover, from the findings of Figure 5.6, Figure 5.8 and Table 5.2, we can interpret that for the range of values of $\eta > 0.06$, solutions of system (5.1.1) becomes chaotic and ultimately unstable. Hence, incorporating an abruptly higher drug dose is unsafe for the leprosy patients and would eventually have a negative effect on the human body because it induces drug resistance and severe adverse drug effects such as irreversible nerve damages, blindness etc. [Guragain et al. (2017); Sansarricq et al. (2004)].

Considering the Ridley–Jopling classification of leprosy Ridley et al. (1962), we can see that due to higher values of intrinsic growth rate (r) and carrying capacity (K) of *M. leprae*, higher range of values of η in between $0.052 - 0.059$ should necessarily be used as an effective treatment method for lepromatous leprosy cases (LL). For PB cases (especially in tuborculoid TT), our analytical and numerical findings from Figure 5.5, Figure 5.6 and Figure 5.8 suggests that a lesser efficacy rate of varying η within the range $0.025 - 0.04$ for nearly 120 days will be more beneficial due to the smear-negative property and low bacterial index with BI < 2 (skin lesions ≤ 5). Furthermore, recent experimental studies suggest that framing a shorter period of effective treatment policy is of major importance always to avoid relapse and irregularities in treatment [Gelber et al. (2004)]. The reduced multidrug therapy regimen recommended by WHO for leprosy is scheduled as 6 months in PB cases and 6 - 12 months in MB cases [Organization et al. (1998); Rodrigues and Lockwood (2011)].

During the numerical simulation portion, specifically in Fig. 5.6, we have chosen the value of infection rate $\beta = 0.0032$ considerably low to indicate actually the infection of PB types of leprosy patients. This produces the result that the system starts getting stabilized after 120 days i.e. at least 120 days (or 4 months) of treatment with maintaining the efficacy range $\eta \in (0.025, 0.059)$ is recommended for PB cases. For the infection of MB types of patients, bacterial load is much higher as BI ≥ 2 and hence, $\beta = 0.0071$ is chosen to simulate Fig 5.7. In this case, our outcomes in Figure 5.4, Figure 5.7 suggest that drug efficacy rate η cannot be increased more than 0.059 as the cell concentrations of our system becomes unstable. After 12 months, presence of viable load of bacilli after treatment with MDT are observed in some specific cases for patients with high bacillary load [Shetty et al. (2003); Kar et al. (2004); Gupta et al. (2005); Narang et al. (2022)]. Hence, strict long-term followup is needed and the overall health situations of every leprosy patient should be monitored very carefully after RFT (release for treatment). Indeed, if required, for the PB patients and especially, for the MB patients with high initial BI [Prasad and Kaviarasan (2010)], the pattern of sensitivity profile of η vs. β demonstrated in Figure 5.8 and Table 5.2 suggests that treatment can be continued after the recommended period within the prescribed drug efficacy zone for some cases considering different status of the disease.

Chapter 6

A Caputo-Fabrizio Fractionalized Mathematical Model for Investigating the Memory-regulated Infection Mechanism in Leprosy

Dynamical behavior of any living microorganism such as *M. leprae* not only depends on the conditions of its current state (e.g., substrate concentration, medium condition, etc.) but also on those of its previous states. The associated *M. leprae*-induced infection procedure and the pattern of cellular interactions are distinguishable in different memory stages. We have precisely utilized this phenomena in this Chapter[6] and extended our previously constructed integer-order derivative model to a fractionalized system. Here, we have developed a three-dimensional Caputo-Fabrizo fractionalized mathematical model involving concentrations of healthy Schwann cells, infected Schwann cells, and *M. leprae* bacteria in order to predict the dynamical changes in the cells during the disease dissemination process while incorporating the effect of memory on system cell populations, especially on the *M. leprae* bacterial population. The memory effect can be incorporated into an ODE-based system by introducing fractional-order ($\zeta \in (0, 1]$) derivatives as an index of memory [Du et al. (2013)]. The significance of varying the fractional order in $(0, 1]$ is that ζ tends to zero, which indicates that the fractionalized system has ideal memory and that the system is free from memory as ζ approaches 1. Most importantly, we have

[6] *The major portion of this chapter is published in the Journal Mathematics, MDPI, 11, 3630, August, 2023.*

formulated and investigated a fractionalized optimal-control-induced system comprising the combined drug dose therapy of Ofloxacin and Dapsone intended to achieve a more realistic treatment regime for leprosy. We have proved the existence and uniqueness of solutions of the fractionalized model with the help of the renowned Banach Fixed-Point theorem and investigated the stability by adopting Picard's T-stability theory. Furthermore, we have generated the necessary conditions for optimality by investigating a generalized fractional optimal control problem (FOCP) and then, utilized the results for our system. The main goal of this Chapter is to compare this fractional-order system with the corresponding integer-order model and also to distinguish the rich dynamics exhibited by the optimal-control-induced system based on different values of the fractional order $\zeta \in (0, 1)$.

6.1 The Basic Integer-Order Model and the Caputo–Fabrizio Fractionalized Mathematical Model Formulation

In recent years, fractional-order derivatives have gained huge importance in the field of modeling real-world biological phenomena. The fractional-order derivative is in fact a much generalized version of the integer-order derivative. In this Chapter, we now introduce the basic three-dimensional nonlinear ODE-based mathematical model developed in Chapter 2 that describes the fundamental disease dynamics of leprosy.

$$\begin{aligned} \frac{dS_u}{dt} &= \nu_1 S_u \left(1 - \frac{S_u}{S_{u_{max}}}\right) - \beta_1 S_u B_l, \\ \frac{dS_i}{dt} &= \beta_1 S_u B_l - \mu S_i, \\ \frac{dB_l}{dt} &= \nu_2 B_l \left(1 - \frac{B_l}{B_{l_{max}}}\right) - \beta_2 S_u B_l + \sigma S_i, \end{aligned} \tag{6.1.1}$$

with initial values $S_u(0) = S_{u_0} \geq 0$, $S_i(0) = S_{i_0} \geq 0$ and $B_l(0) = B_0 \geq 0$ at $t = 0$. Here, $S_u(t)$, $S_i(t)$ and $B_l(t)$ denote the concentrations of healthy Schwann cells, infected Schwann cells and *M. leprae* bacteria at any time t. ν_1 and ν_2 describe the intrinsic growth rates of the $S_u(t)$ and $B_l(t)$ populations, where $S_{u_{max}}$ and $B_{l_{max}}$ are the carrying capacity of the same. β_1 is the rate at which healthy cells are infected by *M. leprae* and μ denotes the natural mortality rate of S_i cells. The bacterial clearance rate results from the infection and the proliferation rates of newly produced free *M. leprae* bacteria, which are indicated

by the parameters β_2 and σ, respectively. Modifying the above system in terms of the CF (Caputo–Fabrizio) fractional differential system of equations, we obtain

$$\begin{aligned} {}^{CF}D_t^{\zeta} S_u(t) &= \nu_1 S_u \left(1 - \frac{S_u}{S_{u_{max}}}\right) - \beta_1 S_u B_l, \\ {}^{CF}D_t^{\zeta} S_i(t) &= \beta_1 S_u B_l - \mu S_i, \\ {}^{CF}D_t^{\zeta} B_l(t) &= \nu_2 B_l \left(1 - \frac{B_l}{B_{l_{max}}}\right) - \beta_2 S_u B_l + \sigma S_i \end{aligned} \tag{6.1.2}$$

with initial values $S_u(0) = S_{u_0} \geq 0$, $S_i(0) = S_{i_0} \geq 0$ and $B_l(0) = B_0 \geq 0$ at $t = 0$.

6.1.1 The iterative scheme

We now consider system (6.1.2). The term $S_u B_l$ is a nonlinear term and, hence, applying the Laplace transformation operator ($\mathcal{L}$) on both sides of the system (6.1.2), we obtain that

$$\begin{aligned} \frac{p\mathcal{L}\left(S_u(t)\right) - S_u(0)}{p + \zeta(1-p)} &= \mathcal{L}\left(\nu_1 S_u \left(1 - \frac{S_u}{S_{u_{max}}}\right) - \beta_1 S_u B_l\right), \\ \frac{p\mathcal{L}\left(S_i(t)\right) - S_i(0)}{p + \zeta(1-p)} &= \mathcal{L}\left(\beta_1 S_u B_l - \mu S_i\right), \\ \frac{p\mathcal{L}\left(B_l(t)\right) - B_l(0)}{p + \zeta(1-p)} &= \mathcal{L}\left(\nu_2 B_l \left(1 - \frac{B_l}{B_{l_{max}}}\right) - \beta_2 S_u B_l + \sigma S_i\right). \end{aligned} \tag{6.1.3}$$

The set in Equation (6.1.3) can now be rewritten in the following form:

$$\begin{aligned} \mathcal{L}(S_u(t)) &= \frac{S_u(0)}{p} + \left(\frac{p + \zeta(1-p)}{p}\right) \mathcal{L}\left(\nu_1 S_u \left(1 - \frac{S_u}{S_{u_{max}}}\right) - \beta_1 S_u B_l\right), \\ \mathcal{L}(S_i(t)) &= \frac{S_i(0)}{p} + \left(\frac{p + \zeta(1-p)}{p}\right) \mathcal{L}(\beta_1 S_u B_l - \mu S_i), \\ \mathcal{L}(B_l(t)) &= \frac{B_l(0)}{p} + \left(\frac{p + \zeta(1-p)}{p}\right) \mathcal{L}\left(\nu_2 B_l \left(1 - \frac{B_l}{B_{l_{max}}}\right) - \beta_2 S_u B_l + \sigma S_i\right). \end{aligned} \tag{6.1.4}$$

Using the inverse Laplace, we obtain

$$\begin{aligned} S_u(t) &= S_u(0) + \mathcal{L}^{-1}\left[\frac{p + \zeta(1-p)}{p} \mathcal{L}\left(\nu_1 S_u \left(1 - \frac{S_u}{S_{u_{max}}}\right) - \beta_1 S_u B_l\right)\right], \\ S_i(t) &= S_i(0) + \mathcal{L}^{-1}\left[\frac{p + \zeta(1-p)}{p} \mathcal{L}\left(\beta_1 S_u B_l - \mu S_i\right)\right], \\ B_l(t) &= B_l(0) + \mathcal{L}^{-1}\left[\frac{p + \zeta(1-p)}{p} \mathcal{L}\left(\nu_2 B_l \left(1 - \frac{B_l}{B_{l_{max}}}\right) - \beta_2 S_u B_l + \sigma S_i\right)\right]. \end{aligned} \tag{6.1.5}$$

We now present the series solutions generated by this method as follows:

$$S_u = \sum_{n=0}^{\infty} S_{u_n}, \quad S_i = \sum_{n=0}^{\infty} S_{i_n}, \quad B_l = \sum_{n=0}^{\infty} B_{l_n}. \tag{6.1.6}$$

Furthermore, the series solution representation of the only existing nonlinear term $S_u B_l$ is given as

$$S_u B_l = \sum_{n=0}^{\infty} G_n \quad \text{where} \quad G_n = \sum_{k=0}^{n} S_{u_k} \sum_{k=0}^{n} B_{l_k} - \sum_{k=0}^{n-1} S_{u_k} \sum_{k=0}^{n-1} B_{l_k}. \tag{6.1.7}$$

We now use the initial conditions to achieve the following recursive formulas:

$$\begin{aligned}
S_{u_{n+1}} &= S_{u_n}(0) + \mathcal{L}^{-1}\left[\frac{p+\zeta(1-p)}{p}\mathcal{L}\left(\nu_1 S_{u_n}\left(1-\frac{S_{u_n}}{S_{u_{max}}}\right) - \beta_1 S_{u_n} B_{l_n}\right)\right], \\
S_{i_{n+1}} &= S_{i_n}(0) + \mathcal{L}^{-1}\left[\frac{p+\zeta(1-p)}{p}\mathcal{L}\left(\beta_1 S_{u_n} B_{l_n} - \mu S_{i_n}\right)\right], \\
B_{l_{n+1}} &= B_{l_n}(0) + \mathcal{L}^{-1}\left[\frac{p+\zeta(1-p)}{p}\mathcal{L}\left(\nu_2 B_{l_n}\left(1-\frac{B_{l_n}}{B_{l_{max}}}\right) - \beta_2 S_{u_n} B_{l_n} + \sigma S_{i_n}\right)\right].
\end{aligned} \tag{6.1.8}$$

The approximate solution is assumed to be obtained as a limit when $n \to \infty$, i.e., $S_u(t) = \lim_{n\to\infty} S_{u_n}(t)$, $S_i(t) = \lim_{n\to\infty} S_{i_n}(t)$ and $B_l(t) = \lim_{n\to\infty} B_{l_n}(t)$.

6.1.2 Stability analysis

It is known that iteration methods are numerical procedures which compute a sequence of gradually accurate iterations to approximate the solution of a class of problems. These methods are truly useful tools of applied mathematics for solving real life problems ranging from economics, finance, various types of biological problems to transportation, network analysis, or optimization. An iteration method is considered to be sound if it possesses some qualitative properties such as convergence and stability. That is why several scientists paid and still pay attention to the qualitative study of iteration methods. In this Section, first, we present the detailed definition of the T-stability of Picard's iteration [Qing and Rhoades (2008)].

Definition 6.1.1 *Suppose T is a self-map on a complete metric space (Y, d). Consider an iteration $y_{n+1} = g(T, y_n)$. Furthermore, let us assume that $\mathcal{P}(T)$ is the fixed-point set of T with $\mathcal{P}(T) \neq \phi$ and let $\{y_n\}$ converge to some point $y \in \mathcal{P}(T)$. Let $\{z_n\} \subset Y$ and define $\{u_n\} = d(Z_{n+1}, g(T, z_n))$. Now, if $u_n \to 0$ implies that $z_n \to y$, then the iteration method $y_{n+1} = g(T, y_n)$ is said to be T-stable. Furthermore, note that the convergence of $\{z_n\}$ guarantees that $\{z_n\}$ must be bounded above. If all these conditions hold true for $y_{n+1} =$*

$g(T, y_n)$, then Picard's iteration method is called T-stable.

Let $(\mathbb{X}, \|.\|)$ be a Banach space. As every Banach space is a complete metric space with the metric induced by the associated norm, Definition 6.1.1 holds true for $(\mathbb{X}, \|.\|)$ also. [In this context, it is important to mention that in general, a metric space is said to be complete if every Cauchy sequence defined on it converges to a point in the space with respect to the metric defined on it.]

Theorem 6.1.1 *Let T be a self-map on the space $(\mathbb{X}, \|.\|)$, which satisfies the following:*

$$\|T_x - T_y\| \leq \Lambda\|x - T_x\| + \varrho\|x - y\| \quad \textit{for all} \quad x, y \in \mathbb{X}$$

where $\Lambda \geq 0$ and $\varrho \in [0, 1)$. Suppose T has a fixed point. Then, T is Picard's T-stable.

Now, let us define a self-map T as

$$\begin{aligned}
T(S_{u_n}(t)) = S_{u_{n+1}} &= S_{u_n}(0) + \mathcal{L}^{-1}\left[\frac{p+\zeta(1-p)}{p}\mathcal{L}\left(\nu_1 S_{u_n}\left(1 - \frac{S_{u_n}}{S_{u_{max}}}\right) - \beta_1 S_{u_n} B_{l_n}\right)\right], \\
T(S_{i_n}(t)) = S_{i_{n+1}} &= S_{i_n}(0) + \mathcal{L}^{-1}\left[\frac{p+\zeta(1-p)}{p}\mathcal{L}\left(\beta_1 S_{u_n} B_{l_n} - \mu S_{i_n}\right)\right], \\
T(B_{l_n}(t)) = B_{l_{n+1}} &= B_{l_n}(0) + \mathcal{L}^{-1}\left[\frac{p+\zeta(1-p)}{p}\mathcal{L}\left(\nu_2 B_{l_n}\left(1 - \frac{B_{l_n}}{B_{l_{max}}}\right) - \beta_2 S_{u_n} B_{l_n} + \sigma S_{i_n}\right)\right].
\end{aligned} \tag{6.1.9}$$

For all $m, n \in \mathbb{N}$, let us first construct the following differences:

$$\begin{aligned}
T(S_{u_n}(t)) - T(S_{u_m}(t)) &= S_{u_n}(t) - S_{u_m}(t) \\
&\quad + \mathcal{L}^{-1}\left[\frac{p+\zeta(1-p)}{p}\mathcal{L}\left(\nu_1 S_{u_n}\left(1 - \frac{S_{u_n}}{S_{u_{max}}}\right) - \beta_1 S_{u_n} B_{l_n}\right)\right] \\
&\quad - \mathcal{L}^{-1}\left[\frac{p+\zeta(1-p)}{p}\mathcal{L}\left(\nu_1 S_{u_m}\left(1 - \frac{S_{u_m}}{S_{u_{max}}}\right) - \beta_1 S_{u_m} B_{l_m}\right)\right], \\
T(S_{i_n}(t)) - T(S_{i_m}(t)) &= S_{i_n}(t) - S_{i_m}(t) + \mathcal{L}^{-1}\left[\frac{p+\zeta(1-p)}{p}\mathcal{L}\left(\beta_1 S_{u_n} B_{l_n} - \mu S_{i_n}\right)\right] \\
&\quad - \mathcal{L}^{-1}\left[\frac{p+\zeta(1-p)}{p}\mathcal{L}\left(\beta_1 S_{u_m} B_{l_m} - \mu S_{i_m}\right)\right], \\
T(B_{l_n}(t)) - T(B_{l_m}(t)) &= B_{l_n}(t) - B_{l_m}(t) \\
&\quad + \mathcal{L}^{-1}\left[\frac{p+\zeta(1-p)}{p}\mathcal{L}\left(\nu_2 B_{l_n}\left(1 - \frac{B_{l_n}}{B_{l_{max}}}\right) - \beta_2 S_{u_n} B_{l_n} + \sigma S_{i_n}\right)\right] \\
&\quad - \mathcal{L}^{-1}\left[\frac{p+\zeta(1-p)}{p}\mathcal{L}\left(\nu_2 B_{l_m}\left(1 - \frac{B_{l_m}}{B_{l_{max}}}\right) - \beta_2 S_{u_m} B_{l_m} + \sigma S_{i_m}\right)\right]
\end{aligned} \tag{6.1.10}$$

where $\frac{p+\zeta(1-p)}{p}$ is a Lagrange multiplier in fractional form. As all the solutions S_{u_n}, S_{i_n}, B_{l_n} are Cauchy sequences in the Banach space $(\mathbb{X}, \|.\|)$, it is true that $\|S_{u_n} - S_{u_m}\| \to 0$, $\|S_{i_n} - S_{i_m}\| \to 0$ and $\|B_{l_n} - B_{l_m}\| \to 0$ as $n, m \to \infty$. Due to this similar behavior of the solutions, i.e., comparative influence of the solutions [Gao et al. (2021)], we have

$$\begin{aligned} \|S_{u_n}(t) - S_{u_m}(t)\| &\cong \|S_{i_n}(t) - S_{i_m}(t)\|, \\ \|S_{u_n}(t) - S_{u_m}(t)\| &\cong \|B_{l_n}(t) - B_{l_m}(t)\|. \end{aligned} \tag{6.1.11}$$

Now, applying the norm on both sides of the first equation of (6.1.10), we obtain

$$\begin{aligned} \|T(S_{u_n}(t)) - T(S_{u_m}(t))\| &= \|S_{u_n}(t) - S_{u_m}(t) \\ &\quad + \mathcal{L}^{-1}\left[\frac{p+\zeta(1-p)}{p}\mathcal{L}\left(\nu_1 S_{u_n}\left(1 - \frac{S_{u_n}}{S_{u_{max}}}\right) - \beta_1 S_{u_n} B_{l_n}\right)\right] \\ &\quad - \mathcal{L}^{-1}\left[\frac{p+\zeta(1-p)}{p}\mathcal{L}\left(\nu_1 S_{u_m}\left(1 - \frac{S_{u_m}}{S_{u_{max}}}\right) - \beta_1 S_{u_m} B_{l_m}\right)\right] \| \\ &= \|S_{u_n}(t) - S_{u_m}(t) + \mathcal{L}^{-1}\left[\frac{p+\zeta(1-p)}{p}\mathcal{L}\Big[\nu_1(S_{u_n}(t) - S_{u_m}(t)\right. \\ &\quad + \left(-\frac{\nu_1}{S_{u_{max}}} S_{u_n}(S_{u_n} - S_{u_m})\right) + \left(-\frac{\nu_1}{S_{u_{max}}} S_{u_m}(S_{u_n} - S_{u_m})\right) \\ &\quad \left. + (-\beta_1 B_{l_n}(S_{u_n} - S_{u_m})) + (-\beta_1 S_{u_m}(B_{l_n} - B_{l_m}))\Big]\right] \|. \end{aligned}$$

Using triangle inequality, we obtain

$$\begin{aligned} \|T(S_{u_n}(t)) - T(S_{u_m}(t))\| \leq \|S_{u_n}(t) - S_{u_m}(t)\| + \mathcal{L}^{-1}\Bigg[\frac{p+\zeta(1-p)}{p}\mathcal{L}\Big[\|\nu_1(S_{u_n}(t) - S_{u_m}(t)\| \\ + \| - \frac{\nu_1}{S_{u_{max}}} S_{u_n}(S_{u_n} - S_{u_m})\| + \| - \frac{\nu_1}{S_{u_{max}}} S_{u_m}(S_{u_n} - S_{u_m})\| \\ + \| - \beta_1 B_{l_n}(S_{u_n} - S_{u_m})\| + \| - \beta_1 S_{u_m}(B_{l_n} - B_{l_m})\|\Big]\Bigg]. \end{aligned}$$

Then, using the relations in (6.1.11), we obtain

$$\begin{aligned}\|T(S_{u_n}(t)) - T(S_{u_m}(t))\| &\leq \|S_{u_n}(t) - S_{u_m}(t)\| + \mathcal{L}^{-1}\left[\frac{p+\zeta(1-p)}{p}\mathcal{L}\Big[\|\nu_1(S_{u_n}(t) - S_{u_m}(t)\|\right.\\ &+ \| - \frac{\nu_1}{S_{u_{max}}}S_{u_n}(S_{u_n} - S_{u_m})\| + \| - \frac{\nu_1}{S_{u_{max}}}S_{u_m}(S_{u_n} - S_{u_m})\|\\ &\left.+ \| - \beta_1 B_{l_n}(S_{u_n} - S_{u_m})\| + \| - \beta_1 S_{u_m}(S_{u_n} - S_{u_m})\|\Big]\right]\\ &\leq \|S_{u_n}(t) - S_{u_m}(t)\|\left[1 + \nu_1 E_1(\zeta) - 2M_1\frac{\nu_1}{S_{u_{max}}}E_2(\zeta)\right.\\ &\left.- \beta_1(M_1 + M_3)E_3(\zeta)\right]\end{aligned} \tag{6.1.12}$$

where $E_1(\zeta)$, $E_2(\zeta)$ and $E_3(\zeta)$ are functions of $\mathcal{L}^{-1}\left[\frac{p+\zeta(1-p)}{p}\mathcal{L}(.)\right]$ and $\|S_{u_n}\| < M_1$, $\|S_{i_n}\| < M_2$ and $\|B_{l_n}\| < M_3$. Proceeding similarly, we obtain from the second and third equations of (6.1.10),

$$\|T(S_{i_n}(t)) - T(S_{i_m}(t))\| \leq \|S_{i_n}(t) - S_{i_m}(t)\|\left[1 + \beta_1(M_1 + M_3)E_3(\zeta) - \mu E_4(\zeta)\right] \tag{6.1.13}$$

and

$$\begin{aligned}\|T(B_{l_n}(t)) - T(B_{l_m}(t))\| \leq \|B_{l_n}(t) - B_{l_m}(t)\|&\left[1 + \nu_2 E_5(\zeta) - 2M_3\frac{\nu_2}{B_{l_{max}}}E_6(\zeta)\right.\\ &\left.- \beta_2(M_1 + M_3)E_3(\zeta) + \sigma E_7(\zeta)\right]\end{aligned} \tag{6.1.14}$$

where $E_4(\zeta)$, $E_5(\zeta)$, $E_6(\zeta)$ and $E_7(\zeta)$ are functions of $\mathcal{L}^{-1}\left[\frac{p+\zeta(1-p)}{p}\mathcal{L}(.)\right]$ and

$$\begin{aligned}\left[1 + \nu_1 E_1(\zeta) - 2M_1\frac{\nu_1}{S_{u_{max}}}E_2(\zeta) - \beta_1(M_1 + M_3)E_3(\zeta)\right] &< 1,\\ \left[1 + \beta_1(M_1 + M_3)E_3(\zeta) - \mu E_4(\zeta)\right] &< 1,\\ \left[1 + \nu_2 E_5(\zeta) - 2M_3\frac{\nu_2}{B_{l_{max}}}E_6(\zeta) - \beta_2(M_1 + M_3)E_3(\zeta) + \sigma E_7(\zeta)\right] &< 1.\end{aligned} \tag{6.1.15}$$

So, we can conclude that the self-map T defined in (6.1.9) has a fixed point. In view

of (6.1.15) and also choosing $\varrho = (0, 0, 0)$ and

$$\Lambda = \begin{cases} 1 + \nu_1 E_1(\zeta) - 2M_1 \frac{\nu_1}{S_{u_{max}}} E_2(\zeta) - \beta_1(M_1 + M_3)E_3(\zeta), \\ 1 + \beta_1(M_1 + M_3)E_3(\zeta) - \mu E_4(\zeta), \\ 1 + \nu_2 E_5(\zeta) - 2M_3 \frac{\nu_2}{B_{l_{max}}} E_6(\zeta) - \beta_2(M_1 + M_3)E_3(\zeta) + \sigma E_7(\zeta), \end{cases}$$

we can see that all the conditions of Theorem 6.1.1 are satisfied. Thus, the self-mapping T is Picard's T-stable. Summarizing the discussions, we now present the following theorem.

Theorem 6.1.2 *Consider system (6.1.2) with the set of equations in system (6.1.8). Let T be a self-map as defined by (6.1.9). If the conditions (6.1.15) are satisfied by T, then T has a fixed point and, hence, T is Picard's T-stable.*

6.1.3 Existence of the solutions

Using fixed-point theory, we now show the existence of the solutions of system (6.1.2) in this Subsection. For this, let us first observe that

$$\begin{aligned} S_u(t) - S_{u_0}(t) =& \frac{2(1-\zeta)}{M(\zeta)(2-\zeta)} \left(\nu_1 S_u(t) \left(1 - \frac{S_u(t)}{S_{u_{max}}} \right) - \beta_1 S_u(t) B_l(t) \right) \\ &+ \frac{2\zeta}{M(\zeta)(2-\zeta)} \int_0^t \left(\nu_1 S_u(y) \left(1 - \frac{S_u(y)}{S_{u_{max}}} \right) - \beta_1 S_u(y) B_l(y) \right) dy, \\ S_i(t) - S_{i_0}(t) =& \frac{2(1-\zeta)}{M(\zeta)(2-\zeta)} \left(\beta_1 S_u B_l - \mu S_i \right) \\ &+ \frac{2\zeta}{M(\zeta)(2-\zeta)} \int_0^t \left(\beta_1 S_u(y) B_l(y) - \mu S_i(y) \right) dy, \\ B_l(t) - B_{l_0}(t) =& \frac{2(1-\zeta)}{M(\zeta)(2-\zeta)} \left(\nu_2 B_l(t) \left(1 - \frac{B_l(t)}{B_{l_{max}}} \right) - \beta_2 S_u(t) B_l(t) + \sigma S_i \right) \\ &+ \frac{2\zeta}{M(\zeta)(2-\zeta)} \int_0^t \left(\nu_2 B_l(y) \left(1 - \frac{B_l(y)}{B_{l_{max}}} \right) - \beta_2 S_u(y) B_l(y) + \sigma S_i(y) \right) dy. \end{aligned}$$

Let T_1 be an operator on H to itself, i.e., $T_1 : H \to H$. Here, T_1 is chosen as an operator for the entire system. Applying it, we obtain that

$$\begin{aligned} T_1(S_u(t)) &= \frac{2(1-\zeta)}{M(\zeta)(2-\zeta)} K_1(t, S_u(t)) + \frac{2\zeta}{M(\zeta)(2-\zeta)} \int_0^t \left(K_1(y, S_u(y)) \right) dy, \\ T_1(S_i(t)) &= \frac{2(1-\zeta)}{M(\zeta)(2-\zeta)} \left(K_2(t, S_i(t)) \right) + \frac{2\zeta}{M(\zeta)(2-\zeta)} \int_0^t \left(K_2(y, S_i(y)) \right) dy, \\ T_1(B_l(t)) &= \frac{2(1-\zeta)}{M(\zeta)(2-\zeta)} \left(K_3(t, B_l(t)) \right) + \frac{2\zeta}{M(\zeta)(2-\zeta)} \int_0^t \left(K_3(y, B_l(y)) \right) dy \end{aligned}$$

where

$$K_1(t, S_u(t)) = \nu_1 S_u(t)\left(1 - \frac{S_u(t)}{S_{u_{max}}}\right) - \beta_1 S_u(t) B_l(t),$$
$$K_2(t, S_i(t)) = \beta_1 S_u(t) B_l(t) - \mu S_i(t),$$
$$K_3(t, B_l(t)) = \nu_2 B_l(t)\left(1 - \frac{B_l(t)}{B_{l_{max}}}\right) - \beta_2 S_u(t) B_l(t) + \sigma S_i(t).$$

Let $P \subset H$ be bounded. We aim to show that $\overline{T_1(P)}$ is compact to ensure the existence and boundedness of the solutions of system (6.1.2), where T_1 is defined as above. We can see that there exist positive reals κ_1, κ_2 and κ_3 such that $\|S_u\| < \kappa_1$, $\|S_i\| < \kappa_2$ and $\|B_l\| < \kappa_3$. From the definition of T_1, we can write

$$\begin{aligned}
\|T_1(S_u(t))\| &= \|\frac{2(1-\zeta)}{M(\zeta)(2-\zeta)} K_1(t, S_u(t)) + \frac{2\zeta}{M(\zeta)(2-\zeta)} \int_0^t (K_1(y, S_u(y)))\, dy\| \\
&\leq \frac{2(1-\zeta)}{M(\zeta)(2-\zeta)} \|K_1(t, S_u(t))\| + \frac{2\zeta}{M(\zeta)(2-\zeta)} \| \int_0^t (K_1(y, S_u(y)))\, dy\| \\
&\leq \left[\frac{2(1-\zeta)}{M(\zeta)(2-\zeta)} + a_1 \frac{2\zeta}{M(\zeta)(2-\zeta)}\right] \|K_1(t, S_u(t))\| \\
&\leq R_1 \left[\frac{2(1-\zeta)}{M(\zeta)(2-\zeta)} + a_1 \frac{2\zeta}{M(\zeta)(2-\zeta)}\right]
\end{aligned}$$

which implies

$$\|T_1(S_u(t))\| \leq \frac{2R_1}{M(\zeta)(2-\zeta)}(1 + \zeta a_1 - \zeta)$$

and also proceeding similarly, we can obtain

$$\|T_1(S_i(t))\| \leq \frac{2R_2}{M(\zeta)(2-\zeta)}(1 + \zeta a_2 - \zeta),$$
$$\|T_1(B_l(t))\| \leq \frac{2R_3}{M(\zeta)(2-\zeta)}(1 + \zeta a_3 - \zeta)$$

where

$$R_1 = \max_{\substack{t\in[0,1] \\ S_u \in [0,\kappa_1]}} K_1(t, S_u(t)),$$

$$R_2 = \max_{\substack{t\in[0,1] \\ S_i \in [0,\kappa_2]}} K_2(t, S_i(t)),$$

$$R_3 = \max_{\substack{t\in[0,1] \\ B_l \in [0,\kappa_3]}} K_3(t, B_l(t)).$$

Hence, we have proved that $T_1(P)$ is bounded. Let, $t_2 > t_1$ and $S_u, S_i, B_l \in P$. So, for a given $\epsilon > 0$, there exists η satisfying that $\|(t_2 - t_1)\| < \eta$, and we can write the following:

$$\begin{aligned}\|K_1(t_2, S_u(t_2)) - K_1(t_1, S_u(t_1))\| &\leq \nu_1 \|S_u(t_2) - S_u(t_1)\| \\ &+ \frac{\nu_1}{S_{u_{max}}} \|S_u(t_2) + S_u(t_1)\| \, \|S_u(t_2) - S_u(t_1)\| \\ &+ \beta_1 \|B_l\| \, \|S_u(t_2) - S_u(t_1)\| \\ &\leq \nu_1 \|S_u(t_2) - S_u(t_1)\| + 2\kappa_1 \frac{\nu_1}{S_{u_{max}}} \|S_u(t_2) - S_u(t_1)\| \\ &+ \beta_1 \kappa_3 \|S_u(t_2) - S_u(t_1)\| \\ &\leq \left[\nu_1 + \frac{2\kappa_1 \nu_1}{S_{u_{max}}} + \beta_1 \kappa_3\right] \|S_u(t_2) - S_u(t_1)\|. \end{aligned} \tag{6.1.16}$$

Assuming that if the function $S_u(t)$ is Lipschitz-continuous, i.e., for some real number $L_1 \geq 0$ and for all t_1, t_2, the inequality $\|S_u(t_2) - S_u(t_1)\| \leq L_1 \|t_2 - t_1\|$ holds, we can rewrite (6.1.16) as

$$\|K_1(t_2, S_u(t_2)) - K_1(t_1, S_u(t_1))\| \leq G_1 \|t_2 - t_1\| \tag{6.1.17}$$

where $G_1 = L_1 \left[\nu_1 + \frac{2\kappa_1 \nu_1}{S_{u_{max}}} + \beta_1 \kappa_3\right]$. Similarly, we have

$$\|K_2(t_2, S_i(t_2)) - K_2(t_1, S_i(t_1))\| \leq G_2 \|t_2 - t_1\|, \tag{6.1.18}$$

$$\|K_3(t_2, B_l(t_2)) - K_3(t_1, B_l(t_1))\| \leq G_3 \|t_2 - t_1\| \tag{6.1.19}$$

if $S_i(t)$ and $B_l(t)$ are also Lipschitz-continuous, i.e., for some real numbers $L_2, L_3 \geq 0$, the conditions

$$\begin{aligned}&\|S_i(t_2) - S_i(t_1)\| \leq L_2 \|t_2 - t_1\|, \\ &\|B_l(t_2) - B_l(t_1)\| \leq L_3 \|t_2 - t_1\| \;\text{ hold, respectively, for all } t_1, t_2.\end{aligned}$$

Furthermore,

$$\begin{aligned}\|T_1(S_u(t_2)) - T_1(S_u(t_1))\| &\leq \frac{2(1-\zeta)}{M(\zeta)(2-\zeta)}\|K_1(t_2, S_u(t_2)) - K_1(t_1, S_u(t_1))\| \\ &+ \frac{2\zeta}{M(\zeta)(2-\zeta)}R_1\|K_1(t_2, S_u(t_2)) - K_1(t_1, S_u(t_1))\| \\ &\leq \frac{2(1-\zeta)}{M(\zeta)(2-\zeta)}G_1\|t_2 - t_1\| + \frac{2\zeta}{M(\zeta)(2-\zeta)}R_1G_1\|t_2 - t_1\| \\ &\text{(using inequality (6.1.17)).}\end{aligned}$$

Finally, choosing

$$\eta = \frac{\epsilon}{\frac{2(1-\zeta)}{M(\zeta)(2-\zeta)}G_1 + \frac{2\zeta}{M(\zeta)(2-\zeta)}R_1G_1},$$

we can see that $\|T_1(S_u(t_2)) - T_1(S_u(t_1))\| \leq \epsilon$ holds.

Similarly proceeding and using inequalities (6.1.18) and (6.1.19), we can also easily show that $\|T_1(S_i(t_2)) - T_1(S_i(t_1))\| \leq \epsilon$ and $\|T_1(B_l(t_2)) - T_1(B_l(t_1))\| \leq \epsilon$ hold, which guarantees the equicontinuity of T_1. Hence, according to the well-known Arzela–Ascoli theorem, we can say that $\overline{T_1(P)}$ is compact. Next, we present the following theorem by summarising the previous discussions on the existence of the solutions of system (6.1.2), and then we move forward to show the uniqueness of the solutions of system (6.1.2).

Theorem 6.1.3 *Let $P \subset H$ be bounded. Then, for the operator T_1, there exist κ_1, κ_2 and κ_3 such that if the functions $S_u(t)$, $S_i(t)$ and $B_l(t)$ are Lipschitz-continuous, i.e., if for some real numbers, L_1, L_2 and $L_3 \geq 0$, the following conditions hold*

$$\begin{aligned}\|S_u(t_2) - S_u(t_1)\| &\leq L_1\|t_2 - t_1\|, \\ \|S_i(t_2) - S_i(t_1)\| &\leq L_2\|t_2 - t_1\|, \\ \|B_l(t_2) - B_l(t_1)\| &\leq L_3\|t_2 - t_1\|,\end{aligned}$$

for all t_1, t_2, then $\overline{T_1(P)}$ is compact. Thus, all the solutions of system (6.1.2) exist and are bounded.

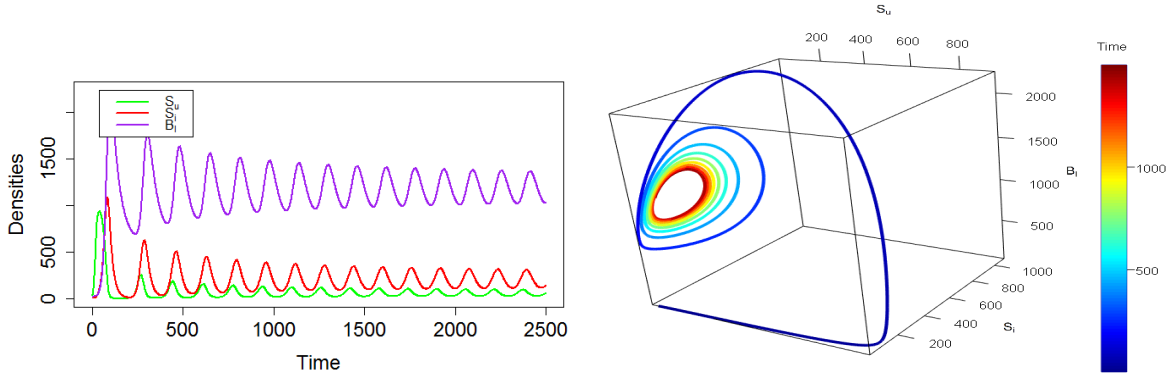

(a) *(b)*

*Figure 6.1: Behavior of the solutions of the system populations and 3-D phase portrait diagrams of the CF fractionalized system (6.1.2) depicting the oscillatory dynamics and appearance of limit cycles for $\zeta = 1$. Values of $\nu_2 = 0.03$, $S_{u_{max}} = 1000$ were used to simulate the Subfigures in this Figure, where all the other parameter values were chosen from Table 6.1. (**a**) Behavior of the trajectories of system (6.1.2); (**b**) 3-D phase diagram for system (6.1.2) in $S_u - S_i - B_l$ space.*

6.1.4 Uniqueness of the solutions

To prove the uniqueness of the solutions of system (6.1.2), let us consider the mapping T_1 again which was defined previously. Now,

$$\begin{aligned}\|T_1(S_u(t)) - T_1(\tilde{S}_u(t))\| &= \|\frac{2(1-\zeta)}{M(\zeta)(2-\zeta)}(K_1(t, S_u(t)) - K_1(t, \tilde{S}_u(t))) \\ &+ \frac{2\zeta}{M(\zeta)(2-\zeta)}\int_0^t (K_1(y, S_u(y)) - K_1(y, \tilde{S}_u(y)))\| \\ &\leq \left[\frac{2D_1}{M(\zeta)(2-\zeta)}\right]\|S_u(t) - \tilde{S}_u(t)\|.\end{aligned}$$

Similarly, we can obtain

$$\|T_1(S_i(t)) - T_1(\tilde{S}_i(t))\| \leq \left[\frac{2D_2}{M(\zeta)(2-\zeta)}\right]\|S_i(t) - \tilde{S}_i(t)\|,$$
$$\|T_1(B_l(t)) - T_1(\tilde{B}_l(t))\| \leq \left[\frac{2D_3}{M(\zeta)(2-\zeta)}\right]\|B_l(t) - \tilde{B}_l(t)\|$$

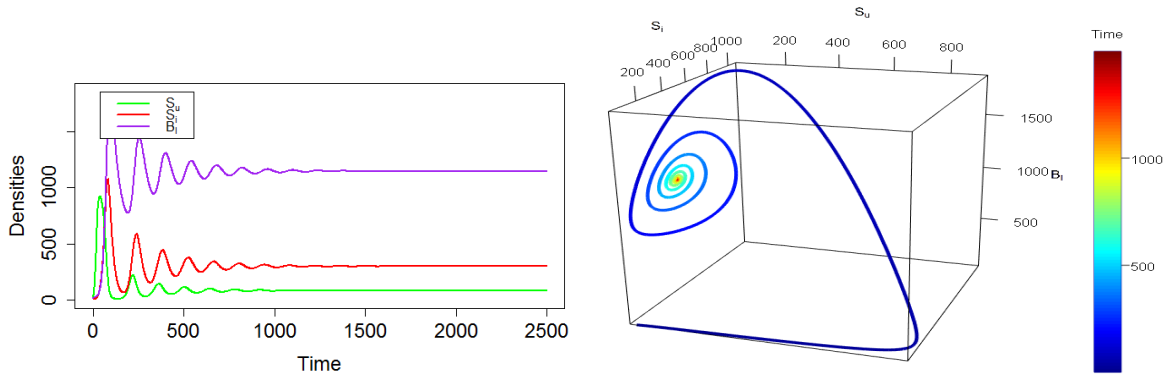

(a) *(b)*

*Figure 6.2: Behavior of the solutions of the system populations and 3-D phase portrait diagrams of the CF fractionalized system (6.1.2) depicting the stable behavior for $\zeta = 1$. Values of $\nu_2 = 0.05$ and $S_{u_{max}} = 1000$ were used to simulate the Subfigures in this Figure where other parameter values were chosen from Table 6.1. (**a**) Behavior of the trajectories of system (6.1.2); (**b**) 3-D phase diagram for system (6.1.2) in $S_u - S_i - B_l$ space.*

where $D_1, D_2, D_3 \in \mathbb{R}$. Hence, the operator T_1 is a contraction if the following conditions hold:

$$\frac{2D_1}{M(\zeta)(2-\zeta)}\|S_u(t) - \tilde{S}_u(t)\| < 1,$$
$$\frac{2D_2}{M(\zeta)(2-\zeta)}\|S_i(t) - \tilde{S}_i(t)\| < 1,$$
$$\frac{2D_3}{M(\zeta)(2-\zeta)}\|B_l(t) - \tilde{B}_l(t)\| < 1$$

which ensures the existence of unique positive solutions of system (6.1.2) using fixed-point theorem.

6.2 Equilibria and Stability

Our CF fractionalized mathematical model (6.1.2) has two equilibria, namely the disease-free equilibrium E_0 and the endemic equilibrium E^*. Here, E_0 is given as $E_0 = (S_{u_{max}}, 0, 0)$. The value of the basic reproduction number R_0 is given as $R_0 = \frac{\beta_1 \sigma S_{u_{max}}}{\mu(\beta_2 S_{u_{max}} - \nu_2)}$. R_0 is actually interpreted as the secondary number of new infections in a completely susceptible healthy

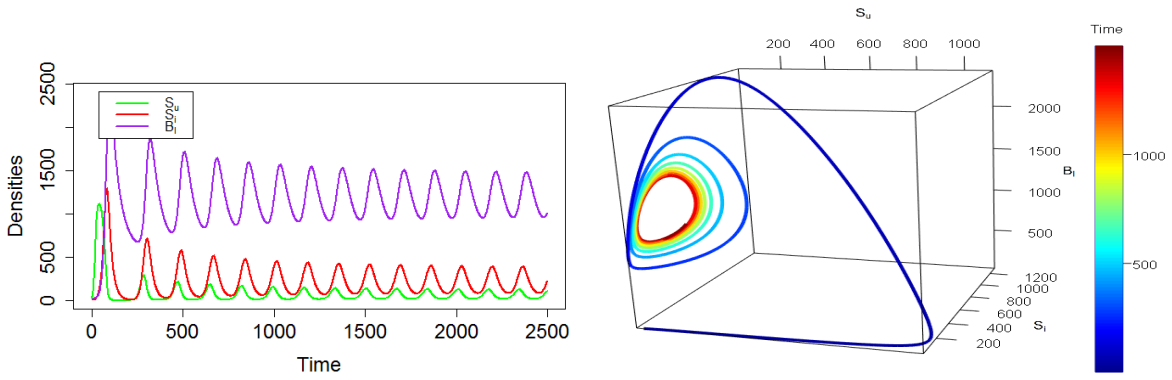

(a) *(b)*

*Figure 6.3: Time series and phase portrait diagram of the CF fractionalized system (6.1.2) depicting the unstable oscillatory behavior of the system state populations and appearance of stable limit cycles for $\zeta = 0.8$. Values of $\nu_2 = 0.03$ and $S_{u_{max}} = 1200$ were used to simulate the Subfigures in this Figure where other parameter values were chosen from Table 6.1. (**a**) Behavior of the trajectories of system (6.1.2); (**b**) 3-D phase diagram for system (6.1.2) in $S_u - S_i - B_l$ space.*

Schwann cell population and, based on the above, we now present the following theorem on the stability of E_0 for our system (6.1.2) as follows:

Theorem 6.2.1 *The disease-free equilibrium E_0 of system (6.1.2) is locally asymptotically stable if $R_0 < 1$.*

To obtain the coordinates of the endemic equilibrium E^*, we now set the right-hand sides of system (6.1.2) to zero. Hence, we obtain the values of S_u^*, S_i^* and B_l^*, which are already described in Chapter 2. In this context, we now present the following theorem, which describes the required criterion about the stability of E^* [Li et al. (2019)].

Theorem 6.2.2 *If the matrix $(I - (1-\zeta)\mathcal{J})$ is invertible, then the endemic equilibrium E^* of the CF fractionalized system (6.1.2) is locally asymptotically stable if all the roots of the characteristic equation $det(x(I - (1-\zeta)\mathcal{J}) - \zeta\mathcal{J}) = 0$ of system (6.1.2) evaluated at E^* are negative real or have negative real parts where $\mathcal{J}$ denotes the Jacobian matrix of system (6.1.2) at $E^* = (S_u^*, S_i^*, B_l^*)$.*

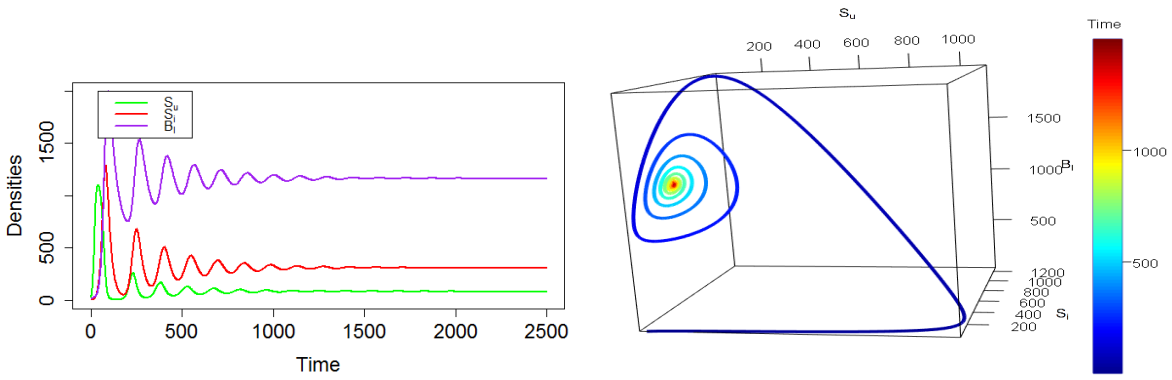

(a) *(b)*

Figure 6.4: Time series and phase portrait diagram of the CF fractionalized system (6.1.2) depicting the asymptotically stable behavior of the system state populations for $\zeta = 0.8$. *Here, values of* $\nu_2 = 0.05$ *and* $S_{u_{max}} = 1200$ *were used to simulate the Subfigures in this Figure. Values of all the other parameters were chosen from Table 6.1. (**a**) Behavior of the trajectories of system (6.1.2); (**b**) 3-D phase diagram for system (6.1.2) in* $S_u - S_i - B_l$ *space.*

6.3 Optimal Control Induced Caputo-Fabrizio Fractional Mathematical Model

Optimal control is a very useful tool for controlling the progression of a disease in the human body. Furthermore, this tool has gained major importance lately for the investigation of efficient and cost-effective drug treatment policies for various infectious diseases and for other different important biological problems based on fractional mathematical models [Kamocki (2014); Chatterjee et al. (2021); Vellappandi et al. (2022); Baba and Bilgehan (2021)]. In this Chapter, we have analyzed our formulated CF fractionalized model (6.1.2) by incorporating two control functions, $u_1(t)$ and $u_2(t)$; one is an effect of the drug Ofloxacin and another is of Dapsone on various cell densities, respectively. Here, Ofloxacin blocks the occurrence of new infections, and by preventing the formation of folic acid, Dapsone specifically inhibits replication of *M. leprae* bacteria. The optimal-control-induced CF fractional mathematical

model is presented as:

$$\begin{aligned} {}^{CF}D_t^{\zeta} S_u(t) &= \nu_1 S_u \left(1 - \frac{S_u}{S_{u_{max}}}\right) - \beta_1 (1 - u_1(t)) S_u B_l, \\ {}^{CF}D_t^{\zeta} S_i(t) &= \beta_1 (1 - u_1(t)) S_u B_l - \mu S_i, \\ {}^{CF}D_t^{\zeta} B_l(t) &= \nu_2 (1 - u_2(t)) B_l \left(1 - \frac{B_l}{B_{l_{max}}}\right) - \beta_2 (1 - u_1(t)) S_u B_l + \sigma S_i \end{aligned} \tag{6.3.1}$$

with initial values $S_u(0) = S_{u_0} \geq 0$, $S_i(0) = S_{i_0} \geq 0$ and $B_l(0) = B_0 \geq 0$ at $t = 0$.

Our main aim is to decrease the number of infected cells and the bacterial density as well as to increase the healthy cell concentrations. Let us now consider the state system given by (6.3.1) with the class of admissible controls defined as

$$\begin{aligned} \mathcal{U} = \{(u_1(\cdot), u_2(\cdot)) : u_1,\ u_2 \ \text{ are Lebesgue measurable functions on [0,1]} \\ \text{and} \quad 0 \leq u_i(t) \leq 1 \ \text{ for } \ i = 1, 2\}. \end{aligned} \tag{6.3.2}$$

So, the objective function for the CF fractionalized optimal control system (6.3.1), (6.3.2) is given as

$$\mathcal{J}(u_1(\cdot), u_2(\cdot)) = \int_0^{t_f} \left[\frac{1}{2} C_1 u_1^2(t) + \frac{1}{2} C_2 u_2^2(t) + S_i^2(t) + B_l^2(t)\right] dt \tag{6.3.3}$$

where C_1 and C_2 measure the cost associated with the control functions $u_1(t)$ and $u_2(t)$, respectively. Then, we find the optimal controls u_1 and u_2 to minimize the cost function

$$\mathcal{J}(u_1, u_2) = \int_0^{t_f} [\psi(S_u(t), S_i(t), B_l(t), u_1(t), u_2(t),\ t)]\, dt \tag{6.3.4}$$

subject to the constraints ${}_0^{CF}D_t^{\zeta}(S_u(t)) = \alpha_1$, ${}_0^{CF}D_t^{\zeta}(S_i(t)) = \alpha_2$ and ${}_0^{CF}D_t^{\zeta}(B_l(t)) = \alpha_3$, where $\alpha_j = \alpha_j(S_u, S_i, B_l, u_1, u_2,\ t)$ and $j = 1, 2, 3$, and the given initial conditions are $S_u(0) = S_{u_0}$ and $S_i(0) = S_{i_0}$, $B_l(0) = B_{l_0}$.

Now, we first present a formulation of a generalized fractional optimal control problem (FOCP) and deduce the necessary conditions for its optimality. For this, let us consider a generalized FOCP as

$$J(v) = \int_0^{t_f} [L(t, x, v)dt]\, dt \tag{6.3.5}$$

subject to the constraints ${}_0^{CF}D_t^{\zeta}(x(t)) = g(t, x, v)$ with initial condition $x(0) = x_0$. Here, $x(t)$ and $v(t)$ are state and control vectors, respectively, and L and g are differentiable functions

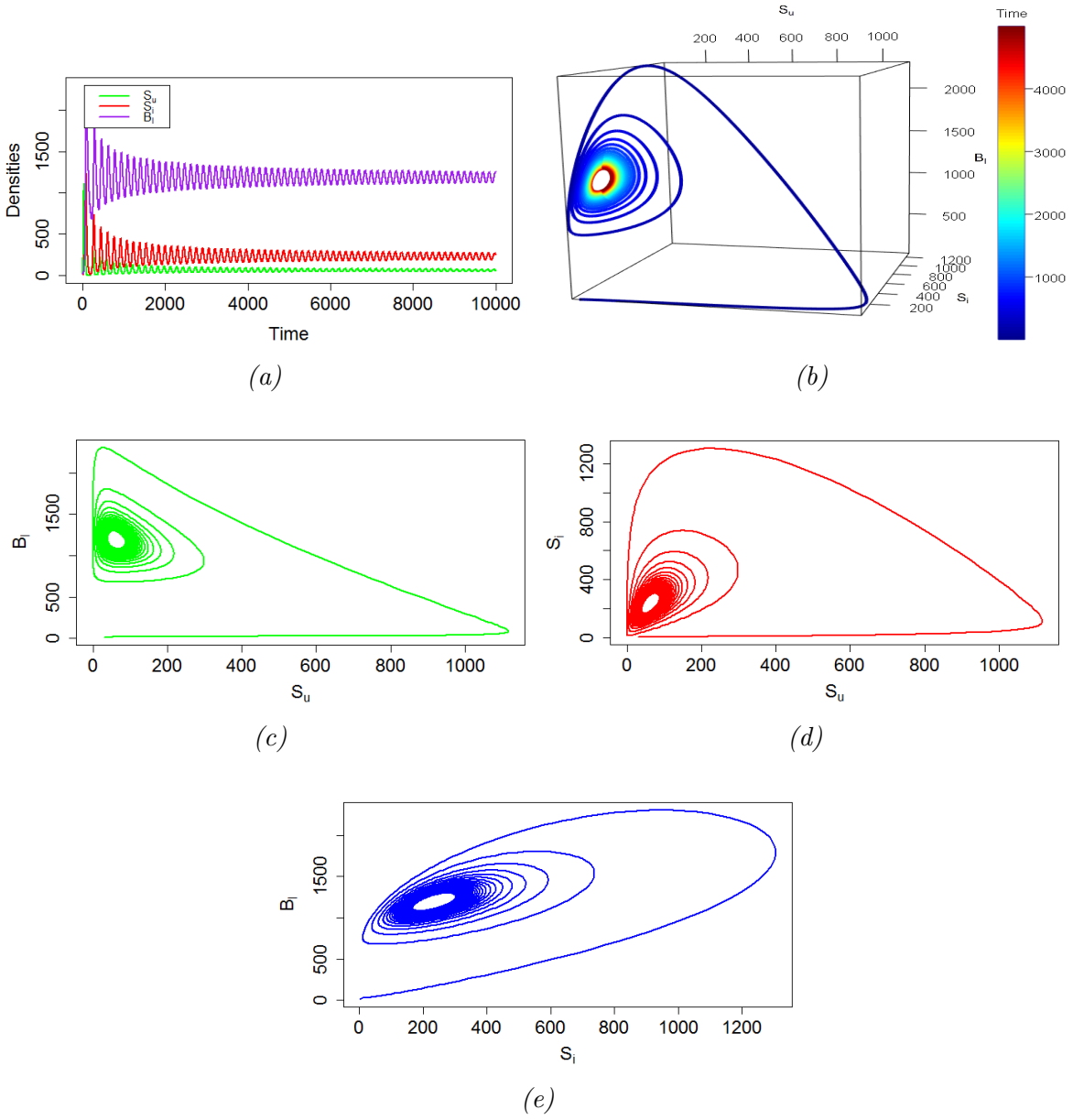

*Figure 6.5: Times series and phase portrait diagrams of the CF fractionalized system (6.1.2) depicting the sustained oscillatory unstable behavior of the system state populations and appearance of limit cycles for $\zeta = 1$. Here, values of $\nu_2 = 0.035$ and $S_{u_{max}} = 1200$ were used for simulating the Subfigures in this Figure. All the other parameter values were chosen from Table 6.1. (**a**) Behavior of the trajectories of system (6.1.2); (**b**) 3-D phase diagram for system (6.1.2) in $S_u - S_i - B_l$ space; (**c**) 2-D phase diagram of system (6.1.2) in the $S_u - B_l$ plane; (**d**) 2-D phase diagram for system (6.1.2) in the $S_u - S_i$ plane; (**e**) 2-D phase diagram for system (6.1.2) in the $S_i - B_l$ plane.*

with $0 < \zeta \leq 1$.

Theorem 6.3.1 *We define a Hamiltonian as follows:*

$$\mathcal{H}(t, x, v, \phi) = L(t, x, v) + \phi * g(t, x, v) \tag{6.3.6}$$

where $\phi \in C^1[0, t_f]$ is a function. If ϕ, x, v satisfy the following equations:

$$\begin{aligned} {}_0^{CF}D_t^{\zeta}(x(t)) = \frac{\partial \mathcal{H}(t, x(t), v(t), \phi(t))}{\partial \phi}, \quad {}_t^{CF}D_{t_f}^{\zeta}(\phi(t)) = \frac{\partial \mathcal{H}(t, x(t), v(t), \phi(t))}{\partial x}, \\ \frac{\partial \mathcal{H}(t, x(t), v(t), \phi(t))}{\partial v} = 0, \qquad \phi(t_f) = 0 \end{aligned}$$

then (x, v) is the minimizer of (6.3.5).

Proof. Let us first substitute Equation (6.3.6) in (6.3.5); hence, we obtain

$$J(v) = \int_0^{t_f} \{\mathcal{H}(t, x, v, \phi) - \phi * g(t, x, v)\}\, dt. \tag{6.3.7}$$

The necessary condition for the optimality of the FOCP is

$$\delta J(v) = 0. \tag{6.3.8}$$

To obtain the optimal control laws, we choose the variation of equation (6.3.7) as

$$\delta J(v) = \left[\delta x \frac{\partial \mathcal{H}}{\partial x} + \delta v \frac{\partial \mathcal{H}}{\partial v} + \delta \phi \frac{\partial \mathcal{H}}{\partial \phi} - \delta \phi\ {}_0^{CF}D_t^{\zeta}(x(t)) - \phi \left({}_0^{CF}D_t^{\zeta}(\delta x(t))\right)\right] dt \tag{6.3.9}$$

where δx, δv, $\delta \phi$ are variations of x, v and ϕ, respectively.

Again,

$$\int_0^{t_f} \phi(t) \left({}_0^{CF}D_t^{\zeta}(\delta x(t))\right) dt = \int_0^{t_f} \delta x \left({}_0^{CF}D_t^{\zeta}(\phi(t))\right) dt - \left({}_t^{CF}I_{t_f}^{1-\zeta}(\phi(t)\right) \delta x. \tag{6.3.10}$$

Substituting (6.3.10) in (6.3.9), we obtain

$$\begin{aligned} \delta J(v) = \int_0^{t_f} \left[\delta(x) \left[\frac{\partial \mathcal{H}}{\partial x} - {}_0^{CF}D_t^{\zeta}(\phi(t))\right] + \delta v s.\ \frac{\partial \mathcal{H}}{\partial v} + \delta \phi \left[\frac{\partial \mathcal{H}}{\partial \phi} - {}_0^{CF}D_t^{\zeta}(x(t))\right]\right] dt \\ + {}_t^{CF}I_{t_f}^{1-\zeta}(\phi(t))\delta x\Big|_{t=t_f}. \end{aligned} \tag{6.3.11}$$

Now, we know $\delta J(v) = 0$. Hence, considering equation (6.3.11), the coefficients of δx, δv, $\delta\phi$ must be equal to zero, which leads us to the following equations:

$$
\begin{aligned}
{}_{0}^{CF}D_{t}^{\zeta}(x(t)) = \frac{\partial \mathcal{H}(t, x(t), v(t), \phi(t))}{\partial \phi}, \quad {}_{t}^{CF}D_{t_f}^{\zeta}(\phi(t)) = \frac{\partial \mathcal{H}(t, x(t), v(t), \phi(t))}{\partial x}, \\
\frac{\partial \mathcal{H}(t, x(t), v(t), \phi(t))}{\partial v} = 0, \quad {}_{t}^{CF}I_{t_f}^{1-\zeta}(\phi(t))\Big|_{t=t_f} = \phi(t_f) = 0.
\end{aligned}
$$

In addition, the following necessary conditions must also hold for the optimality of the FOCP defined in (6.3.5), which are noted here in the form of the following lemma.

Lemma 6.3.1 *The following conditions hold true for the generalized FOCP described in (6.3.5):*

$$
{}_{t}^{CF}D_{t_f}^{\zeta}(\phi(t)) = \frac{\partial \mathcal{H}(t, x(t), v(t), \phi(t))}{\partial x} \tag{6.3.12}
$$

$$
\text{and} \quad {}_{0}^{CF}D_{t}^{\zeta}(\phi(t_f - t)) = \frac{\partial \mathcal{H}(t_f - t, x(t_f - t), v(t_f - t), \phi(t_f - t))}{\partial x} \tag{6.3.13}
$$

where $0 < \zeta \leq 1$.

Proof. The definition of the CF fractional derivative (1.10.14) is given as

$$
{}_{0}^{CF}D_{t}^{\zeta}(f(t)) = \frac{1}{1-\zeta}\int_{0}^{t} \exp\left[-\frac{\zeta(t-x)}{1-\zeta}\right] f'(x)dx, \quad t \geq 0, \quad 0 < \zeta < 1.
$$

From the above-mentioned definition of the CF fractional derivative, it follows that

$$
{}_{t_f-t}^{CF}D_{t_f}^{\zeta}(\phi(t_f - t)) = \frac{1}{1-\zeta}\int_{t_f-t}^{t_f} \exp\left[-\frac{\zeta(t_f - t - x)}{1-\zeta}\right] \phi'(x)dx. \tag{6.3.14}
$$

Now, assuming $t_f - x = y$, from equation (6.3.14), we obtain that

$$
\begin{aligned}
{}_{t_f-t}^{CF}D_{t_f}^{\zeta}(\phi(t_f - t)) &= \frac{1}{1-\zeta}\int_{t}^{0} \exp\left[-\frac{\zeta(y-t)}{1-\zeta}\right] \phi'(t_f - y)(-dy) \\
&= \frac{1}{1-\zeta}\int_{0}^{t} \exp\left[-\frac{\zeta(y-t)}{1-\zeta}\right] \phi'(t_f - y)dy.
\end{aligned} \tag{6.3.15}
$$

Hence, the optimality conditions are achieved as

$$\begin{cases} {}_0^{CF}D_t^{\zeta}(x(t)) = \dfrac{\partial \mathcal{H}(t, x(t), v(t), \phi(t))}{\partial \phi}, \\ {}_0^{CF}D_t^{\zeta}(\phi(t_f - t)) = \dfrac{\partial \mathcal{H}(t_f - t, x(t_f - t), v(t_f - t), \phi(t_f - t))}{\partial x} \\ \text{and} \quad \dfrac{\partial \mathcal{H}}{\partial v} = 0 \ \text{ where } \ \mathcal{H} := \mathcal{H}(t, x(t), v(t), \phi(t)). \end{cases} \tag{6.3.16}$$

We now shift our focus from the generalized point of view, specifically to our CF fractionalized optimal-control-induced (CFOC) system (6.3.1), (6.3.3), (6.3.4). Let us first consider the following modified cost function:

$$\hat{Z} = \int_0^T \left[\mathcal{H}(S_u, S_i, B_l, u_1, u_2, t) - \sum_{j=1}^{3} \theta_j \alpha_j(S_u, S_i, B_l, u_1, u_2, t) \right] dt. \tag{6.3.17}$$

Hence, the Hamiltonian is defined as

$$\mathcal{H}(S_u, S_i, B_l, u_1, u_2, t) = \psi(S_u, S_i, B_l, u_1, u_2, t) + \sum_{j=1}^{3} \theta_j \alpha_j(S_u, S_i, B_l, u_1, u_2, t). \tag{6.3.18}$$

Then, utilizing (6.3.16), the necessary and sufficient conditions for the CF fractional optimal control (CFOC) problem defined in (6.3.1), (6.3.3), (6.3.4) are given as

$$\begin{gathered} {}_0^{CF}D^{\zeta}\theta_1 = \frac{\partial \mathcal{H}}{\partial S_u}, \quad {}_0^{CF}D^{\zeta}\theta_2 = \frac{\partial \mathcal{H}}{\partial S_i}, \quad {}_0^{CF}D^{\zeta}\theta_3 = \frac{\partial \mathcal{H}}{\partial B_l}, \quad \frac{\partial \mathcal{H}}{\partial u_i} = 0, \quad i = 1, 2, \\ \text{and } \ {}_0^{CF}D_t^{\zeta}(S_u(t)) = \frac{\partial \mathcal{H}}{\partial \theta_1}, \ \ {}_0^{CF}D_t^{\zeta}(S_i(t)) = \frac{\partial \mathcal{H}}{\partial \theta_2}, \ \ {}_{.0}^{CF}D_t^{\zeta}(B_l(t)) = \frac{\partial \mathcal{H}}{\partial \theta_3}. \end{gathered}$$

Moreover, θ_1, θ_2 and θ_3 are Lagrange's multipliers, which express the necessary and sufficient conditions in terms of the Hamiltonian for the fractional optimal control problem defined above.

Now, consider system (6.3.1). Let us consider the Hamiltonian defined in (6.3.18). Rewrit-

ing it in the following form, we obtain

$$\begin{aligned}\mathcal{H}(S_u, S_i, B_l, u_1, u_2, \theta) = \frac{1}{2}C_1u_1^2 + \frac{1}{2}C_2u_2^2 + S_i^2 + B_l^2 \\ + \theta_1\left(\nu_1 S_u\left(1 - \frac{S_u}{S_{u_{max}}}\right) - \beta_1(1-u_1(t))S_uB_l\right) \\ + \theta_2\left(\beta_1(1-u_1(t))S_uB_l - \mu S_i\right) \\ + \theta_3\left(\nu_2(1-u_2(t))B_l\left(1 - \frac{B_l}{B_{l_{max}}}\right) - \beta_2(1-u_1(t))S_uB_l + \sigma S_i\right).\end{aligned} \tag{6.3.19}$$

Theorem 6.3.2 *If u_1^*, u_2^* are optimal controls of the given CFOC system defined by (6.3.1), (6.3.3), (6.3.4), and if S_u^*, S_i^*, B_l^* are the corresponding optimal paths, then there exist co-state variables θ_1^*, θ_2^*, θ_3^* such that besides the given control system being satisfied, the following conditions, i.e., the co-state equations, hold true also. The co-state equations are given as*

$$\begin{aligned}{}_0^{CF}D_t^{\zeta}\theta_1^* &= -\theta_1^*\left[\nu_1 - \frac{2S_u\nu_1}{S_{u_{max}}} - \beta_1(1-u_1)B_l\right] - \theta_2^*\beta_1(1-u_1)B_l \\ &\quad +\theta_3^*\beta_2(1-u_1)B_l, \\ {}_0^{CF}D_t^{\zeta}\theta_2^* &= \theta_2^*\mu - \theta_3^*\sigma - 2S_i, \\ {}_0^{CF}D_t^{\zeta}\theta_3^* &= \theta_1^*\beta_1(1-u_1)S_u - \theta_2^*\beta_1(1-u_1)S_u \\ &\quad -\theta_3^*\left[\nu_2(1-u_2)\left[1 - \frac{2B_l}{B_{l_{max}}}\right] - \beta_2(1-u_1)S_u\right] - 2B_l\end{aligned} \tag{6.3.20}$$

with transversality conditions $\theta_1^*(t_f) = 0$, $\theta_2^*(t_f) = 0$, $\theta_3^*(t_f) = 0$, and the optimality conditions are given by

$$\begin{aligned}\mathcal{H}(S_u^*(t), S_i^*(t), B_l^*(t), u_1^*(t), u_2^*(t)) = \min_{0\le u_i\le 1}\mathcal{H}(S_u^*, S_i^*, B_l^*, u_i^*), \\ u_1^*(t) = \min\left\{1, \max\left(0, \frac{S_uB_l(\beta_1\theta_2^* - \beta_2\theta_3^* - \beta_1\theta_1^*)}{C_1}\right)\right\}, \\ u_2^*(t) = \min\left\{1, \max\left(0, \frac{\theta_3^*\nu_2B_l\left(1 - \frac{B_l}{B_{l_{max}}}\right)}{C_2}\right)\right\}.\end{aligned} \tag{6.3.21}$$

Proof. The adjoint system (6.3.20) is obtained from $\mathcal{H}$ as follows

$$-\frac{d\theta_1}{dt} = \frac{\partial\mathcal{H}}{\partial S_u}, \quad -\frac{d\theta_2}{dt} = \frac{\partial\mathcal{H}}{\partial S_i}, \quad -\frac{d\theta_3}{dt} = \frac{\partial\mathcal{H}}{\partial B_l}$$

with transversality conditions given as $\theta_1(t_f) = \theta_2(t_f) = \theta_3(t_f) = 0$. Furthermore, the characterization of the CF fractionalized optimal controls $u_1^*(t)$ and $u_2^*(t)$ are achieved by solving the following equations

$$\frac{\partial \mathcal{H}}{\partial u_1} = 0, \quad \frac{\partial \mathcal{H}}{\partial u_2} = 0$$

on the interior of the control set and utilizing the properties of the control space $\mathcal{U}$.

The analytical Sections of our study come to an end here and next we proceed to the numerical outcomes for validation of the analytical portions of our proposed systems.

6.4 Numerical Simulation

In this Section, we perform numerical simulations for both the Caputo–Fabrizo fractional system denoted by (6.1.2) and also the CF fractionalized optimal control system (6.3.1). All the numerical results are compared with the analytical and theoretical outcomes previously achieved. We chose the initial values according to the cardinal rule of scientific hypothesis. Some values of the parameters were chosen from the numerical table in Chapter 2 and the research article [Masaki et al. (2013)], and the other values were estimated. The values of the parameters which we have used here are described in the following table denoted by Table 6.1. All of our numerical findings here were obtained using MATLAB 2016A. Throughout the Chapter, the interval of consideration was chosen as $[0, 2.5 \times 10^3]$.

Here, we want to mention that Table 6.1 actually refers to the values of the system parameters for system (6.1.2) and system (6.3.1) for the fractional order $\zeta = 1$. During the simulations of the Figures for $\zeta \in (0, 1)$, we adopted the technique proposed by Atangana et al. [Khan and Atangana (2020)]. To avoid the dimension mismatching of $(time)^{-1}$ and $(time)^{(-\zeta)}$ between the left- and right-hand sides of the systems, the dimensions of the system parameters were modified accordingly and the corresponding values were utilized for the numerical simulations.

In Figures 6.1 and 6.2, the behavior of the cell densities and the phase portrait diagrams of the healthy Schwann cells, infected Schwann cells and *M. leprae* bacteria for system (6.1.2) in the 3-D phase space are exhibited, respectively, for $\zeta = 1$, i.e., for the classical integer-order system. Figure 6.1 depicts oscillatory periodic solutions and stable limit cycles. On the contrary, in Figure 6.2, stable solutions are observed whenever the value of ν_2 is increased from 0.03 to 0.05, which describes that the intrinsic growth rate of the bacterial population is a very crucial parameter for demonstrating the dynamical shift in system (6.1.2).

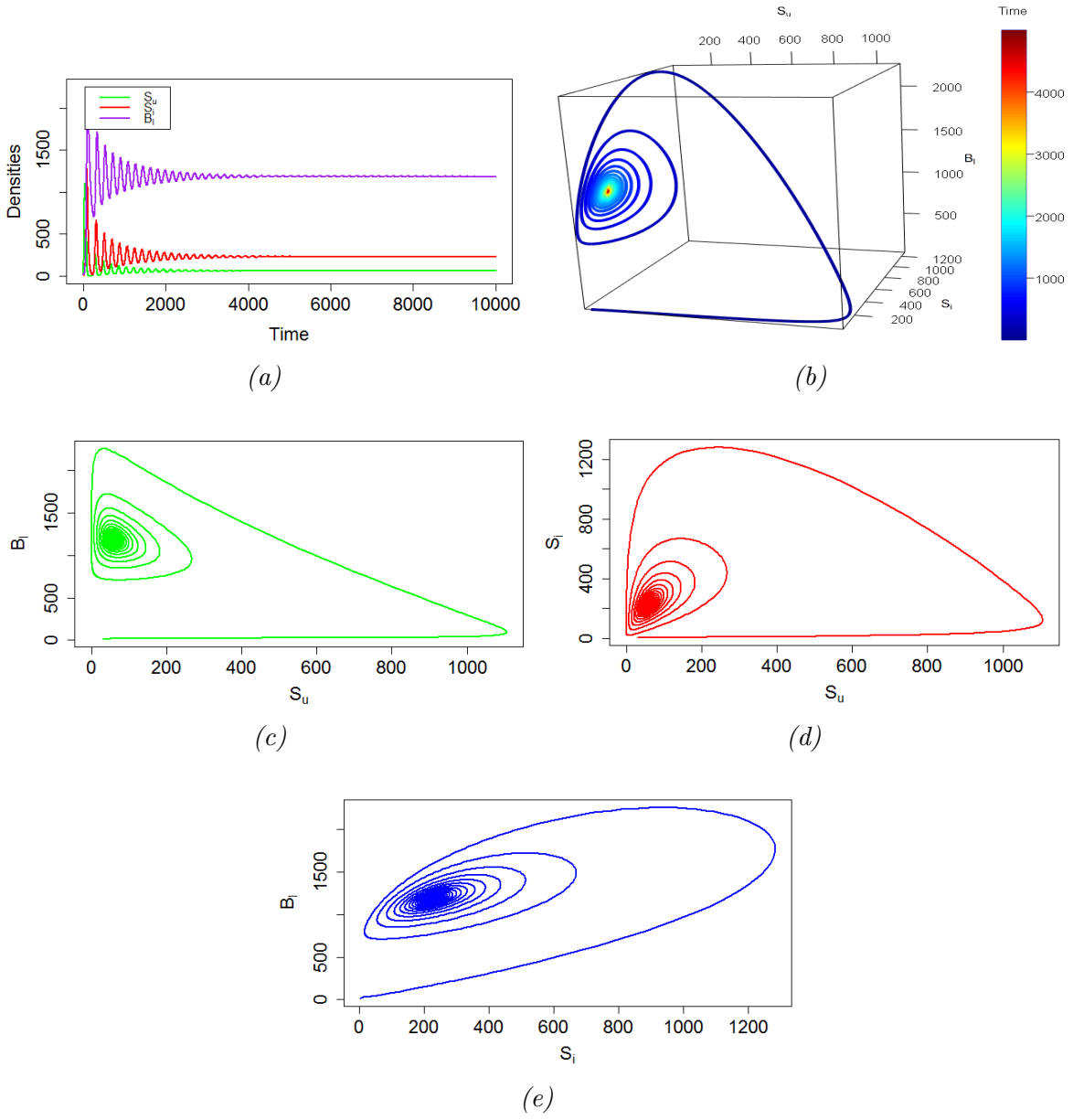

Figure 6.6: Times series and phase portrait diagrams of the CF fractionalized system (6.1.2) depicting the asymptotically stable dynamics of the system state populations for $\zeta = 0.6$. *Here, major observations are noted by studying the comparative behavior of system (6.1.2) between the CF-fractional order* $\zeta = 1$ *(unstable in the form of stable periodic solutions and limit cycles shown in Figure 6.5) and* $\zeta = 0.6$ *(stable behavior demonstrated in this Figure, i.e., in Figure 6.6). Here, values of* $\nu_2 = 0.035$ *and* $S_{u_{max}} = 1200$ *were used for simulating the Subfigures in this Figure. All the other parameter values were chosen from Table 6.1. (**a**) Behavior of the trajectories of system (6.1.2); (**b**) 3-D phase diagram for system (6.1.2) in* $S_u - S_i - B_l$ *space; (**c**) 2-D phase diagram of system (6.1.2) in the* $S_u - B_l$ *plane; (**d**) 2-D phase diagram for system (6.1.2) in the* $S_u - S_i$ *plane; (**e**) 2-D phase diagram for system (6.1.2) in the* $S_i - B_l$ *plane.*

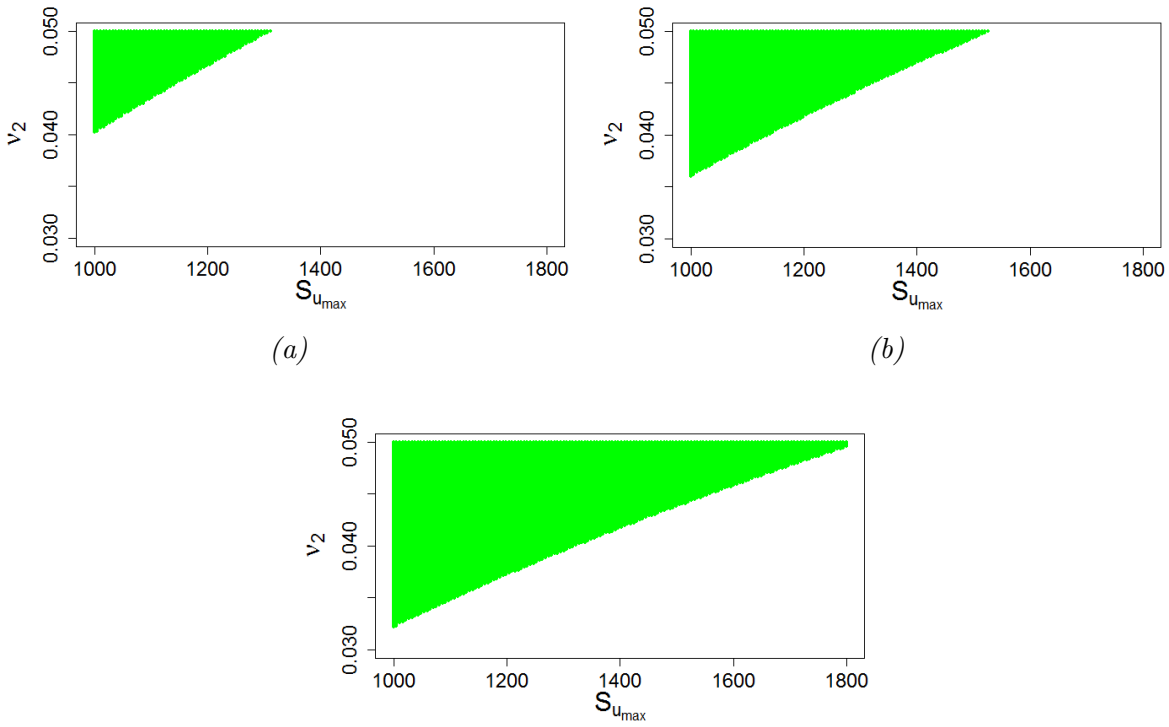

*Figure 6.7: Representation of the stability regions for the Caputo–Fabrizio (CF) fractionalized system (6.1.2) for different values of CF fractional order ζ. Values of the parameters were chosen as $\nu_1 = 0.4$, $B_{l_{max}} = 530$, $\mu = 0.1$, $\beta_1 = 0.00032$, $\sigma = 0.3$, $\beta_2 = 0.00024$ and all the values of other parameters were taken from Table 6.1. (**a**) Stability region for CF fractional order $\zeta = 1$; (**b**) stability region for CF fractional order $\zeta = 0.8$; (**c**) stability region for CF fractional order $\zeta = 0.6$.*

Table 6.1: List of parameter values used in numerical simulation for systems (6.1.2) and (6.3.1) for $\zeta = 1$.

Parameter	**Parameter Definition**	**Assigned Value**
ν_1	growth rate of S_u	0.4
ν_2	growth rate of B_l	0.01–0.05
$S_{u_{max}}$	carrying capacity of S_u	600–1400
$B_{l_{max}}$	carrying capacity of B_l	400–550
μ	natural death rate of S_i	0.1
β_1	infection rate	0.0003–0.0046
σ	proliferation rate of B_l	0.1–0.35
β_2	clearance rate of B_l	0.00015–0.0003

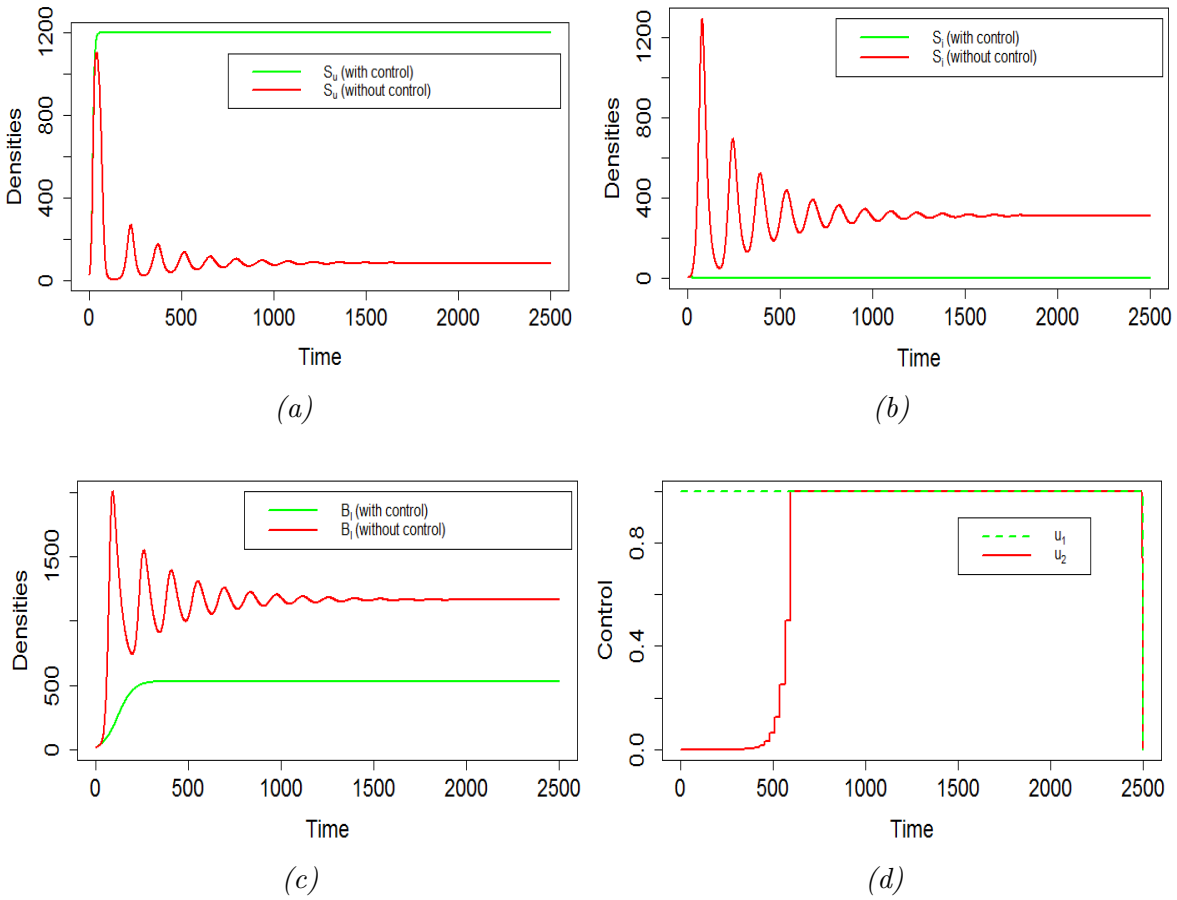

*Figure 6.8: Trajectories of the cell populations of the optimal-control-induced Caputo–Fabrizio fractional (CFOC) system (6.3.1). Scenarios for both with and without control are exhibited here in Subfigures (**a**), (**b**) and (**c**), respectively, denoted by green and red color. In Subfigure (**d**), optimal control profiles of u_1^* and u_2^* are shown for CFOC system (6.3.1). Values of the parameters were chosen as $\zeta = 0.9$, $\nu_2 = 0.03$, $S_{u_{max}} = 1200$ for simulating the Subfigures of this Figure and other parameter values were selected from Table 6.1. (**a**) Behavior of the densities of healthy Schwann cells S_u; (**b**) behavior of the densities of infected Schwann cells S_i; (**c**) behavior of the concentrations of M. leprae bacteria B_l; (**d**) dynamics of the optimal control profiles u_1^* and u_2^* for system (6.3.1).*

We now move on to understand the behavior of system (6.1.2) in the previous memory states, i.e., for the non-integer cases or fractional-order cases for the value of $\zeta \in (0, 1)$. Considering $\zeta = 0.8$, Figure 6.3 shows that system (6.1.2) produces oscillatory solutions and stable limit cycles for $\nu_2 = 0.03$, while S_u cell, S_i cell and B_l bacteria reach the stable concentrations of approximately 50 mm^3, 120 mm^3 and 1100 mm^3, respectively, at the endemic steady state E^* described in Figure 6.4.

Next, a comparison of system (6.1.2)'s behavior is investigated for two different values of ζ. Keeping the whole parameter set fixed, we varied the fractional order from $\zeta = 1$ to $\zeta = 0.6$. The numerical outcomes in Figure 6.5 exhibit unstable behavior with sustained oscillations of the cell population densities of system (6.1.2) for $\zeta = 1$, but moving towards the previous memory state for $\zeta = 0.6$, Figure 6.6 shows that after a little initial fluctuation, the system state populations become asymptotically stable. In addition, in Figure 6.7, the stability regions of the interior equilibrium $E^*(S_u^*, S_i^*, B_l^*)$ for the CF fractionalized system (6.1.2) for three different values of ζ, i.e., for $\zeta = 1, 0.8, 0.6$, are clearly demonstrated in Figures 6.7a, 6.7b and 6.7c, respectively.

In Figures 6.8 and 6.9, the effect of the optimal control treatment policy has been demonstrated on the Caputo–Fabrizio fractionalized optimal control (CFOC) system for the fractional orders $\zeta = 0.9$ and $\zeta = 0.6$, respectively. In both cases, the concentrations of healthy Schwann cells (S_u) are observed to be increased, and also the densities of S_i and B_l are decreased in the body of a leprosy-infected person. The bacterial concentration B_l decreases to 510 mm^3 in Figure 6.8c, while it decreases to a stable concentration of 420 mm^3 depicted in Figure 6.9c. This indicates that the CFOC system (6.3.1) acts better when more previous memory states are considered for $\zeta = 0.6$. Now, looking into the optimal control profiles of u_1^* and u_2^*, we can see that the drug therapy Dapsone denoted by $u_2^*(t)$ needs to be increased after 520 days in case of $\zeta = 0.9$, while it should be increased after nearly 1100 days up to the range 0.8–0.9 for $\zeta = 0.6$ described in Figures 6.8d and 6.9d, respectively. This happens due to the memory effect of *M. leprae*-induced infection and as the previous memory stages of the bacteria are extremely correlated with the drug resistance scenarios during the treatment [Wolf et al. (2008)]. Indeed, the *M. leprae* bacteria are highly Dapsone-resistant [Wu et al. (2022); Williams et al. (2018)]. To tackle the dissemination of leprosy into the human body and to effectively inhibit bacterial drug resistance, applying the optimal control treatment approach for the previous memory state of $\zeta = 0.6$ is more realistic in nature and appropriate than the present state or the states very adjacent to $\zeta = 0.9$.

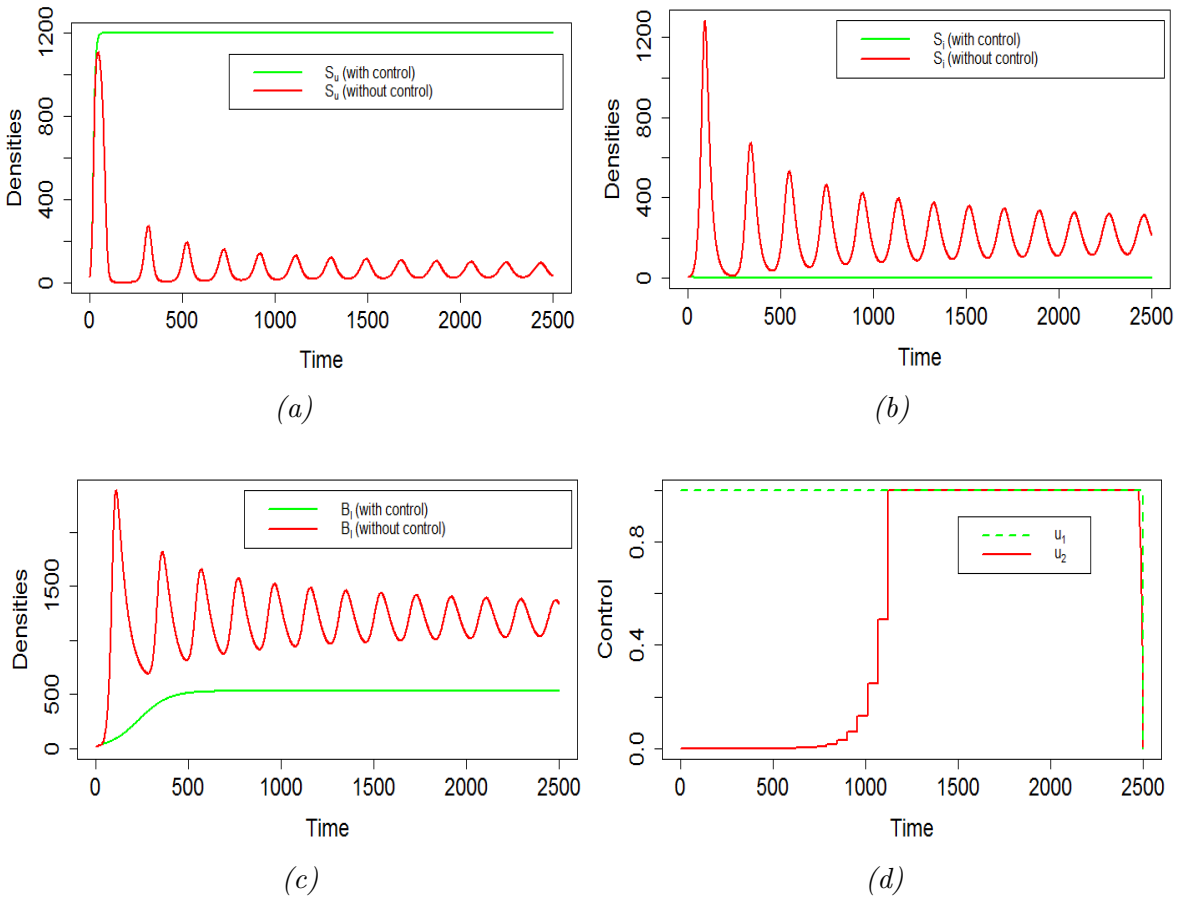

*Figure 6.9: Trajectories of the cell populations of the optimal-control-induced Caputo–Fabrizio fractional (CFOC) system (6.3.1). Scenarios for both with and without control are exhibited here in Subfigures (**a**), (**b**) and (**c**), respectively, denoted by green and red colors. In Subfigure (**d**), optimal control profiles of u_1^* and u_2^* are shown for CFOC system (6.3.1). Values of the parameters were chosen as $\zeta = 0.6$, $\nu_2 = 0.03$, $S_{u_{max}} = 1200$ for simulating the Subfigures of this Figure and other parameter values were selected from Table 6.1. (**a**) Behavior of the densities of healthy Schwann cells S_u; (**b**) behavior of the densities of infected Schwann cells S_i; (**c**) behavior of the concentrations of M. leprae bacteria B_l; (**d**) dynamics of the optimal control profiles u_1^* and u_2^* for system (6.3.1).*

6.5 Discussion

In this Chapter, we have formulated and analyzed a three-dimensional CF fractional-order-based mathematical system and, most importantly, investigated the impacts of memory effects on the CF fractionalized optimal control system by incorporating a combined drug therapy. We have formulated an iterative scheme using the Laplace and inverse Laplace transformations in Section 6.1.1. Following that, we established the stability of the solutions using Picard's T-stability iterative criterion in Theorem 6.1.2 in Section 6.1.2. For demonstrating the existence and uniqueness of the solutions (Theorem 6.1.3 in Section 6.1.3 and Section 6.1.4) of system (6.1.2), we used the well-known Banach fixed-point theorem and Arzela–Ascoli theorem. The formula for the basic reproduction number R_0 was derived and the local asymptotic stability of E_0 for the CF fractionalized system (6.1.2) was investigated with respect to the threshold value of $R_0 = 1$. Besides this, we also described the stability criterion of the endemic equilibrium E^* of system (6.1.2) in Theorem 6.2.2 in Section 6.2. Furthermore, the CFOC system (6.3.1) was investigated by suitably defining the control set $\mathcal{U}$ in Equation (6.3.2) and the objective function (6.3.3) in Section 6.3. A generalized FOCP was formed in (6.3.5) and optimality conditions were proven in detail for this FOCP denoted by (6.3.16). Then, the formulas in (6.3.16) were applied to achieve the necessary and sufficient optimality conditions for system (6.3.1), and also the values of the optimal control pair u_1^* and u_2^* and the co-state or the adjoint equations with the corresponding transversality conditions were described elaborately in Theorem 6.3.2.

In Chapter 2, we have described three strategies and among them, Strategy-III was found to be the most effective one. However, serious matters of concern in determining a realistic and accurate therapy for leprosy are the high cost and extreme adverse effects of the combined drug therapy. Here, in this Chapter, from Figures 6.8d and 6.9d, we can observe that after introducing the memory effect, the amount of the drugs needed initially is much less for system (6.3.1) than for Strategy-III in both the memory-free model and integer-ordered system, which is much better in terms of cost-effectiveness and safe therapeutics.

Furthermore, comparing Figures 6.8 and 6.9, we can notice that if the value of ζ is decreased from 0.9 to 0.6, oscillatory solutions appear for the specific range of the parameter set, but in both cases, under the optimal treatment policy, the densities of the cell populations approach a stable concentration. The dynamics of the optimal control profile of Ofloxacin remain almost similar for both $\zeta = 0.9, 0.6$, but the control profile of Dapsone provides notable differences. More specifically, for $\zeta = 0.6$, the drug dose of Dapsone, i.e., $u_2^*(t)$, needs to be increased after 1100 days to tackle the highly Dapsone-drug-resistant *M. leprae* [Wu et al. (2022); Williams et al. (2018)] and the associated infection procedure. Thus, to build a perfect

regimen for combined therapy, acquiring enough knowledge from the previous memory states about drug-resistance issues [Matsuoka (2010); Williams and Gillis (2012); Benjak et al. (2018)] is essential and, hence, CFOC system (6.3.1) with $\zeta = 0.6$ is very fruitful in this context. The more we reduce the value of ζ and approach the previous memory states, the more accurate the precision will be. Still, future works on leprosy in this aspect should also focus on investigating the memory stages for the value of $\zeta < 0.6$, and before implementation, the outcomes should be validated properly by clinical and experimental researchers.

Chapter 7

Analysis of a Stochastic Mathematical Model for Examining the Extinction of Infected Schwann Cells in Leprosy

Stochastic systems has the capacity to handle uncertainties in the inputs applied. Stochastic models possess some inherent randomness i.e. noise and the unique characteristic a stochastic system holds is that the same set of parameter values and initial conditions will lead to an ensemble of different outputs. In this Chapter[7], we have extended the deterministic ODE-based system developed in Chapter 5 and formulated a stochastic version of the system. Long term behavior of the model is investigated by calculating a stationary distribution and normal approximation of the distribution. The quasi-stationary distribution of the model is studied to examine the models' behavior before extinction and to achieve the time to extinction of the infected Schwann cells. Our main aim of this Chapter is to predict the probability that the infectious cells have died out at a given time while comparing different scenarios incorporated as a result of the most dominant parameter, the drug-efficacy rate of MDT treatment. All of the analytical results are validated through numerical simulations in Matlab 2016a and are compared with existing clinical data.

[7] *The bulk of this chapter is communicated in a peer-reviewed journal.*

7.1 The Deterministic Mathematical Model

We have first considered the four-dimensional mathematical model developed in Chapter 5 here in this Section and extended this system later through constructing a stochastic version of it. The four dimensional nonlinear ODE-based system is presented as:

$$\begin{aligned}
\frac{dS_h}{dt} &= \Pi - \beta S_h B + \alpha f(X) S_i - \lambda g(X) S_h - d S_h, \\
\frac{dS_i}{dt} &= \beta S_h B - \alpha f(X) S_i + \lambda g(X) S_h - d_i S_i, \\
\frac{dB}{dt} &= rB\Big(1 - \frac{B}{K}\Big) - d_b X B + \kappa S_i, \\
\frac{dX}{dt} &= e\eta S_i - \theta X
\end{aligned} \tag{7.1.1}$$

with initial values $S_h(0) = S_{h0} > 0$, $S_i(0) = S_{i0} > 0$ and $B(0) = B_0 > 0$ and $X(0) = X_0 > 0$ at $t = 0$.

Here, the concentrations of healthy Schwann cells, infected Schwann cells, *M. leprae* bacteria and MDT drug therapy are represented by $S_h(t)$, $S_i(t)$, $B(t)$ and $X(t)$, respectively, at any time t. Π denotes the constant production rate of healthy Schwann cells from neural crest cells into human body. β is the effective contact rate between the healthy Schwann cells and the bacteria. α be the rate at which infected cells become recovered due to the effect of MDT. The rate at which healthy Schwann cells are getting infected again as a result of waning effect of MDT is indicated by λ. The parameters, r and K describe the intrinsic growth rate and carrying capacity of *M. leprae* bacteria as presented in a logistic manner. The level of treatment i.e. the concentration of MDT is proportional to the number of infected Schwann cells and it is represented by the term, $e\eta S_i$, where e denotes the proportionality constant and η denotes the efficacy rate of MDT. Moreover, θ reflects the natural drug washout rate through various physiological processes into a human body. d, d_i and d_b signify the natural death rate or mortality rate healthy Schwann cells, infected Schwann cells and the rate at which *M. leprae* bacteria is killed by MDT, respectively. By the rate κ, we have denoted the proliferation rate of newly produced free *M. leprae* bacteria from infected Schwann cells which via releasing bacteria-laden macrophages, further disseminates the infection into the whole human body. The effective drug-treatment is directed by the increasing function, $f(X)$ with $f(0) = 0$ and $\sup f(X) = 1$. It is considered that the effectiveness of drug is fading for which the healthy Schwann cells are becoming infected again. Therefore, $g(X)$ is chosen as a decreasing function of X with $g(0) = 1$ and $\inf g(X) = 0$.

Let us denote the total number of Schwann cells at any time t into a human body by $N_S(t)$ i.e $N_S(t) = S_h(t) + S_i(t)$. Adding the first and second equations of system (7.1.1), we get

$$\frac{N_S}{dt} = \Pi - d_s S_h \tag{7.1.2}$$

where $d_s = d + d_i$. From equation (7.1.2), we get

$$\frac{dN_S}{\Pi - d_s N_S} = dt. \tag{7.1.3}$$

Integrating this, we obtain

$$N_S(t) = \frac{1}{d_s}(\Pi - ce^{-d_s t}) \quad \text{where} \quad c \quad \text{is an arbitrary constant.}$$

This clearly implies that

$$N_s \to \frac{\Pi}{d_s} \quad as \quad t \to \infty. \tag{7.1.4}$$

Using equation (7.1.4) in system (7.1.1), we get that

$$\begin{aligned} \frac{dS_i}{dt} &= \beta(N_S - S_i)B - \alpha f(X)S_i + \lambda g(X)(N_S - S_i) - d_i S_i, \\ \frac{dB}{dt} &= rB\Big(1 - \frac{B}{K}\Big) - d_b XB + \kappa S_I, \\ \frac{dX}{dt} &= e\eta S_i - \theta X. \end{aligned} \tag{7.1.5}$$

For the quasi-steady state (QSS) approximation to achieve an accurate and precise interpretation of the dynamics of the system, it is required to consider the MDT drug dose concentration in an equilibrium state i.e. more precisely, we need to put the third equation of system (7.1.5) to be zero which implies that $\frac{dX}{dt} = 0$.

From this equation, we get

$$X = \frac{e\eta S_i}{\theta}. \tag{7.1.6}$$

From equation (7.1.6), substituting the value of X, model (7.1.5) assumes the following form:

$$\begin{cases} \dfrac{dS_i(t)}{dt} = \beta(N_S - S_i)B - \alpha f(\dfrac{e\eta S_i}{\theta})S_i + \lambda g(\dfrac{e\eta S_i}{\theta})(N_S - S_i) - d_i S_i, \\ \dfrac{dB(t)}{dt} = rB\Big(1 - \dfrac{B}{K}\Big) - d_b \dfrac{e\eta S_i}{\theta} B + \kappa S_i. \end{cases} \tag{7.1.7}$$

Previously, it was mentioned in the model formulation and assumption Section that f and g

are chosen as two functions of X, monotonically increasing and decreasing, respectively such that $f(0) = 0$, $g(0) = 1$, $\limsup f(X) = 1$ and $\liminf g(X) = 0$. Let us now use the explicit forms in place of the functional forms $f(X)$ and $g(X)$ as $f(X) = \frac{X}{1+X}$ and $g(X) = \frac{1}{1+X}$. Under these assumptions, the deterministic system (7.1.7) can be written as:

$$\begin{cases} \dfrac{dS_i(t)}{dt} = \beta(N_S - S_i)B - \dfrac{\alpha e\eta}{\theta + e\eta S_i}S_i^2 + \dfrac{\lambda\theta}{\theta + e\eta S_i}(N_S - S_i) - d_i S_i, \\ \dfrac{dB(t)}{dt} = rB\Big(1 - \dfrac{B}{K}\Big) - \dfrac{d_b e\eta}{\theta}S_i B + \kappa S_i. \end{cases} \tag{7.1.8}$$

To investigate the dynamical behaviour of system (7.1.8), we have to discuss the local asymptotic stability of the equilibrium points for the system. For evaluating the equilibrium points, let us put the right hand sides of the equations of system (7.1.8) equals to zero. Hence, we obtain the following set of equations:

$$\beta(N_S - S_i^*)(B^*) - \frac{\alpha e\eta}{\theta + e\eta S_i^*}(S_i^*)^2 + \frac{\lambda\theta}{\theta + e\eta S_i^*}(N_S - S_i^*) - d_i S_i^* = 0, \tag{7.1.9}$$

$$\kappa S_i^* - \frac{d_b e\eta}{\theta}S_i^*(B^*) + r(B^*)\Big(1 - \frac{(B^*)}{K}\Big) = 0. \tag{7.1.10}$$

From equation (7.1.9), it implies that

$$S_i^* = \frac{rB^*(K - B^*)\theta}{K(d_b e\eta B^* - \kappa\theta)}. \tag{7.1.11}$$

Replacing the value of S_i^* in the equation (7.1.10) , we get

$$h(B^*) = (B^*)^5 + \psi_1(B^*)^4 + \psi_2(B^*)^3 + \psi_3(B^*)^2 + \psi_4(B^*) + \psi_5 = 0 \tag{7.1.12}$$

where

$$\psi_1 = \frac{G_2H_2 + G_1H_3}{G_2H_3}, \quad \psi_2 = \frac{G_2H_1 + G_1H_2 + G_0H_3 + \Lambda_1}{G_2H_3}, \quad \psi_3 = \frac{G_1H_1 + G_0H_2 + \Lambda_2}{G_2H_3},$$
$$\psi_4 = \frac{G_0H_1 + \Lambda_3}{G_2H_3}, \quad \psi_5 = \frac{\Lambda_4}{G_2H_3}$$

and

$G_0 = -\kappa K\theta^2$, $G_1 = e\eta r\theta K + K\theta d_b e\eta$, $G_2 = -e\eta r\theta$, $H_1 = -(K\beta N_S\kappa\theta + d_i r\theta K)$, $H_2 = (K\beta N_S d_b e\eta + d_i r\theta - r\theta K\beta)$, $H_3 = r\theta\beta$, $\Lambda_1 = \theta^2 r\lambda K d_b e\eta$, $\Lambda_2 = \lambda\theta N_S K^2 d_b^2 e^2\eta^2 + \alpha e\eta r\theta - r\lambda\theta^2 K^2 d_b e\eta - r\lambda\theta^3\kappa K$, $\Lambda_3 = r\theta^3\kappa K - 2\lambda\theta N_S K^2 d_b e\eta\kappa\theta$, $\Lambda_4 = \lambda\theta N_S\kappa^2 K^2\theta^2 - \alpha re\theta\eta K\beta$.

Positive interior equilibrium $E^* = (S_i^*, B^*)$ exists for system (7.1.8) if there exists S_i^*, B^* such that both $S_i^* > 0$ and $B^* > 0$. The endemic state bacterial density can not exceed

the carrying capacity of the population which means $B^* < K$ always holds true. So, from equation (7.1.11), it follows that $S_i^* > 0$ whenever

$$d_b e\eta B^* > \kappa\theta \tag{7.1.13}$$

where B^* is the positive root of equation (7.1.12). Now, it is remaining to show that there exists a positive root of (7.1.12) i.e. there exists $B^* > 0$ such that $h(B^*) = 0$. It is important to note that $h(+\infty)$ is always positive and hence, existence of at least one positive root of $h(B^*) = 0$ is guaranteed if $\psi_5 < 0$. So, there exists at least one positive $B^* \in (0, \infty)$ satisfying equation (7.1.12) if the following condition is satisfied:

$$\alpha r e\eta\beta < \lambda N_S K \kappa^2 \theta^2. \tag{7.1.14}$$

In view of the previous discussion, we now construct the following lemma.

Lemma 7.1.1 *For the positive value of B^* i.e. if $\alpha r e\eta\beta < \lambda N_S K\kappa^2\theta^2$ holds and if $d_b e\eta B^* > \kappa\theta$, then the positive endemic equilibrium $E^* = (S_i^*, B^*)$ of system (7.1.8) exists.*

The Jacobian matrix of system (7.1.8) at the endemic equilibrium point $E^* = (S_i^*, B^*)$ is given as:

$$\mathcal{J}(S_i, B) = \begin{pmatrix} A_{11} & A_{12} \\ A_{21} & A_{22} \end{pmatrix}. \tag{7.1.15}$$

where

$$A_{11} = -\beta B^* - \frac{(2\alpha e\eta S_i^* + \lambda\theta)}{\theta + e\eta S_i^*} + \frac{e\eta}{(\theta + e\eta S_i^*)^2}(\alpha e\eta S_i^2 - \lambda\theta N_S) - d_i, \quad A_{12} = \beta(N_S - S_i^*),$$
$$A_{21} = -\frac{-d_b e\eta}{\theta} B^* + \kappa, \quad A_{22} = r - \frac{2rB^*}{K} - \frac{d_b e\eta}{\theta} S_i^*.$$

This implies that the corresponding characteristic equation of system (7.1.8) at E^* is

$$\det(\mathcal{J} - \omega I_2) = 0 \tag{7.1.16}$$

which indicates that

$$\omega^2 + D_0\omega + D_1 = 0 \tag{7.1.17}$$

where the values of D_0 and D_1 are given as:

$$D_0 = -(A_{11} + A_{14}), \quad D_1 = (A_{11}A_{14} - A_{12}A_{13}). \tag{7.1.18}$$

Clearly, equation (7.1.8) is quadratic equation with real coefficients. Either both of the two

roots $\omega_i,\ i = 1, 2$ are real or complex conjugate to each other. So, two cases are arising in this situation and are described below.

- When the roots are real, we can see that $\omega_1 + \omega_2 = -D_0$ and $\omega_1\omega_2 = D_1$. This implies that both of the roots will be negative if the conditions $D_0 > 0$ and $D_1 > 0$ are satisfied.
- When the roots are complex conjugate to each other, let us assume that these roots are in the form ω and $\bar{\omega}$. From equation (7.1.17), it follows that $-D_0 = \omega + \bar{\omega} = 2Re(\omega)$ where $Re(\omega)$ denotes the real part of ω. This clearly implies that complex roots with negative real part exists whenever $D_0 > 0$.

Considering the previous discussions and results, we now present the following theorem which explains the local asymptotic stability of E^* for system (7.1.8).

Theorem 7.1.1 *The endemic equilibrium $E^* = (S_i^*, B^*)$ of system (7.1.8) will be locally asymptotically stable i.e. the characteristic equation (7.1.17) possesses negative real roots or roots with negative real parts if the following inequalities are satisfied:*

$$A_{11} + A_{14} > 0 \quad \textit{and} \quad A_{11}A_{14} > A_{12}A_{13}.$$

7.2 Stochastic Model Formulation

A full stochastic version of our modified deterministic system (7.1.8) is formulated and described in this Section. Here, we have considered two state variables at time t, namely

- the number of infected Schwann cells denoted by $S_i(t)$,
- the number of *M. leprae* bacteria denoted by $B(t)$.

These state variables take the values in the state space $\mathcal{S}$ which is specifically described in the form: $\mathcal{S} = \{(S_i, B) : S_i = 0, 1, 2, ... ; B = 0, 1, 2....\}$. Let us consider that $P_{S_i,B}$ be the joint probability distribution of the number of infected Schwann cells and the number of *M. leprae* bacteria with possible transition rate at the time interval $[t, t + \Delta t]$.

7.2.1 Formulation of Kolmogorov's forward equation

Our model accounts for seven basic events namely, new infections of healthy Schwann cells, reinfection of the recovered cells for fading effect of MDT, removal of infected cells due to recovery through MDT treatment, natural death of infected cells, intracellular growth of *M.*

leprae bacteria, proliferation of *M. leprae* from the infected Schwann cells and the natural death rate of the bacteria. All these state transitions and the corresponding transition rates are demonstrated in detail in the fully stochastic version of the model mentioned in Table 7.1. Then, the Kolmogorov's forward equation which constructs a set of differential equation for the state probabilities along with the appropriate transition rates is as follows:

$$\begin{aligned}\frac{dP_{S_i,B}}{dt} &= \lim_{\Delta t\to 0}\frac{P_{S_i,B}(t+\Delta t)-P_{S_i,B}(t)}{\Delta t}\\ &= P_{S_i-1,B}\left[\beta B+\frac{\lambda\theta}{\theta+e\eta(S_i-1)}\left(N_s-S_i+1\right)\right]\\ &+ P_{S_i+1,B}\left[\frac{\alpha e\eta}{\theta+e\eta(S_i+1)}(S_i+1)^2+d_i(S_i+1)\right]\\ &+ P_{S_i,B-1}\left[\kappa S_i+r\left(1-\frac{(B-1)}{K}\right)(B-1)\right]\\ &+ P_{S_i,B+1}\left[\frac{d_b e\eta}{\theta}S_i(B+1)\right]-P_{S_i,B}\ \Lambda(S_i,B).\end{aligned} \tag{7.2.1}$$

Now, rewriting equation (7.2.1), we obtain the compact form of the Kolmogorov's forward equation given as:

$$\begin{aligned}\dot{P}_{S_i,B} &= \lambda_1(S_i-1,B)P_{S_i-1,B}+\mu_1(S_i+1,B)P_{S_i+1,B}\\ &+\lambda_2(S_i,B-1)P_{S_i,B-1}+\mu_2(S_i,B+1)P_{S_i,B+1}-\Lambda(S_i,B)P_{S_i,B}\end{aligned} \tag{7.2.2}$$

where

$$\begin{aligned}\lambda_1(S_i-1,B) &= \beta B+\frac{\lambda\theta}{\theta+e\eta(S_i-1)}\left(N_s-S_i+1\right),\\ \mu_1(S_i+1,B) &= \frac{\alpha e\eta}{\theta+e\eta(S_i+1)}(S_i+1)^2+d_i(S_i+1),\\ \lambda_2(S_i,B-1) &= \kappa S_i+r\left(1-\frac{(B-1)}{K}\right)(B-1),\\ \mu_2(S_i,B+1) &= \frac{d_b e\eta}{\theta}S_i(B+1)\end{aligned}$$

and

$$\Lambda(S_i,B)=\lambda_1(S_i,B)+\mu_1(S_i,B)+\lambda_2(S_i,B)+\mu_2(S_i,B).$$

Furthermore, we construct a method to map the two-dimensional $P_{S_i,B}$ into a one-dimensional

vector P such that the equation (7.2.2) gets converted into the following form:

$$\frac{dP}{dt} = PV. \tag{7.2.3}$$

Here, the probability P_{S_iB} is set to be as the $(N_S+1)(K+1)$ th element of the vector and V is a matrix which is comprised of the transition rates obtained from the transition rate table denoted by Table 7.1.
Now, The matrix V is of the form :

$$V = \{V_{ij}\} = \begin{pmatrix} V_{11} & V_{12} & V_{13} & V_{14} & ..... & 0 \\ V_{21} & V_{22} & V_{23} & V_{24} & ..... & 0 \\ . & V_{31} & V_{33} & V_{34} & ..... & 0 \\ . & V_{41} & ..... & V_{44} & ..... & 0 \\ . & . & . & . & . & . \\ . & . & . & . & . & . \end{pmatrix} \tag{7.2.4}$$

where

$$V_{11} = -\frac{\lambda\theta}{\theta + e\eta}(N_S + 1) + d_i,\ V_{22} = \beta + \frac{\lambda\theta}{\theta + e\eta}N_S + \kappa + r(1 - \frac{1}{K}) + \frac{2d_b e\eta}{\theta}$$

and the other diagonal elements $\{V_{jj}\}$ can be obtained by increasing the value of j in place of (S_i, B). The sub-diagonal elements are described as

$$V_{21} = \kappa + r(1 - \frac{1}{K}) + \frac{2d_b e\eta}{\theta},\ V_{31} = 2\kappa + 2r(1 - \frac{2}{K}) + 1 + \frac{2d_b e\eta}{\theta},\ \text{ and so on ....}$$

The rest of the sub-diagonal terms are evaluated also by increasing the value of (S_i, B). Similarly, the super-diagonal elements are determined as follows:

$$V_{12} = \beta + \frac{\lambda\theta}{\theta + e\eta}N_s + 2\left[\frac{\alpha e\eta}{\theta + e\eta} + 1\right],$$
$$V_{23} = 2\beta + \frac{\lambda\theta}{\theta + 2e\eta}(N_s - 1) + 2\left[\frac{2\alpha e\eta}{\theta + 2e\eta} + d_i\right] \text{ and so on ....}$$

Similarly, by performing one increment of (S_i, B), one can get the rest of the elements of the super-diagonal of V.

Since, all the parameters of our model are strictly positive, then our disease process is a Markov process on a finite, irreducible state space $\mathcal{C}$. Therefore, it is to be considered that

the transition rate matrix V has a unique left eigenvector denoted by

$$\Gamma = (\gamma_1, \gamma_2, ..., \gamma_{(N_S+1)(K+1)}) \tag{7.2.5}$$

with eigenvalue 0. i.e,

$$\sum_{i=1}^{(N_S+1)(K+1)} \gamma_i = 1. \tag{7.2.6}$$

The remaining eigenvalues are negative. Thus, this eigenvector gives the unique limiting distribution of the process and irrespective of the initial state of the process, it can be written that

$$\lim_{t\to\infty} P(S_i(t), B(t)) \quad = \quad \gamma. \tag{7.2.7}$$

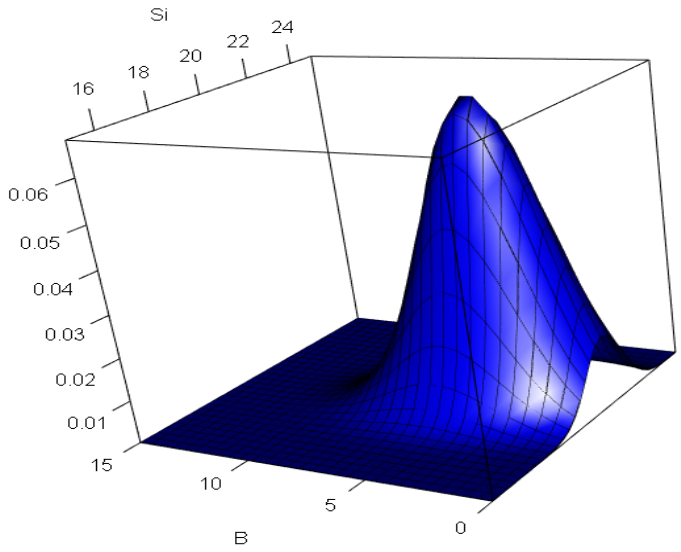

Figure 7.1: The distribution of infected Schwann cells (S_i) and M. leprae bacteria (B) generated by the bivariate normal distribution approximation. The values of the parameters for simulating this Figure are chosen as: $\beta = 1.5$, $\alpha = 0.8$, $\lambda = 0.1$, $d = 0.0016$, $d_i = 0.0046$, $\eta = 0.026$, $r = 1$, $K = 10$, $d_b = 0.0046$, $e = 0.25$, $\theta = 0.0007$, $\kappa = 0.05$, $N_s = 20$, $N = N_s + K$.

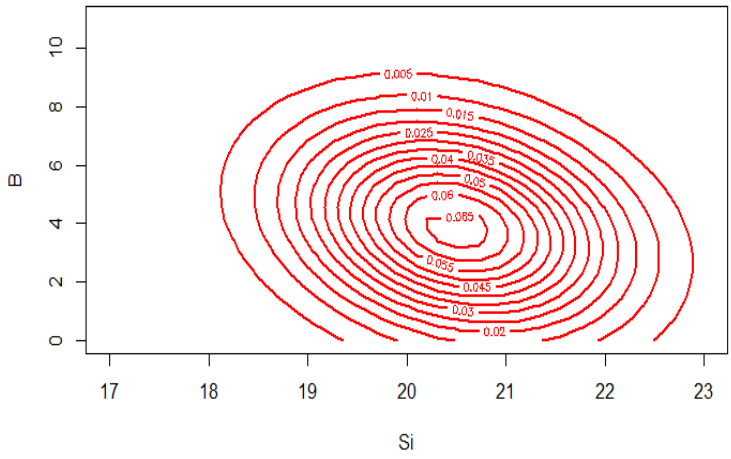

Figure 7.2: Contour plot of the approximated bivariate normal distribution of of S_i and B. We have simulated this Figure by keeping the parameter set same as mentioned for Figure 7.1.

7.3 Quasi Stationary Distribution

In our Stochastic model, we can observe that the disease transmission process is a Markov process on a finite reducible state space. The state space $(0, 0)$ is the only absorbing state here and the rest of the states are transient states. Thus, instead of studying stationary distribution, here we consider especially the quasi stationary distribution which is applicable for the transient states.

Now, we reconstruct the joint probability distribution $P_{mn}(t) = P\{S_i(t) = m; B(t) = n\}$ and putting $m = 0$ on our Kolmogorov's forward equation (7.2.2), we get

$$\dot{P}_{00} = P_{-1,0}\ \lambda_1(-1, 0) + P_{1,0}\ \mu_1(1, 0) + P_{0,-1}\ \lambda_2(0, -1) + P_{0,1}\ \mu_2(0, 1) \tag{7.3.1}$$

$$= \left(\frac{\alpha e\eta}{\theta + e\eta} + d_i\right) P_{10}. \tag{7.3.2}$$

Since $P_{-1,0}$ and $P_{0,-1}$ are not the feasible states here, the corresponding probabilities are set to zero. Let us assume that $q_{mn}(t)$ be the corresponding state probability condition on

non-extinction. Then, $q_{mn}(t)$ can be rewritten in the following form:

$$\begin{aligned} q_{mn}(t) &= P\{S_i(t) = m, B(t) = n \mid S_i(t) \neq 0\} \\ &= \frac{P_{mn}(t)}{1 - P_{00}(t)}. \end{aligned} \tag{7.3.3}$$

Differentiating equation (7.3.3), we get

$$\begin{aligned} \dot{q}_{mn}(t) &= \frac{(1 - P_{00}(t))\dot{P}_{mn}(t) + P_{mn}(t)\dot{P}_{00}(t)}{(1 - P_{00}(t))^2} \\ &= \frac{\dot{P}_{mn}(t)}{1 - P_{00}(t)} + \frac{P_{mn}(t)}{(1 - P_{00}(t))^2}\left(\frac{\alpha e\eta}{\theta + e\eta} + d_i\right) P_{10} \\ &= \frac{\dot{P}_{mn}(t)}{1 - P_{00}(t)} + \frac{P_{mn}(t)}{(1 - P_{00}(t))}\left(\frac{\alpha e\eta}{\theta + e\eta} + d_i\right) q_{10}. \end{aligned} \tag{7.3.4}$$

Thus,

$$\dot{q}(t) = q(t)V_0 + \left(\frac{\alpha e\eta}{\theta + e\eta} + d_i q_{10}\right) q(t) \tag{7.3.5}$$

where the sub-matrix V_0 is derived by eliminating first row and first column of the matrix V. Therefore, the quasi stationary distribution is the stationary solution of our Kolmogorov's forward equation (7.2.2).

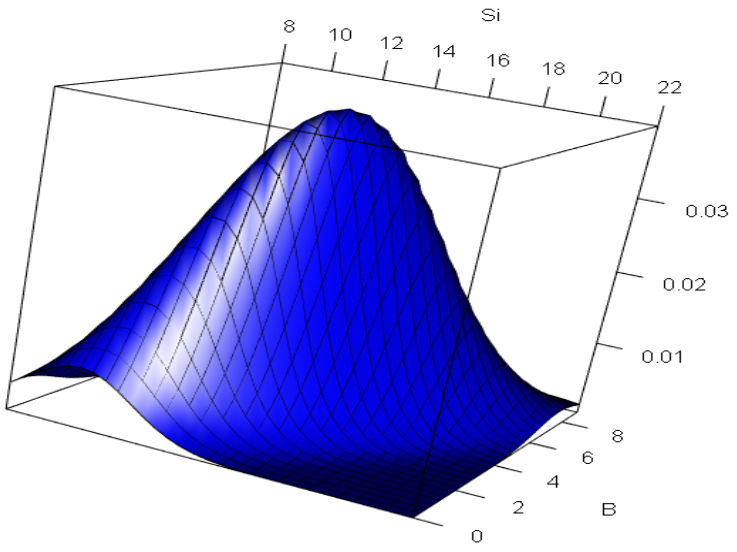

Figure 7.3: Surface plot of the bivariate normal distribution of S_i and B considering the proliferation rate of M. leprae bacteria $\kappa = 0$. Rest of the parameter values are chosen from Table 7.2.

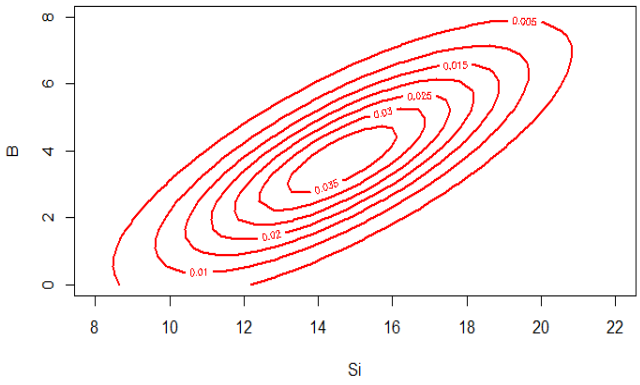

Figure 7.4: Contour plot of the bivariate normal distribution of S_i and B considering $\kappa = 0$. Values of the other parameters are chosen from Table 7.2.

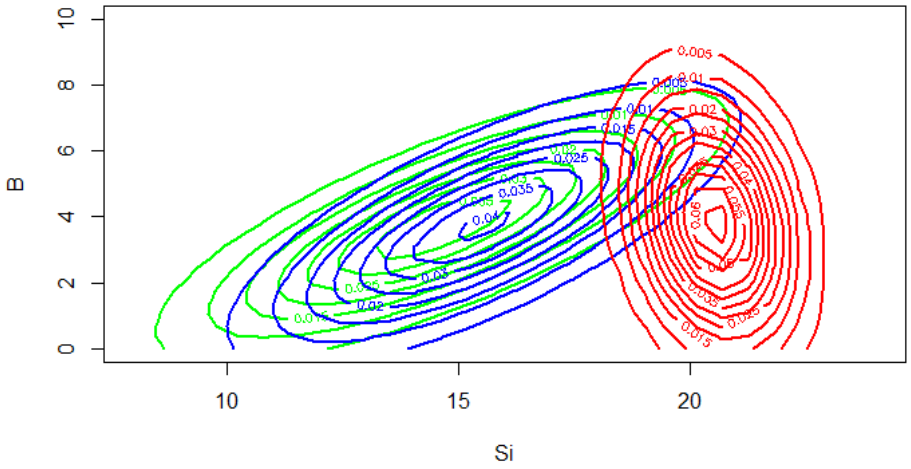

Figure 7.5: Demonstration of different contour plots for the bivariate normal distribution by varying κ. Contours of colors green, blue and red are obtained for the three different values of κ; i.e. for $\kappa = 0,\ 0.01$ and 0.05, respectively. For this simulation, we have chosen the other parameter values from Table 7.2.

7.3.1 Exact distribution of the time to extinction

Let us consider that τ be the time to extinction for the Markov process. Then, we have

$$\begin{aligned} P(\tau > t) &= P\{S_i(t) > 0, B(t) > 0\} \\ P(\tau \leq t) &= P\{S_i(t) = 0, B(t) = 0\} \quad = P_{00}(t) \end{aligned}$$

So, from equation (7.3.4), we get

$$\dot{q}_{mn}(t) = \frac{\dot{P}_{mn}(t)}{1 - P_{00}(t)} + \frac{P_{mn}(t)}{(1 - P_{00}(t))} \left[\frac{\alpha e \eta}{\theta + e\eta} + d_i \right] q_{10} \tag{7.3.6}$$

$$\implies \dot{P}_{mn}(t) = (1 - P_{00}(t))\dot{q}_{mn} - P_{mn}(t) \left[\frac{\alpha e \eta}{\theta + e\eta} + d_i \right] q_{10}. \tag{7.3.7}$$

Now, for obtaining stabilized condition, we put $\dot{q}_{mn}(t) = 0$ which presents us the result given as

$$\dot{P}_{mn}(t) \quad = \quad -P_{mn}(t) \left[\frac{\alpha e \eta}{\theta + e\eta} + d_i \right] q_{10} \tag{7.3.8}$$

Furthermore, integrating equation (7.3.8) with respect to the initial condition $P_{mn}(0) = q_{mn}$, we have

$$P_{mn}(t) = q_{mn} \exp \left[- \left(\frac{\alpha e \eta}{\theta + e\eta} + d_i \right) q_{10} t \right].$$

Therefore,

$$\begin{aligned} P_{00}(t) &= q_{00}(t) \exp \left[- \left(\frac{\alpha e \eta}{\theta + e\eta} + d_i \right) q_{10} t \right] \\ &= \frac{P_{00}(t)}{1 - P_{00}(t)} \exp \left[- \left(\frac{\alpha e \eta}{\theta + e\eta} + d_i \right) q_{10} t \right] \end{aligned}$$

which gives us

$$P_{00}(t) \quad = \quad 1 - \exp \left[- \left(\frac{\alpha e \eta}{\theta + e\eta} + d_i \right) q_{10} t \right]. \tag{7.3.9}$$

Thus, if the initial condition equals the quasi stationary distribution, then from result (7.3.9), we get the distribution of τ is exponential with the exact parameter $\left(\frac{\alpha e \eta}{\theta + e\eta} + d_i \right) q_{10}$. Hence, it can be written that

$$E(\tau) = \frac{1}{\left(\frac{\alpha e \eta}{\theta + e\eta} + d_i \right) q_{10}}. \tag{7.3.10}$$

7.4 Normal Approximation and Approximation of the Quasi Stationary Distribution

It is important to note that when the number of infected Schwann cells is extremely large, the behaviour of the stochastic process tends to a deterministic limit. Thus, we now approximate

Table 7.1: Hypothesized transition rates for the fully stochastic version of model (7.1.8)

Description of events	**State transitions**	**Transition rates**
New infections of S_h cells	$(S_i, B) \to (S_i + 1, B)$	$\beta(N_S - S_i)B$
Reinfection of S_h cells	$(S_i, B) \to (S_i + 1, B)$	$\frac{\lambda\theta}{\theta + e\eta S_i}(N_S - S_i)$
Removal of S_i cells due to recovery	$(S_i, B) \to (S_i - 1, B)$	$\frac{\alpha e\eta}{\theta + e\eta S_i}S_i^2$
Natural death of S_i cells	$(S_i, B) \to (S_i - 1, B)$	$d_i S_i$
Intracellular growth of *M. leprae*	$(S_i, B) \to (S_i, B + 1)$	$rB\Big(1 - \frac{B}{K}\Big)$
Proliferation of *M. leprae* from S_i	$(S_i, B) \to (S_i, B + 1)$	κS_i
Natural death of *M. leprae*	$(S_i, B) \to (S_i, B - 1)$	$\frac{d_b e\eta}{\theta}S_i B$

a diffusion process to investigate the statistical properties of the stationary distribution.

To do this i.e. to approximate system (7.1.8), we first define a family of scaled process. Let us consider, $N = N_S + K$. Utilizing this and also, assuming

$$X = \frac{S_i}{N} \quad \text{and} \quad Y = \frac{B}{N},$$

we now parameterize system (7.1.8) which takes the following form:

$$\begin{cases} \dfrac{dX(t)}{dt} = \beta NY(\dfrac{N_S}{N} - X) - \dfrac{\alpha e\eta}{\theta + e\eta NX}NX^2 + \dfrac{\lambda\theta}{\theta + e\eta NX}(\dfrac{N_S}{N} - X) - d_i X, \\ \dfrac{dY(t)}{dt} = rY\Big(1 - \dfrac{NY}{K}\Big) - \dfrac{d_b e\eta}{\theta}NXY + \kappa X. \end{cases} \tag{7.4.1}$$

System (7.1.8) has endemic equilibrium (S_i^*, B^*) and it is locally asymptotically stable which is previously discussed in the Section 7.1. Therefore, the endemic point (X^*, Y^*) of our parameterised version of system (7.1.8) denoted by system (7.4.1) also satisfies system (7.1.8) and hence, is essentially locally asymptotically stable also.

Now, we consider a process, $Z_N(t) = \sqrt{N}[V_N(t) - (X(t) - Y(t))]$ which can be approximated by a two dimensional Ornstein-Uhlenbeck process, whose local drift matrix $U(X^*, Y^*)$ and local covariance matrix C^*, close to the equilibrium, are evaluated. The local drift matrix of system (7.1.8) is given as

$$U(X^*, Y^*) = \begin{pmatrix} \mathcal{A}_{11} & \mathcal{A}_{12} \\ \mathcal{A}_{21} & \mathcal{A}_{22} \end{pmatrix} \tag{7.4.2}$$

where the entries of $U(X^*, Y^*)$ are given as

$$\begin{cases} \mathcal{A}_{11} = -\beta N Y^* + \dfrac{e\eta N\theta X^*(\lambda - 2\alpha) - \lambda\theta^2 - \lambda\theta e\eta(N_s + NX^*) - \alpha e^2\eta^2 N^2 (X^*)^2}{(\theta + e\eta N X^*)^2} - d_i, \\ \mathcal{A}_{12} = \beta(N_s - NX^*), \\ \mathcal{A}_{21} = -\dfrac{d_b e\eta}{\theta} N Y^* + \kappa, \\ \mathcal{A}_{22} = r - \dfrac{2rNY^*}{K} - \dfrac{d_b e\eta}{\theta} N X^*. \end{cases}$$

The local covariance matrix C^* is of the form

$$C^* = \begin{pmatrix} \mathcal{B}_{11} & 0 \\ 0 & \mathcal{B}_{22} \end{pmatrix} \tag{7.4.3}$$

where

$$\begin{cases} \mathcal{B}_{11} = \beta N Y^* (\dfrac{N_S}{N} - X^*) - \dfrac{\alpha e\eta}{\theta + e\eta N X^*} N X^{*2} + \dfrac{\lambda\theta}{\theta + e\eta N X^*} (\dfrac{N_S}{N} - X^*) - d_i X^*, \\ \mathcal{B}_{22} = rY^* \Big(1 - \dfrac{NY^*}{K}\Big) - \dfrac{d_b e\eta}{\theta} N X^* Y^* + \kappa X^*. \end{cases}$$

Now, we proceed to obtain the distribution of the Ornstein-Uhlenbeck Process at time t associated with the bivariate normal distribution where the mean vector and the variance matrix are denoted as $(\hat{X}, \hat{Y})$ and $\mathcal{S}(t)$, respectively. From Theorem 7.1.1 in Section 7.1, we can observe that all the eigenvalues of the matrix $U(X^*, Y^*)$ will be negative which results in the strict positivity of $\det(U(X^*, Y^*))$. This further indicates that for the bivariate normal distribution process, the mean vector in equilibrium is zero vector and the variance matrix $\sum$ in equilibrium is actually a solution of the following equation,

$$U(X^*, Y^*) \sum + \sum U^\top (X^*, Y^*) = -C^*(X^*, Y^*) \tag{7.4.4}$$

where $U^\top$ is the transpose of the matrix U.

Therefore, we conclude that the quasi-stationary distribution is approximated with bivariate normal distribution with mean $\hat{S}_i$ i.e. (NX^*) and standard deviation $\sqrt{\frac{\sigma_1}{N}}$ obtained from

$$\sum = \begin{pmatrix} \sigma_1 & \sigma_2 \\ \sigma_2 & \sigma_3 \end{pmatrix}. \tag{7.4.5}$$

Here, formulas for evaluating σ_1, σ_2 and σ_3 are described as

$$\begin{cases} \sigma_1 = \dfrac{-\mathcal{A}_{11}\mathcal{B}_{11} + \mathcal{A}_{12}\mathcal{B}_{22} + \mathcal{B}_{11}\mathcal{A}_{22} - \mathcal{B}_{11}\mathcal{A}_{21}}{2(\mathcal{A}_{11}^2 + \mathcal{A}_{11}\mathcal{A}_{22} - \mathcal{A}_{11}\mathcal{A}_{21} - \mathcal{A}_{12}\mathcal{A}_{21})}, \\ \sigma_2 = \dfrac{\mathcal{A}_{11}\mathcal{B}_{22} + \mathcal{B}_{11}\mathcal{A}_{21}}{2(\mathcal{A}_{11}^2 + \mathcal{A}_{11}\mathcal{A}_{22} - \mathcal{A}_{11}\mathcal{A}_{21} - \mathcal{A}_{12}\mathcal{A}_{21})}, \\ \sigma_3 = \dfrac{-\mathcal{A}_{11}^2\mathcal{B}_{22} - \mathcal{A}_{11}\mathcal{B}_{22}\mathcal{A}_{22} + \mathcal{A}_{12}\mathcal{B}_{22}\mathcal{A}_{21} - \mathcal{B}_{11}\mathcal{A}_{21}^2}{2\mathcal{A}_{22}(\mathcal{A}_{11}^2 + \mathcal{A}_{11}\mathcal{A}_{22} - \mathcal{A}_{11}\mathcal{A}_{21} - \mathcal{A}_{12}\mathcal{A}_{21})}. \end{cases}$$

The equilibrium distribution of the disease process $(S_i(t), B(t))$ can be approximated by a bivariate normal distribution with mean (NX^*, NY^*) and variance matrix $N\Sigma$. The normal density function at the point (S_i, B) can be written as:

$$P(S_i(t), B(t)) = \frac{1}{2\pi\sqrt{det(N\Sigma)}} e^{-(S_i - NX^*,\ B - NY^*)(2N\Sigma)^{-1}(S_i - NX^*,\ B - NY^*)^\top}.$$

Now, for maintaining consistency with the positivity of the number of infected Schwann cells into the human body i.e. $S_i > 0$, the approximated normal distribution is modified by truncation of 0.5 and given as

$$q_{m.} \simeq \frac{1}{(\sqrt{\frac{\sigma_1}{N}})} \frac{\phi\left[\frac{(m-\hat{S}_i)}{(\sqrt{\frac{\sigma_1}{N}})}\right]}{\Phi\left[\frac{(\hat{S}_i - 0.5)}{(\sqrt{\frac{\sigma_1}{N}})}\right]} \tag{7.4.6}$$

where ϕ and Φ are the bivariate normal probability density function (PDF) and normal cumulative distribution function (CDF), respectively.

7.4.1 The expected time to extinction

In this Subsection, using the result (7.4.6), we approximate (7.3.10) to obtain that

$$E(\tau) = \frac{1}{\left(\frac{\alpha e \eta}{\theta + e\eta} + d_i\right) q_{1.}} \tag{7.4.7}$$

where

$$q_{1.} = \frac{1}{(\sqrt{\frac{\sigma_1}{N}})} \frac{\phi\left[\frac{(m-\hat{S}_i)}{\sqrt{\frac{\sigma_1}{N}}}\right]}{\Phi\left[\frac{(\hat{S}_i - 0.5)}{\sqrt{\frac{\sigma_1}{N}}}\right]}. \tag{7.4.8}$$

Thus, we find the expected time to extinction of the infected Schwann cells by putting $m = 1$ in the previous approximation of quasi-stationary distribution $q_{m.}$.

Table 7.2: **List of parameter values used in numerical simulations for our systems**

Parameter	Parameter definition	Assigned Value (Unit)	Range
Π	Production rate of S_h	35 (cells day^{-1})	20 - 70
β	Contact rate of B and S_h	1.5 (mm^3 day^{-1})	0.012 - 1.8
α	Recovery rate of S_i	0.8 (mm^3 day^{-1})	0.2 - 0.9
λ	Reinfection rate of S_h	0.1 (mm^3 day^{-1})	0.02 - 0.4
d	Natural death rate of S_h	0.0016 (day^{-1})	0.001 - 0.008
d_i	Natural death rate of S_i	0.00046 (day^{-1})	0.0001 - 0.00071
η	Drug efficacy rate of MDT	0.026	0.01 - 0.4
r	Growth rate of B	1.01 (day^{-1})	0.01 - 1.32
K	Carrying capacity of B	10 (mm^{-3})	5 - 60
d_b	Killing rate of B by MDT	0.0022 (day^{-1})	0.0014 - 0.005
e	Proportionality constant	0.25	0.1 - 1.2
θ	flushing out rate of MDT	0.00007 (μM day^{-1})	0.00001 - 0.0009
κ	proliferation rate of B	0.02	0.01 - 0.18

7.5 Numerical Simulations

Exhibiting numerical examples is essential for validating the analytical results. Setting suitable parameter values while estimating some of them from existing literatures and Chapter 5, we have performed a few numerical simulations for various distribution processes for our proposed systems. Parameter values are specified in the corresponding Figure diagrams, otherwise collected from Table 7.2.

In Figure 7.1 and Figure 7.2, distribution of infected Schwann cells and *M. leprae* bacteria are exhibited by using the bivariate normal approximation method. for performing this, the density function of the normal approximation and the left eigenvector of the matrix V with respect to the eigenvalue 0, are solved during simulating these Figures numerically. In this context, it is important to note that the proliferation rate of newly produced free *M. leprae* bacteria is one of most important parameters for our system. If the infection of healthy Schwann cells are inhibited by MDT therapy, it eventually reduce or even stops the production of free bacteria. This is the fundamental reason why investigating the distribution of normal approximation is of utmost importance for $\kappa = 0$ which is exactly shown in Figure 7.3 and Figure 7.4. Comparisons between Figure 7.1 and Figure 7.3 clearly indicates that large probabilities are obtained for lower values of B and higher ranges of values of S_i in 7.1 while for $\kappa = 0$, we get large probabilities for higher values of B and lower values of S_i. Also, to make the impact of κ clearer on the system dynamics, intersection three different contours

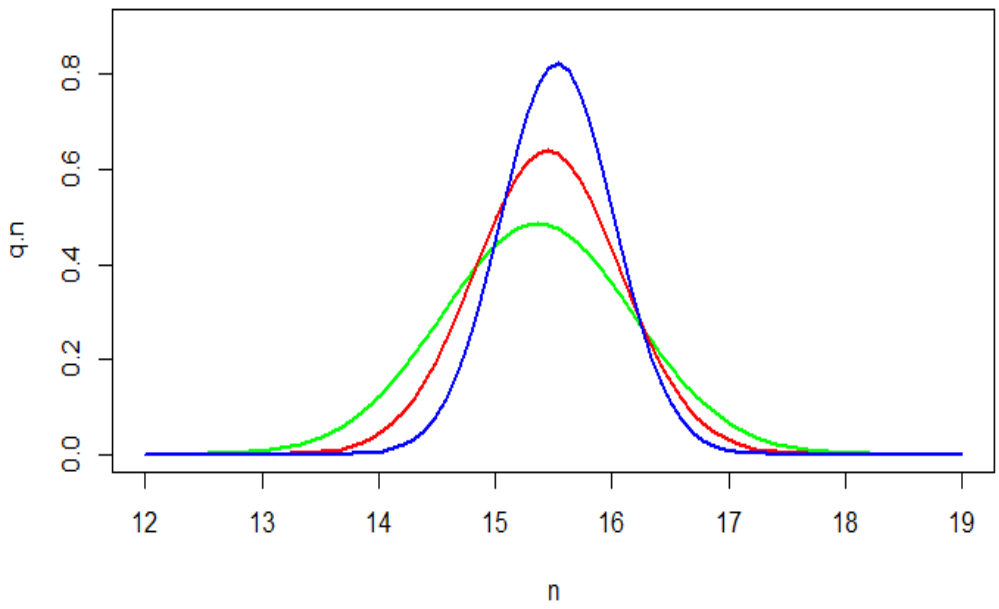

Figure 7.6: Quasi-stationary distribution of the infected Schwann cells for three different values of $N = N_s + K$. Here, K remains fixed and is assigned the value of $K = 10$. The values of N_s are varied as $N_s = 40, 50$ and 60 to respectively denote the simulations for the colors green, red and blue. The values of the other parameters are chosen as $\beta = 1.5$, $\alpha = 0.8$, $\lambda = 0.1$, $d = 0.0016$, $d_i = 0.00046$, $\eta = 0.026$, $r = 1$, $K = 10$, $d_b = 0.0046$, $e = 0.25$, $\theta = 0.00007$ and $\kappa = 0.02$.

for the values of $\kappa = 0,\ 0.01,\ 0.05$ for the normal approximations are manifested in Figure 7.5.

In Figure 7.6, we plot the marginal distribution profile of the infected Schwann cells S_i by varying the values of N, in quasi-stationary state. We consider $N = N_s + K$ and the values of N_s are varied as $N_s = 40, 50$ and 60 to plot the graphs. Trajectories in this Figure show that the distribution is positively skewed for comparatively lower values of N and gradually becomes symmetric for higher magnitude of N. Thus, we can conclude that the density of infected Schwann cells raises with increasing values of N.

In Figure 7.7, we have described the expected time to extinction $E(\tau)$ of the infected cells while varying the values of N_s under the MDT treatment considering $\eta = 0.28$. Up to the value of $N_s = 14$, expected time decreases from nearly 1800 days to 250 days, but for larger values of N_s, the change in the estimated time $E(\tau)$ is relatively very slow. A

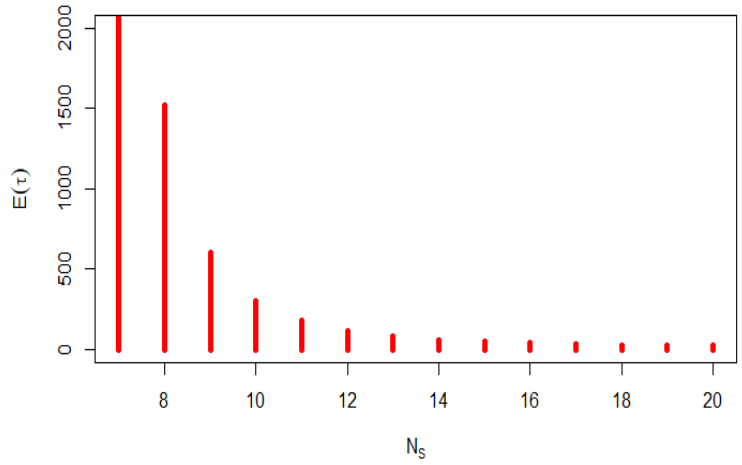

Figure 7.7: Description of the expected time to extinction $E(\tau)$ of the infected Schwann cells S_i with respect to N_s. Here, we have chosen the value of drug-efficacy rate $\eta = 0.28$ and the other parameter values are remained the same as in Figure 7.6.

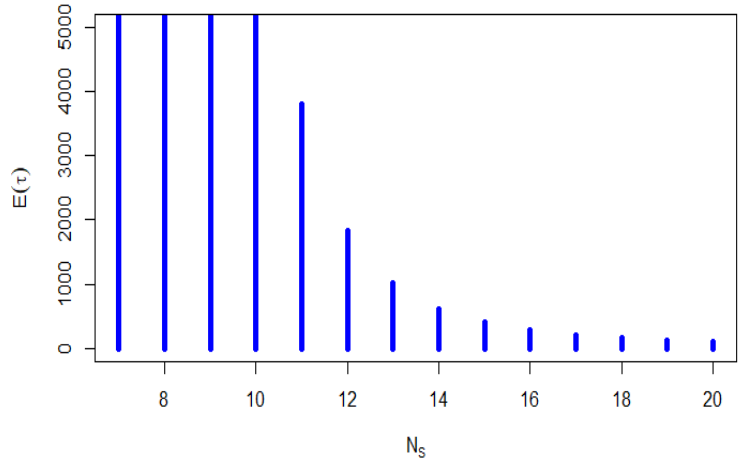

Figure 7.8: Expected time to extinction $E(\tau)$ of the infected Schwann cells S_i with respect to N_s considering the value of drug-efficacy rate $\eta = 0.22$ and the other parameter values are remained the same as in Figure 7.7. The other parameters are chosen from Table 7.2.

comparative analysis is performed in Figure 7.8 for achieving the expected time to extinction

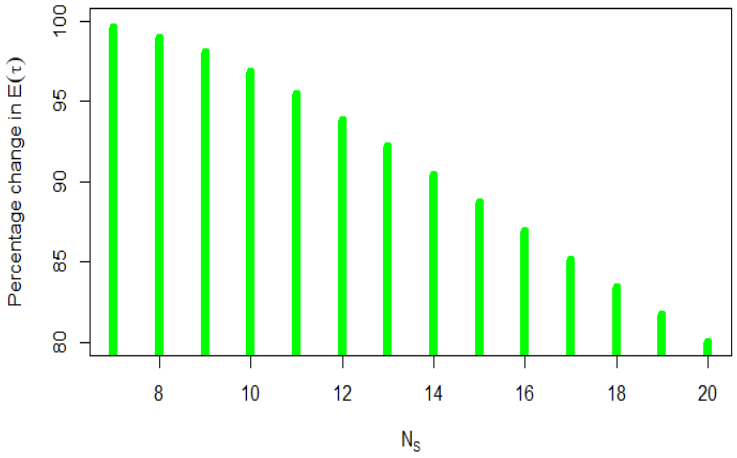

Figure 7.9: Change of percentage fall in the expected time to extinction $E(\tau)$ corresponding to the change in the values of η in the Figures 7.6 and 7.7. The values of the other parameters are chosen from Table 7.2.

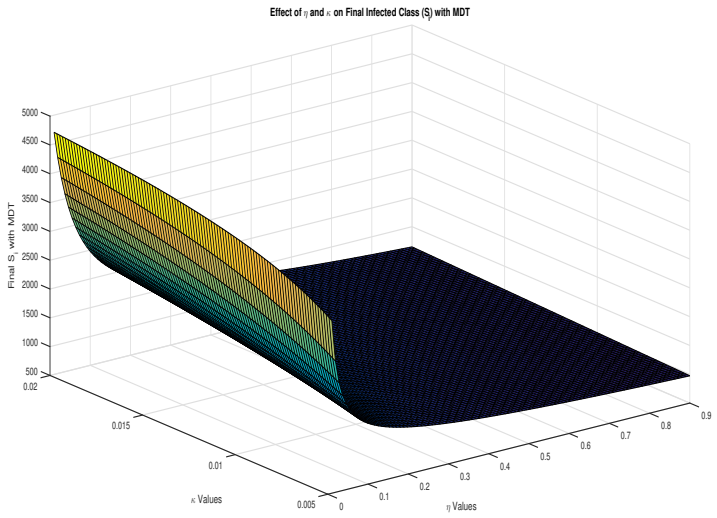

Figure 7.10: 3-D plot of the infected cells' density S_i with respect to η and κ. Rest of parameters' values are chosen from Table 7.2.

$E(\tau)$ by choosing $\eta = 0.22$. Simulations show that for lower value of drug-efficacy rate, longer expected time to extinction is essentially needed up to the values of $N = 14$. Furthermore, in Figure 7.9, change in the percentage fall in $E(\tau)$ between $\eta = 0.22$ and $\eta = 0.28$ is calculated

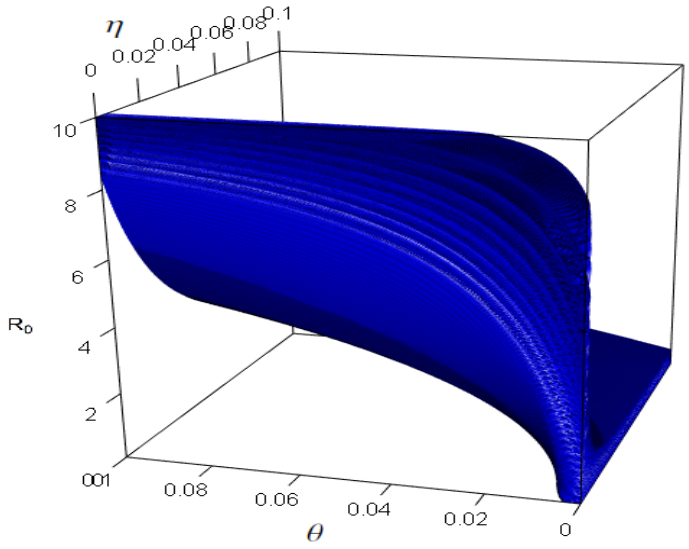

Figure 7.11: 3-D contour plot of the basic reproduction number R_0 with respect to η and θ. The other parameters are chosen from Table 7.2.

for gradually increasing N_s values. Here, it can be observed that the percentage change is gradually decreasing with the increasing values of N_s.

Finally, in Figure 7.10, a 3-D plot is exhibited for depicting the change in the densities of S_i cells with respect to drug-efficacy rate η of MDT therapy and proliferation rate κ which infers that S_i density is the least for combined values of larger η values and relatively low κ values. Finally, a 3-D contour plot demonstrating the coupled effect of η and θ on the basic reproduction number R_0 for system 7.1.7 has been depicted in Figure 7.11.

7.6 Discussion

In this Chapter, firstly, we have investigated the basic system dynamics of a deterministic mathematical model. Then, the deterministic system is extended to a discrete stochastic model with detailed presentation of all the possible transition states. The stochastic mathematical model is analyzed and investigated from different aspects of exact distribution, quasi-stationary distribution and most importantly, bivariate normal distribution.

The analytical and numerical outcomes suggest that the proliferation rate of bacteria and the efficacy of the MDT treatment are the most two important parameters contributing to the exploration of the system dynamics. The expected time to extinction of the infected cells is observed to be lower if the production rate of free bacteria is comparatively low and if MDT is

being administered with high efficacy rate of $\eta = 0.28$. Also, focusing on the long-term system dynamics for achieving the extinction of infected cells into a human body, our obtained results suggests that the bacterial proliferation is inhibited and even, stopped successfully whenever the *M. leprae*-induced infections can be blocked or controlled effectively and the recovery to the healthy class through the proper combined drug therapeutic schedule of $1500 - 1800$ days can be shortened as much as possible.

Chapter 8

Conclusion and Future Direction

In the final chapter, we will review the research contributions of the thesis as well as discuss the future directions for research.

8.1 Conclusions

In this Section, we have discussed research contribution of the thesis chapter wise. The main contribution of the thesis are as follows:

8.1.1 Chapter 2

Three strategies of optimal control are discussed in this Chapter. Strategy-I (with efficiency index 58.74%) is more effective than Strategy-II (efficiency index 50.85%) for having a higher efficiency index. Strategy-III has a much higher efficiency index (71.56%) than both Strategy-I and II as we have used combination of the both drugs in this case. The main motive of Strategy-I is to prevent new infections in a leprosy patient where Strategy-II focuses on suppressing the natural replication of the *M. leprae* bacteria. Our analysis suggests that preventing new infections is more advantageous and useful than only inhibiting bacterial growth as once we can stop spreading the new infections, the bacterial load will automatically decrease gradually. However, Strategy-III performs more effectively than the other two as it concentrates on both of these two points. Hence, it is suggested that the optimal control therapy with Strategy-III discussed in this Chapter is the most beneficial approach of controlling leprosy. Also, after in depth analysis and investigation of a patient's condition, switching from Strategy-III to Strategy-I or even Strategy-II can be a very good option for some specific cases after a certain period of time to avoid adverse drug effects. Finally, the

investigations performed in this Chapter successfully describes the basic cell dynamics of leprosy and the obtained results can further guide in developing a cost-effective drug regimen for leprosy patients successfully.

8.1.2 Chapter 3

In this Chapter, we have incorporated the theta-logistic growth for *M. leprae* bacteria in place of classical logistic growth. Comparing several scenarios for different values of θ (with $\theta < 1,\ \theta = 1$ and $\theta > 1$), we have come into the conclusion that for $\theta > 0.48$, our proposed system produces oscillatory periodic solutions. Biologically, this indicates that the densities of the *M. leprae* bacteria and the infected Schwann cells fluctuate very rapidly in this case and ultimately, lose stability when the intraspecific competition between the bacteria for available resources crosses a specific critical value of $\theta^* = 0.48$. Evidently, the findings of this Chapter completely justify our assumption of theta-logistic growth for the bacterial population and effectively describe the relation of density-dependence and per capita growth rate (PGR) for *M. leprae* which presents a novel insight to unfold the vastly complicated leprosy infection process and the disease progression into the human body.

8.1.3 Chapter 4

Two different variants of delayed mathematical models are constructed in this Chapter and furthermore, optimal control strategy with delay in state variables has been implemented on both of these models. The analytical and the numerical outcomes of this Chapter conclude that our proposed optimal control-induced delayed mathematical systems act very explicitly and unambiguously at giving reliable predictions on the infection and disease transmission process of leprosy. We strongly claim that our proposed systems, more precisely, the second optimal control-induced delayed mathematical model should necessarily be used as a decisive policymaker in a cost-effective preventive control strategy and also as a crucial tool for framing a perfect drug dose regimen for leprosy as a more realistic and practical approach.

8.1.4 Chapter 5

In this Chapter, we have discussed a four dimensional mathematical model which successfully captures some basic and intriguing features of the disease dissemination process and therapeutic approaches for leprosy. Our proposed treatment policy with a flexible version of MDT with the prescribed zone of drug efficacy rate and treatment tenures for both paucibacillary (PB) and multibacillary (MB) types of patients is much safer, effective and can

really be a potential candidate for future clinical trials and for the pharmacists aiming to develop an accurate and novel treatment regime. Our investigations validate the essence of applying a modified version of MDT therapy with efficacy rate η in the safe and effective zone i.e. $\eta \in (0.025, 0.059)$ but necessarily for a longer treatment period of nearly 300 days (10 months) for MB cases in comparisons to the scenarios of PB cases.

8.1.5 Chapter 6

This Chapter demonstrates the memory effect for experimenting with the leprosy pathophysiology which actually involves the entire history before the present instant, and the implication of fractional calculus can surely be viewed as a suitable and exclusive tool for modeling these types of phenomena with hysteresis. The Chapter reveals that the whole *M. leprae*-induced infection in leprosy not only depends on the present state but also on the previous memory stages of the infection process. With the different circumstances and effects that the whole infection mechanism experiences in various memory stages, the CF fractionalized system responds differently to the current conditions. The knowledge accumulated by the metabolic activities in preceding stages confers fitness to the bacteria in an evolutionary way, which validates that the history-dependent drug-resistant behavior is essentially a clear manifestation of the memory effect in leprosy. Thus, to overcome the drug resistance scenario, high-cost-related problems and side-effects of the combined therapy, the three-dimensional Caputo-Fabrizio fractionalized optimal control mathematical model for the fractional order $\zeta = 0.6$ presented in this Chapter should certainly be considered by mathematical and clinical scientists for all future studies on leprosy.

8.1.6 Chapter 7

Due to inherited randomness and noise, a stochastic mathematical model has been investigated in this Chapter to explore the leprosy dynamics involving the joint probability distribution of infected Schwann cells and *M. leprae* bacteria. Our experiments suggest that the expected time to extinction for the infected Schwann cells gets lowered as the total Schwann cell population size increases. Surface plot and contour diagrams generated from the bivariate normal approximation suggests that infected cells' density is strongly correlated with the bacterial proliferation and efficacy of MDT therapy. The basic reproduction number for our system which is a threshold and determining criterion for the disease prevalence into the human body, can necessarily be lowered if MDT drug dose is administered with the proposed regimen which simultaneously kills *M. leprae* as well as recovers the infected Schwann cells.

8.2 Future research: An outline

We have previously discussed the contribution of this thesis in leprosy dynamics, after which research on this topic will necessarily be continued to gain more extensive and profound knowledge. Using some modern mathematical tools while incorporating new deeper biological insights, we will be able to extend our systems and explore new horizons. Futuristic research works can certainly be performed in the following directions.

- Firstly, it is important to note that the long tenure of treatment is still a concerning issue for leprosy. In addition, classification of leprosy is not only limited to the PB and MB cases but also, five different types forming a complete spectrum. To resolve this, different mathematical models should be investigated for all these types and examining the interplay from the point of view of uniform therapeutic schedule should be given major importance.

- Evaluating drug holidays and implementing impulsive biologic therapy is a very intriguing mathematical tool which has been applied lately on many infectious and non-infectious diseases. In leprosy, although the prescribed drug dose schedules support drug-holidays, the perfect regimen is yet to be explored. Thus, to avoid the relapse cases and adverse impacts of MDT, a more beneficial impulsive treatment should necessarily be designed for leprosy.

- Finally, the influence of immune response and vital roles played by the complicated cytokine chains and networks in leprosy can not be neglected. Various inflammatory and anti-inflammatory cytokines, contribute significantly in the immunity and pathogenesis of leprosy. Evidence suggests that the cytokines IL-10, IFN-γ, TNF-α play a crucial roles in the clinical manifestation and progression of the disease in all sub-types of leprosy. Thus, the futuristic works should precisely consider all these aspects whenever aiming to get more elemental and essential insights on leprosy.

Bibliography

Abboubakar, H., Kamgang, J. C., Nkamba, L. N. and Tieudjo, D. (2018). Bifurcation thresholds and optimal control in transmission dynamics of arboviral diseases, *Journal of mathematical biology*. **76**, 379–427.

Adams, L. B., Pena, M. T., Sharma, R., Hagge, D. A., Schurr, E. and Truman, R. W. (2012). Insights from animal models on the immunogenetics of leprosy: a review, *Memórias do Instituto Oswaldo Cruz*. **107**, 197–208.

Al Basir, F. (2020). A multi-delay model for pest control with awareness induced interventions—hopf bifurcation and optimal control analysis, *International Journal of Biomathematics*. **13**(06), 2050047.

Ali, N. and Zaman, G. (2021). Optimal control of double delayed hiv-1 infection model of fighting a virus with another virus, *Computational Methods for Differential Equations*. **9**(3), 874–885.

Baba, B. A. and Bilgehan, B. (2021). Optimal control of a fractional order model for the covid–19 pandemic, *Chaos, Solitons & Fractals*. **144**, 110678.

Banerjee, S. and Sarkar, R. R. (2008). Delay-induced model for tumor–immune interaction and control of malignant tumor growth, *Biosystems*. **91**(1), 268–288.

Becx-Bleumink, M. and Berhe, D. (1992). Occurrence of reactions, their diagnosis and management in leprosy patients treated with multidrug therapy; experience in the leprosy control program of the all africa leprosy and rehabilitation training center (alert) in ethiopia., *International journal of leprosy and other mycobacterial diseases: official organ of the International Leprosy Association*. **60**(2), 173–184.

Bekri, W., Gebre, S., Mengiste, A., Saunderson, P. R. and Zewge, S. (1998). Delay in presentation and start of treatment in leprosy patients: a case-control study of disabled and non-disabled patients in three different settings in ethiopia, *International journal of leprosy and other mycobacterial diseases*. **66**(1), 1–9.

Benjak, A., Avanzi, C., Singh, P., Loiseau, C., Girma, S., Busso, P., Fontes, A. N. B., Miyamoto, Y., Namisato, M., Bobosha, K. et al. (2018). Phylogenomics and antimicrobial resistance of the leprosy bacillus mycobacterium leprae, *Nature communications*. **9**(1), 352.

Birkhoff, G., Ince, E., Mickens, R. E. and Blaksley Bazterrica, E. J. (1989). Introduction to ordinary differential equations.

Birkhoff, G. and Rota, G.-C. (1978). *Ordinary differential equations*, John Wiley & Sons.

Blok, D. J., de Vlas, S. J., Fischer, E. A. and Richardus, J. H. (2015). Mathematical modelling of leprosy and its control, *Advances in parasitology*. **87**, 33–51.

Bodnar, M. (2000). The nonnegativity of solutions of delay differential equations, *Applied Mathematics Letters*. **13**(6), 91–95.

Britton, W. J. and Lockwood, D. N. (2004). Leprosy, *The Lancet*. **9416**(363), 1209–1219.

Cambau, E. and Williams, D. (2019). Anti-leprosy drugs: modes of action and mechanisms of resistance in mycobacterium leprae, *International textbook on leprosy*.

Camuset, G., Lafarge, S., Borgherini, G., Gerber, A., Pouderoux, N., Foucher, A., Poubeau, P., Manaquin, R., Larrieu, S., Vilain, P. et al. (2016). Leprosy on reunion island, 2005-2013: situation and perspectives, *PLoS neglected tropical diseases*. **10**(4), e0004612.

Cao, X., Saha, S. and Roy, P. K. (2019). A statistical inference in an epidemic model with combinational drug treatment: Hiv as a case study, *Results in Applied Mathematics*. **3**, 100066.

Caputo, M. and Fabrizio, M. (2015). A new definition of fractional derivative without singular kernel, *Progress in Fractional Differentiation & Applications*. **1**(2), 73–85.

Chatterjee, A. N., Al Basir, F., Almuqrin, M. A., Mondal, J. and Khan, I. (2021). Sars-cov-2 infection with lytic and non-lytic immune responses: A fractional order optimal control theoretical study, *Results in physics*. **26**, 104260.

Chatterjee, A. N. and Roy, P. K. (2012). Anti-viral drug treatment along with immune activator il-2: a control-based mathematical approach for hiv infection, *International Journal of Control*. **85**(2), 220–237.

Chen, L., Chen, L. et al. (2009). Permanence of a discrete periodic volterra model with mutual interference, *Discrete Dynamics in Nature and Society*. **2009**.

Chu, T., Liu, D., Huai, P., Chen, X., Han, S., Chen, S. and Zhang, F. (2020). Comprehensive measures succeeded in improving early detection of leprosy cases in post-elimination era: Experience from shandong province, china, *PLoS neglected tropical diseases*. **14**(2), e0007891.

Cooke, K. L. and Van Den Driessche, P. (1986). On zeroes of some transcendental equations, *Funkcialaj Ekvacioj*. **29**(1), 77–90.

Deps, P. D., Nasser, S., Guerra, P., Simon, M., Birshner, R. D. C. and Rodrigues, L. C. (2007). Adverse effects from multi-drug therapy in leprosy: a brazilian study., *Leprosy review*. **78**(3), 216–222.

Dieudonné, J. (2011). *Foundations of modern analysis*, Read Books Ltd.

Dogra, S., Narang, T. and Kumar, B. (2013). Leprosy-evolution of the path to eradication, *The Indian Journal of Medical Research*. **137**(1), 15.

Du, M., Wang, Z. and Hu, H. (2013). Measuring memory with the order of fractional derivative, *Scientific reports*. **3**(1), 3431.

Duthie, M. S., Truman, R. W., Goto, W., O'Donnell, J., Hay, M. N., Spencer, J. S., Carter, D. and Reed, S. G. (2011). Insight toward early diagnosis of leprosy through analysis of the developing antibody responses of mycobacterium leprae-infected armadillos, *Clinical and vaccine immunology*. **18**(2), 254–259.

Ffytche, T. (1989). Importance of early diagnosis in ocular leprosy., *The British Journal of Ophthalmology*. **73**(12), 939.

Fischer, M. (2017). Leprosy–an overview of clinical features, diagnosis, and treatment, *JDDG: Journal der Deutschen Dermatologischen Gesellschaft*. **15**(8), 801–827.

Fleming, W. H. and Rishel, R. W. (2012). *Deterministic and stochastic optimal control*, Vol. 1, Springer Science & Business Media.

Flemming, W. and RISHEL, R. (1975). Deterministic and sochastic optimal control springer-verlag, *New York, United State of America*. .

Franke, J. E. and Yakubu, A.-A. (2008). Disease-induced mortality in density-dependent discrete-time sis epidemic models, *Journal of mathematical biology*. **57**, 755–790.

Freedman, H. and Kuang, Y. (1991). Stability switches in linear scalar neutral delay equations, *Funkcialaj Ekvacioj*. **34**(1), 187–209.

Gantmacher, F. (1959). Theory of matrices ams, chelsea publishing, . .

Gao, F., Li, X., Li, W. and Zhou, X. (2021). Stability analysis of a fractional-order novel hepatitis b virus model with immune delay based on caputo-fabrizio derivative, *Chaos, Solitons & Fractals*. **142**, 110436.

Gaschignard, J., Grant, A. V., Thuc, N. V., Orlova, M., Cobat, A., Huong, N. T., Ba, N. N., Thai, V. H., Abel, L., Schurr, E. et al. (2016). Pauci-and multibacillary leprosy: two distinct, genetically neglected diseases, *PLoS neglected tropical diseases*. **10**(5), e0004345.

Gelber, R. H. (1987). Activity of minocycline in mycobacterium leprae-infected mice, *The Journal of infectious diseases*. **156**(1), 236–239.

Gelber, R. H., Balagon, M. V. F. and Cellona, R. V. (2004). The relapse rate in mb leprosy patients treated with 2-years of who-mdt is not low1, *International Journal of Leprosy and Other Mycobacterial Diseases*. **72**(4), 493.

Gelber, R. H., Fukuda, K., Byrd, S., Murray, L., Siu, P., Tsang, M. and Rea, T. H. (1992). A clinical trial of minocycline in lepromatous leprosy., *BMJ: British Medical Journal*. **304**(6819), 91.

Gelber, R. H. and Grosset, J. (2012). The chemotherapy of leprosy: an interpretive history, *Leprosy review*. **83**(3), 221–240.

Giraldo, L., Garcia, U., Raigosa, O., Munoz, L., Dalia, M. M. P. and Jamboos, T. (2018). Multibacillary and paucibacillary leprosy dynamics: a simulation model including a delay, *Appl Math Sci*. **12**(32), 1677–1685.

Göllmann, L. and Maurer, H. (2013). Theory and applications of optimal control problems with multiple time-delays, *Journal of Industrial and Management Optimization*. **10**(2), 413–441.

Goulart, I. M. B. and Goulart, L. R. (2008). Leprosy: diagnostic and control challenges for a worldwide disease, *Archives of dermatological research*. **300**, 269–290.

Grosset, J. H., Ji, B., Guelpa-Lauras, C.-C., Perani, E. G. and N'Deli, L. N. (1990). Clinical trial of pefloxacin and ofloxacin in the treatment of lepromatous leprosy., *International Journal of Leprosy and Other Mycobacterial Diseases: Official Organ of the International Leprosy Association*. **58**(2), 281–295.

Guckenheimer, J., Oster, G. and Ipaktchi, A. (1977). The dynamics of density dependent population models, *Journal of Mathematical Biology*. **4**(2), 101–147.

Gupta, U., Katoch, K., Singh, H., Natrajan, M. and Katoch, V. (2005). Persister studies in leprosy patients after multi-drug treatment, *International journal of leprosy and other mycobacterial diseases*. **73**(2), 100.

Guragain, S., Upadhayay, N. and Bhattarai, B. M. (2017). Adverse reactions in leprosy patients who underwent dapsone multidrug therapy: a retrospective study, *Clinical pharmacology: advances and applications*. pp. 73–78.

Hale, J. K. (1977). Retarded functional differential equations: basic theory, *Theory of functional differential equations*, Springer, pp. 36–56.

Hale, J. K. and Koçak, H. (2012). *Dynamics and bifurcations*, Vol. 3, Springer Science & Business Media.

Hartman, P. (1964). Ordinary differential equations. john willey & sons, *Inc. New York-London-Sydney*. .

Hattaf, K. and Yousfi, N. (2012). Optimal control of a delayed hiv infection model with immune response using an efficient numerical method, *International Scholarly Research Notices*. **2012**.

Heffernan, J. M., Smith, R. J. and Wahl, L. M. (2005). Perspectives on the basic reproductive ratio, *Journal of the Royal Society Interface*. **2**(4), 281–293.

Hu, Z., Teng, Z. and Jiang, H. (2012). Stability analysis in a class of discrete sirs epidemic models, *Nonlinear Analysis: Real World Applications*. **13**(5), 2017–2033.

Ikeda, Y., Takeuchi, Y., Martin, F., Cosset, F.-L., Mitrophanous, K. and Collins, M. (2003). Continuous high-titer hiv-1 vector production, *Nature biotechnology*. **21**(5), 569–572.

Jessen, K. and Mirsky, R. (2016). The repair schwann cell and its function in regenerating nerves, *The Journal of physiology*. **594**(13), 3521–3531.

Ji, B., Perani, E. G., Petinom, C., N'Deli, L. and Grosset, J. H. (1994). Clinical trial of ofloxacin alone and in combination with dapsone plus clofazimine for treatment of lepromatous leprosy, *Antimicrobial agents and chemotherapy*. **38**(4), 662–667.

Job, C. K., Jayakumar, J., Kearney, M. and Gillis, T. P. (2008). Transmission of leprosy: a study of skin and nasal secretions of household contacts of leprosy patients using pcr, *The American journal of tropical medicine and hygiene*. **78**(3), 518–521.

Job, C., Verghese, R. et al. (1975). Schwann cell changes in lepromatous leprosy-an electron-microscope study., *Indian Journal of Medical Research*. **63**(7), 897–901.

Jung, E., Lenhart, S. and Feng, Z. (2002). Optimal control of treatments in a two-strain tuberculosis model, *Discrete and Continuous Dynamical Systems Series B*. **2**(4), 473–482.

Kaluarachchi, S., Fernandopulle, B. and Gunawardane, B. (2001). Hepatic and haematological adverse reactions associated with the use of multidrug therapy in leprosy–a five year retrospective study., *Indian journal of leprosy*. **73**(2), 121–129.

Kamocki, R. (2014). Pontryagin maximum principle for fractional ordinary optimal control problems, *Mathematical Methods in the Applied Sciences*. **37**(11), 1668–1686.

Kar, B. R., Belliappa, P., Ebenezer, G. and Job, C. (2004). Single lesion borderline lepromatous leprosy, *International journal of leprosy and other mycobacterial diseases*. **72**, 45–47.

Khan, M. A. and Atangana, A. (2020). Modeling the dynamics of novel coronavirus (2019-ncov) with fractional derivative, *Alexandria Engineering Journal*. **59**(4), 2379–2389.

Krasnosel, M. (1968). *The Operator of Translation along the Trajectories of Differential Equations*, American Mathematical Society.

Krasnosel'skii, M. (1968). Translation along trajectories of differential equations, transl. math. monographs vol. 19, *Amer. Math. Soc. Providence RI.* .

Kroger, A., Pannikar, V., Htoon, M., Jamesh, A., Katoch, K., Krishnamurthy, P., Ramalingam, K., Jianping, S., Jadhav, V., Gupte, M. et al. (2008). International open trial of uniform multi-drug therapy regimen for 6 months for all types of leprosy patients: rationale, design and preliminary results, *Tropical Medicine & International Health*. **13**(5), 594–602.

Lakshmanan, M. and Rajaseekar, S. (2012). *Nonlinear dynamics: integrability, chaos and patterns*, Springer Science & Business Media.

Lakshmikantham, V., Simeonov, P. S. et al. (1989). *Theory of impulsive differential equations*, Vol. 6, World scientific.

Lee, E. B. and Markus, L. (1967). *Foundations of optimal control theory*, Vol. 87, Wiley New York.

Leprosy, W. (2012). on, organization wh. who expert committee on leprosy: eighth report, *World Health Organization*. .

Li, H., Cheng, J., Li, H.-B. and Zhong, S.-M. (2019). Stability analysis of a fractional-order linear system described by the caputo–fabrizio derivative, *Mathematics*. **7**(2), 200.

Losada, J. and Nieto, J. J. (2015). Properties of a new fractional derivative without singular kernel, *Progr. Fract. Differ. Appl.* **1**(2), 87–92.

Lukes, D. L. (1982). Differential equations: classical to controlled, . .

Masaki, T., Qu, J., Cholewa-Waclaw, J., Burr, K., Raaum, R. and Rambukkana, A. (2013). Reprogramming adult schwann cells to stem cell-like cells by leprosy bacilli promotes dissemination of infection, *Cell*. **152**(1), 51–67.

Mateus, J. P., Rebelo, P., Rosa, S., Silva, C. M. and Torres, D. F. (2017). Optimal control of non-autonomous seirs models with vaccination and treatment, *arXiv preprint arXiv:1706.06843*. .

Matis, J. H., Kiffe, T. R., Renshaw, E. and Hassan, J. (2003). A simple saddlepoint approximation for the equilibrium distribution of the stochastic logistic model of population growth, *Ecological Modelling*. **161**(3), 239–248.

Matsuoka, M. (2010). Drug resistance in leprosy, *Japanese journal of infectious diseases*. **63**(1), 1–7.

Moet, F. J., Pahan, D., Oskam, L. and Richardus, J. H. (2008). Effectiveness of single dose rifampicin in preventing leprosy in close contacts of patients with newly diagnosed leprosy: cluster randomised controlled trial, *Bmj*. **336**(7647), 761–764.

mondiale de la Santé, O., Organization, W. H. et al. (2016). Global leprosy update, 2015: time for action, accountability and inclusion, *Weekly Epidemiological Record= Relevé épidémiologique hebdomadaire*. **91**(35), 405–416.

Murray, J. (1989). 1989mathematical biology, *Berlin: SpringerVerlag. MurrayMathematical biology1989*. .

Narang, T., Kamat, D., Thakur, V., Lavania, M., Singh, I., Ahuja, M. and Dogra, S. (2022). Equal rates of drug resistance in leprosy cases with relapse and recurrent/chronic type 2 reaction: time to revise the guidelines for drug-resistance testing in leprosy?, *Clinical and experimental dermatology*. **47**(2), 297–302.

Nåsell, I. (1999). On the time to extinction in recurrent epidemics, *Journal of the Royal Statistical Society: Series B (Statistical Methodology)*. **61**(2), 309–330.

Neilan, R. L. M. (2009). *Optimal control applied to population and disease models*, PhD thesis, University of Tennessee, Knoxville.

Okosun, K. and Makinde, O. (2013). Optimal control analysis of malaria in the presence of non-linear incidence rate, *Appl. Comput. Math.* **12**(1), 20–32.

Ooi, W. W. and Srinivasan, J. (2004). Leprosy and the peripheral nervous system: basic and clinical aspects, *Muscle & nerve*. **30**(4), 393–409.

Organization, W. H. et al. (1982). *Chemotherapy of leprosy for control programmes: report of a WHO study group [meeting held in Geneva from 12 to 16 October 1981]*, World Health Organization.

Organization, W. H. et al. (1998). *WHO Expert Committee on Leprosy: seventh report*, World Health Organization.

Organization, W. H. et al. (2012). *WHO Expert Committee on leprosy: eighth report*, World Health Organization.

Pardillo, F. E. F., Fajardo, T. T., Abalos, R. M., Scollard, D. and Gelber, R. H. (2007). Methods for the classification of leprosy for treatment purposes, *Clinical Infectious Diseases*. **44**(8), 1096–1099.

Parkash, O. (2009). Classification of leprosy into multibacillary and paucibacillary groups: an analysis, *FEMS Immunology & Medical Microbiology*. **55**(1), 1–5.

Penna, G. O., Bührer-Sékula, S., Kerr, L. R. S., Stefani, M. M. d. A., Rodrigues, L. C., de Araújo, M. G., Ramos, A. M. C., de Andrade, A. R. C., Costa, M. B., Rosa, P. S. et al. (2017). Uniform multidrug therapy for leprosy patients in brazil (u-mdt/ct-br): Results of an open label, randomized and controlled clinical trial, among multibacillary patients, *PLoS neglected tropical diseases*. **11**(7), e0005725.

Penna, M. L. F., Buhrer-Sekula, S., Pontes, M. A. D. A., Cruz, R., Gonçalves, H. D. S. and Penna, G. O. (2014). Results from the clinical trial of uniform multidrug therapy for leprosy patients in brazil (u-mdt/ct-br): decrease in bacteriological index, *Leprosy review*. **85**(4), 262–266.

Penna, M. L. F. et al. (2014). Considerations in the design of clinical trials for multibacillary leprosy treatment., *Clinical Investigation*. **4**(1), 77–86.

Ploemacher, T., Faber, W. R., Menke, H., Rutten, V. and Pieters, T. (2020). Reservoirs and transmission routes of leprosy; a systematic review, *PLoS neglected tropical diseases*. **14**(4), e0008276.

Pontryagin, L. (1987). Mathematical theory of optimal processes, english edn.

Pontryagin, L. S. (2018). *Mathematical theory of optimal processes*, Routledge.

Prasad, P. and Kaviarasan, P. (2010). Leprosy therapy, past and present: can we hope to eliminate it?, *Indian journal of dermatology*. **55**(4), 316.

Qing, Y. and Rhoades, B. (2008). T-stability of picard iteration in metric spaces, *Fixed Point Theory and Applications*. **2008**, 1–4.

Rao, P. N. and Suneetha, S. (2018). Current situation of leprosy in india and its future implications, *Indian dermatology online journal*. **9**(2), 83.

Rees, R. (1994). The microbiology of leprosy, *Leprosy*, pp. 31–43.

Ridéey, D., Jopling, W. H. et al. (1966). Classification of leprosy according to immunity. a five-group system., *International journal of leprosy*. **34**(3), 255–73.

Ridley, D., Jopling, W. et al. (1962). A classification of leprosy for research purposes., *Leprosy review*. **33**(2), 119–28.

Robinson, C. (1998). *Dynamical systems: stability, symbolic dynamics, and chaos*, CRC press.

Rodrigues, F., Silva, C. J., Torres, D. F. and Maurer, H. (2017). Optimal control of a delayed hiv model, *arXiv preprint arXiv:1708.06451*. .

Rodrigues, L. C. and Lockwood, D. N. (2011). Leprosy now: epidemiology, progress, challenges, and research gaps, *The Lancet infectious diseases*. **11**(6), 464–470.

Roy, A. K., Roy, P. K. and Grigorieva, E. (2017). Mathematical insights on psoriasis regulation: Role of th1 and th2 cells, *Mathematical Biosciences & Engineering*. **15**(3), 717–738.

Roy, P. K., Chatterjee, A. N., Greenhalgh, D. and Khan, Q. J. (2013). Long term dynamics in a mathematical model of hiv-1 infection with delay in different variants of the basic drug therapy model, *Nonlinear Analysis: Real World Applications*. **14**(3), 1621–1633.

Roy, P. K., Chowdhury, S., Chatterjee, A. N., Chattopadhyay, J. and Norman, R. (2013). A mathematical model on ctl mediated control of hiv infection in a long-term drug therapy, *Journal of Biological Systems*. **21**(03), 1350019.

Ruan, S., Xiao, D. and Beier, J. C. (2008). On the delayed ross–macdonald model for malaria transmission, *Bulletin of mathematical biology*. **70**(4), 1098–1114.

Sabin, T. D., Ebner, J. D. et al. (1969). Patterns of sensory loss in lepromatous leprosy, *Int J Lepr*. **37**, 239–248.

Saha, S., Roy, P. K. and SMITH?, R. (2018). Modeling monocyte-derived dendritic cells as a therapeutic vaccine against hiv, *Journal of Biological Systems*. **26**(04), 579–601.

Sales, A. M., Campos, D. P., Hacker, M. A., da Costa Nery, J. A., Düppre, N. C., Rangel, E., Sarno, E. N. and Penna, M. L. F. (2013). Progression of leprosy disability after discharge: is multidrug therapy enough?, *Tropical Medicine & International Health*. **18**(9), 1145–1153.

Salzer, J. L. (2015). Schwann cell myelination, *Cold Spring Harbor perspectives in biology*. **7**(8), a020529.

Samko, S. G., Kilbas, A. A. and Marichev, O. I. (1993). Fractional integrals and derivatives, translated from the 1987 russian original.

Sansarricq, H. et al. (2004). *Multidrug therapy against leprosy: development and implementation over the past 25 years*, number WHO/CDS/CPE/CEE/2004.46, World Health Organization.

Schättler, H. and Ledzewicz, U. (2015). Optimal control for mathematical models of cancer therapies, *An application of geometric methods*. .

Scollard, D. M., Adams, L., Gillis, T., Krahenbuhl, J., Truman, R. and Williams, D. (2006). The continuing challenges of leprosy, *Clinical microbiology reviews*. **19**(2), 338–381.

Sekiguchi, M. and Ishiwata, E. (2010). Global dynamics of a discretized sirs epidemic model with time delay, *Journal of Mathematical Analysis and Applications*. **371**(1), 195–202.

Sen, A. and Mukhejee, D. (2011). Study of stability of a discrete two-predators and one prey model, *Int. J. Contemp. Math. Sciences*. **6**(13), 637–646.

Setia, M. S., Shinde, S. S., Jerajani, H. R. and Boivin, J.-F. (2011). Is there a role for rifampicin, ofloxacin and minocycline (rom) therapy in the treatment of leprosy? systematic review and meta-analysis, *Tropical Medicine & International Health*. **16**(12), 1541–1551.

Sharma, R., Lahiri, R., Scollard, D. M., Pena, M., Williams, D. L., Adams, L. B., Figarola, J. and Truman, R. W. (2013). The armadillo: a model for the neuropathy of leprosy and potentially other neurodegenerative diseases, *Disease models & mechanisms*. **6**(1), 19–24.

Shepard, C. et al. (1981). A brief review of experiences with short-term clinical trials monitored by mouse-foot-pad inoculation., *Leprosy Review*. **52**(4), 299–308.

Shetty, V., Wakade, A., Ghate, S., Pai, V., Ganapati, R. and Antia, N. (2003). Viability and drug susceptibility testing of m. leprae using mouse footpad in 37 relapse cases of leprosy, *International journal of leprosy and other mycobacterial diseases*. **71**(3), 210–217.

Silva, C. J. and Torres, D. F. (2013). Optimal control for a tuberculosis model with reinfection and post-exposure interventions, *Mathematical Biosciences*. **244**(2), 154–164.

Smith, C. S., Aerts, A., Saunderson, P., Kawuma, J., Kita, E. and Virmond, M. (2017). Multidrug therapy for leprosy: a game changer on the path to elimination, *The Lancet Infectious Diseases*. **17**(9), e293–e297.

Smith, R. and Wahl, L. (2005). Drug resistance in an immunological model of hiv-1 infection with impulsive drug effects, *Bulletin of Mathematical Biology*. **67**(4), 783–813.

Spierings, E., De Boer, T., Zulianello, L. and Ottenhoff, T. (2000). The role of schwann cells, t cells and mycobacterium leprae in the immunopathogenesis of nerve damage in leprosy, *Lepr Rev*. **71**(Suppl), S121–S129.

Talhari, C., Talhari, S. and Penna, G. O. (2015). Clinical aspects of leprosy, *Clinics in dermatology*. **33**(1), 26–37.

Tapinos, N. and Rambukkana, A. (2005). Insights into regulation of human schwann cell proliferation by erk1/2 via a mek-independent and p56lck-dependent pathway from leprosy bacilli, *Proceedings of the National Academy of Sciences*. **102**(26), 9188–9193.

Van den Driessche, P. and Watmough, J. (2002). Reproduction numbers and sub-threshold endemic equilibria for compartmental models of disease transmission, *Mathematical biosciences*. **180**(1-2), 29–48.

van Hooij, A. and Geluk, A. (2021). In search of biomarkers for leprosy by unraveling the host immune response to mycobacterium leprae, *Immunological Reviews*. **301**(1), 175–192.

Vellappandi, M., Kumar, P., Govindaraj, V. and Albalawi, W. (2022). An optimal control problem for mosaic disease via caputo fractional derivative, *Alexandria Engineering Journal*. **61**(10), 8027–8037.

Walker, S. and Lockwood, D. (2006). The clinical and immunological features of leprosy, *British medical bulletin*. **77**(1), 103–121.

Wang, X., Xiao, Y., Wang, J. and Lu, X. (2013). Stochastic disease dynamics of a hospital infection model, *Mathematical biosciences*. **241**(1), 115–124.

Westerlund, S. (1991). Dead matter has memory!, *Physica scripta*. **43**(2), 174.

Wilder-Smith, E. P. and Van Brakel, W. H. (2008). Nerve damage in leprosy and its management, *Nature Clinical Practice Neurology*. **4**(12), 656–663.

Williams, D. L., Araujo, S., Stryjewska, B. M. and Scollard, D. (2018). Dapsone resistance in leprosy patients originally from american samoa, united states, 2010–2012, *Emerging Infectious Diseases*. **24**(8), 1584.

Williams, D. L. and Gillis, T. P. (2012). Drug-resistant leprosy: monitoring and current status, *Leprosy review*. **83**(3), 269–281.

Wolf, D. M., Fontaine-Bodin, L., Bischofs, I., Price, G., Keasling, J. and Arkin, A. P. (2008). Memory in microbes: quantifying history-dependent behavior in a bacterium, *PLOS one*. **3**(2), e1700.

Wu, Z., Wang, C., Wang, Z., Shi, Y., Jiang, H. and Wang, H. (2022). Risk factors for dapsone resistance in leprosy patients: A systematic meta-analysis, *Journal of Global Antimicrobial Resistance*. **30**, 459–467.

Yang, C.-Y., Bialecka-Fornal, M., Weatherwax, C., Larkin, J. W., Prindle, A., Liu, J., Garcia-Ojalvo, J. and Süel, G. M. (2020). Encoding membrane-potential-based memory within a microbial community, *Cell systems*. **10**(5), 417–423.

Yang, H. M. and Ferreira, C. P. (2008). Assessing the effects of vector control on dengue transmission, *Applied mathematics and computation*. **198**(1), 401–413.

Yang, X., Chen, L. and Chen, J. (1996). Permanence and positive periodic solution for the single-species nonautonomous delay diffusive models, *Computers & Mathematics with Applications*. **32**(4), 109–116.

Zuidema, J., Hilbers-Modderman, E. and Merkus, F. (1986). Clinical pharmacokinetics of dapsone, *Clinical pharmacokinetics*. **11**, 299–315.

List of Publications

Based on this thesis, the following papers have been published and communicated:

- **Papers Published/Communicated in Journals**

1. **Ghosh, S.**, Chatterjee, A.N., Roy, P.K. et al. Mathematical Modeling and Control of the Cell Dynamics in Leprosy. *Computational Mathematics and Modeling*, 32, 52–74 (2021). DOI: https://doi.org/10.1007/s10598-021-09516-z

2. **Ghosh, S.**, Rana, S., Roy, P.K. Leprosy: Considering the Effects on Density-Dependent Growth of Mycobacterium leprae. *Differential Equations and Dynamical Systems*, 1-15 (2022). DOI: https://doi.org/10.1007/s12591-022-00608-9

3. **Ghosh, S.**, Saha, S., Roy, P.K, Critical observation of WHO recommended multidrug therapy on the disease leprosy through mathematical study, *Journal of Theoretical Biology*, Volume 567, 111496 (2023). DOI: https://doi.org/10.1016/j.jtbi.2023.111496

4. Cao, Xianbing., **Ghosh, S.**, Bose, H., Rana, S., Roy, P.K, Application of Optimal Control Therapeutic Approach on Memory Regulated Infection Mechanism for the Disease Leprosy through Caputo-Fabrizio Fractional Derivative, *MDPI-Mathematics*, 11(17),p 3630 (2023). DOI: https://doi.org/10.3390/math11173630

5. **Ghosh, S.**, Roy, A.K., Roy, P.K. Implementation of suitable optimal control strategy through introspection of different delay induced mathematical models for leprosy: A comparative study. *Optimal Control Applications and Methods* (2023). DOI: https://doi.org/10.1002/oca.3060

6. **Ghosh, S.**, Rana, S., Mukherjee, S., Roy, P.K., Gaining insights on the extinction of infected Schwann cells in leprosy: A stochastic mathematical model-based study. (Communicated in a peer-reviewed Journal)

– – – – – – – –